

Development of an automated analysis of
TDEM data for the delineation of a finite
conductor in a conductive half space.

by

Magdalena Combrinck

A thesis submitted in partial fulfillment of the
requirements for the degree of

Doctor in Philosophy in Exploration Geophysics

In the Faculty of Natural and Agricultural Science
of the University of Pretoria.

PRETORIA

2006

Development of an automated analysis of
TDEM data for the delineation of a finite
conductor in a conductive half space.

by

Magdalena Combrinck

Supervisor: Professor W. J. Botha

Degree: Doctor of Philosophy in Exploration Geophysics

Department: Geology

Abstract

The objective of this work is to find an efficient, preferably automated, algorithm or interpretational procedure that can be applied in real time to localise conductors buried in a host rock, with special attention given to a conductor in a conductive environment. The Time Domain Electromagnetic (TDEM) method is considered and more specifically the central loop configuration which can be found in both ground and airborne acquisition systems. The traditional interpretation approach of decay curve analysis is automated and combined with an adapted S-layer differential transform (Sidorov and Tiskshaev, 1969) to produce conductivity-depth sections with superimposed decay behaviour at every station. The adaptations made to the S-layer differential transform include:

- a noise filter to improve performance on field data
- the S-layer differential transform compatibility (SLTC) filter which only allows data conforming to the basic mathematical assumptions made in the transform to be processed (This “compatible” behaviour is derived through a number of synthetic model studies.)
- a depth correction based on the implications of approximating an infinite number of currents with a single filament.

A remaining concern when implementing the S-layer transform is found in two consecutive numerical differentiations and various approaches are analysed to ensure stable differentiation procedures. The automated algorithm is applied to a variety of synthetic models to validate its accuracy and finally examples are shown of its application to both ground and airborne data sets.

TABLE OF CONTENTS

1	INTRODUCTION	1
1.1	General overview.....	1
1.2	Objective.....	3
2	OVERVIEW OF ELECTROMAGNETIC THEORY FOR GROUND, IN- LOOP TDEM DATA	4
2.1	Introduction.....	4
2.2	System geometry and operating specifications.....	4
2.3	Analytical TDEM responses for four common models.....	5
2.3.1	TDEM central-loop response over a conductive half space.....	7
2.3.2	Thin, conductive sheet (S-layer).....	9
2.3.3	Finite conductor in a resistive host rock (half space).....	11
2.3.4	Finite conductor in a conductive host rock (half space).....	12
2.4	Conclusion.....	17
3	CONVENTIONAL INTERPRETATION TECHNIQUES	18
3.1	Introduction.....	18
3.2	Profiles versus soundings.....	19
3.3	Forward Modelling and Inversion.....	20
3.4	Limitations on automation of inversion techniques.....	21
3.5	Decay curve analysis.....	22
3.6	Transforms (Depth imaging).....	24
3.6.1	Conductivity Depth Images (CDI's).....	24
3.6.2	Stationary current images (SCI) (SCI - trademark of Geotrex-Dighem Pty Limited).....	24
3.6.3	S-layer differential transform.....	25
3.7	Combining Strategies.....	27
4	AUTOMATED INTEGRATED ANALYSIS OF TDEM DATA	28
4.1	An integrated analysis algorithm.....	28
4.2	Visualization of the field data for rapid anomaly detection.....	28
4.3	Decay curve analysis.....	30
4.3.1	Layered earth behaviour.....	31
4.3.2	Confined conductor behaviour.....	32
4.3.3	IP effect or severe lateral variation in subsurface conductivity.....	33
4.3.4	Results, output and presentation.....	33
4.4	Numerical calculation of the S-layer differential transform.....	33
4.4.1	Defining the S-layer transform.....	33
4.4.2	Numerical differentiation of TEM data.....	36
4.4.3	Comparison of differentiation methods applied to synthetic data.....	45
4.4.5	Concluding remarks on numerical differentiation.....	54
4.5	The S-layer correction factor.....	55
4.5.1	Defining a S-layer correction factor.....	55
4.5.3	Behaviour of the S-layer transform when applied to synthetic data.....	68
4.5.4	S-layer differential transform compatibility filter.....	92

4.5.5	Imaged conductivity depth sections generated from synthetic data	93
5	APPLICATION TO FIELD DATA.....	100
5.1	Introduction.....	100
5.2	Ground survey.....	100
5.2.1	Data acquisition and system parameters	100
5.2.2	Objective	102
5.2.3	Application of S-layer differential transform.....	102
5.2.4	Comparison of 25Hz (high, H) and 6.25Hz (medium, M) base frequency data	110
5.2.5	Imaged conductivity sections	114
5.2.6	Comparison of automated conductor location with Maxwell plate model results	117
5.3	Airborne survey.....	121
5.3.1	Data acquisition and system parameters	121
5.3.2	Automated processing	122
5.4	Conclusions and recommendations	125

LIST OF FIGURES

Figure 2-1	The use of equivalent current filament concept in understanding the behaviour of TEM fields over a conducting half space (after Nabighian and Macnae, 1991).....	8
Figure 2-2	Conductive sheet parameters.....	9
Figure 2-3	Equivalent current filaments (images) for a conducting thin sheet at various times after current interruption in the transmitter loop (after Nabighian and Macnae, 1991).....	10
Figure 2-4	Sphere currents at various times (a – surface currents; b-d – equatorial/plane currents) (after McNeill, 1980).	12
Figure 2-5	A permeable conducting sphere embedded in a conducting infinite space. The dipolar source is located at $S(r_0,0,0)$ outside the sphere (after Singh 1973).	14
Figure 2-6	Time characteristic of $h_{1r}^v(t)$ for $r/a=2$, $\mu_2/\mu_1=1$, and variable σ_1/σ_2 (after Singh 1973).....	14
Figure 2-7	Time characteristic of $h_{10r}^v(t)$ for $r/a=2$, $\mu_2/\mu_1=1$, and variable σ_1/σ_2 (after Singh 1973).....	15
Figure 2-8	Time characteristic of $h_{10\theta}^u(t)$ for $r/a=2$, $\mu_2/\mu_1=1$, and variable σ_1/σ_2 (after Singh 1973).....	15
Figure 2-9	“Reflected” smoke-rings. Electric field intensity is presented as sections for 20 consecutive time channels. The cyan and black contour lines present the electric field intensity for a homogeneous 50 Ohm.m half space and indicate the well-known diffusive smoke-ring behaviour. The colour contours indicate electric field intensity of currents for a 5 Ohm.m prism (black rectangle) in a 50 Ohm.m half space as percentage of the half space response. The “reflected” currents are clearly visible in channels 13 to 20.	16
Figure 3-1	Comparison of apparent conductivity (calculated by differentiating the fitted slowness with respect to reference depth curve) with the actual conductivity for four three-layer models (after Macnae and Lamontagne, 1987).	25
Figure 3-2	Cross-section of the model (top); Conductivity-depth image obtained by differential S-transformation (centre); Conductivity-depth image obtained by regularized S-inversion (bottom). (After Tartaras et. al., 2000).....	26
Figure 4-1	In (a) the raw data are presented in a contoured log-scale. In (b) the data were normalised using the half space value used in the forward model. In (c) the data were normalised as discussed above.	30
Figure 4-2	Flow diagram for decay curve slope analysis.	32
Figure 4-3	Percentage errors for differentiation in different domains of TDEM data for a 10 Ohm.m half space.	38
Figure 4-4	A Lagrange interpolating polynomial fitted to the data points outlining the back of a duck (top) and a cubic spline curve fitted to the same data points (bottom). (From Burden and Faires, 1993, Figures 3.11 and 3.12).....	40
Figure 4-5:	Comparison of differentiation methods applied to (a) unequally spaced points without smoothing of data, (b) unequally spaced points with smoothing of	

data, (c) equally spaced points without smoothing of data and (d) equally spaced points with smoothing.	46
Figure 4-6: A summary (in ascending order) of the average error over twenty data points for each of the alternatives in Figure 4.5. (ES: equal spacing, US: unequal spacing)	47
Figure 4-7: Synthetic data and model for three-layer earth.....	47
Figure 4-8: Effects of smoothing at different points in S-layer transform algorithm.....	49
Figure 4-9: Comparison of S-layer differential transform results for the three numerical differentiation methods applied on (a) unequally spaced data points without smoothing of data, (b) unequally spaced data points with smoothing of data, (c) equally spaced data without smoothing and (d) equally spaced data with smoothing.....	50
Figure 4-10: Four field data soundings; 1 to 4 are very smooth and considered to be clean data, while 5 & 6 contains noise.	51
Figure 4-11: S-layer differential transform results for Sounding 1.	51
Figure 4-12: S-layer differential transform results for Sounding 2.	52
Figure 4-13: S-layer differential transform results for Sounding 3.	53
Figure 4-14: S-layer differential transform results for Sounding 4.	54
Figure 4-15: Half space resistivities compared to resistivities from S-Layer differential transform.	56
Figure 4-16: Values for S and d corrections giving correct resistivity values and the effective depth correction resulting from each pair. (from Excel: summary of depth conversion factor models)	58
Figure 4-17: Cumulative conductance curves for late time halfspace approximations.	60
Figure 4-18: Cumulative conductance curves for late time half space and S-layer approximations.....	61
Figure 4-19: Comparison of S-layer differential transform (SLDT) solutions using different depth factors and layered earth inversions of synthetic data for a two layer earth.	63
Figure 4-20: Comparison of S-layer differential transform (SLDT) solutions using different depth factors and layered earth inversions of synthetic data for a three layer earth (thin conductive layer).....	64
Figure 4-21: Comparison of S-layer differential transform (SLDT) solutions using different depth factors and layered earth inversions of synthetic data for a three layer earth (thick conductive layer). Top: negative values included; Bottom: no negative values.....	65
Figure 4-22: Comparison of S-layer differential transform (SLDT) solutions using different depth factors and layered earth inversions of synthetic data for a thin conductive plate in a resistive half space.	66
Figure 4-23: Comparison of S-layer differential transform (SLDT) solutions using different depth factors and layered earth inversions of synthetic data for a conductive prism in a resistive half space.....	67
Figure 4-24 Cumulative conductance versus depth, 0.02 S/m (50 Ω .m) half space.....	69
Figure 4-25 Conductivity versus depth, 0.02 S/m (50 Ω .m) half space.....	69
Figure 4-26: Cumulative conductance versus depth for two layers of decreasing conductivity; first layer thickness 200m.....	70

Figure 4-27: Imaged conductivity versus depth for two layers of decreasing conductivity; first layer thickness 200m.....	71
Figure 4-28: Cumulative conductance versus depth for two layers of increasing conductivity; first layer thickness 200m.....	72
Figure 4-29: Imaged conductivity versus depth for two layers of increasing conductivity; first layer thickness 200m.	73
Figure 4-30: Imaged conductivity versus depth for two layers of increasing conductivity; first layer thickness 200m – linear scale.....	73
Figure 4-31: Cumulative conductance for a 15m thick layer of varying conductivity at 150m depth in a 0.02 S/m half space.....	74
Figure 4-32: Imaged conductivity versus depth for a 15m thick layer of varying conductivity at 150m depth in a 0.02 S/m half space.....	75
Figure 4-33: Imaged conductivity versus depth for a 15m thick layer of varying conductivity at 150m depth in a 0.02 S/m half space; linear scale.	75
Figure 4-34: Cumulative conductance for a 0.2 S/m layer of varying thickness at 150m depth in a 0.02 S/m half space.....	76
Figure 4-35: Imaged conductivity for a 0.2 S/m layer of varying thickness at 150m depth in a 0.02 S/m half space.....	77
Figure 4-36: Imaged conductivity for a 0.2 S/m layer of varying thickness at 150m depth in a 0.02 S/m half space; linear scale.....	77
Figure 4-37: Cumulative conductance for a 2 S/m layer of varying thickness at 150m depth in a 0.02 S/m half space.....	78
Figure 4-38: Imaged conductivity for a 2 S/m layer of varying thickness at 150m depth in a 0.02 S/m half space.....	78
Figure 4-39: Imaged conductivity for a 2 S/m layer of varying thickness at 150m depth in a 0.02 S/m half space – linear scale.	79
Figure 4-40: Cumulative conductance for a 0.2 S/m layer of 20 m thickness at various depths in a 0.02 S/m half space.	80
Figure 4-41: Imaged conductivity for a 0.2 S/m layer of 20 m thickness at various depths in a 0.02 S/m half space.	80
Figure 4-42: Imaged conductivity for a 0.2 S/m layer of 20 m thickness at various depths in a 0.02 S/m half space – linear scale.....	81
Figure 4-43: Cumulative conductance for a 0.2 S/m layer of 20 m thickness at 150 m depth in various host rock conductivities.....	82
Figure 4-44: Imaged conductivity for a 0.2 S/m layer of 20 m thickness at 150 m depth in various host rock conductivities.....	82
Figure 4-45: Imaged conductivity for a 0.2 S/m layer of 20 m thickness at 150 m depth in various host rock conductivities - linear scale.....	83
Figure 4-46: Cumulative conductance for a 0.2 S/m plate of 20 m thickness at 150 m depth in 0.02 S/m host rock. The horizontal dimensions vary from 100 m to infinite.	84
Figure 4-47: Imaged conductivity for a 0.2 S/m plate of 20 m thickness at 150 m depth in 0.02 S/m host rock. The horizontal dimensions vary from 100 m to infinite.	84
Figure 4-48: Imaged conductivity for a 0.2 S/m plate of 20 m thickness at 150 m depth in 0.02 S/m host rock. The horizontal dimensions vary from 100 m to infinite; linear scale.....	85

Figure 4-49: Cumulative conductance for a 2 S/m plate of 20 m thickness at 150 m depth in 0.02 S/m host rock. The horizontal dimensions vary from 100 m to infinite.	85
Figure 4-50: Imaged conductivity for a 2 S/m plate of 20 m thickness at 150 m depth in 0.02 S/m host rock. The horizontal dimensions vary from 100 m to infinite.	86
Figure 4-51: Imaged conductivity for a 2 S/m plate of 20 m thickness at 150 m depth in 0.02 S/m host rock. The horizontal dimensions vary from 100 m to infinite; linear scale.	86
Figure 4-52: Cumulative conductance for a 0.2 S/m prism at 150 m depth in a 0.02 S/m host rock. The prism dimensions vary from 100 m to 400 m.	87
Figure 4-53: Imaged conductivity for a 0.2 S/m prism at 150 m depth in a 0.02 S/m host rock. The prism dimensions vary from 100 m to 400 m.	88
Figure 4-54: Imaged conductivity for a 0.2 S/m prism at 150 m depth in a 0.02 S/m host rock. The prism dimensions vary from 100 m to 400 m; linear scale.	88
Figure 4-55: Comparison between imaged conductivities of a 0.2 S/m prism, 20 m thick plate and infinite sheet of 20 m thickness at 150 m depth in a 0.02 S/m host rock. Both the plate and prism have horizontal dimensions of 300 m.	89
Figure 4-56: Cumulative conductance for 2 S/m prisms at 150 m depth in a 0.02 S/m host rock. The prism dimensions vary from 100 m to 400 m.	90
Figure 4-57: Imaged conductivity for 2 S/m prisms at 150 m depth in a 0.02 S/m host rock. The prism dimensions vary from 100 m to 400 m.	90
Figure 4-58: Imaged conductivity for 2 S/m prisms at 150 m depth in a 0.02 S/m host rock. The prism dimensions vary from 100 m to 400 m; linear scale.	91
Figure 4-59 : Comparison between imaged conductivities of 2 S/m prisms, 20 m thick plates and infinite sheet of 20 m thickness at 150 m depth in a 0.02 S/m host rock. Plates and prisms with horizontal dimensions of 200 m and 300 m are shown.	91
Figure 4-60: Examples of field data showing "returning smoke ring" behaviour (stations -1200 and -150 from line 4950, Rosh Pinah data set).	92
Figure 4-61: S-layer differential transform results (conductivity depth section) on synthetic data. Top: Thin vertical plate (400mX 400m X 20m)	94
Figure 4-62: Same models as in Figure 4-63. Red dots indicate half space decay behaviour and blue dots indicate conductor in "free air" decay.	95
Figure 5-1: Mountain with TDEM survey team.	101
Figure 5-2: Grid locality and layout.	102
Figure 5-3: Line 4950, Station 100. <i>Top</i> : Raw data with calculated cumulative conductance and imaged conductivity. <i>Middle</i> : No filter effect on input data values, only on cumulative conductance curve with imaged conductivity of filtered conductance values. <i>Bottom</i> : Input data filtered for late channel erratic behaviour and filtered cumulative conductance values.	104
Figure 5-4: Line 4950, Station 300. <i>Top</i> : Raw data with calculated cumulative conductance and imaged conductivity. <i>Middle</i> : No filter effect on input data values, only on cumulative conductance curve with imaged conductivity of filtered conductance values. <i>Bottom</i> : Input data filtered for late channel erratic behaviour and filtered cumulative conductance values.	105

Figure 5-5: Line 4950, Station 400. <i>Top:</i> Raw data with calculated cumulative conductance and imaged conductivity. <i>Middle:</i> No filter effect on input data values, only on cumulative conductance curve with imaged conductivity of filtered conductance values. <i>Bottom:</i> Input data filtered for late channel erratic behaviour and filtered cumulative conductance values.	106
Figure 5-6: Line 4950, Station 450. <i>Top:</i> Raw data with calculated cumulative conductance and imaged conductivity. <i>Middle:</i> No filter effect on input data values, only on cumulative conductance curve with imaged conductivity of filtered conductance values. <i>Bottom:</i> Input data filtered for late channel erratic behaviour and filtered cumulative conductance values.	107
Figure 5-7: Line 4950, Station -1550. <i>Top:</i> Raw data with calculated cumulative conductance and imaged conductivity. <i>Middle:</i> No filter effect on input data values, only on cumulative conductance curve with imaged conductivity of filtered conductance values. <i>Bottom:</i> Input data filtered for late channel erratic behaviour and filtered cumulative conductance values.	108
Figure 5-8: Comparison of SDTC filter only (top) and SDTC with additional noise filter (bottom). Black dots are station elevations (DTM) and white dots represent depths at which conductivities are calculated.	110
Figure 5-9: Line 450N showing good correlation between conductivity depth sections obtained from the high (top) and medium frequencies (bottom).	111
Figure 5-10: Line 1650N showing poor correlation between the high (top) and medium frequencies (bottom).	112
Figure 5-11: Line 450; Stations 750 and 1450; medium and high frequency measured data...	113
Figure 5-12: Line 1650; Stations -200, 150 and 250; medium and high frequency measured data.	114
Figure 5-13: Contour map of conductor decay constants draped over topography and conductivity depth sections in 3D. Top viewpoint is from inclination 20°, declination 180° and 5km distance. Bottom viewpoint is inclination 10°, declination -100° and distance 5km. Axes are Northing, Easting and Elevation above sea level.	115
Figure 5-14: 3D view from inclination 60°, declination 180° and 5km distance with and without contour map of conductor decay constants.	116
Figure 5-15: Line 4050. EM response profiles and sections from automated processing procedures.	118
Figure 5-16: Line 4150. EM response profiles and sections from automated processing procedures.	119
Figure 5-17: Line 4050. Comparison of Maxwell plate model and conductivity depth section.	120
Figure 5-18: Line 4150. Comparison of Maxwell plate model and conductivity depth section.	120
Figure 5-19: EM Response over conductor.....	122
Figure 5-20: Conductivity depth section from S-layer transform, showing dipping conductor.....	123
Figure 5-21: Conductivity depth section in greyscale with channels corresponding to half space power law decay indicated in red.	123

Figure 5-22: Conductivity depth section in greyscale with conductor decay constants plotted at scaled channel positions.	124
Figure 5-23: Conductivity depth section in greyscale with channels on stations showing sign changes indicated in blue.....	124

ACKNOWLEDGMENTS

The author wishes to thank Prof. Willem Botha (my supervisor) for his patience and when it was required, the lack thereof. Many other people including family, friends, training partners and colleagues contributed to this work through their continued moral support. To Melinda de Swardt who took me for tea when the end seemed too far away a special word of gratitude, as well as to all my students who stimulated my own growth with their questions and enthusiasm.

Sincere gratitude is also extended to BHP Billiton for allowing me to use their data and to that very special breed of geophysicists specialising in EM who published and shared their knowledge without whom there would have been nothing to build this work on. Lastly, to the Creator who thought it well to hide the earth's riches from us, but not without endowing us with the capabilities to find it if looking with courage and persistence.

Chapter 1

1 INTRODUCTION

"I believe that we cannot live better than seeking to become still better than we are."

(Socrates)

1.1 General overview

The Time Domain Electromagnetic (TDEM) method, also referred to as Transient EM (TEM), has been used in mineral exploration since the late 1950's. The basic theory of this method is defined in totality by four differential equations, known as Maxwell's equations. These equations describe the relationships between electric and magnetic fields and sources, enabling the geophysicist to derive the electric field (E) in the earth through measuring the magnetic field (B), or its time derivative (dB/dt) on, above or below the surface. The electric field in the earth is a function of the electromagnetic (EM) source and of the earth's conductivity distribution. If the source is known, the geophysicist should be able to derive the conductivity distribution of the subsurface (and therefore be able to isolate and interpret zones with contrasting conductivities).

- The success of this procedure is dependant on three factors:
- Choosing a source (transmitter) of appropriate dimensions and magnetic moment to induce currents in the subsurface volume of interest
- Measuring the induced magnetic field and/or its derivative with the required accuracy and resolution in time and space (receiver) to resolve the target
- Accurately solving Maxwell's equations

The first two factors are concerned with the design of the measuring instrument and data acquisition parameters. Survey costs are the largest limiting influence on these factors and increases in cost can only be justified by producing increasingly accurate geological models leading to savings in other stages of exploration expenses, e.g. drilling.

Theoretically, within some engineering constraints, one can choose to measure or "know" the whole field exactly. This is a scenario utilised very effectively through

forward modeling and is the reason why synthetic data is normally used as a first run to test new interpretation algorithms.

The third factor proves to be the most difficult – accurately solving Maxwell's equations. These equations can only be solved analytically for a few very simple geometrical models and only if assumptions regarding homogeneity, isotropy, frequency dependence, and frequency and conductivity ranges are made. Kaufman and Keller (1983) makes use of asymptotic equations based on even more assumptions and terms like “far away”, “late time”, “early time” and “large loops” are found extensively in EM literature. Solutions are calculated for these very special instances of system geometry and conductivity models, but the results are applied and compared to real earth situations, not complying with these assumptions. Following this reasoning it is understandable why geophysicists sometimes experience frustration in terms of knowing that there is a conductive unit but not being able to say exactly what or where, leading to simply drilling anomalies – also known as “bump-hunting”.

Accepting that Maxwell's equations cannot be solved analytically for a general situation, the next option would be to solve them numerically making use of standard numerical solutions for differential equations. The complexity of these equations, numerical instabilities under certain conditions (e.g. high conductivity contrasts), and the very long computer calculation times, imply that full three dimensional solutions (and especially inversion) of realistic geological models are not yet reaching industry expectations as an efficient interpretation tool.

The only option left at this stage is to develop time- and cost efficient algorithms to find solutions based on some of these assumptions and apply these *only* to geological settings and data *satisfying* those assumptions. An example of this is the mathematical assumption of one dimensionality of the earth, which is met when horizontally layered geology is investigated. This approach implies a number of different interpretational procedures and algorithms to be developed. It is of course possible to apply one algorithm or procedure to all data acquired over a range of different geological settings, but the obtained results would only be reliable if the inherent assumptions of the algorithm are met.

One of the most common assumptions is that the host rock containing the ore body of interest is very resistive. This implies a significant decrease in computational effort, but unfortunately is one of the assumptions not always met in true field conditions. The non-compliance of this assumption is of great importance in the closely related field of landmine detection where small pieces of metal are looked for, often in very conductive and magnetite rich top soils (Butler, 2003).

1.2 Objective

The objective of this work is to find an efficient, preferably automated, algorithm or interpretational procedure that can be applied in real time to scenarios of conductors buried in a resistive and/or conductive host rock or half space. This will not provide the ultimate answer, but can be considered another useful tool available to the geophysicist to reduce some assumptions. Real-time conductor location and imaging (i.e. estimating size, depth and conductance) can attribute significantly to reduction of processing and interpretation cost in the mineral industry and might also encourage the development of new instruments. For example, a multi-channel metal detector with real-time processing and conductivity imaging of data might prove to be very valuable in the field of landmine detection, especially in conductive top soil regions where traditional metal detectors sometimes prove to be inadequate (Butler, 2003).

Chapter 2

2 OVERVIEW OF ELECTROMAGNETIC THEORY FOR GROUND, IN- LOOP TDEM DATA

"There is a theory which states that if ever anybody discovers exactly what the Universe is for and why it is here, it will instantly disappear and be replaced by something even more bizarre and inexplicable. There is another theory which states that this has already happened."

(from "The Hitchhiker's guide to the Galaxy", Douglas Adams)

2.1 Introduction

It is the inherent complexity contained in the electromagnetic method that on the one hand forces us to simplify it almost beyond recognition in order to apply it practically; and on the other hand compels us to keep on searching for the "truth" (or the most complete set of information that can be obtained from EM measurements). This continued search is conducted in many, painstakingly slow, very small steps – sometimes referred to as *research*.

All EM methods (except the magneto-telluric method) utilise active sources, or transmitters, in order to generate measurable fields. This is in contrast to passive methods such as the potential field methods (e.g. the gravity and magnetic techniques) where the earth's natural occurring magnetic field is measured. Passive source method instruments only consist of receivers and the data acquired by different instruments are all reduced to the earth's total field with no or minimal computational effort. Active source instruments, on the other hand, require the complete specifications of the source and receiver to be incorporated into the processing and interpretational procedures. Unless stated otherwise, algorithms derived in this study are only suitable for systems conforming to the same basic geometrical set-up and operating parameters as described in the following paragraphs.

2.2 System geometry and operating specifications

The theory developed in this study is directly applicable to central-loop ground TDEM systems with step-current excitation, e.g. Geonics EM37 or EM47 and interpretation

strategy allows for both 1D and 3D model considerations. The late time mathematical approximations are implemented for most procedures.

2.3 Analytical TDEM responses for four common models

Analytical responses for TDEM data are calculated by solving Maxwell's equations. The differential forms of the equations are valid at points in space only, but comparatively easy to calculate, while the integral forms are valid at boundaries of units, more difficult to calculate and used primarily to generate boundary conditions.

Table 2-1 Maxwell's equations (Compiled from Ward and Hohmann (1988) and Kaufman and Keller (1983)).

Maxwell's equations in integral form:	Maxwell's equations in differential form:
$\int_S \mathbf{D} \cdot d\mathbf{S} = q$ $\int_S \mathbf{B} \cdot d\mathbf{S} = 0$ $\oint \mathbf{E} \cdot d\mathbf{l} = -\frac{d\Phi_B}{dt}$ $\Phi_B = \int_S \mathbf{B} \cdot d\mathbf{S} = \text{Flux through surface}$ $\oint \mathbf{H} \cdot d\mathbf{l} = \mathbf{I} + \int_S \frac{\partial \mathbf{D}}{\partial t} \cdot d\mathbf{S}$	$\nabla \cdot \mathbf{D} = \rho$ $\nabla \cdot \mathbf{B} = 0$ $\nabla \times \mathbf{E} = -\frac{\partial \mathbf{B}}{\partial t}$ $\nabla \times \mathbf{H} = \mathbf{j} + \frac{\partial \mathbf{D}}{\partial t}$

Maxwell's equations are uncoupled differential equations that need to be coupled using the constitutive equations that contain all the electrical and magnetic properties of the medium through which EM propagation occurs (i.e. the earth in geophysics). The constitutive equations are given by Ward and Hohmann (1988) as:

$$\mathbf{D} = \underline{\underline{\epsilon}} \cdot \mathbf{E}$$

$$\mathbf{B} = \underline{\underline{\mu}} \cdot \mathbf{H}$$

$$\mathbf{j} = \underline{\underline{\sigma}} \cdot \mathbf{E}.$$

\mathbf{E} : electric field intensity [V/m]

\mathbf{D} : dielectric displacement [C/m²]

\mathbf{I} : current [A]

ρ : electric charge density [C/m³]

$\sigma, \underline{\underline{\sigma}}$: conductivity [S/m]

$\epsilon, \underline{\underline{\epsilon}}$: dielectric permittivity [F/m]

\mathbf{B} : magnetic induction [Tesla]

\mathbf{H} : magnetic field intensity [A/m]

\mathbf{j} : current density [A/m²]

q : charge [Coulomb]

$\mu, \underline{\underline{\mu}}$: magnetic permeability [H/m]

In these equations the dielectric permittivity, magnetic permeability and electric conductivity should all be regarded as tensor functions of angular frequency, position, time, temperature, pressure and magnetic/electric field strength. However, in order to derive analytical solutions some assumptions regarding these parameters are necessary.

ASSUMPTIONS:

- All media are linear, isotropic and homogeneous and possess physical properties, which are independent of time, temperature and pressure (implying scalar presentation of physical properties rather than tensors).
- The magnetic permeability of all media is assumed to be equal to that of free space, i.e. $\mu = \mu_0$.

The TDEM solutions are derived by calculating the frequency domain electromagnetic (FDEM) responses for equivalent models and then applying Fourier transforms to these results. In order to solve the FDEM equations analytically some further assumptions are necessary.

ADDITIONAL ASSUMPTIONS:

- There are no free electric charges or current in the medium, i.e.

$$\rho = 0; \quad \nabla \cdot \mathbf{D} = \nabla \cdot \mathbf{E} = 0.$$

- We assume a harmonic time varying field, i.e.

$$\mathbf{E} = \mathbf{E}_0 e^{-i\omega t} \text{ and } \mathbf{B} = \mathbf{B}_0 e^{-i\omega t}.$$

- Displacement currents are much smaller than induction currents, i.e.

$$\frac{\partial \mathbf{D}}{\partial t} \ll \mathbf{j} \text{ and } \nabla \times \mathbf{H} = \sigma \mathbf{E} \text{ implying a wavenumber of}$$

$k^2 = i\omega\mu\sigma$ in the solution of the wave (Helmholz) equation.

The receiver and transmitter are in the same plane of observation ($z=0$), also indicating the air-surface boundary in the case of a half space or layered earth.

Incorporating these assumptions into calculations the analytical solutions for a number of different geological models can be found. For the purposes of this study there are four cases deserving special attention, namely:

- Conductive half space

- Thin, conductive sheet (S-layer)
- Finite conductor in a resistive host rock (half space)
- Finite conductor in a conductive host rock (half space).

2.3.1 TDEM central-loop response over a conductive half space

The quasi-static approximation of EM-field propagation in a half space can be described as a diffusion process (Nabighian, 1979). When doing a TDEM survey the current in the transmitter loop is switched off very abruptly, causing a sudden change in the associated magnetic field (large $\partial\mathbf{B}/\partial t$). Following from Maxwell's third equation the electric field (\mathbf{E}) associated with this sudden change in magnetic field will cause a current to flow in the conductive half space ($\mathbf{j} = \sigma\mathbf{E}$). This current will mimic the primary transmitter loop geometry but will only exist in that form for a fraction of a second as it is not confined to a specific path or circuit and has no source (battery) to maintain current flow. The induced current will therefore immediately start to dissipate, generating a new magnetic field that changes with time and consequently induce new currents in the half space. This behaviour was discussed extensively by Nabighian (1979), leading to the smoke-ring concept of EM propagation in a homogeneous half space. In short, a number of EM induced currents exist in the half space after the primary field is terminated and the maximum current density retains a transmitter loop-like shape expanding with time. Contouring the electric field at different points in time clearly show the maxima of the electric field (most dominant currents) migrating outward and downward into the half space at an angle of approximately 30° . Nabighian (1979) also introduced the mathematical alternative of a single equivalent current filament that will produce, with a high degree of accuracy, the same EM fields measured on the surface of the earth, as would the whole system of real currents. This equivalent current filament moves outward and downward at an angle of approximately 47° . A comparison of these two approaches is shown in figure 2.1. The advantage of using the single equivalent current filament is the dramatic simplification in mathematical description that allows the calculation of parameters such as velocity and depth with time as well as relationships of these to half space conductivity.

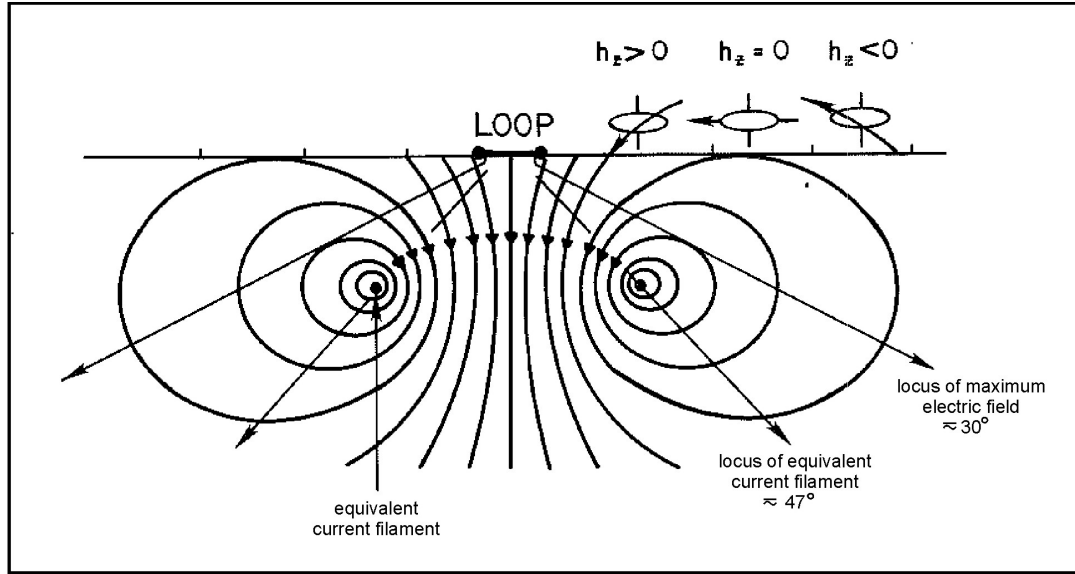


Figure 2-1 The use of equivalent current filament concept in understanding the behaviour of TEM fields over a conducting half space (after Nabighian and Macnae, 1991).

The quasi-stationary (derivative of) magnetic field transient response of a central-loop, step-current system over a conductive earth is given by Kaufman and Keller (1985) as

$$\frac{\partial H_z}{\partial t} = -\frac{I}{\mu_0 \sigma a^3} \left[3 \operatorname{erf}(u) - \frac{2}{\pi^{1/2}} u (3 + 2u^2) e^{-u^2} \right] \quad (2.1)$$

where

$$\operatorname{erf}(u) = \frac{2}{\sqrt{\pi}} \int_0^u e^{-x^2} dx$$

$$u = \frac{\pi \sqrt{2} a}{\tau}$$

$$\tau = 2\pi \left(\frac{2t}{\mu_0 \sigma} \right)^{1/2}$$

a = radius of the transmitter loop[m]

t = time [s],

with a late time asymptotic approximation of

$$\frac{\partial H_z}{\partial t} = (\operatorname{emf}) \cdot (\text{effective receiver area}) = -\frac{I a^2 (\sigma \mu_0)^{3/2}}{20\pi^{1/2}} t^{-5/2}. \quad (2.2)$$

In the “late time” (which can be achieved through either large values of t , or small values of σ), it can be seen from equation 2.2 that the vertical component of the measured

electromotive force (emf) is directly proportional to $t^{-5/2}$ for an ideal step function excitation. This behaviour is described as a power-law decay with time and manifests as a straight line with a slope of $m = -5/2$ on a graph of $\log(\text{emf})$ versus $\log(t)$. The horizontal component of the emf can be shown to exhibit the same behaviour (Kaufman and Keller, 1983); the only difference being that it shows a time-decay proportional to t^{-3} in the late time. In terms of the smoke-ring analogy, the “late time” for profiling commences when the equivalent current filament is so far away that any receiver position can be approximated to be at the centre of the smoke-ring. With the central-loop system (as used in this study) this is always the case and it is easy to see why the late time approximations are particularly useful for this survey geometry.

2.3.2 Thin, conductive sheet (S-layer)

Parameters used in the conductive sheet model are shown in figure 2.2.

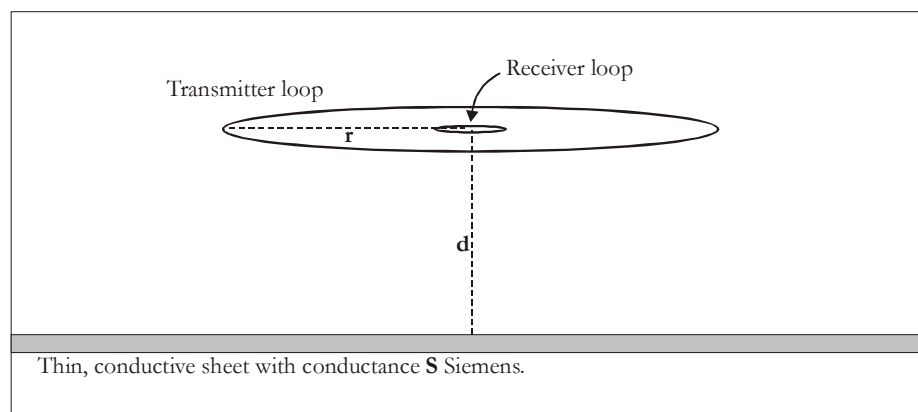


Figure 2-2 Conductive sheet parameters.

The equivalent current smoke-ring behaviour for an S-layer (originally solved by Maxwell) is described by Nabighian and Macnae (1991). With the primary field termination currents are induced in the S-layer, once again representing the geometry of the transmitter loop. As time passes the equivalent current filament retains its original size and intensity and only appears to migrate downwards with a velocity related to the conductance of the S-layer as $v = 2/S\mu_0 \text{ ms}^{-1}$ (figure 2.3). This is an exact solution for velocity (v).

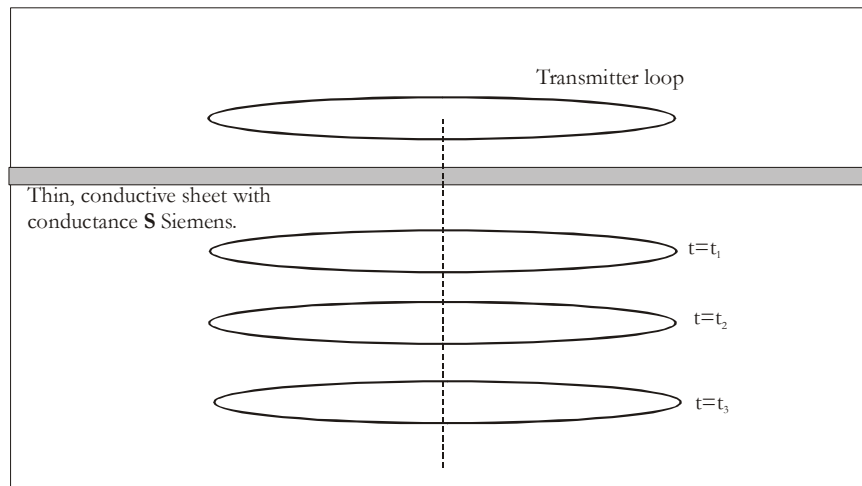


Figure 2-3 Equivalent current filaments (images) for a conducting thin sheet at various times after current interruption in the transmitter loop (after Nabighian and Macnae, 1991).

The emf induced in a loop which is located in the horizontal plane, with a small dipole source located at its centre, is given by Kaufman and Keller (1983) as:

$$emf = -\frac{M}{Sr^2} \frac{3(\tau_s + 2h_0)}{[1 + (\tau_s + 2h_0)^2]^{3/2}} \quad (2.3)$$

where

M = magnetic dipole moment of the transmitter (small) loop

$$\tau_s = \frac{2t}{\mu_0 S r}$$

r = radius of the large receiver loop [m]

t = time [s]

S = conductance of the thin plate [S]

$$h_0 = \frac{d}{r}$$

d = vertical distance between the loops and the conductive plate.

The quasi-stationary (derivative of) magnetic field transient response of a central-loop, step current system over a thin conductive sheet can be calculated from equation 2.3 by applying the principle of reciprocity (i.e. in any system the same emf will still be measured if the transmitter and receiver geometries are interchanged). Making the late time approximation

of $\frac{2t}{\mu_0 S} + 2d \gg r$ (where r now represents the small loop radius after reciprocity) and

simplifying equation 2.3 we have

$$emf_{late\ time} = -\frac{3M}{16Sr^2} \frac{1}{(\tau + d)^4} \quad (2.4)$$

$$\frac{\partial H_z}{\partial t} = \frac{emf_{late\ time}}{\text{effective Rx area}} = \frac{emf_{late\ time}}{n_r \pi r^2} = -\frac{3M}{16S\pi} \frac{1}{(\tau + d)^4} \quad (2.5)$$

where

M = magnetic dipole moment of the transmitter (large) loop

$$\tau = \frac{t}{\mu_0 S}$$

n_r = number of turns in receiver loop

r = radius of the small receiver loop[m].

This is a very good approximation for the chosen system geometry as the radius of the receiver loop is always in the order of one meter and the late time condition is always satisfied under field conditions. The “late time” approximation of the S-layer response is therefore directly proportional to t^{-4} . This behaviour manifests as a straight line with a slope of $m = -4$ on a graph of $\log(emf)$ versus $\log(t)$.

2.3.3 Finite conductor in a resistive host rock (half space)

The significance of having a confined target surrounded by an insulator is that there is always some stage of time (“late time”) when the current distribution in the conductor becomes invariant with time and the decay becomes exponential at a rate determined by the shape, size, and conductivity of the body (McNeill, 1980). An intuitive feeling for the general behaviour of isolated (confined) conductors can be developed from examining the simplified case of a conducting sphere assumed to be in a region of uniform magnetic field that is suddenly terminated. Immediately after termination of the primary current (early time) the secondary currents flow on the surface of the sphere and are independent of its conductivity (figure 2.4a). From then on the currents diffuse radially inwards, similar to the smoke-ring propagation found in a half space. This stage of changing current distribution is referred to as intermediate time (figure 2.4c). The late time commences when the inductance and resistance associated with each current ring, have stabilized and from this time onwards both the currents and their associated external magnetic field commence to decay exponentially with a time-constant given by

$$\tau = \frac{\sigma \mu a^2}{\pi^2} \quad (2.6)$$

σ = conductivity of sphere [S]

a = radius of sphere [m],

so that

$$emf_{sphere \text{ late time}} = A e^{-t/\tau} \quad (2.7)$$

A = constant containing geometrical information.

Emf measurements taken at this stage of “late time” will manifest as a straight line when plotted on a semi-log graph of $\ln(emf)$ versus time.

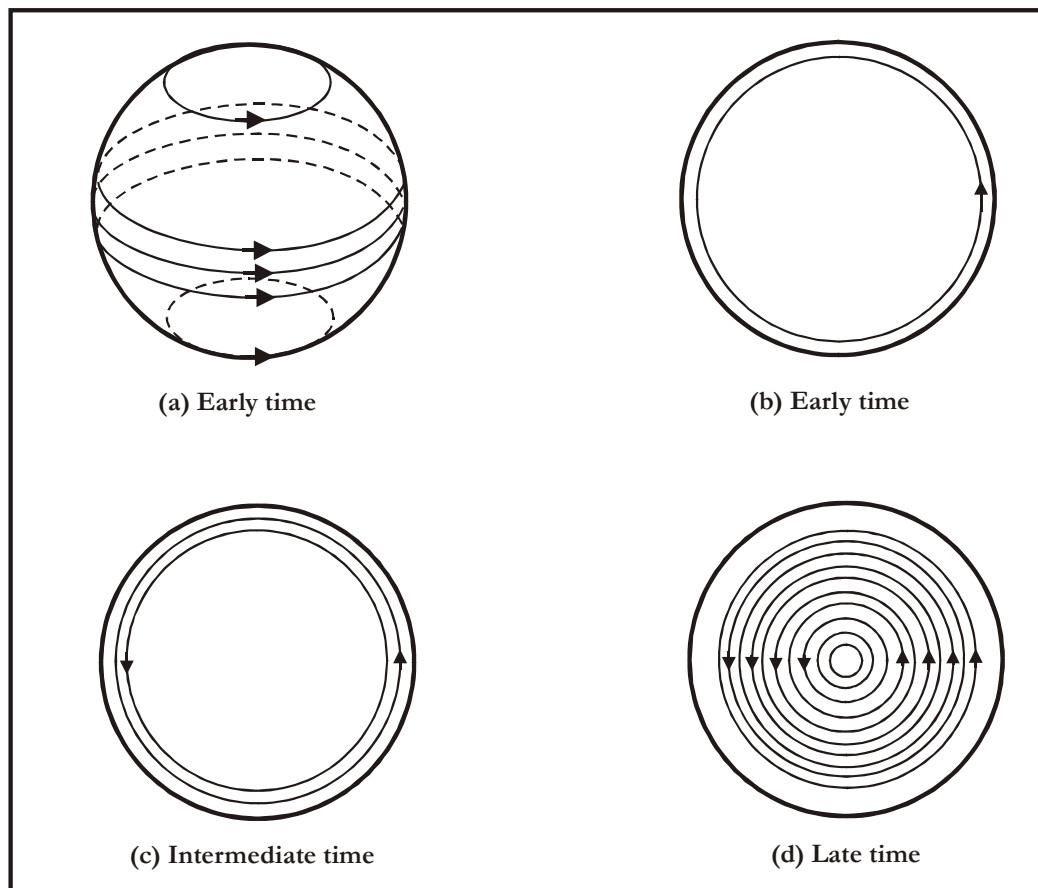


Figure 2-4 Sphere currents at various times (a – surface currents; b-d – equatorial/plane currents) (after McNeill, 1980).

2.3.4 Finite conductor in a conductive host rock (half space)

When a conductive target is located in a conductive host rock the inducing magnetic field, at the location of the target, is no longer a step function but a slowly varying field due to

the diffusion of the smoke-ring currents (Nabighian and Macnae, 1991) and the assumptions stated in 2.3 are not valid anymore. This different nature of the inducing field has two consequences. Firstly, the toroidal vortex (induced) currents will not be as strong as in the case of a conductor in free space, because of the reduced $\partial\mathbf{B}/\partial t$ component (fields are varying slower with time). Secondly, the smoke-rings will also cause galvanic currents to flow in the conductor and lead to charge accumulation on the boundaries between the conductor and the host rock. The smoke-ring electric field will instantaneously be opposed within the target by the field of this electric charge distribution created at the target boundaries. A secondary electric field created by these charges will cause a poloidal current flow that tends to cancel most of the primary electric field (i.e. the field associated with the smoke-rings) inside the conducting target (Nabighian and Macnae, 1991). This cancellation is more effective for short strike length bodies which, therefore, have less poloidal (galvanic) current flow than longer bodies. The strength of these currents depends mainly on the conductivity of the host rock and is only weakly dependent on the much higher conductivity of the target. As such, the secondary magnetic field will decay at a rate governed chiefly by the host rock conductivity. Anomalies due to both poloidal (galvanic) and toroidal (inductive) currents are generally of the same sign and increase the detectability of a given target according to Nabighian and Macnae (1991). However, the combined anomaly will be spatially smeared toward longer wavelengths compared to that of vortex currents alone – leading to erroneous interpretation if modelled using a conductor in free-space approach. Singh (1973) has calculated the TDEM response for a conductive sphere in a conducting infinite space and shown that the late time response can also be presented as an inverse power law that is characteristic of whole- and half space responses (i.e. straight-line behaviour in the late time on a logarithmic graph of emf versus time). In the following graphs, h refers to the magnetic field component, the first subscript 1 to the multi-pole, the second to the spherical component (r , θ , or ϕ), and the third to the orientation of the magnetic dipole (r for radial, θ for transverse). The superscripts v and u refer to the magnetic mode or transverse electric (TE) and electric mode or transverse magnetic (TM) solutions. In free space (i.e. making the quasi-static approximation) only TE solutions are generated with a radial magnetic dipole as source (horizontal loop above sphere). Figures 2.6 to 2.8 show the differences in late time decay behaviour between a conductive sphere in free space ($\sigma_1/\sigma_2=0$) and a conductive sphere in a conducting infinite space for various conductivity contrasts ($\sigma_1/\sigma_2=1/10$ to $1/100$). The secondary magnetic field component $h_{1r}^v(t)$ in figure 2.6, is equivalent to the vertical

component ($h_z(t)$) generated from a vertical magnetic dipole source through abrupt termination of current in a horizontal loop. The response for a sphere in free space ($\sigma_1/\sigma_2=0$) corresponds with solutions obtained by Nabighian (1971) and McNeill (1980).

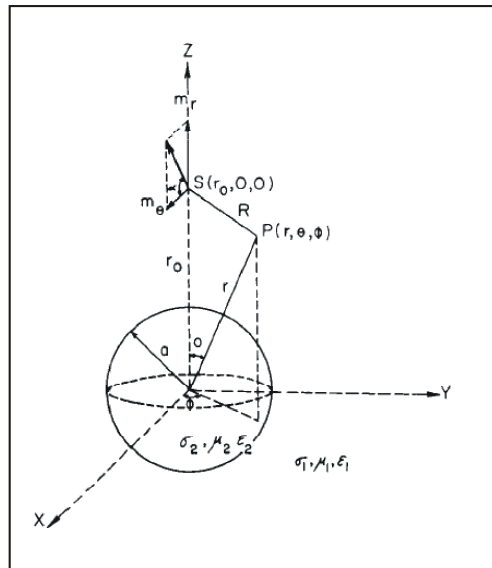


Figure 2-5 A permeable conducting sphere embedded in a conducting infinite space. The dipolar source is located at $S(r_0,0,0)$ outside the sphere (after Singh 1973).

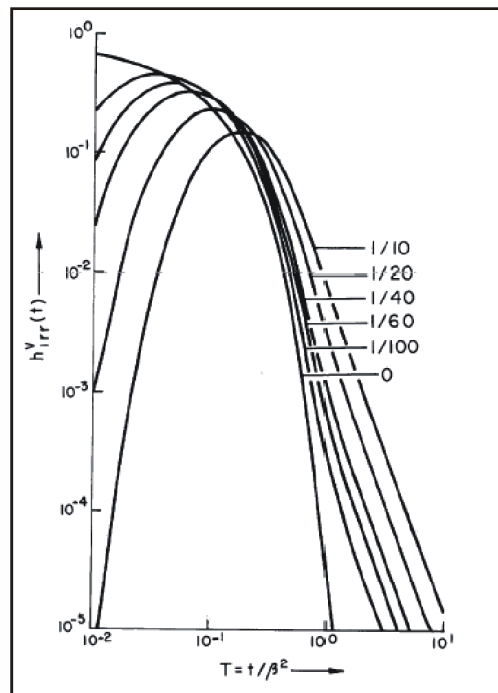


Figure 2-6 Time characteristic of $h^v_{1rr}(t)$ for $r/a=2$, $\mu_2/\mu_1=1$, and variable σ_1/σ_2 (after Singh 1973).

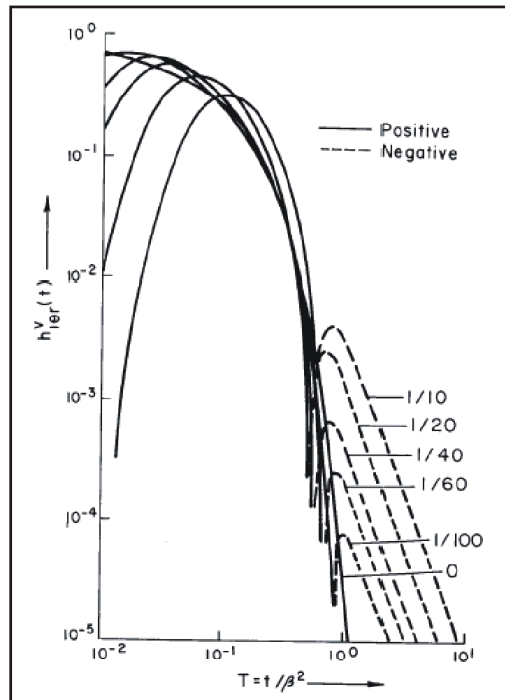


Figure 2-7 Time characteristic of $h^v_{10r}(t)$ for $r/a=2$, $\mu_2/\mu_1=1$, and variable σ_1/σ_2 (after Singh 1973).

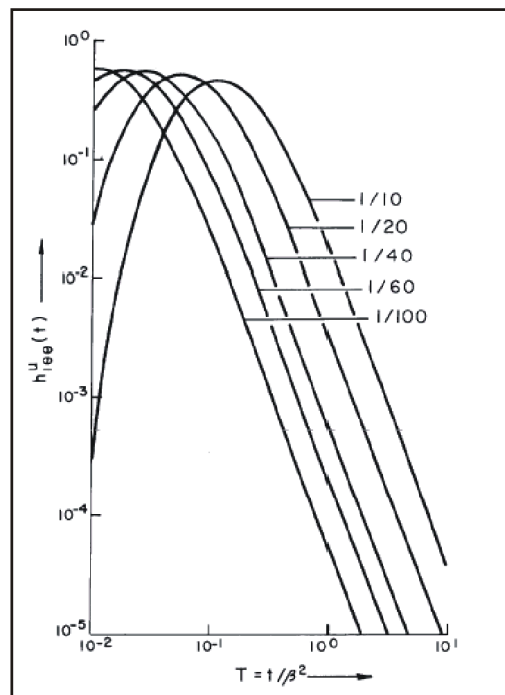


Figure 2-8 Time characteristic of $h^u_{10\theta}(t)$ for $r/a=2$, $\mu_2/\mu_1=1$, and variable σ_1/σ_2 (after Singh 1973).

The curves for $h^v_{1rr}(t)$ reach a maximum at $T > 0$ and then decay at a rate slower than the case $\sigma_1/\sigma_2=0$, whose maximum occurs at $T = 0$. With increasing σ_1/σ_2 (lower contrast between sphere and conducting space implying more conductive space), the peak value of $h^v_{1rr}(t)$ is reduced and delayed in time. Also, in late time the curves exhibit typical inverse

power law decays; straight lines with equal slopes, independent of the actual conductivity values. Figure 2.7 shows the $h_{1\theta r}^v(t)$ component as a function of time, once again comparing free space with conducting space responses. The delayed and reduced peaks with straight-line behaviour in the late time are still present, but the most interesting feature is the sign change that occurs in this response when a conducting space is introduced. The last component of interest is the $h_{1\theta\theta}^u(t)$ in figure 2.8. This component doesn't exist for the free-space case and presents the magnetic field components associated with galvanic currents generated in the sphere. These responses are comparable in magnitude to the fields generated by the vortex currents. The sign changes observed in figure 2.7 can be explained by thinking of the sphere acting as a secondary source of smoke-rings. Smoke-rings (or more probably shells) move out from this source in all directions and the moment they pass the receiver position a sign change is recorded in the measured radial component (figure 2.9).

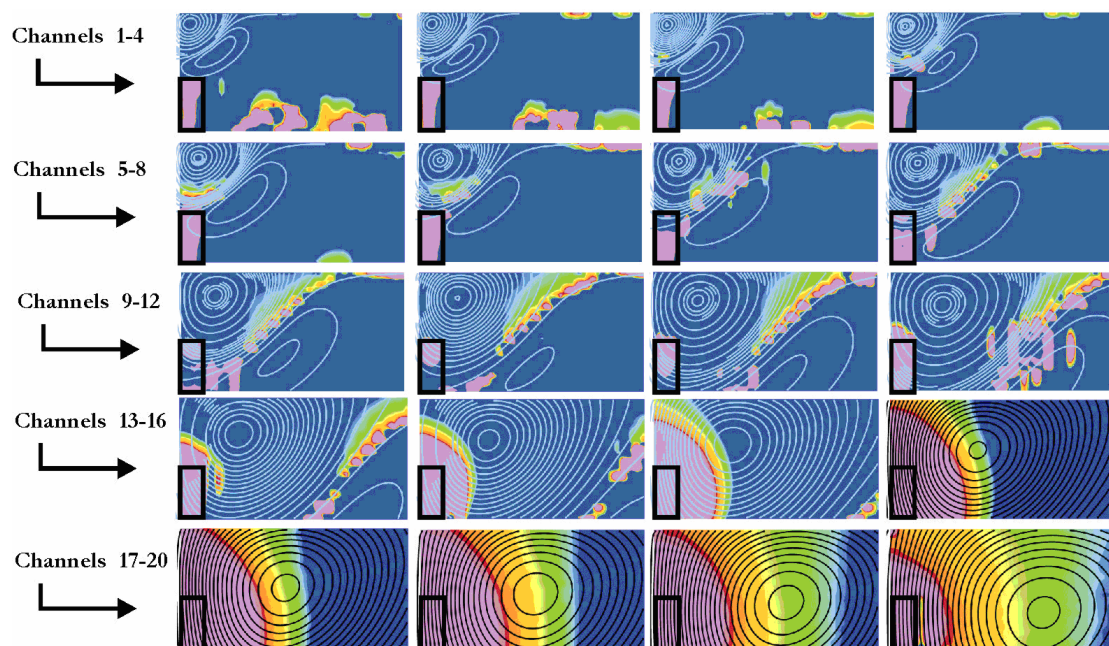


Figure 2-9 “Reflected” smoke-rings. Electric field intensity is presented as sections for 20 consecutive time channels. The cyan and black contour lines present the electric field intensity for a homogeneous 50 Ohm.m half space and indicate the well-known diffusive smoke-ring behaviour. The colour contours indicate electric field intensity of currents for a 5 Ohm.m prism (black rectangle) in a 50 Ohm.m half space as percentage of the half space response. The “reflected” currents are clearly visible in channels 13 to 20.

2.4 Conclusion

It is possible to describe electromagnetic field propagation analytically for only a few simplified earth models. Modelling realistic geological environments imply numerical solution of Maxwell's equations which are very time-consuming and not yet commonly used in industry. Several interpretation techniques and strategies have therefore been developed based on the simplified equations given above and these will be discussed in the following chapters.

Chapter 3

3 CONVENTIONAL INTERPRETATION TECHNIQUES

"The definition of insanity is doing the same thing over and over and expecting different results."

(Benjamin Franklin, 1706-1790)

3.1 Introduction

The ultimate goal of doing any geophysical survey is to deliver a map or model indicating the subsurface distribution of physical properties, i.e. conductivity in the case of TEM and to interpret this data in terms of geology. When geological information are added to the geophysical model it is possible to link lithology or structures to distinct geophysical units of different conductivities and this serves as a very useful tool in constructing a final geological model.

This study is concerned mainly with the conversion of TEM data to a reliable subsurface conductivity distribution. Traditionally there are two separate classes of exploration targets for TEM surveys and based on these classes different survey geometries and interpretational procedures are followed. In modern day geophysics these two classes of surveys increasingly overlap but it is still important to understand the different approaches that were followed in the past as most of the interpretation techniques being used today were developed for very specific target conditions.

The first type of target is considered to be a confined conductor(s) in a resistive host rock. The theoretical assumptions made in this case are basically that the host rock has no influence on the electromagnetic propagation of fields and conductors are considered to be suspended in free space for all mathematical purposes. TEM surveys to detect this type of target are designed to emphasize lateral variations in conductivity and are called profiling surveys. The geophysical model derived from interpreting a survey like this would contain the location, conductivity and geometrical parameters of one or more finite conductors (two- or three-dimensional). These conductors would be simplified geometrical shapes such as spheres, ellipsoids, plates or prisms approximating true geological units. Typical geological targets are massive sulphides or linear structures like weathered faults or shear zones.

The second type of target is considered to be a half space or layered earth. The theoretical assumptions made in this case are that there are no finite conductors present and that the subsurface layers are perfectly horizontal. Mathematically this means that all processing reduces to one dimension. TEM surveys designed for this type of target emphasize vertical variations in conductivity and are called sounding surveys. Fairly realistic models of the subsurface are obtained by stitching together a number of sounding models to produce a conductivity depth section and effectively resolving geological features in two dimensions and not only one. Practical applications would include determining depth to bedrock or mapping saltwater intrusions into aquifers.

In reality a combination of these two approaches are necessary to obtain a complete subsurface conductivity distribution and it is towards this goal that most TEM research is currently focused. The most important factor when dealing with the huge amounts of data gathered in this instance is to automate as much of the processing and interpretation as possible in order to keep survey time and costs competitive in the exploration industry. At the same time it is important to resolve less conspicuous anomalies and map them more accurately as the tradition of “bump-hunting” is not profitable in modern day exploration. In the rest of this chapter the different techniques used in TEM interpretation will be discussed with reference to the optimum targets for interpretation as well as the potential for automation of these techniques.

3.2 Profiles versus soundings

Profiling and sounding can refer to different survey geometries or just to the way data is viewed, processed and interpreted. The same data set (or parts of it) can therefore be treated as either sounding- or profile data or both. The most relevant view or interpretation strategy is dependent on the primary target or goal of the survey as described in 3.1. Interpreting data in profile format involves looking at measured values as a function of distance, removing a half space response if required, and interpreting anomaly shapes associated with two- or three-dimensional conductors either through forward modelling, inversion or curve matching. This is very similar to modelling potential field data, but with some important differences.

There are as many profiles to consider as there were time channels measured (varying anywhere from 7 to 100) and often it is not possible to obtain a good fit for a specific conductor on all of these channels simultaneously. This can be ascribed to the fact that

modelling software still approximates complex geological units in terms of simplified geometries as well as mathematical simplifications sometimes needed to solve a problem (see 2.3). Since TEM is an active source method (as opposed to magnetics and gravity) the transmitter current waveform, geometry and position all determine the actual shape and amplitude of anomalies. Different systems also measure different components of the magnetic field or its time derivative, again resulting in different anomaly shapes and amplitudes. Even if all the above factors are accounted for, the TEM method allows only for modelling of time varying current distributions unlike gravity, for example, where the measured field is a direct and unique consequence of the subsurface density distribution.

Interpretation of data in sounding format implies that a model is constructed with variation in depth only, and such a model always takes the form of a number of layer thicknesses and corresponding conductivities. Data are presented either as $\text{emf}(t)$, $\partial\mathbf{B}/\partial t$, $\mathbf{B}(t)$ or more commonly, apparent resistivity as a function of time. As with profiling data, a model is determined through forward modelling, inversion or curve matching. Due to the one-dimensional nature of this interpretation, inversion can be applied successfully provided that the number of layers is known, a good starting model is used and the geology conforms fairly closely to the one-dimensional assumption made in these algorithms.

3.3 Forward Modelling and Inversion

Forward modelling is a process whereby a geophysicist tries to match field data with calculated values from a specified model by changing the model parameters until there is a close correlation between the field and calculated data. Inversion is a mathematical approach also described as optimization, minimization or solution of a system of non-linear equations. Most of the various inversion approaches (an exception is Occam's inversion) reduce to the guessing of an initial model (initial parameters), forward calculating the response of this model, determining the difference (error) between the calculated and measured response and adjusting the initial parameters in a way that would minimize this difference. A number of forward modelling and inversion algorithms have been published ranging from a single current filament approximation (Barnett, 1984) through to the most general case of complete three-dimensional models (Newman et. al., 1986; Newman and Hohmann, 1988; Xiong, 1992; Wang and Hohmann, 1993).

3.4 Limitations on automation of inversion techniques

Forward modelling as defined in 3.3 cannot be automated as it includes the active involvement of a geophysicist at every guess of a new model. In fact, inversion is the process whereby “guessing of models” is taken over by an algorithm or computer. Although mathematically sound, in practice there are a number of problems which often inhibits the successful implementation and automation of inversion procedures.

- A priori knowledge of the geology under investigation is needed; i.e. should inversion be run for a layered earth (with how many layers) or should it be done for multiple plates (and how many plates)?
- Even if the general structure is known, the initial model should be close to the real model to obtain mathematical convergence.
- In the case of convergence, it can be difficult to decide whether convergence was to the desired global minimum or just a local minimum which adds yet another unknown to the interpretation process.
- Equivalence
- Validity of assumptions; e.g. late time behaviour of models are compared with time channels exhibiting early or intermediate time behaviour.
- There have to be more data than free parameters which would become a problem when trying to implement a totally general three-dimensional cube as model (this would of course be the ultimate solution).
- The most limiting factor however, is the need for a very fast forward modelling algorithm. TEM algorithms are still very time-consuming for all but the simplest cases of layered earths and multiple plates.

Practical experience in the interpretation of TEM data with inversion software has shown that extensive forward modelling was needed before inversions could be run successfully and that the 3-10% statistical reduction in error did not always mean that a more geologically plausible model was achieved. In fact, correlation with geological data such as borehole and structural information proved invaluable to distinguish between mathematical equivalent models and more often than not mathematical accuracy had to be sacrificed to obtain geological feasibility in a model. This is especially true in a geologically complex area. The best of both worlds would naturally be the application of constrained inversion,

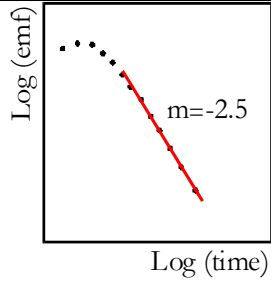
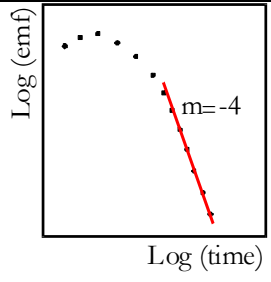
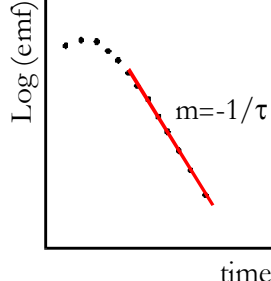
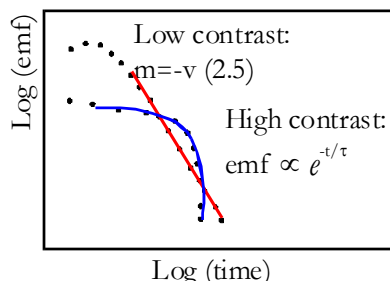
where mathematical solutions are found subject to geological truths such as dip, strike, conductivity ranges and limits on dimensions of bodies. However, this information is very rarely available in the exploration industry before TEM interpretations have to be done. Consequently, it is very difficult at this point in time to see inversion as a fully automated procedure for interpretation of TEM data, although it could possibly be involved as a final stage of processing after initial models have been found through alternative routes.

3.5 Decay curve analysis

Decay curve analysis is an extremely useful tool with its major strength probably being simplicity. The TEM method is based on current distribution changes with time, and decay curve analysis is the simplest way of analysing the time-varying fields associated with this phenomenon. In Chapter 2 the specific equations describing the decay behaviour for general models were given with specific reference to the late time. A summary of these late time approximations is given in Table 3.1. Decay curve analysis is a tool that helps the interpreter to distinguish between the two basic classes and subsequent interpretation strategies as mentioned in 3.1. Plotting all data, station by station, on both log-log and log-linear graphs and analysing the slopes of any data forming straight lines in the late time yields very good information on the geological structure in two dimensions. It allows the interpreter to immediately divide the survey area up into regions containing the four models shown in Table 3.1, with the only complication that a conductor in conductive host rock and with very low contrast may be grouped with half space occurrences at this point. However, what is more likely to happen from experience in Case History 1, Chapter 5, is to find stations showing both isolated conductor and half space behaviour but at different time channels. Similar behaviour was also described at the Elura massive sulphide deposit which is situated under a conductive overburden, Australia, by Spies (1980). Decay curve analysis as described here doesn't give any information on depth of conductors, although the decay constant (τ) found from inverse slope of model 3 (and sometimes model 4) graphs is related to the dimensions and conductivity of the causative conductor McNeill (1980), allowing a further division to be made between targets worth further investigating or not. In instances where the subsurface geo-electrical structure is too complex to be approximated by either of the models in Table 3.1, neither of the described characteristics will be found on the decay curve and stations like this will form a class of their own and require some special attention in later stages of interpretation. One of these more complex decay curves involves a sign change in the vertical component of the $\partial\mathbf{B}/\partial t$ measurements

inside the transmitter loop. It is impossible to see this behaviour in a conductive half space or layered earth environment and it therefore implies either an IP effect or extensive lateral variations (including two- or three-dimensional conductors) in the subsurface.

Table 3-1 Summary of late time approximations and behaviour for four general models.

Model	Late time behaviour	Decay plot properties
1. Conductive half space	$\frac{\partial H_z}{\partial t} \propto t^{-3/2}$ (Power law)	
2. Thin, conductive layer	$\frac{\partial H_z}{\partial t} \propto t^{-4}$ (Power law)	
3. Confined conductor in resistive host rock.	$\frac{\partial H_z}{\partial t} \propto e^{-t/\tau}$ (Exponential)	
4. Conductor in conductive host rock.	High contrast: $\frac{\partial H_z}{\partial t} \propto e^{-t/\tau}$ (Exponential) Low contrast: $\frac{\partial H_z}{\partial t} \propto t^{-v}$ (Power law)	

Decay curve analysis as described here, although not yielding the complete solution, can be applied without any user input and therefore has the potential to be fully automated. It is also very fast compared to inversion and can be applied to data in real time.

3.6 Transforms (Depth imaging)

Spies and Frischknecht (1991) describe depth imaging techniques as low cost (i.e. fast and automated) alternatives to modelling and inversion to provide an approximate image of the resistivity section directly from observed data. Originally developed as a “processing” step they now appear very useful for interpretation. Today there are a number of different imaging schemes or transforms (Macnae and Lamontagne, 1987; Nekut, 1987; James, 1988; Eaton and Hohmann, 1989; Smith et. al., 1994; Wolfgram et al., 1998; Tartaras et al., 2000), all based on simplifying some of the governing equations to such an extent that a direct solution for the depth and conductivity parameters can be found either analytically or through curve matching. Although not as accurate as full modelling or inversion the advantages of these schemes are computational speed and no need for initial models or other interactive user input. These methods can therefore be considered as completely automated.

3.6.1 Conductivity Depth Images (CDI's)

This technique has been developed by Macnae and Lamontagne (1987) for step-response sounding data and is routinely used in processing airborne TEM data. At each delay time the variation of the step-response as a function of geometry is transformed to an equivalent reference depth h , which can be related to the depth of electromagnetic field diffusion. The behaviour of h as a function of delay time is nearly independent of the source-receiver geometry. The slowness $\partial t / \partial h$ divided by the magnetic permeability is almost exactly proportional to the cumulative conductance measured from the surface down to a depth h . Thus an apparent conductivity (termed the “imaged conductivity”) can be estimated at depth by $\partial^2 t / \mu_0 \partial h^2$. The result is a conductivity-depth section that can be generated automatically with no prior input needed from the operator. This method is based on the receding image theory of a plane (or S-layer).

3.6.2 Stationary current images (SCI) (SCI - trademark of Geotrex-Digheem Pty Limited)

This method highlights the edges of conductors, gives an indication of dip and allows a qualitative estimate of the conductance of localized conductors (Wolfgram et al., 1998). The SCI emphasizes structural features because it is optimised for lateral contrasts in electrical conductivity. It is an empirically developed method only applied to GEOTEM®

system data and only results applied to synthetic data are available in literature (GEOTEM is a registered trademark of Geotrex).

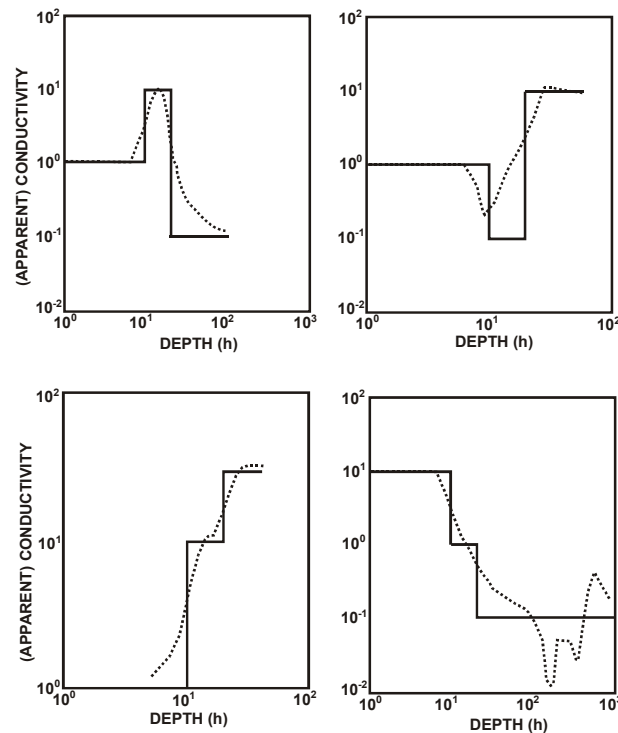


Figure 3-1 Comparison of apparent conductivity (calculated by differentiating the fitted slowness with respect to reference depth curve) with the actual conductivity for four three-layer models (after Macnae and Lamontagne, 1987).

3.6.3 *S-layer differential transform*

The S-layer differential transform was originally developed by Sidorov and Tikshaev (1969) and extended to an inversion technique by Tartaras et al., (2000). It is based on the late-time $\partial B_z / \partial t$ approximation of the S-layer model. The derivative of this equation ($\partial^2 B_z / \partial t^2$) is calculated and from these two equations the variables S (cumulative conductance) and d (depth) can be solved for at every time channel. Taking the partial derivative of S to d ($\partial S / \partial d$) gives the conductivity of a thin layer at depth d. The actual calculations are remarkably simple and when working in a conductive, layered region this method gives good results. The main criticism against the method (Tartaras et al., 2000) is the fact that it contains two numerical differentiations which are numerically unstable operators and therefore is extremely sensitive to noise. It is further based on the one-dimensional and late-time assumptions. Although, for the central-loop sounding geometry it can be shown (Tartaras et. al., 2000) that measured data almost always satisfy the late-time prerequisite.

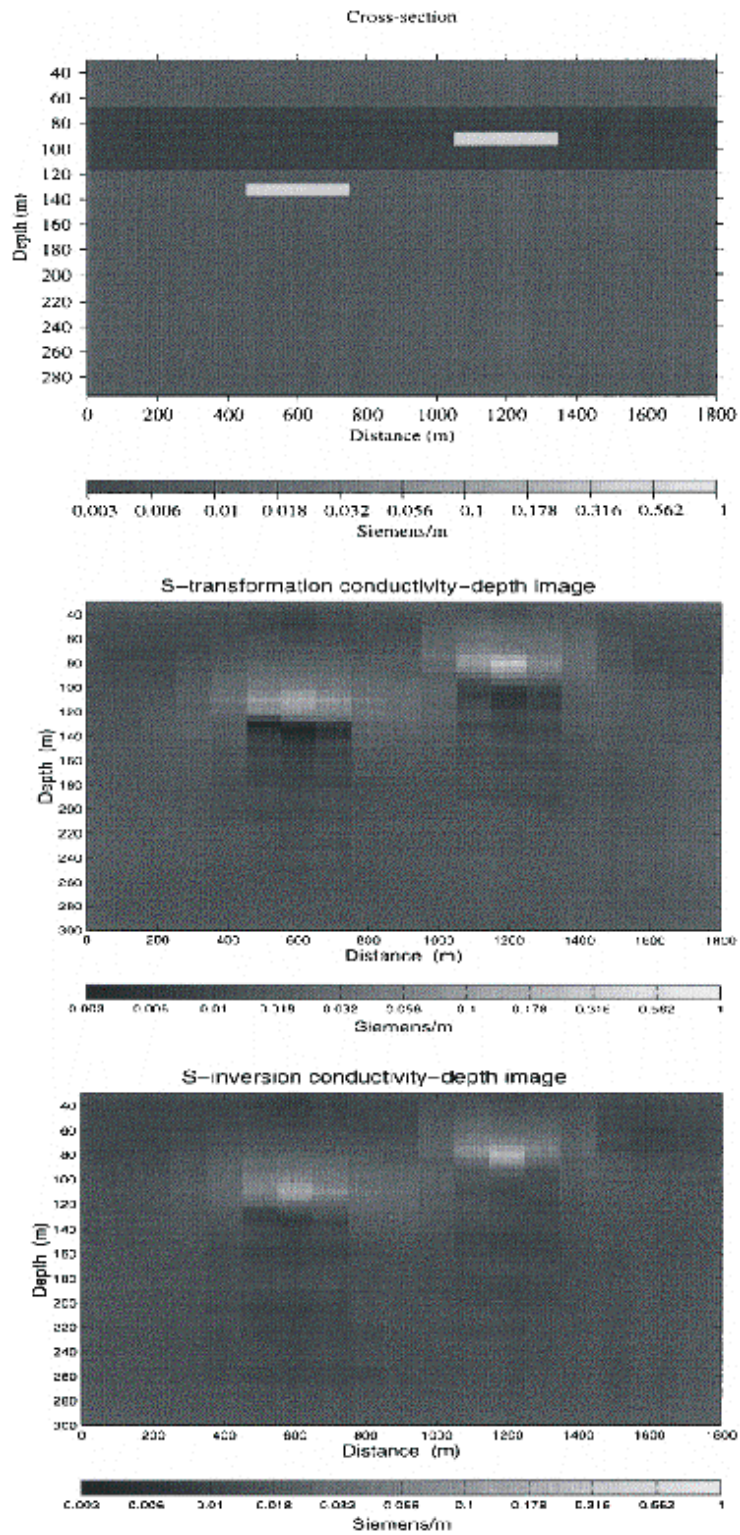


Figure 3-2 Cross-section of the model (top); Conductivity-depth image obtained by differential S-transformation (centre); Conductivity-depth image obtained by regularized S-inversion (bottom). (After Tartaras et. al., 2000)

3.7 Combining Strategies

Interpreting geophysical data almost never comprises the straightforward application of a fixed procedure. As with putting together the different pieces of a puzzle, the more information you have and the more angles you can view it from, the better your chances are of success. TEM data and processing are no different. Especially in TEM data there are still so many approximations made in even the best processing and interpretation algorithms that not one of them can be considered completely accurate. Automatically implementing and combining decay curve analysis with an improved imaging algorithm to isolate conductors will be discussed in the next chapter.

Chapter 4

4 AUTOMATED INTEGRATED ANALYSIS OF TDEM DATA

"Nature is not a competition. It doesn't really matter, when you go out, if you don't identify anything. What matters is the feeling in the heart." (Richard Adams, B. 1920, British Writer)

"Exploring the unknown defines the essence of humanity." (The author)

4.1 An integrated analysis algorithm

A software supported approach was developed for the:

- More effective visualization of the field data for rapid anomaly detection
- Automatic calculation and visualization of decay curve characteristics
- The use of the S-layer transform for the creation of conductivity-thickness cross section for the outline of finite conductors.

An automation of some strategies as outlined in chapter 3 was implemented in a C++ algorithm. Data analysis is performed on a time basis (i.e. decay curves) and not on a spatial basis (i.e. profile plots). Furthermore, the S-layer transform part of the algorithm assumes centre of the loop (sounding) data only. The algorithm does an automatic analysis, discussed below, of each measured decay curve. The only user input required is to specify system parameters and regression analysis limits, although default values for these are given.

4.2 Visualization of the field data for rapid anomaly detection

Even though the ultimate goal of TEM interpretation is to end up with a conductivity-depth section or conductor location and properties, it is always good to have the original data readily available as well. This often helps to clarify ambiguities in interpretations or models, e.g. the presence of a small, three-dimensional feature visible on raw data profiles would imply possible failure of layered interpretations in that region. Noise is also identified with more confidence on original data than after processing or transforms. TEM data can, however, be quite challenging to present in a complete manner without losing detail. Two factors contributing to this are the logarithmic span of data (with the small,

late time values often being more significant) and the fact that the half space (or background) response often dominates that of the target.

A very simple approach was followed to minimize the effects of these two factors. Data at every station are presented as a fraction of an average response calculated over the complete data set. The reasoning behind this is that background (half space or layered earth) should contribute the most to measured values over a large data set (as conductor responses are considered “anomalous” to this background). Adding all these responses together and calculating an average value at each time channel leads to the average response expected in a specific survey area. The fraction responses ($\partial B_z / \partial t$ divided by average) at every station then show deviations of a station from the average or background response. The advantage of this type of data presentation above standard profiles is that it can be displayed as colour contoured pseudo-sections giving the same priority to all time channels and very successfully enhancing anomalous regions. An example of this procedure on synthetic data is shown in figure 4.1. The success of this procedure is of course dependent on a relatively similar background response over a given survey area, although fairly good results have been obtained in the case history discussed in chapter 5, which was conducted over a complex geological area. The same presentation of data (although independently developed) was also found in a paper by Eaton and Hohmann (1987). In their case, however, the conductor to half space response was considered as a signal to noise ratio and was examined for different survey geometries.

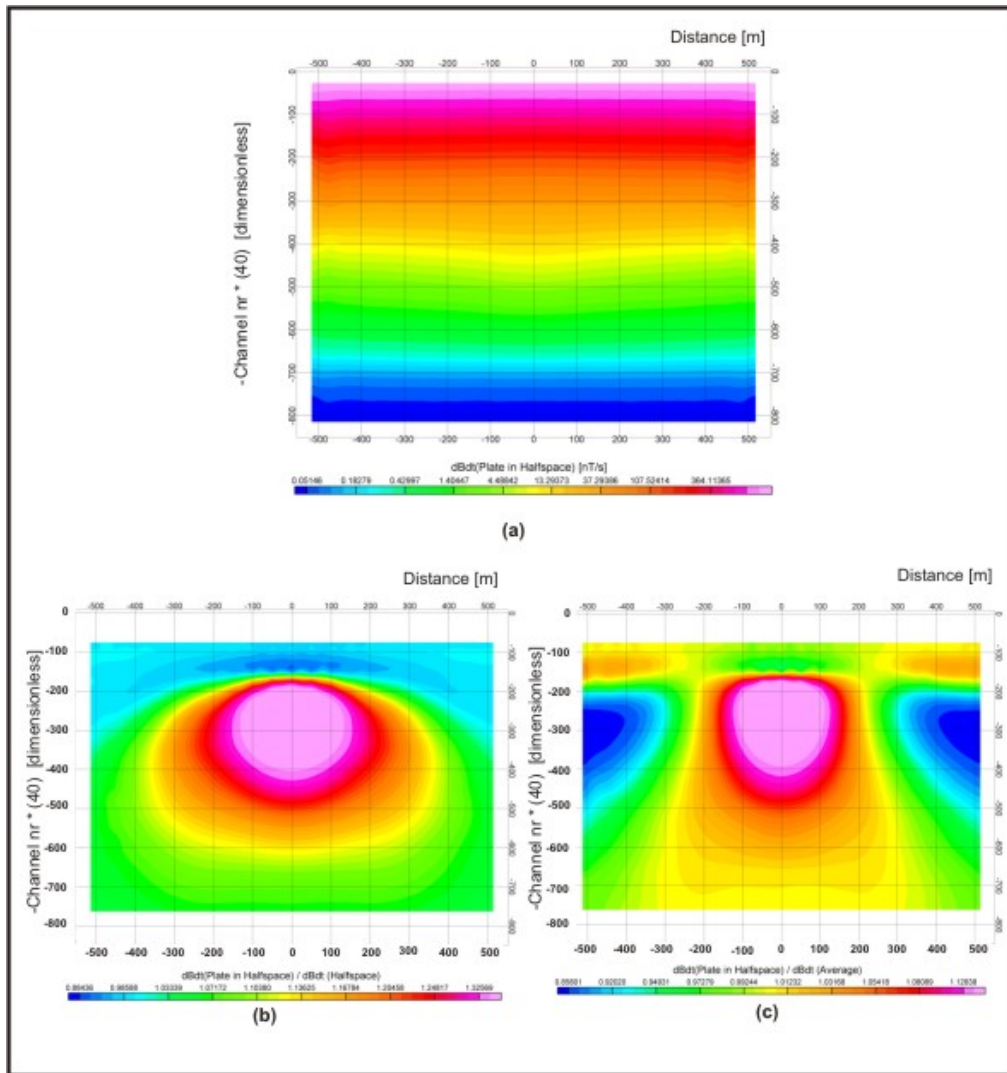


Figure 4-1 In (a) the raw data are presented in a contoured log-scale. In (b) the data were normalised using the half space value used in the forward model. In (c) the data were normalised as discussed above.

4.3 Decay curve analysis

The decay curve analysis is implemented in three steps.

- Decay curves analyzed for layered earth (i.e. power law) behaviour.
- Decay curves analyzed for exponential decay indicating confined conductors.
- Decay curves analyzed for sign changes not related to noise.

4.3.1 *Layered earth behaviour*

The objectives of this analysis are:

- to determine whether there is any straight line behaviour in the logarithmic domain of a sounding data set;
- to determine the largest number of channels (and channel numbers) on which the behaviour can be found;
- to test whether these slopes are close to either -2.5 or -4 and consequently
- to classify the sounding as half space or S-layer type.

Firstly, the time channels and corresponding absolute $\partial B_z / \partial t$ values are transformed to the logarithmic domain. The next step is to determine which channels (if any) approximate straight line behaviour the best. The “best fit” is based on the correlation coefficient (R^2); the closer it is to one, the closer the data display power law decay behaviour. All possible combinations of channels are tested starting with the user-specified minimum number of channels, the default being four. The least squares fit for channels one to four is therefore calculated, followed by two to five, three to six, etc. Then the number of channels is increased by one and the whole process repeated, i.e. channels one to five are analysed, followed by two to six, etc. This process continues until the number of data points evaluated is equal to the number of points in the data set and only one least squares fit is done, e.g. channels one to twenty. For every combination of channels the results are tested to determine the “best fit”. The “best fit” combination will have a R^2 value that falls within a specified range; it will have the slope closest to either -2.5 or -4; and if there are two combinations having the same properties thus far priority is given to the value corresponding to the largest number of channels and latest times (figure 4.2).

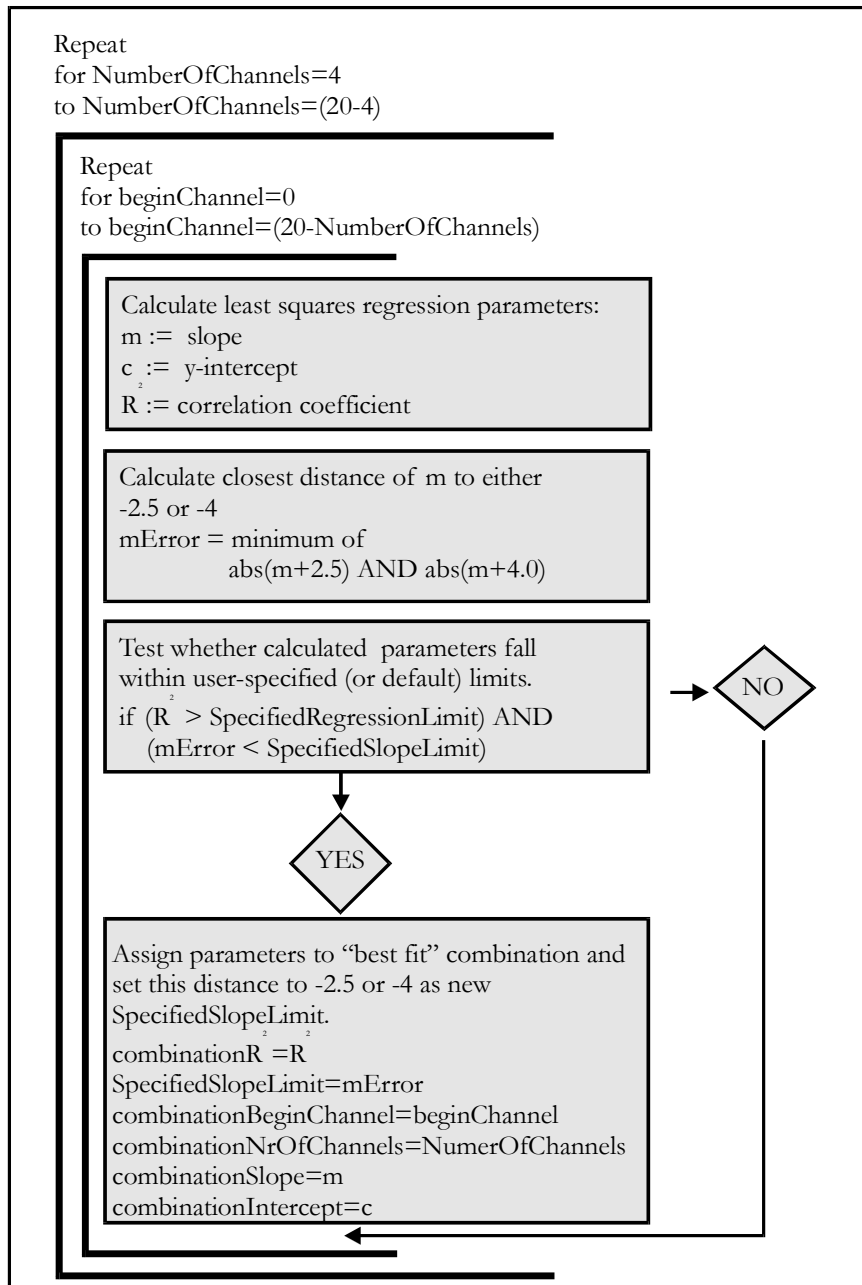


Figure 4-2 Flow diagram for decay curve slope analysis.

Based on the decay curve analysis function every sounding is classified as exhibiting half space behaviour, S-layer behaviour or neither of these.

4.3.2 *Confined conductor behaviour*

Analysing soundings for behaviour typical of confined conductors is done very similar to the layered earth case. Once again, all stations and all channel combinations are analysed with higher priority to more channels and later times. The main difference is that straight line behaviour is now looked for in the semi-logarithmic environment, i.e. only the $\partial B_z / \partial t$ values are transformed to the logarithmic domain. Furthermore, there are no predefined

slope values that need to be tested for and any regression fit within the specified R^2 limit is accepted as a possible conductor. The channels exhibiting the exponential decay are stored as well as the decay constant which is calculated as the inverse of the “best fit” slope.

4.3.3 IP effect or severe lateral variation in subsurface conductivity

The test for sign change of the $\partial B_z / \partial t$ component is done because with the central loop sounding configuration it implies a deviation from a layered, quasi-static subsurface. Sign changes can be ascribed to an IP (induced polarization) effect or significant lateral variations in the subsurface conductivity distribution, including two- or three-dimensional geological units. Having negative values of $\partial B_z / \partial t$ in a data set does not necessarily imply a sign change and it is important to distinguish between a well sampled, repeatable sign change and (normally late time) erratic noise. This was done by requiring at least two points of a specific sign to be followed by four points of opposite sign before a sign change is flagged in the data.

4.3.4 Results, output and presentation

The process of decay curve analysis as described here is extremely quick and takes less than a second for 1600 stations on a Pentium IV PC. The parameters determined through these functions are written to the output ASCII file and can be presented in GEOSOFT as symbols on plan or pseudo-section format. A very useful presentation for first anomaly isolation was also found through contouring the calculated decay constants (see Chapter 5). This immediately allowed areas of anomalous conductivities to be isolated in plan view. It is important to remember that all these procedures will indicate positions of anomalous data points and not yet positions of conductors themselves.

4.4 Numerical calculation of the S-layer differential transform

4.4.1 Defining the S-layer transform

The S-layer differential transform was discussed briefly in paragraph 3.4.3. It was chosen as the preferred imaging algorithm to include in the Sounding Interpretation program for the following reasons,

- Speed
- No need for an initial model
- Although it is based on the same imaging principles as the CDI transform it is easier to implement with fewer empirical factors that need to be included
- The late time approximation used in the algorithm is very applicable to the impulse response, central-loop configuration this work is based on
- For the specific case of a conductive host rock environment the S-layer differential transform shows good resolving capabilities
- As mentioned by Tartaras et. al. (2000) the main drawback of this method is the fact that it requires a numerical differentiation scheme which tends to introduce noise in the interpretation results. The implementation of a robust, yet accurate numerical differentiation scheme based on the specific properties of TEM data therefore receives high precedence. Further enhancements include a noise filter based on data points satisfying the theoretical conditions for the S-layer transform.

The S-layer differential transformation results in two equations that have to be solved for every time channel obtained at every station. Originally derived by Sidorov and Tikshaev (1969) these are summarised by Tartaras et. al. (2000) as:

$$S = \frac{16\pi^{1/3}}{(3M\Sigma n)^{1/3} \mu_0^{4/3}} \frac{\left(|V|^{5/3}\right)}{\left(|V'|^{4/3}\right)} \quad (4.1)$$

$$d = \frac{1}{\mu_0 S} \left(-\frac{4|V|}{|V'|} - t \right) \quad (4.2)$$

where

S = cumulative conductance [S]

d = depth [m]

M = magnetic dipole moment of transmitter [Am^2]

Σ = receiver area [m^2]

n = number of turns of receiver coil

t = time [s]

$|V|$ = electromotive force of ideal receiver loop [V] = $-\Sigma n \left(\frac{\partial B_z}{\partial t} \right)$

$|V|'$ = time derivative of measured voltage $|V|$ [V/s].

The time derivative of the measured voltage ($|V|'$) is the parameter that has to be determined through numerical differentiation. This value is used to calculate both cumulative conductance (S) and depth (d) of an equivalent S-layer for each time channel and noise generated by differentiation will consequently be introduced into both these numbers. However, in order to find the earth parameter of interest, conductivity (σ), another numerical differentiation has to be performed as,

$$\sigma(d) = \frac{\partial S}{\partial d} \text{ [Siemens.m}^{-1}\text{]} \quad (4.3)$$

which follows from the definition of cumulative conductance. Thus, not only is a new set of errors generated in this step, but all errors from the first differentiation are carried over and enlarged by this second differentiation.

The following features are investigated:

- three numerical differentiation techniques are analysed in terms of the specific nature of TDEM data, as described above
- the most appropriate use of smoothing filters
- the effects of the re-sampling of data points to equal time intervals.

4.4.2 Numerical differentiation of TEM data

In the late time, TDEM responses measured over a one-dimensional subsurface can be described as a power-law function, equation 4.4, with $k=2.5$ for a half space and $k=4$ for a thin conductive layer (S-layer). This creates the possibilities of using standard polynomial approximations, but in the logarithmic and semi logarithmic domains. Consider the following power-law decay:

$$V(t) = At^{-k} \quad (4.4)$$

$A = \text{constant}$
 $k = \text{decay constant}$

If the natural logarithm of this function is taken on both sides, it becomes,

$$\ln(V(t)) = \ln A - k \ln(t) \quad (4.5)$$

Substituting $\ln(V(t))$ with $y(x)$, $\ln(t)$ with x and $-k$ with m , we end up with the equation of a straight line (and a polynomial function) in the logarithmic domain.

If there is a two- or three-dimensional conductor present it will contribute to the late-time response in the form of an exponential function as shown in equation 4.6.

$$V(t) = Ae^{-kt} \quad (4.6)$$

$A = \text{constant}$
 $k = \text{decay constant}$

If the natural logarithm of this function is taken on both sides, it becomes,

$$\left. \begin{aligned} \ln(V(t)) &= \ln(Ae^{-kt}) \\ \ln(V(t)) &= \ln A - kt \end{aligned} \right\} \quad (4.7)$$

Equation 4.7 is again a linear function in the semi-logarithmic domain. This behaviour only becomes dominant on TDEM sounding data if the conductor is much more conductive than the surrounding host rock or when the host rock response has been removed from the data through subtraction or deconvolution. Raw field data (as on which the S-layer differential transform is normally applied) would mostly exhibit predominantly power-law decay, although it will be distorted slightly in the presence of conductive layers or finite conductors. In the logarithmic domain TDEM data appear as functions deviating from a general linear trend and can be locally approximated by second or third order polynomials. Finding a relationship between the derivative of a function and the derivative of the same function in the logarithmic or semi-logarithmic domains would enable us to

apply polynomial-based differentiation techniques to data in the domain where they can be approximated best by polynomial functions. These very specific properties of being logarithmically sampled and exhibiting power-law or exponential decays make TEM data distinctly unsuitable for the most common numerical differentiation schemes such as the Lagrange formulas (Burden and Faires, 1993) which are based on functions exhibiting polynomial behaviour.

4.4.2.1 Analytical relationship between derivative transforms in the various domains

The objective is to find an analytical relationship between the derivative of a function in the linear domain ($V'(t)$) and the derivatives calculated in the semi-logarithmic ($g'(t)$) and logarithmic domains ($h'(\ln(t))$) respectively. The strategy is simply to apply the chain rule of differentiation to functions presenting the data in the different domains.

Semi-logarithmic domain

In the semi-logarithmic domain the natural logarithms of the V values are taken and treated as a function of (linear) time. It is presented by the function $g(t)=\ln(V(t))$.

$$\begin{aligned} g(t) &= \ln V(t) \\ \therefore V'(t) &= V(t) \cdot g'(t) \end{aligned} \quad (4.8)$$

Logarithmic domain

In the logarithmic domain the natural logarithms of both the V values and times are taken and the function $h(\ln(t))=g(t)=\ln(V(t))$ is plotted against $\ln(t)$. A substitution of variables is made to simplify the derivation.

$$\begin{aligned} h[\ln(t)] &= \ln[V(t)] \\ h[\ln(t)] &= \ln[V(e^{\ln(t)})] \\ \text{Now, let } x &= \ln(t) \text{ and } t = e^x. \\ \text{Then} \\ h(x) &= \ln[V(e^x)] \\ h'(x) &= D_x \{ \ln[V(e^x)] \} \\ h'(x) &= \frac{1}{V(e^x)} \cdot V'(e^x) \cdot e^x \\ h'(x) \cdot V(e^x) \cdot \frac{1}{e^x} &= V'(e^x) \\ \therefore V'(t) &= h'(\ln(t)) \cdot V(t) \cdot \frac{1}{t} \end{aligned} \quad (4.9)$$

The formulas for transforming the derivatives are straightforward, trivial to apply, and analytically correct (i.e. no truncation error is induced in the transformation process). This enables us to choose the best domain for performing numerical differentiation based on the nature of data and available differentiation schemes.

Synthetic TEM data for a 10 ohm.m half space are used to illustrate this point. The Lagrange 3-point formula was applied to the example data set in the three different domains and transformed back to the linear domain using the appropriate formulas. The results were compared to the analytical derivative of the data and the percentage errors are shown in Figure 4-3. The advantage of differentiating in the logarithmic domain is very clear. Also indicated on this graph are derivative values obtained from a two-point power-law formula in the linear domain. These values are exactly equal to the Lagrange 3-point formula applied in the logarithmic domain. This formula was derived by fitting a power-law function to two points and taking the derivative of this interpolating function in exactly the same way as the Lagrange formulas are derived from polynomials.

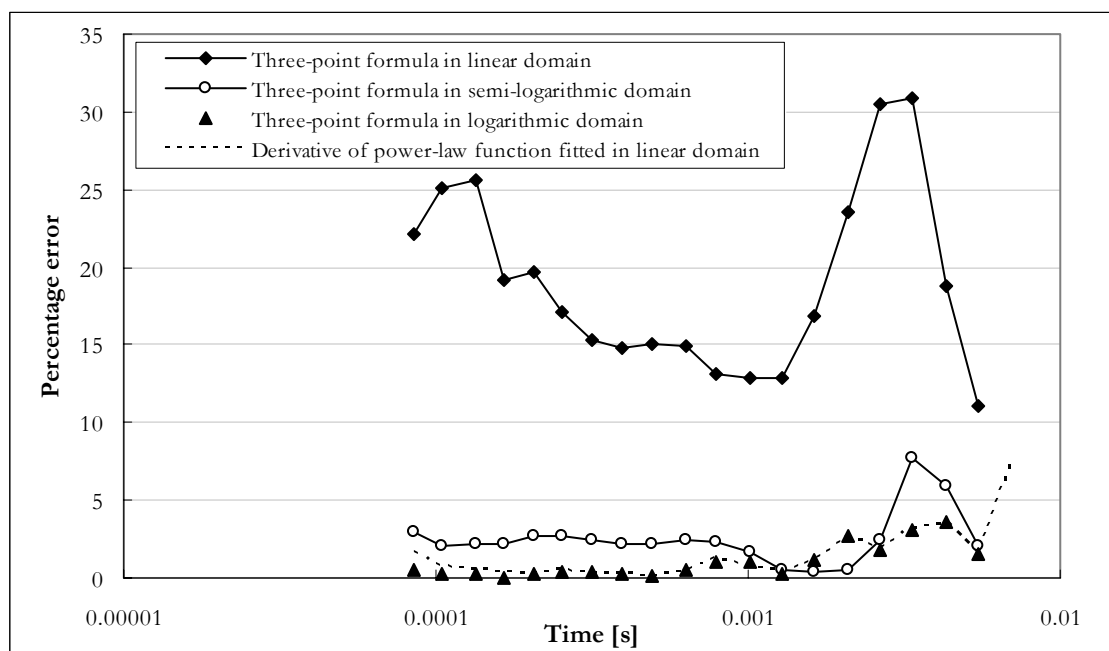


Figure 4-3 Percentage errors for differentiation in different domains of TDEM data for a 10 Ohm.m half space.

4.4.2.2 Description of three polynomial based numerical differentiation techniques

The specific numerical differentiation implemented by Tartaras et. al. (2000) is described only as “... a numerical differentiation scheme that computes a first order derivative for the provided TDEM data using polynomial interpolation.” This is unfortunately not clear

enough to reconstruct with confidence and an exact comparison of this method with the other methods is not included in this study. Tartaras et. al. (2000) also applied smoothing of data "... prior to and following differentiation". This is a common technique applied to reduce noise but ultimately alters data.

Numerical differentiation is an unstable method, because although the accuracy of the formulas increases with smaller values of "h" (distance between successive nodes), this also causes the round-off error to increase. Divisions by small numbers tend to exaggerate round-off errors and should be avoided if possible. A better way of increasing the accuracy is to use formulas derived from higher order polynomials with the same inter-node distance "h", e.g. the three-point and five-point Lagrange polynomial-based formulas (Burden and Faires, 1993).

Three different strategies for differentiation are compared in this study.

4.4.2.2.1 Lagrange three-point formula

The Lagrange three-point numerical differentiation formula is described in most text books on numerical analysis and a detailed derivation can be found in Burden and Faires (1993).

In short, derivative values of discretely sampled data points are approximated by the analytical derivative of a second order Lagrange polynomial fitted through three consecutive data points, i.e.

$$f'(x) \approx D_x \left[\frac{(x-x_i)(x-x_{i+1})}{(x_{i-1}-x_i)(x_{i-1}-x_{i+1})} f(x_{i-1}) + \frac{(x-x_{i-1})(x-x_{i+1})}{(x_i-x_{i-1})(x_i-x_{i+1})} f(x_i) + \frac{(x-x_{i-1})(x-x_i)}{(x_{i+1}-x_{i-1})(x_{i+1}-x_i)} f(x_{i+1}) \right]$$

$$= D_x [L_{i-1}(x)f(x_{i-1}) + L_i(x)f(x_i) + L_{i+1}(x)f(x_{i+1})], \text{ for } x \in \{x_{i-1}; x_i; x_{i+1}\}. \quad (4.10)$$

Effectively the method reduces to a sum of weighted function values and for the special case of calculating $f'(x_i)$ (the derivative at the centre point) for equally spaced data points it reduces to

$$f'(x_i) \approx \frac{1}{h} \left(-\frac{1}{2} \cdot f(x_{i-1}) + 0 \cdot f(x_i) + \frac{1}{2} \cdot f(x_{i+1}) \right) \quad (4.11)$$

where $h = (x_i - x_{i-1})$.

End points of equally spaced values have weights of $(-1.5; 2; -0.5)$ and $(0.5; -2; 1.5)$ for first and last points respectively while the weights for unequally spaced data points have to be calculated for every point using equation 4.10. Errors (and noise) in the calculated derivative are dependent on sampling interval, errors in data values (small errors in data are

enhanced in derivative calculations), computer round-off effects and how accurately the causative function can be approximated locally by a second order polynomial.

4.4.2.2.2 *Derivative of cubic spline interpolated function (referred to as “cubic spline derivative method”)*

The Lagrange three-point method will give analytically correct results for functions of order one or two. The most intuitive way to extend the approximation for a wider range of functions is to increase the degree of the Lagrange approximating polynomial. However, this does not always improve the final result as is illustrated by Burden and Faires (1993) in Figure 4-4.

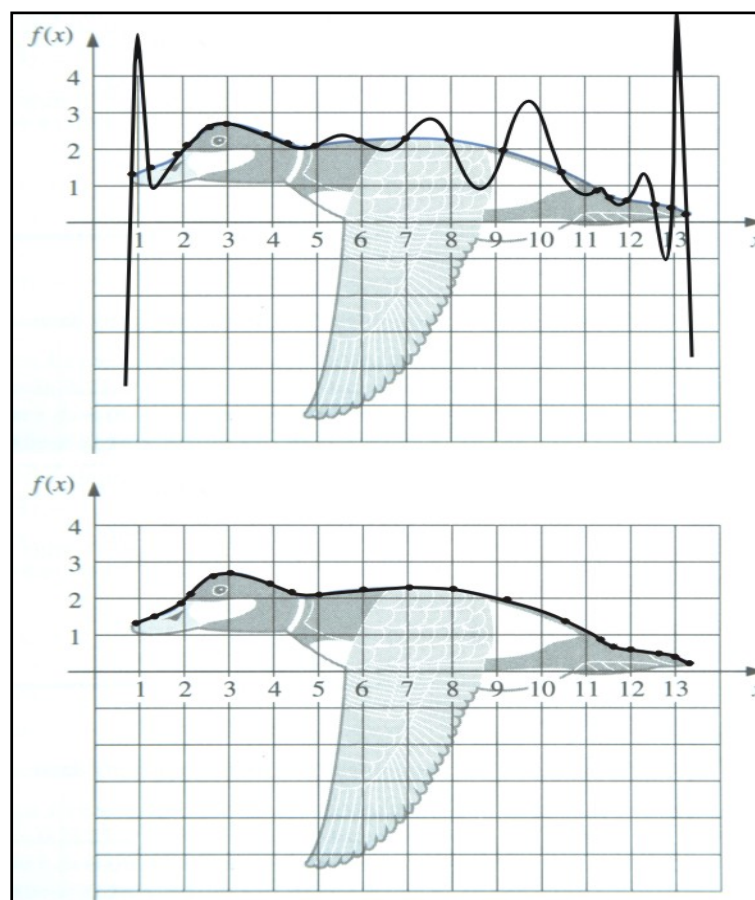


Figure 4-4 A Lagrange interpolating polynomial fitted to the data points outlining the back of a duck (top) and a cubic spline curve fitted to the same data points (bottom). (From Burden and Faires, 1993, Figures 3.11 and 3.12)

Lagrange interpolation requires that the approximated function values on the measured positions be exactly equal to the discrete data points. This introduces unwanted oscillations which are especially detrimental to any consecutive derivative calculations. An alternative is to fit higher order functions using the least squares errors approach.

However, low order polynomials will result in loss of high frequency information and high degree polynomials still suffer from unwanted oscillations.

TEM is based on diffusion of electrical currents into the earth and this is a smooth process, never oscillating in nature, and therefore not suited to this type of interpolation.

Furthermore, although TEM data locally approximate polynomial functions in the logarithmic domain they cannot in general be represented by the same order polynomial on all time channels. A better strategy to follow is piecewise polynomial approximation. One method to interpolate data under these conditions is known as the cubic spline method that involves fitting third order polynomials to each consecutive pair of data points, requiring the function values to be equal to the measured data values as well as continuity of the first and second order derivatives ensuring smoothness of the function. As with the Lagrange three-point formula, an approximation to the derivative of the sampled function is obtained by taking the analytical derivative of the third order cubic spline polynomials at every point. The cubic spline method is computationally more intensive than the Lagrange three-point formula but it can also be used to resample data to equally spaced intervals (which simplifies smoothing of data) if required. The free (or natural) boundary conditions were invoked in this study (assume that the second derivatives of the end points are zero) as the information required for clamped boundary points are not available.

4.4.2.2.3 *Differentiation as the inverse of integration*

In contrast to numerical differentiation, numerical integration (its inverse) is a stable method and not particularly sensitive to noise. The same relationship holds for the downward (unstable) and upward (stable) continuation filters used in processing of potential field data. Cooper (2004) introduced the “inverse of upward continuation” as a more stable downward continuation filter. The same principle can now be extended to the problem at hand and differentiation can be substituted by a stable “inverse of integration” filter. This can be formulated as follows. Define $f(x_i)$ as the n data points to be differentiated, $f'(x_i)$ as the required derivative values and \mathbf{A} an operator of integration.

Then

$$\mathbf{A} \cdot f'(x_i) = f(x_i), \quad i = 0 \dots n. \quad (4.12)$$

For the case where \mathbf{A} is singular, not square or a non-linear operator, equation 4.12 must be solved with a method such as generalised least squares inversion or other equivalent techniques (Cooper, 2004). Disadvantages of solving systems of equations in this way are:

- need for a good initial model
- no guarantee for convergence
- no guarantee for uniqueness of the solution
- mathematical intensity

However, if \mathbf{A} can be formulated as a non-singular, square and linear matrix, equation 4.12 becomes a system of linear equations with the same number of unknowns as equations (implying the existence of an inverse operator and a unique solution) which can be solved by multiplying both sides with \mathbf{A}^{-1} .

$$f'(x_i) = \mathbf{A}^{-1} \cdot f(x_i), \quad i = 0 \dots n. \quad (4.13)$$

In this case equation 4.12 can also be solved by applying Gaussian elimination with backward substitution. Depending on whether \mathbf{A} and \mathbf{A}^{-1} will be calculated only once (for a fixed number of equally spaced data points) or whether it will have to be recalculated (for unequally spaced data points). For 20 data points it will require 3060 multiplications/divisions and 2850 additions/subtractions to solve equation 4.12 using Gauss elimination with backward substitution. The equivalent numbers for calculating \mathbf{A}^{-1} are 10 660 and 10 070. Thereafter 400 multiplications/divisions and 380 additions/subtractions are required to solve for the $f'(x_i)$.

Construction of the integration matrix

Integration and differentiation can be done very simply in the frequency domain by respective division or multiplication with the factor $(i\omega)$ where ω is angular frequency and $i = \sqrt{-1}$. However, the process of Fourier transformation on discrete data points adds noise to data and time (or spatial) domain calculations, although more complex and time-consuming, are preferred in order to obtain cleaner data.

The first point that has to be addressed in any integration procedure is that of the integration constant, formulated as

$$\int f'(x) dx = f(x) + c, \quad (4.14)$$

where c can take on any value (implying an infinite number of solutions). An easy solution is to use definite integrals instead, so that

$$\int_a^b f'(x)dx = f(b) - f(a). \tag{4.15}$$

From equation 4.12, the system of equations that has to be solved now reduces to a general form as shown in equation 4.16.

$$\begin{bmatrix} a_{11} & a_{12} & \dots & a_{1n} \\ a_{21} & \dots & \dots & \dots \\ \dots & \dots & \dots & \dots \\ a_{n1} & \dots & \dots & a_{nn} \end{bmatrix} \begin{bmatrix} f'(x_1) \\ \dots \\ \dots \\ f'(x_n) \end{bmatrix} = \begin{bmatrix} f(x_b) - f(x_a) \\ \dots \\ \dots \\ f(x_n) - f(x_{n-1}) \end{bmatrix}. \tag{4.16}$$

The elements of \mathbf{A} (a_{ii}) must now be defined so as to produce numerical integration of the $f'(x_i)$. Simpson’s rule is a standard and very effective method suitable for polynomial functions. For equally spaced points it is given by

$$\int_{x_{i-1}}^{x_{i+1}} f'(x)dx = f(x_{i+1}) - f(x_{i-1}) \approx \frac{h}{3} [f'(x_{i-1}) + 4 \cdot f'(x_i) + f'(x_{i+1})] \tag{4.17}$$

where

$$h = (x_{i+1} - x_i) = (x_i - x_{i-1})$$

This formula will generate $n-2$ equations. In order to have a square matrix and unique solutions we need two more independent equations. This is done by deriving two end-point Simpson’s rule formulas. The midpoint Simpson’s rule is derived by fitting a second order polynomial through three consecutive points and integrating this polynomial from the first to the third point. The same strategy is followed for the end points except that we integrate from the first to the second point at the start of the sequence and from the second to the third point at the end. This results in the following two equations.

$$\int_{x_1}^{x_2} f'(x)dx = f(x_2) - f(x_1) \approx \frac{h}{3} \left[\frac{5}{4} f'(x_1) + 2 \cdot f'(x_2) - \frac{1}{4} f'(x_2) \right], \tag{4.18}$$

and

$$\int_{x_{n-1}}^{x_n} f'(x)dx = f(x_n) - f(x_{n-1}) \approx \frac{h}{3} \left[-\frac{1}{4} f'(x_{n-2}) + 2 \cdot f'(x_{n-1}) + \frac{5}{4} f'(x_n) \right], \tag{4.19}$$

where

$$h = (x_{i+1} - x_i).$$

For equally spaced points, equation 4.16 can thus be rewritten as

$$\frac{h}{3} \begin{bmatrix} 5/4 & 2 & -1/4 & 0 & . & . & 0 \\ 1 & 4 & 1 & 0 & . & . & 0 \\ 0 & 1 & 4 & 1 & 0 & . & 0 \\ 0 & 0 & 1 & 4 & 1 & . & 0 \\ 0 & . & . & . & . & . & 0 \\ 0 & . & . & 0 & 1 & 4 & 1 \\ 0 & . & . & 0 & -1/4 & 2 & 5/4 \end{bmatrix} \begin{bmatrix} f'(x_1) \\ f'(x_2) \\ . \\ . \\ . \\ f'(x_{n-1}) \\ f'(x_n) \end{bmatrix} = \begin{bmatrix} f(x_2) - f(x_1) \\ f(x_3) - f(x_1) \\ f(x_4) - f(x_2) \\ \dots \\ f(x_{n-1}) - f(x_{n-3}) \\ f(x_n) - f(x_{n-2}) \\ f(x_n) - f(x_{n-1}) \end{bmatrix} \quad (4.20)$$

or

$$\begin{bmatrix} 2\ 1/2 & 4 & -1/2 & 0 & . & . & 0 \\ 1 & 4 & 1 & 0 & . & . & 0 \\ 0 & 1 & 4 & 1 & 0 & . & 0 \\ 0 & 0 & 1 & 4 & 1 & . & 0 \\ 0 & . & . & . & . & . & 0 \\ 0 & . & . & 0 & 1 & 4 & 1 \\ 0 & . & . & 0 & -1/2 & 4 & 2\ 1/2 \end{bmatrix} \begin{bmatrix} f'(x_1) \\ f'(x_2) \\ . \\ . \\ . \\ f'(x_{n-1}) \\ f'(x_n) \end{bmatrix} = \frac{3}{h} \begin{bmatrix} 2[f(x_2) - f(x_1)] \\ f(x_3) - f(x_1) \\ f(x_4) - f(x_2) \\ \dots \\ f(x_{n-1}) - f(x_{n-3}) \\ f(x_n) - f(x_{n-2}) \\ 2[f(x_n) - f(x_{n-1})] \end{bmatrix} \quad (4.21)$$

The matrix \mathbf{A} is square and symmetrical with the highest values on the diagonal as pivot elements except for the first and last rows. The inverse of this matrix, \mathbf{A}^{-1} , depends on the number of data points, n , and can be calculated using any standard algorithm. In the general case where data points are unequally spaced the weights (a_{ii}) are different for every data set and both the matrix and its inverse have to be recalculated for every sounding. The derivation of Simpson's rule for unequally spaced points is given in APPENDIX A.

4.4.2.3 Smoothing and re-sampling of data points

Before testing of the three integration methods discussed above, one need to consider the process and effect of smoothing of the data at various stages of the differentiation process. Smoothing of data before and after numerical differentiation is an accepted method of reducing the noise in data (Tartaras et. al., 2000). However, any smoothing applied to the data, will change the data and will influence the final interpretation. In the S-layer differential transform algorithm there are four possible opportunities to smooth data and the question arises which of these will optimise the algorithm with minimum alteration of the data.

The last factor taken into consideration is the spacing of data points. The time channels at which data are measured are almost equally spaced in the logarithmic domain. The calculated depths (to which the second differentiation has to be performed) will have intervals dependent on the conductivity of the subsurface. The advantage of re-sampling

data to equal intervals is that the weights (and inverse matrices) used for differentiation and smoothing only has to be calculated once. Applying the transform to unequally spaced data points means less tampering with the original data but it is much more time intensive. The method use for smoothing is the three-point moving average filter for equally spaced points and a weighted extension for unequally spaced points (equation 4.22).

$$f(x_2)_{\text{Weighted Moving Average}} = \frac{2 \cdot (x_3 - x_2)}{(x_3 - x_1)} \cdot f(x_1) + f(x_2) + \frac{2 \cdot (x_2 - x_1)}{(x_3 - x_1)} \cdot f(x_3) \quad (4.22)$$

4.4.3 Comparison of differentiation methods applied to synthetic data

4.4.3.1 First order numerical differentiations compared to the analytical derivative of a function

A TDEM decay curve is simulated by an analytical function (equation 4.23), defined as the sum of exponential and power law terms. (There are no analytical formulations of complete layered earth TEM responses in closed form, therefore an “equivalent” analytical function is used.)

$$f(x) = 0.000001 \cdot t^{-5/2} + 0.00000000001 \cdot t^{-4} + 0.00000001 \cdot t^{-3} + 2000 \cdot e^{-2500t} + 12000 \cdot e^{-8000t} + 10 \cdot e^{-400t} \quad (4.23)$$

The first order analytical derivative of this function is compared to the following numerical scenarios:

- All three numerical differentiation algorithms are applied to unequally spaced data points and without smoothing of the data. The results are shown in figure 4.5(a).
- The same as (1) but with smoothing of the function before the derivatives were calculated. The results are shown in figure 4.5(b).
- The same as (1), but with the unequally spaced data points re-sampled to equally spaced data points using the cubic spline interpolation method. Figure 4.5(c) shows the results without smoothing of the data, as in Figure 4.5(a).
- The results in Figure 4.5(d) is the equally spaced data points equivalent of 4.5(b).
- A summary of the average errors (absolute values) for every alternative is given in Figure 4.6.

From these comparisons the following are concluded:

The inversion method gives the smallest average error, followed by the cubic spline and three point methods.

For unsmoothed data the equally spaced points slightly outperform the unequally spaced points, but the reverse is true for smoothed data.

Smoothing of data seems to be the largest contributing factor to errors in noise-free data.

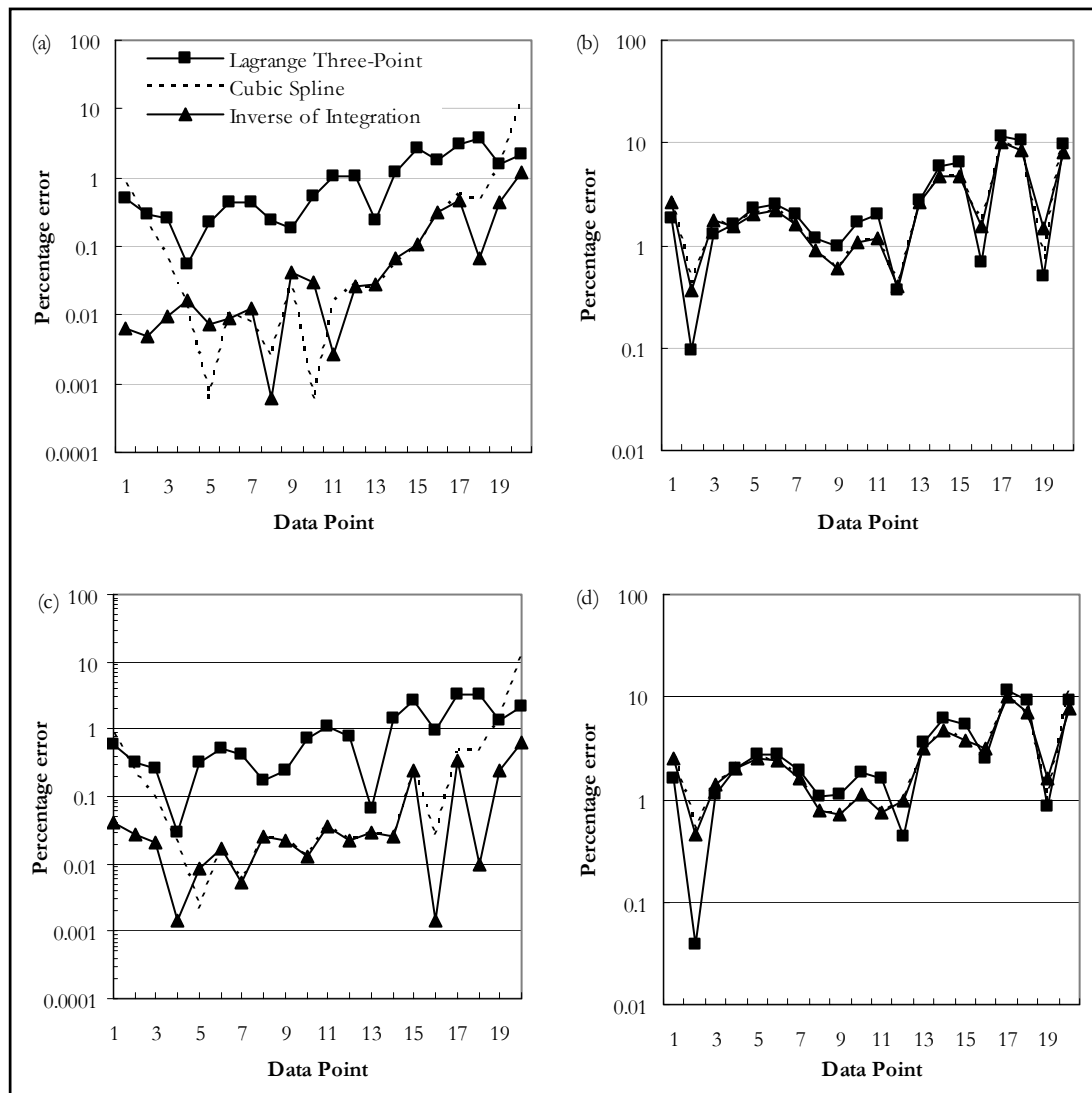


Figure 4-5: Comparison of differentiation methods applied to (a) unequally spaced points without smoothing of data, (b) unequally spaced points with smoothing of data, (c) equally spaced points without smoothing of data and (d) equally spaced points with smoothing.

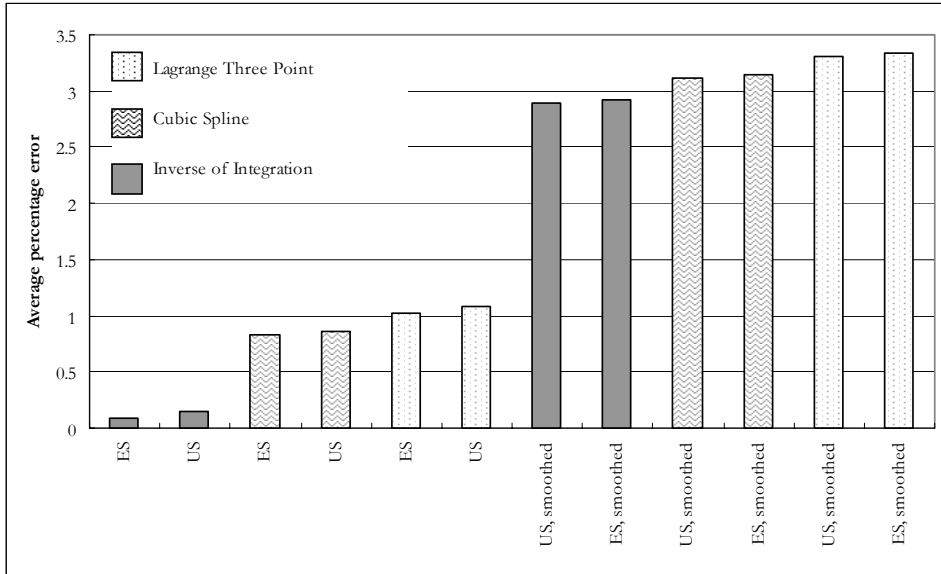


Figure 4-6: A summary (in ascending order) of the average error over twenty data points for each of the alternatives in Figure 4.5. (ES: equal spacing, US: unequal spacing)

4.4.3.2 *S-layer differential transform applied to forward modelled data*

A set of data was calculated for a three-layer earth using MARCO software developed by AMIRA. The model and data are shown in Figure 4-7.

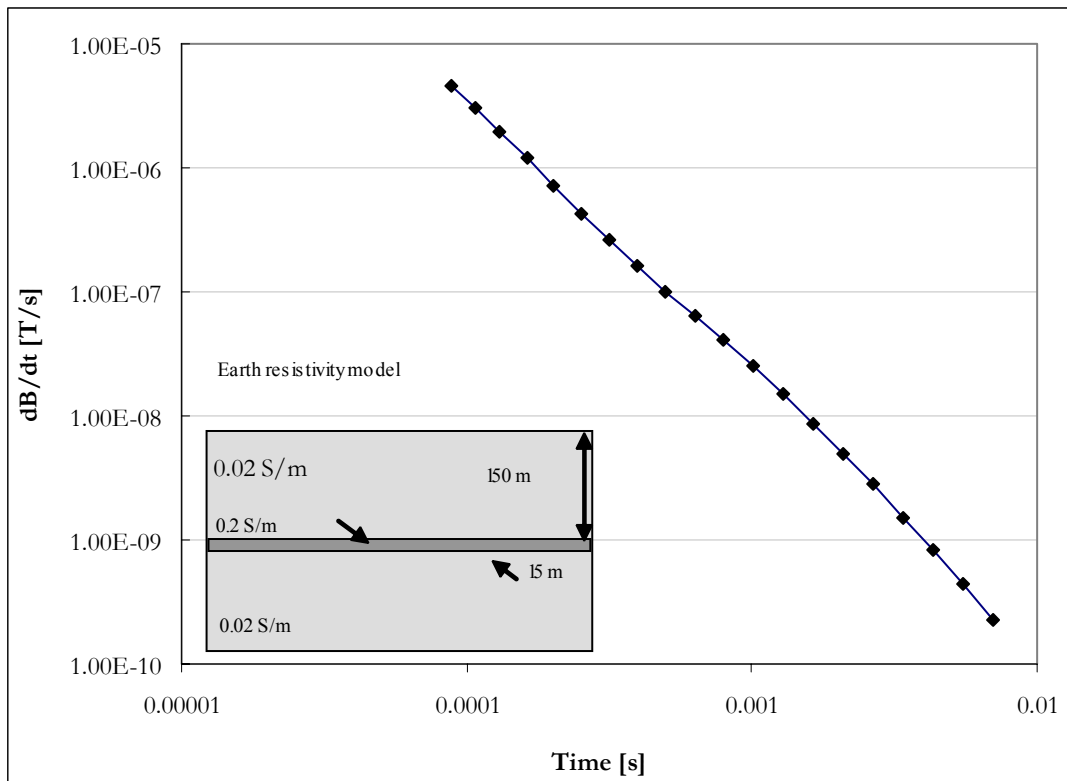


Figure 4-7: Synthetic data and model for three-layer earth.

The numerical calculation of the S-layer transform was done using the following steps:

1. Input $|V|$ values $\left(= \frac{\partial B_z}{\partial t} \text{ if normalised to receiver area of } 1\text{m}^2 \right)$
2. Calculate $|V|'$, i.e. $\frac{\partial^2 B_z}{\partial t^2}$
3. Calculate S from equation 4.1
4. Calculate d from equation 4.2
5. Calculate $\frac{\partial S}{\partial d} = \sigma$

Numerical differentiations are performed in steps 2 and 5. Smoothing filters are applied at various stages in the algorithm culminating up to the strategy proposed by Tartaras et. al. (2000) which is smoothing before and after each differentiation. Figure 4-8 top shows the results of three variations:

- smoothing of $|V|$ before step 1
- smoothing of $|V|$ before step 1 and S after step 3
- smoothing of $|V|$ before step 1, S after step 3 and σ after step 5.

As can be expected the successive smoothing slightly lowers the maximum amplitude and widens the response curve. However, it is critical *not* to smooth $|V|'$ (figure 4.8 bottom), which introduces extensive noise. This is due to the ratios of $|V|$ and $|V|'$ used to calculate S and d .

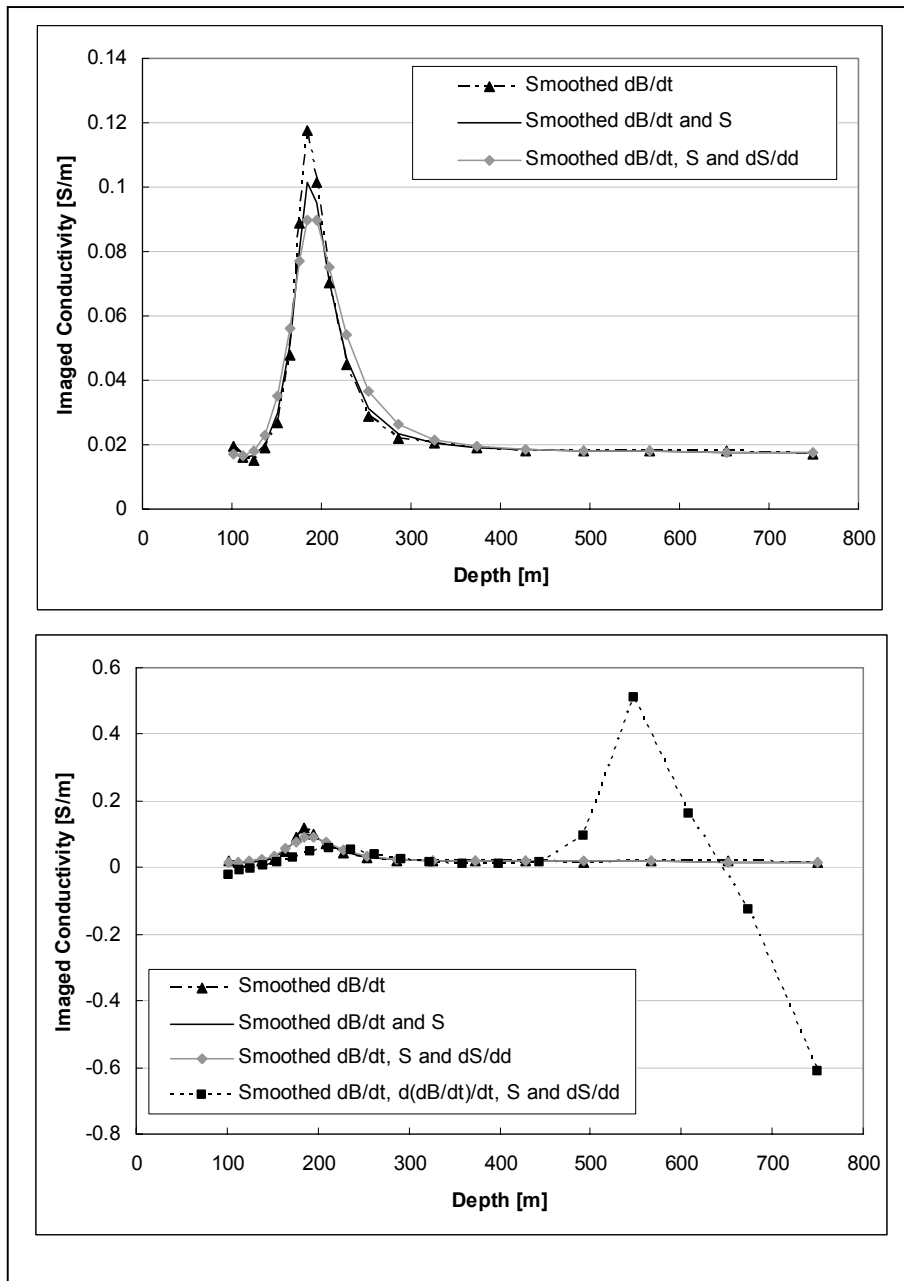


Figure 4-8: Effects of smoothing at different points in S-layer transform algorithm.

Figure 4-9 shows the output of the S-layer transform (imaged conductivity versus depth) for twelve different combinations of differentiation method, smoothing and spacing of data. (Smoothing of data here implies smoothing $|V|$, S and σ .) Both smoothing and resampling of data reduces the maxima of responses leading to an underestimation of the conductivity contrast.

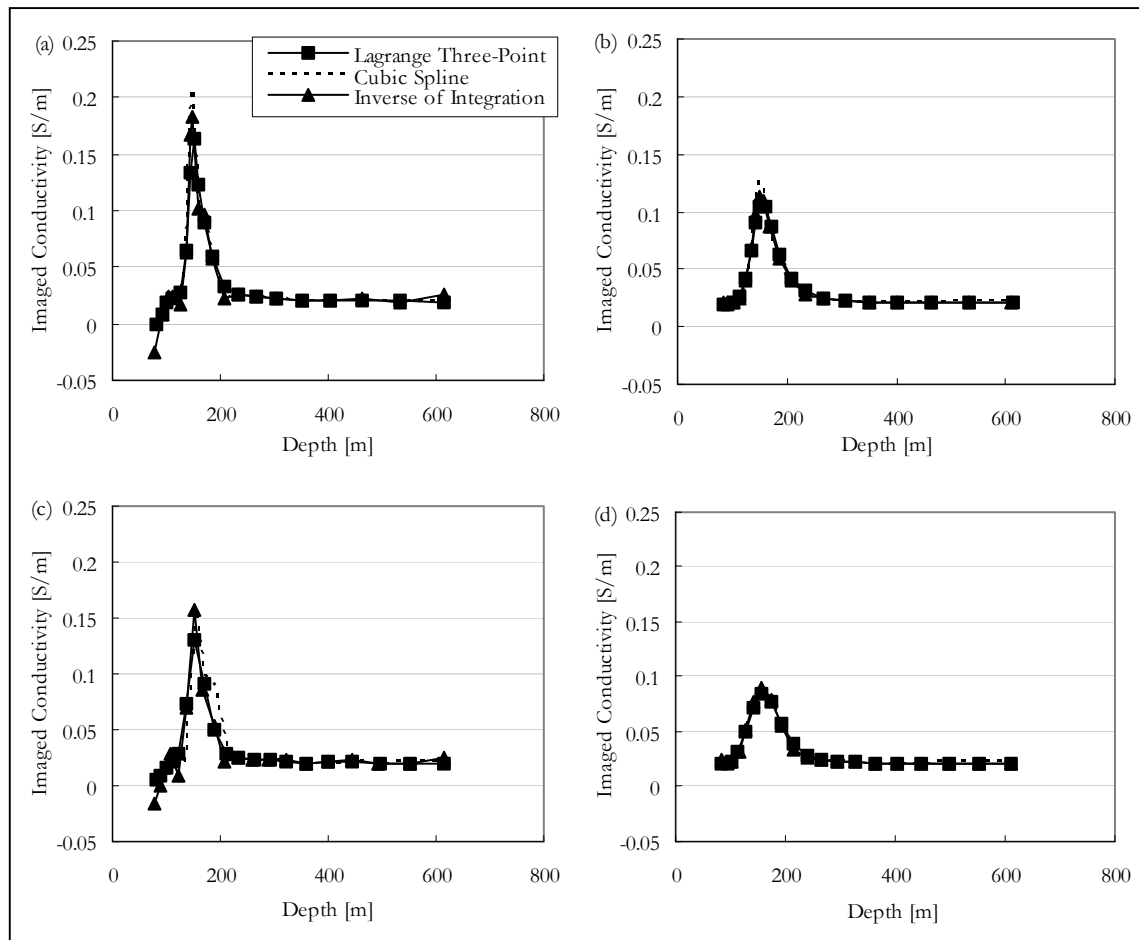


Figure 4-9: Comparison of S-layer differential transform results for the three numerical differentiation methods applied on (a) unequally spaced data points without smoothing of data, (b) unequally spaced data points with smoothing of data, (c) equally spaced data without smoothing and (d) equally spaced data with smoothing.

1.4.4 Comparison of differentiation methods on field data

Four soundings are chosen from a field data set to represent both clean and noisy data (Figure 4-10) and all twelve processing combinations are applied to these soundings. The data were acquired with a Geonics Protem system in the central loop sounding configuration utilising a 100mX100m transmitter loop, 15A current, 25Hz base frequency and effective receiver area of 100m². Figures 4-11 to 4-16 summarise the results with (a) unequally spaced data points without smoothing of data, (b) unequally spaced data points with smoothing of data, (c) equally spaced data points without smoothing of data and (d) equally spaced data points with smoothing every time.

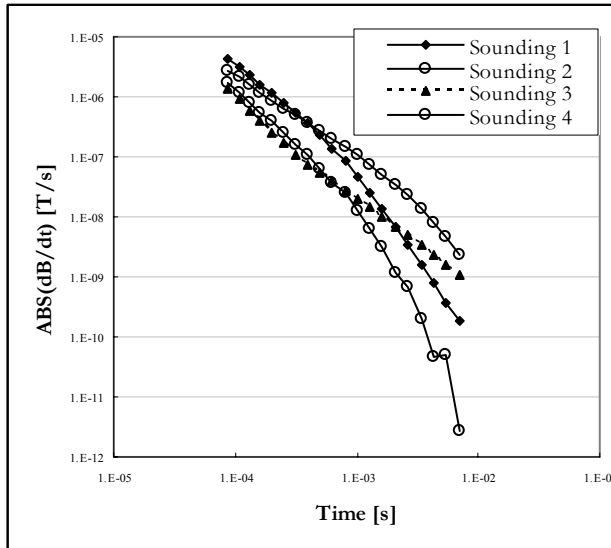


Figure 4-10: Four field data soundings; 1 to 4 are very smooth and considered to be clean data, while 5 & 6 contains noise.

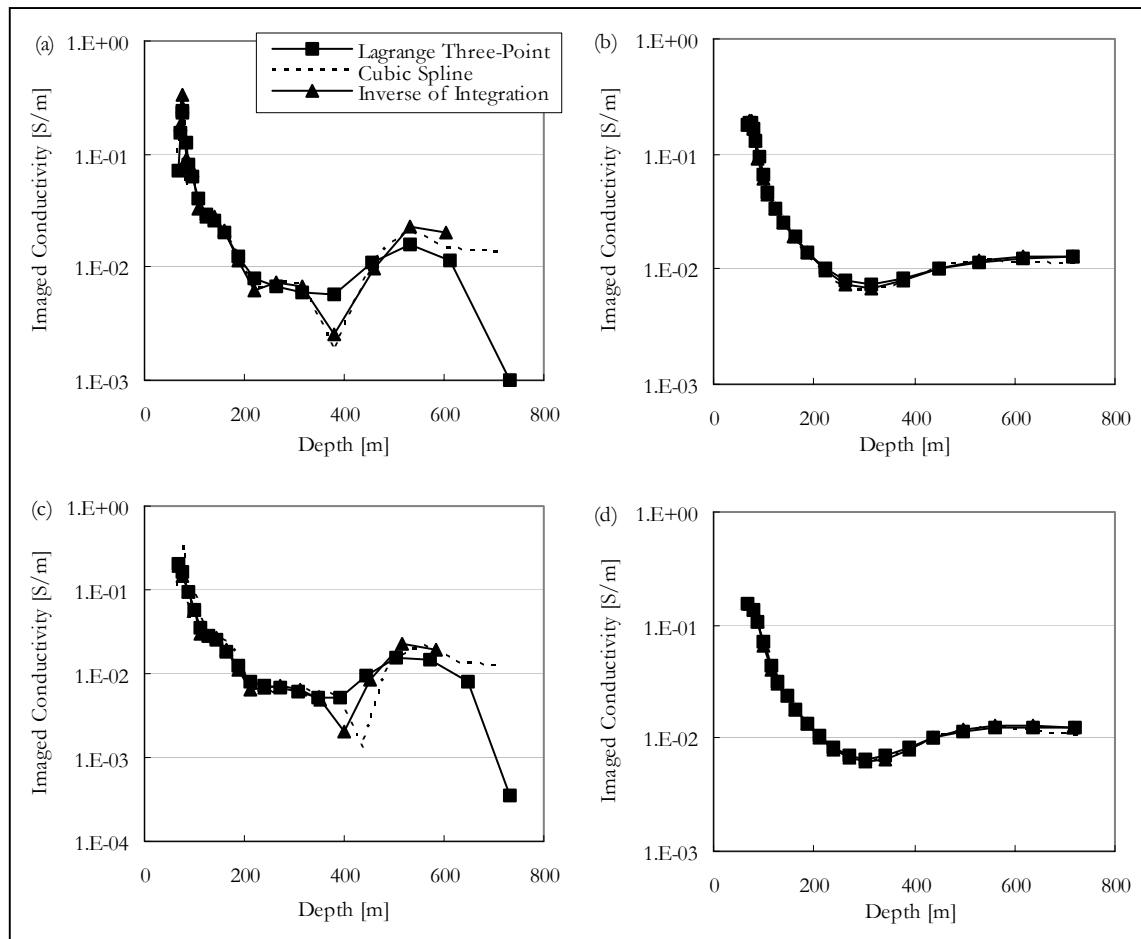


Figure 4-11: S-layer differential transform results for Sounding 1.

Sounding 1 (Figure 4-11) would be considered “noise-free” in that none of the data points would probably be masked (ignored) in manual interpretation of the data. However, comparing the smoothed and unsmoothed results it is clear that it does contain some noise which can be filtered out successfully with the weighted moving average filter. The unequally spaced points are less sensitive to the noise and after smoothing there is no noticeable difference between the three different methods of differentiation. (With field data it is not possible to calculate percentage errors and smoothness of conductivity-depth curves are used as an indication of accuracy based on the smoothly dissipative nature of TEM currents.)

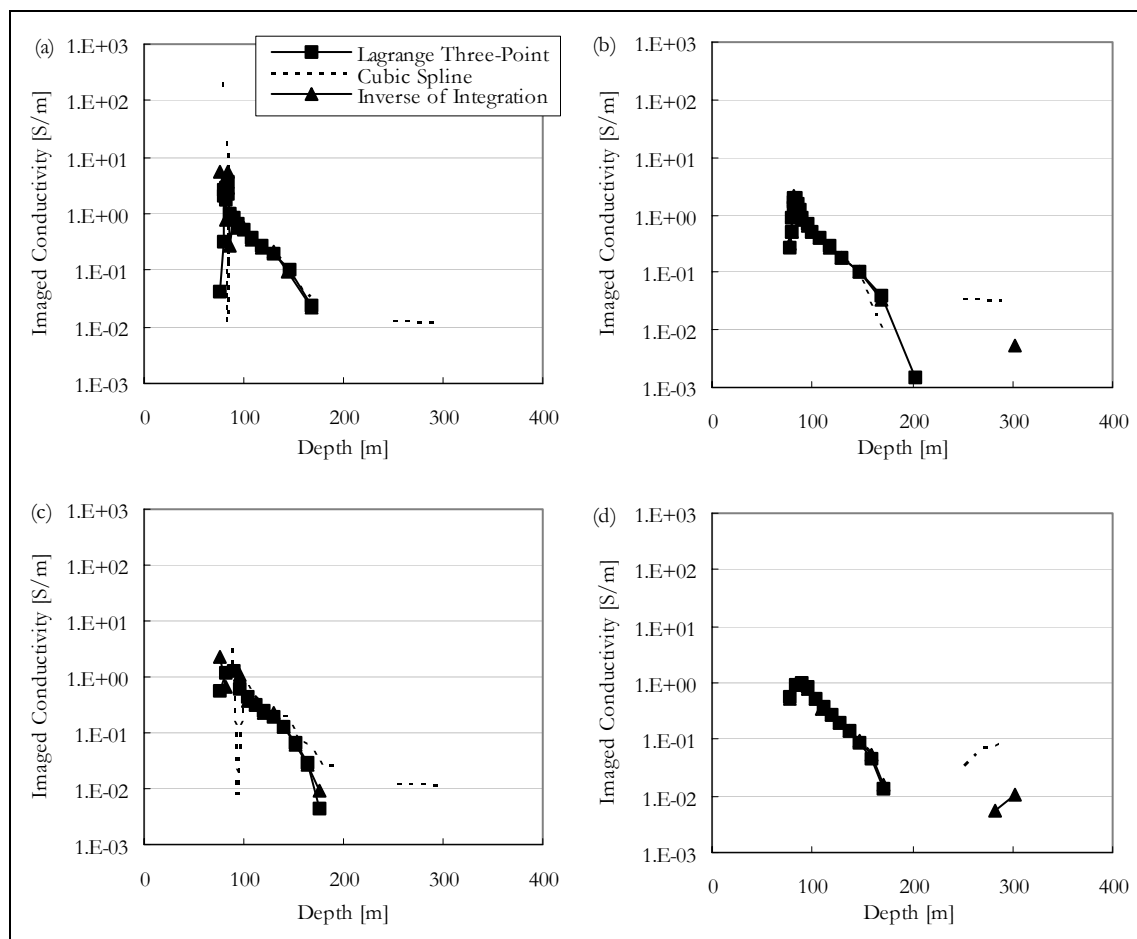


Figure 4-12: S-layer differential transform results for Sounding 2.

Sounding 2 contains slightly more noise (Figure 4-12). The most noticeable effect is that the re-sampling to equally spaced data points causes the method to fail. (This is mostly due to re-sampling of the cumulative conductance (S) curve which is differentiated in step 5 of the algorithm. This curve, although smooth, sometimes forms a relation rather than a

function, implying more than one S value for each depth and this is not accounted for in re-sampling with the cubic spline method.)

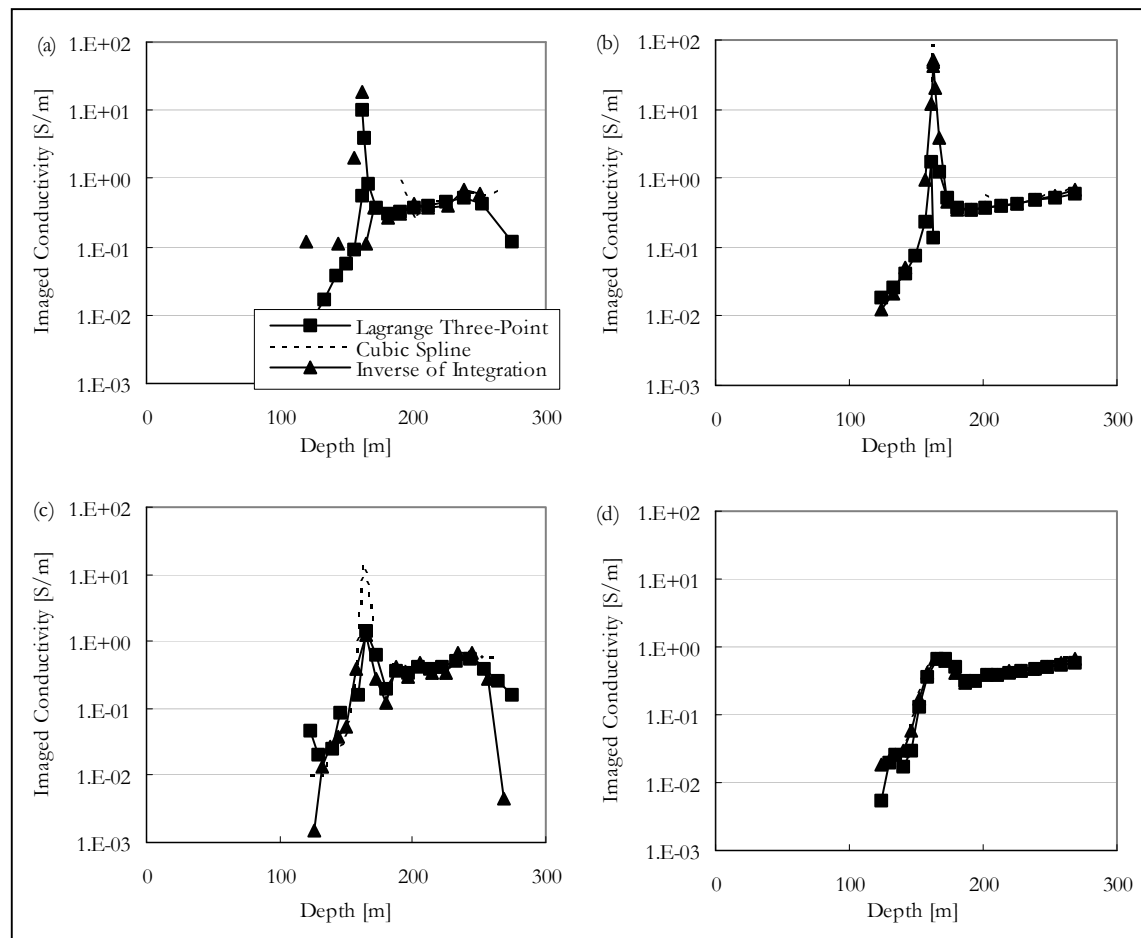


Figure 4-13: S-layer differential transform results for Sounding 3.

For Sounding 3 (Figure 4-13) the same pattern holds. Here the advantage of smoothing is very clear, especially on the “inverse of integration” method. In Sounding 4 (Figure 4-14) even the unequally spaced, smoothed data become noisy with gaps (indicating negative conductivities having no physical meaning). This is once again due to the cumulative conductance curve not increasing monotonically, although the measured data is smooth the algorithm might fail in this case as the assumption of cumulative conductance on which the S-layer transform is based, is violated.

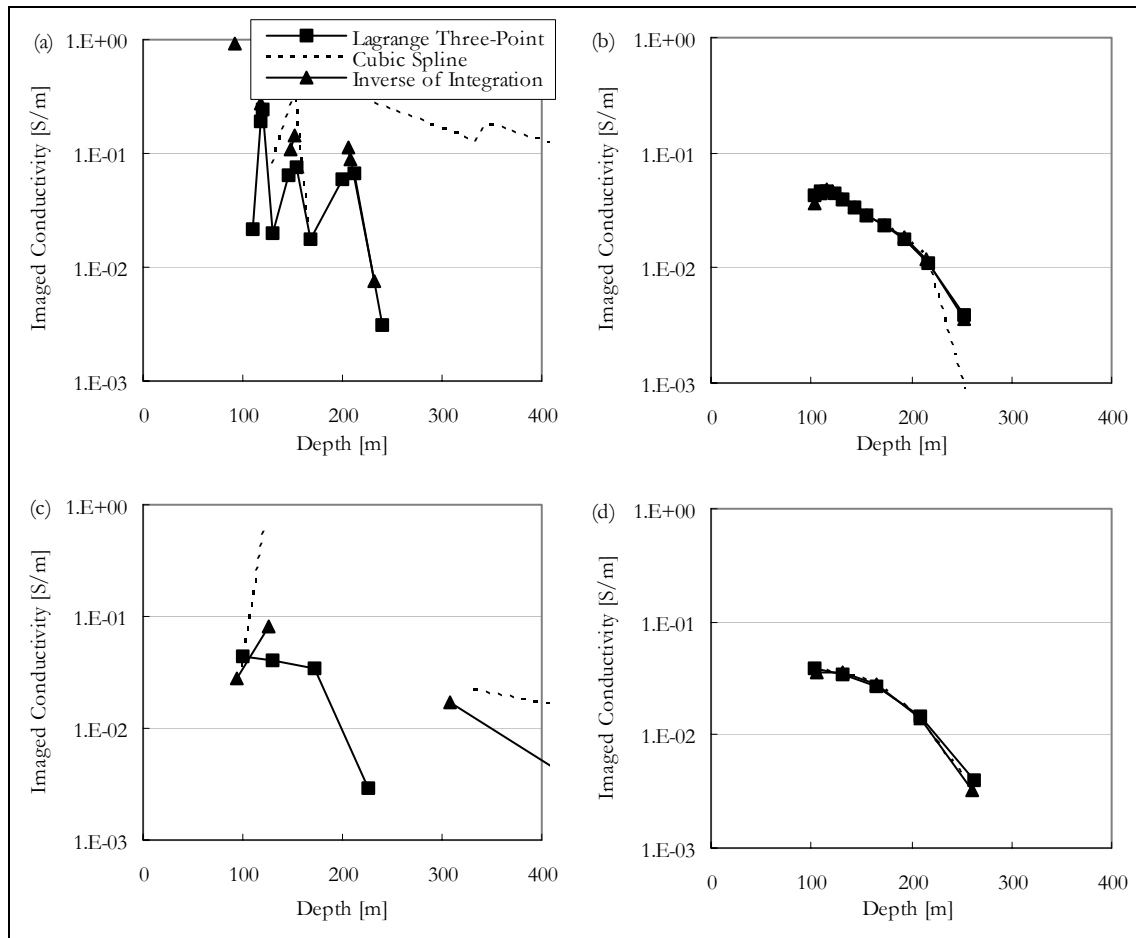


Figure 4-14: S-layer differential transform results for Sounding 4.

4.4.5 Concluding remarks on numerical differentiation

The S-layer differential transform (and other imaging techniques) are useful tools in automated interpretation of TDEM data because it is fast and do not require a starting model. It is not as accurate as inversion methods but remains useful in providing starting models for these more time consuming procedures. As numerical differentiation is very unstable, it is important to take great care when applying this operator in the S-layer transform. When working with field data, data have to be smoothed but with cognizance of the influence on the final result. Even though time-effectiveness can be increased in using algorithms for equally spaced data points it produces very poor results when applied to the S-layer transform. As for the method of differentiation, the “inverse of integration” performed best on synthetic data but it is arguable whether the 0.4% increase in accuracy is worth the additional effort compared to the Lagrange three-point formula. However, the

S-layer transform remains very fast (less than five seconds on a PC for 1500 soundings) no matter which differentiation method is chosen. Finally, only good quality data can be expected to give good quality results and if a truly automated process is required a filter passing only relatively noise-free data should be applied before the S-layer differential transform is applied

4.5 The S-layer correction factor

4.5.1 Defining a S-layer correction factor

The S-layer algorithm applied to the synthetic examples above, necessitated the implementation of a scale factor in order to obtain the correct depths and conductivity values. This factor is determined empirically as follows.

Half space responses were calculated using the late time approximation (Kaufman and Keller, 1983) as well as a numerical implementation of the solution valid for all times (W. J. Botha, unpublished). The S-layer transform is applied to these voltages in order to obtain depths and conductivities (resistivities for comparison). These resistivity values are compared to the original input values. Resistivities used were 10 ohm.m, 50 ohm.m, 100 ohm.m, 500 ohm.m, 1000 ohm.m and 5000 ohm.m with comparative results shown in Fig 4.15. In the figure, the open diamonds are the values obtained from the S-layer transform applied to the full expression, the filled diamonds those obtained from using the asymptotic values, while the solid line indicate the original resistivity value.

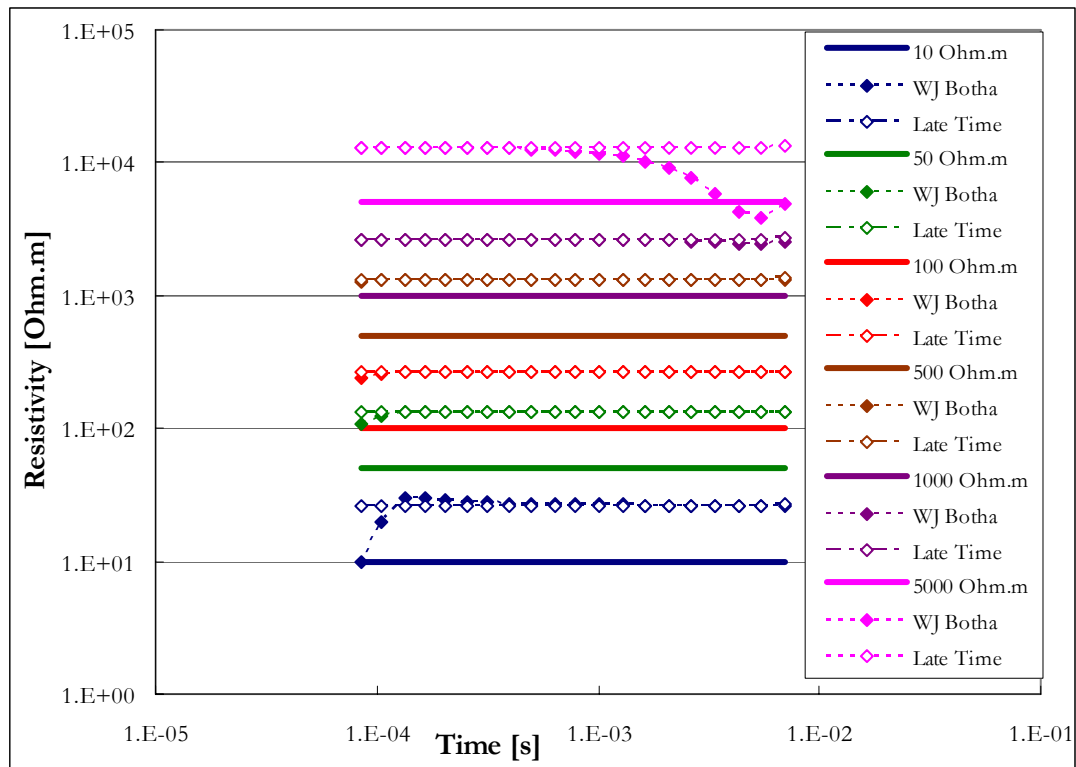


Figure 4-15: Half space resistivities compared to resistivities from S-Layer differential transform.

The 10 ohm.m full solution shows distortions in the first time channels when the late time has not been reached. Distortions are also visible on the late channels of the 5000 ohm.m data. The correlation of the full solution data to the late time approximation results is as expected – in times adhering to the late time approximations the values are equal. From the figure it is immediately obvious that the resistivities produced by the S-Layer transform are consistently higher than that of the input values.

It was found that the ratio of the resistivities calculated from the S-layer transform divided by the modelled resistivity yielded a constant of 2.6192. Since the conductivities ($1/\text{resistivities}$) are calculated in the algorithm as the derivative of conductance (S) to depth (d), this “error” could be produced either in the calculation of S or d, since depth (d) is a function of S (eq. 4.2). Correction factors can be applied in either the S or d formulae and will yield “correct” (i.e. equal to half space) conductivities as long as the following relationships hold.

$$\begin{aligned} \left(\frac{\partial S}{\partial d}\right)_{SCALED} &= \left(\frac{\partial S}{\partial d}\right) / 2.6192 \\ &= \left(\frac{\partial(S \cdot S_{factor})}{\partial\left(d \cdot \frac{d_{factor}}{S_{factor}}\right)} \right) \end{aligned}$$

So that,

$$\begin{aligned} 2.6192 &= \frac{S_{factor}}{\left(\frac{d_{factor}}{S_{factor}}\right)} \\ &= \frac{S_{factor}^2}{d_{factor}} \end{aligned}$$

There are of course an infinite number of correction factors that will satisfy this requirement (Figure 4.16) and an urgent need arose to explain the origin of this discrepancy. Three possibilities are investigated based on comparison with synthetic data from models which have all shown that depths are overestimated by the transform. Only correction factors which will decrease calculated depths are therefore discussed (the red line on Fig 4.16 indicates the possible depth correction factors ranging from almost zero to one). The following possibilities for the observed error were considered.

- A possible error in equation 4.1.
- A possible error in equation 4.2.
- An error in the physical assumptions made during the S-layer transform.

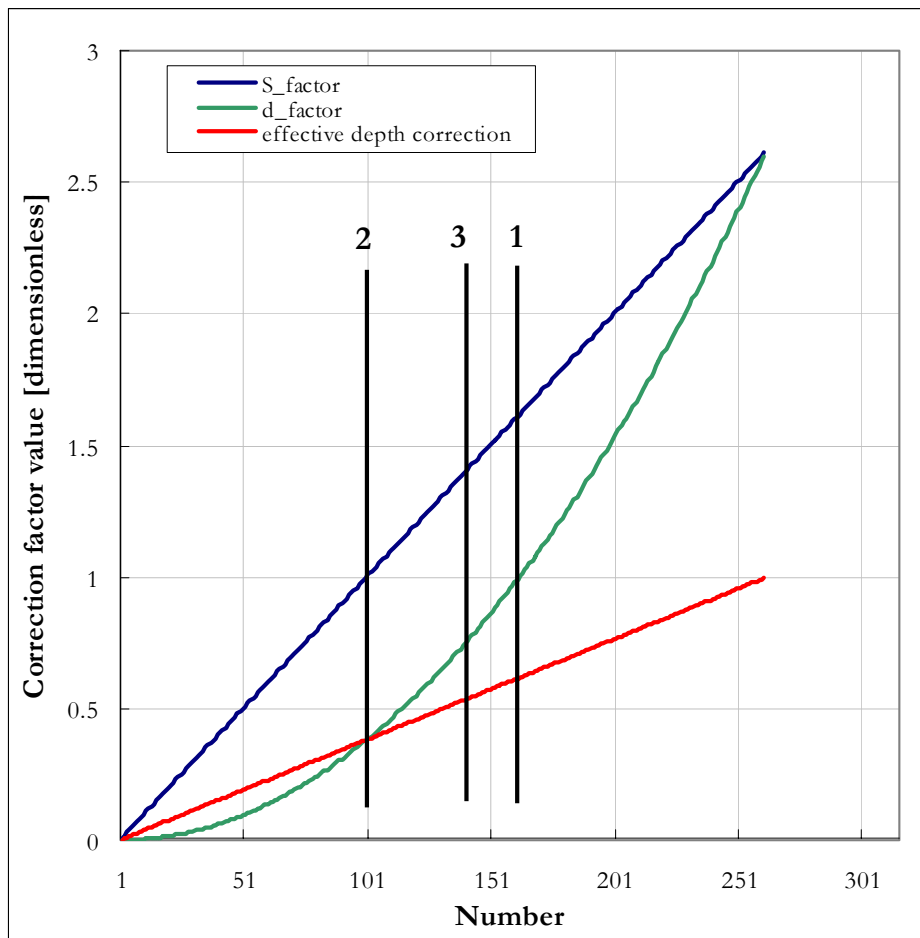


Figure 4-16: Values for S and d corrections giving correct resistivity values and the effective depth correction resulting from each pair. (from Excel: summary of depth conversion factor models)

4.5.1.1 Correction factor: Possibility 1

The assumption made here is that somehow an error is introduced in Eq. 4.1 only and that only this needs to be corrected for. This implies that (vertical line 1, Figure 4.16):

$$d_{FACTOR} = 1$$

$$S_{FACTOR} = \sqrt{2.6192}$$

this leads to a depth correction *multiplication factor* of 0.6185.

4.5.1.2 Correction factor: Possibility 2

Now the assumption is made that an error is introduced in Eq. 4.2 only and that only this needs to be corrected for. This implies that (vertical line 2, Figure 4.16)

$$d_{FACTOR} = \frac{1}{2.6192} = 0.3818$$

$$S_{FACTOR} = 1$$

this leads to a depth correction multiplication factor of 0.3818.

4.5.1.3 Correction factor: Possibility 3

The third possibility is that the equations used in the transform are indeed mathematically sound but that the physical assumptions regarding current distributions made in the S-layer transform lead to poor approximations of the models used. In figure 2.1 it was shown that the equivalent current filament that was successfully used by Nabighian to calculate the half space response, did not spaciouly coincide with the actual maxima of the current distribution in the sub surface. It was decided to test this same discrepancy on the S-layer transform. In other words, it is assumed that the equivalent filament for the S-layer behaviour, as with the equivalent filament for the half space behaviour, does not coincide with the electric field maxima in the subsurface. In order to test this theory the cumulative conductance was calculated, as is done by the S-layer transform, for the electric field maxima and equivalent current filaments (smoke-rings) respectively. The depth expressions given in equation 4.24(a), (After Nabighian and Macnae, 1991) was used in equation 4.24(b) to calculate the cumulative conductances for a 30 ohm.m half space shown in figure 4.17.

$$d_{Electric\ Field\ Maximum} = \sqrt{\frac{2t}{\sigma\mu_0}}$$

$$d_{Equivalent\ Current\ Filament} = 4\sqrt{\frac{t}{\pi\sigma\mu_0}}. \quad 4.24(a)$$

$$S(d_{i+1}) = S(d_i) + \sigma \cdot [d_{i+1} - d_i]. \quad 4.24(b)$$

As can be expected, the cumulative conductance curves are straight lines with slopes $\left(\frac{\partial S}{\partial d}\right)$ equal to the conductivity (Fig 4.17). It can be seen that although both curves will give correct conductivity values the S and d values vary distinctly.

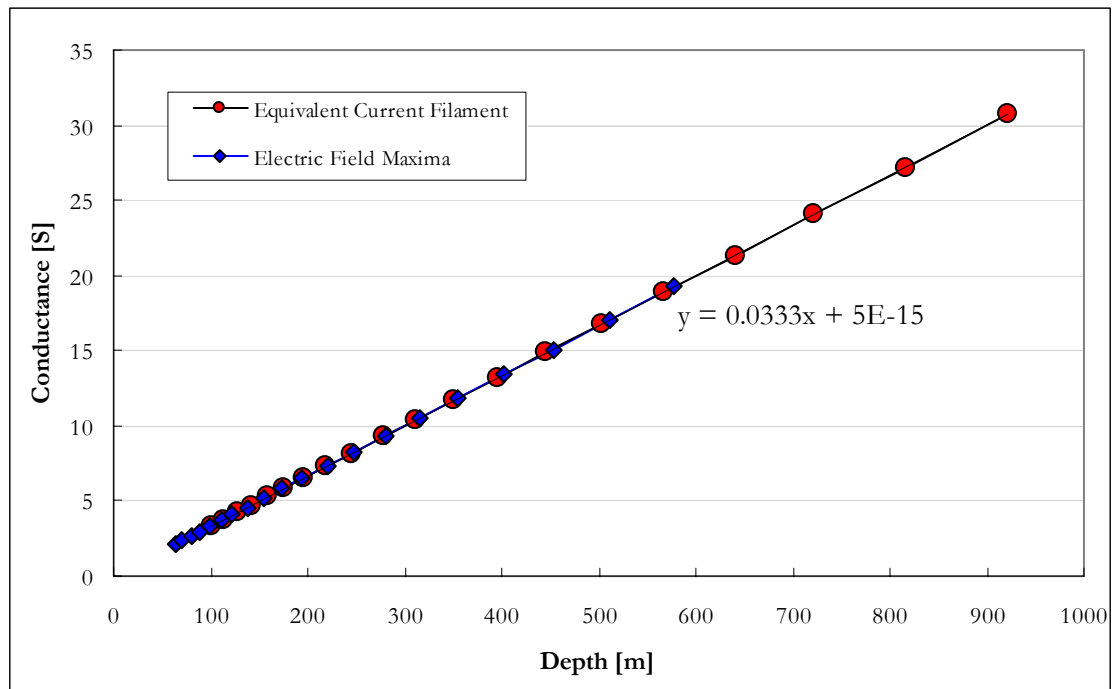


Figure 4-17: Cumulative conductance curves for late time halfspace approximations.

Looking specifically at depths, the equivalent current filament depths range from 99 m to 920 m, while the electric field maxima map between 63 m and 577 m. The S-layer transform is also based on using current filaments to approximate a whole earth response and is it reasonable to expect that the S-layer transform will give similar errors in the depth to current maxima results.

In Figure 4.18 the cumulative conductance curve (green) of the S-layer differential transform is compared with the curves from Figure 4.17. It shows the same approximate depth range as that of the single equivalent current filament but with conductance values much lower than expected (resulting in underestimation of conductivity values). Based on these graphs the third set of correction factors is proposed which will transform the S-layer transform values to coincide with the maxima of the electric field. The corrected conductance curve is shown in pink (Figure 4.18).

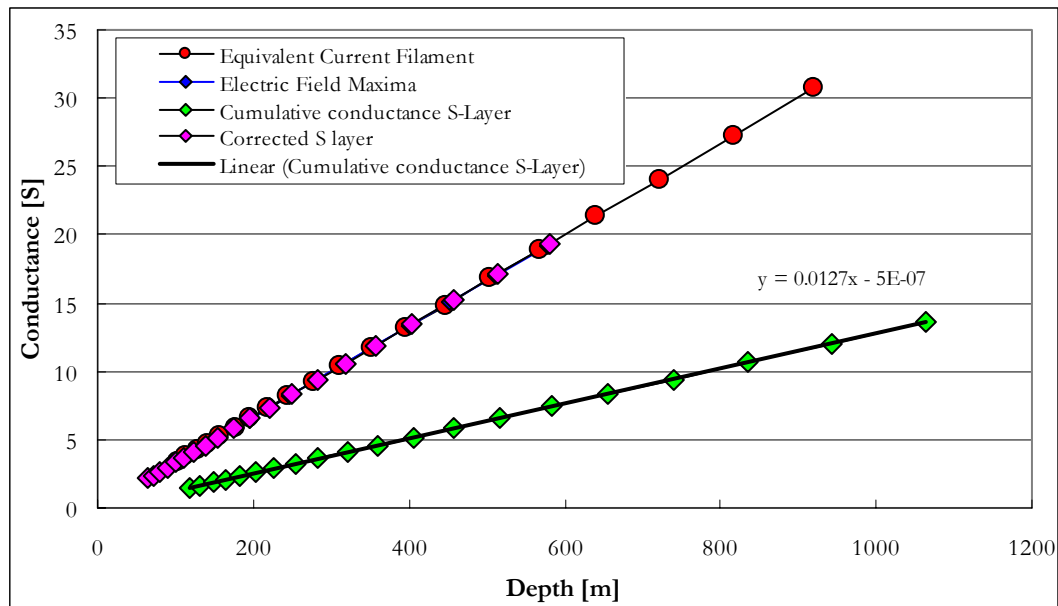


Figure 4-18: Cumulative conductance curves for late time half space and S-layer approximations.

Though the ‘smoke ring’ idea was developed by representing the half space response by a single current filament, expanding outward and downward, the S-layer transform likewise uses a single filament to present the S-layer behaviour. It was consequently assumed that the factor that relates the filament depth to the electrical field maxima in the half space behaviour will be the same in the S-layer approach. This factor of 0.7807 was then used to calculate a correction factor for S, given below.

$$d_{FACTOR} = 0.7807$$

$$S_{FACTOR} = 1.43$$

leading to a depth correction multiplication factor of 0.5460.

1.5.2 Correction factor: Application to synthetic data

The three possibilities for a correction factor are compared on five synthetic data sets in this section. All synthetic data were generated with MARCO software assuming the following system parameters:

Tx loop: 50m X 50m

Tx current: 5 A

Rx loop: 1 m²

Time channels in seconds:

Ch. 1-5	Ch. 6-10	Ch. 11-15	Ch. 16-20
8.8E-05	0.000251	0.000799	0.002648
0.000107	0.000314	0.001014	0.003373
0.000131	0.000396	0.001287	0.004297
0.000162	0.000499	0.001636	0.005475
0.000201	0.000631	0.002081	0.006978

Apart from the S-layer differential transform results (one for each of the 3 correction scenario's) solutions are also shown in Figures 4-19 to 4-23 that were obtained with TEMIX software layered earth inversion (two and three layers) and Occam's smooth model inversion (10 layers). All layered earth inversions have an error of less than 1%. For the two-layer earth (Model 1) the second choice of the correction factor (blue) is the closest to the input model although correction factor 3 (black) correlates best with the smooth layered earth inversion (green).

MODEL 1: Two-layer earth

Layer	Thickness	Resistivity (conductivity)
1	100 m	50 ohm.m (0.02 S/m)
2	infinite	5 ohm.m (0.2 S/m)

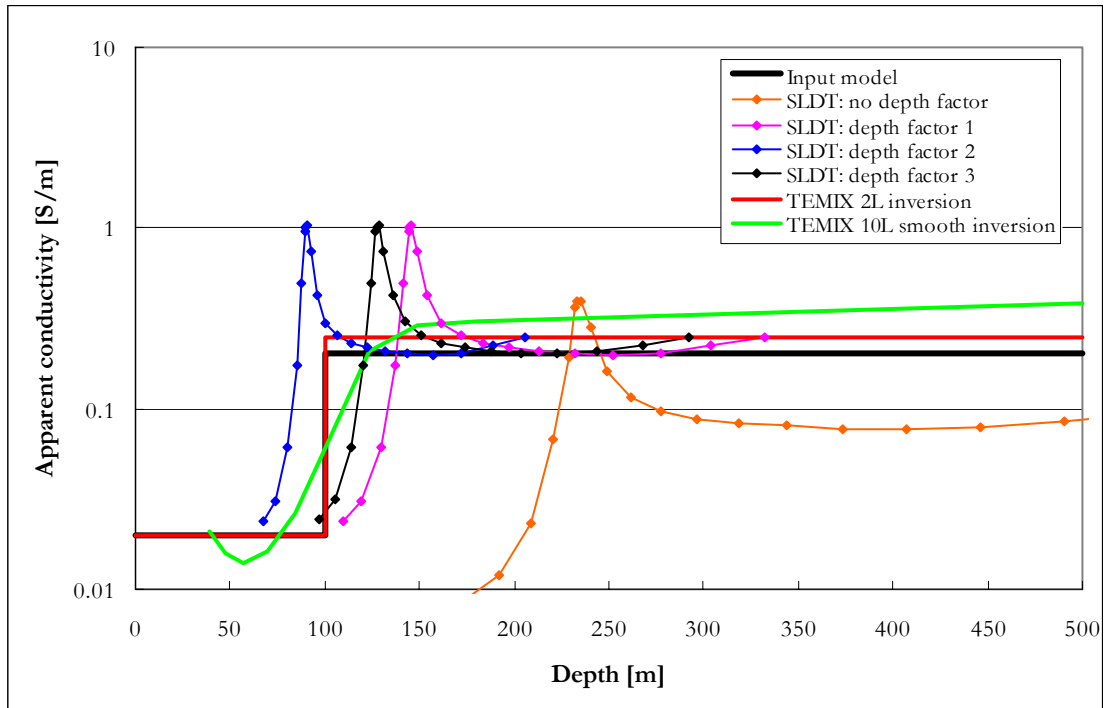


Figure 4-19: Comparison of S-layer differential transform (SLDT) solutions using different depth factors and layered earth inversions of synthetic data for a two layer earth.

MODEL 2: Three-layer earth (thin conductive layer)

Layer	Thickness	Resistivity (conductivity)
1	150 m	50 ohm.m (0.02 S/m)
2	15 m	5 ohm.m (0.2 S/m)
3	infinite	50 ohm.m (0.02 S/m)

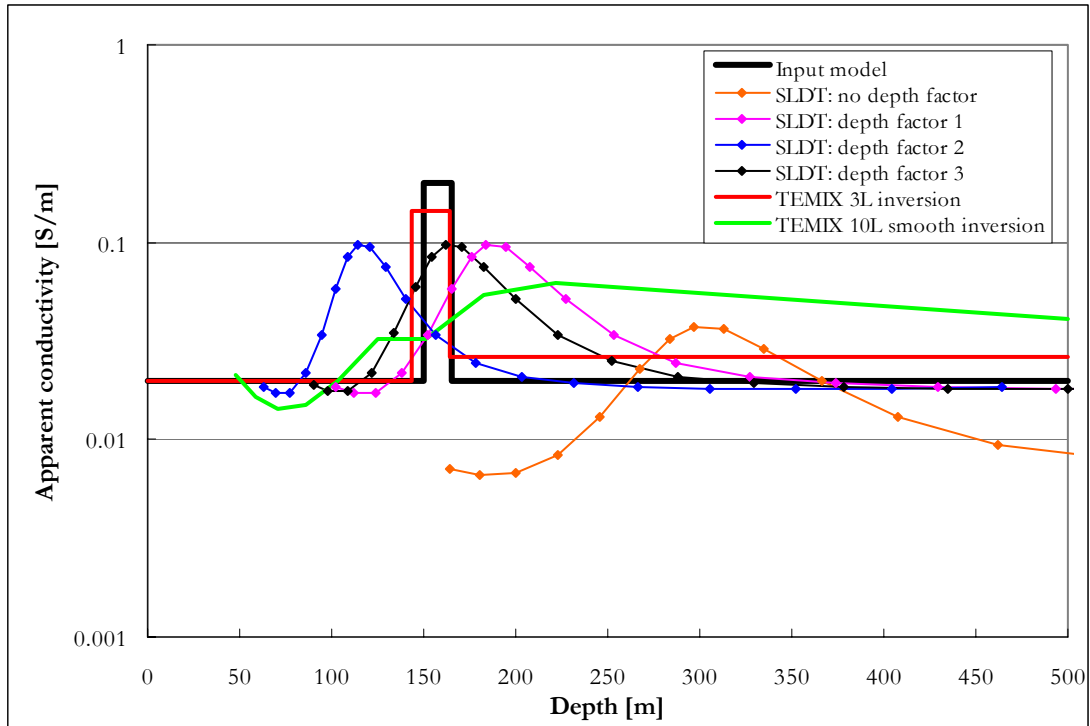


Figure 4-20: Comparison of S-layer differential transform (SLDT) solutions using different depth factors and layered earth inversions of synthetic data for a three layer earth (thin conductive layer).

In the case of a thin conductive layer correction factor 3 is the most accurate of the SLDT's (S-layer differential transform) and also outperforms the smooth layer inversion (Figure 4-20).

MODEL 3: Three-layer earth (thick conductive layer)

Layer	Thickness	Resistivity (conductivity)
1	150 m	50 ohm.m (0.02 S/m)
2	50 m	5 ohm.m (0.2 S/m)
3	inf	50 ohm.m (0.02 S/m)

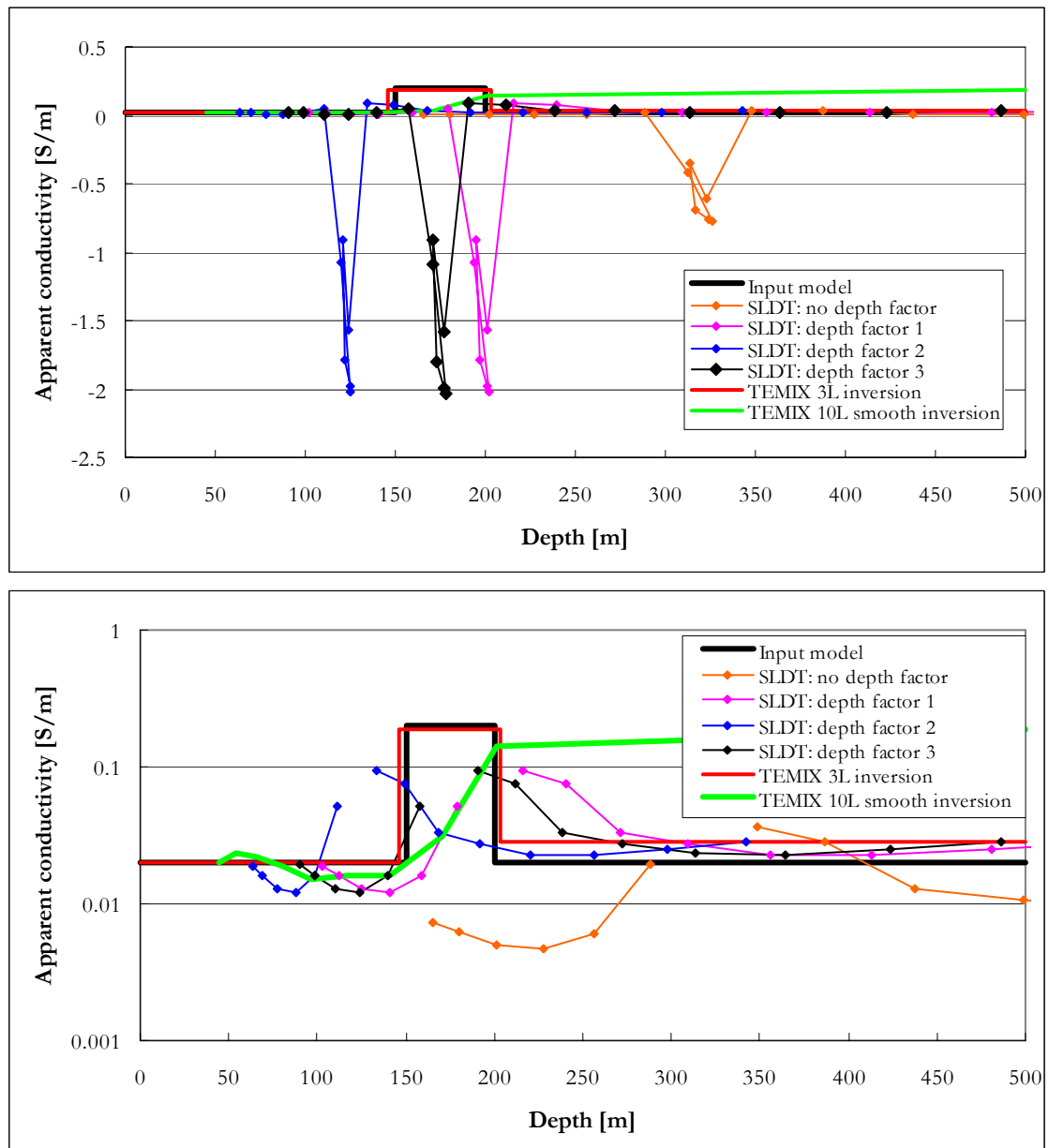


Figure 4-21: Comparison of S-layer differential transform (SLDT) solutions using different depth factors and layered earth inversions of synthetic data for a three layer earth (thick conductive layer). Top: negative values included; Bottom: no negative values.

The thick conductive layer (Model 3) shows an apparent failure of the SLDT algorithm with decreasing depths calculated at increasing times, resulting in negative apparent conductivities (Figure 4-21). This is explained by the “reflecting smoke ring” concept where high conductance features start acting as a secondary source and additional currents are generated diffusing both upward and downward from this point. However, at some stage the primary diffusive pattern outlives the secondary event and the expected increase

in cumulative conductance with time can be mapped again (Figure 4-2 bottom). This behaviour is investigated in more detail in the next section.

MODEL 4: Conductive plate in half space

Half space resistivity (conductivity)	50 ohm.m (0.02 S/m)
Plate resistivity (conductivity)	5 ohm.m (0.2 S/m)
Plate dimensions (horizontal)	200m X 200m
Plate thickness (vertical)	20m
Plate depth to top	150m

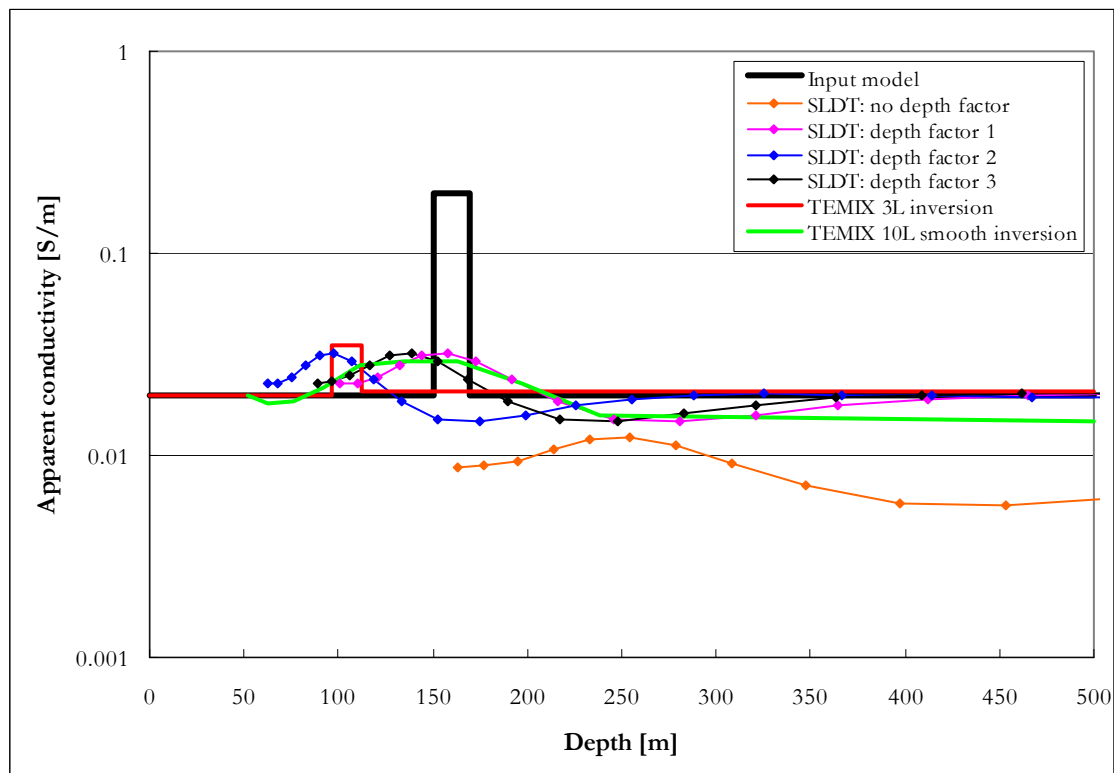


Figure 4-22: Comparison of S-layer differential transform (SLDT) solutions using different depth factors and layered earth inversions of synthetic data for a thin conductive plate in a resistive half space.

The thin conductive plate is underestimated in depth and conductivity by all the methods employed (except the SLDT no correction which still overestimates depth). The SLDT correction factor 3 correlates best with the smooth inversion and is closer to the input

model than the three layer inversion. This is to be expected as the basic assumption of an infinite layer (in horizontal extent) is violated.

MODEL 5: Conductive prism in half space

Half space resistivity (conductivity)	50 ohm.m (0.02 S/m)
Prism resistivity (conductivity)	5 ohm.m (0.2 S/m)
Prism dimensions (horizontal)	200m X 200m
Prism thickness (vertical)	200m
Prism depth to top	150m

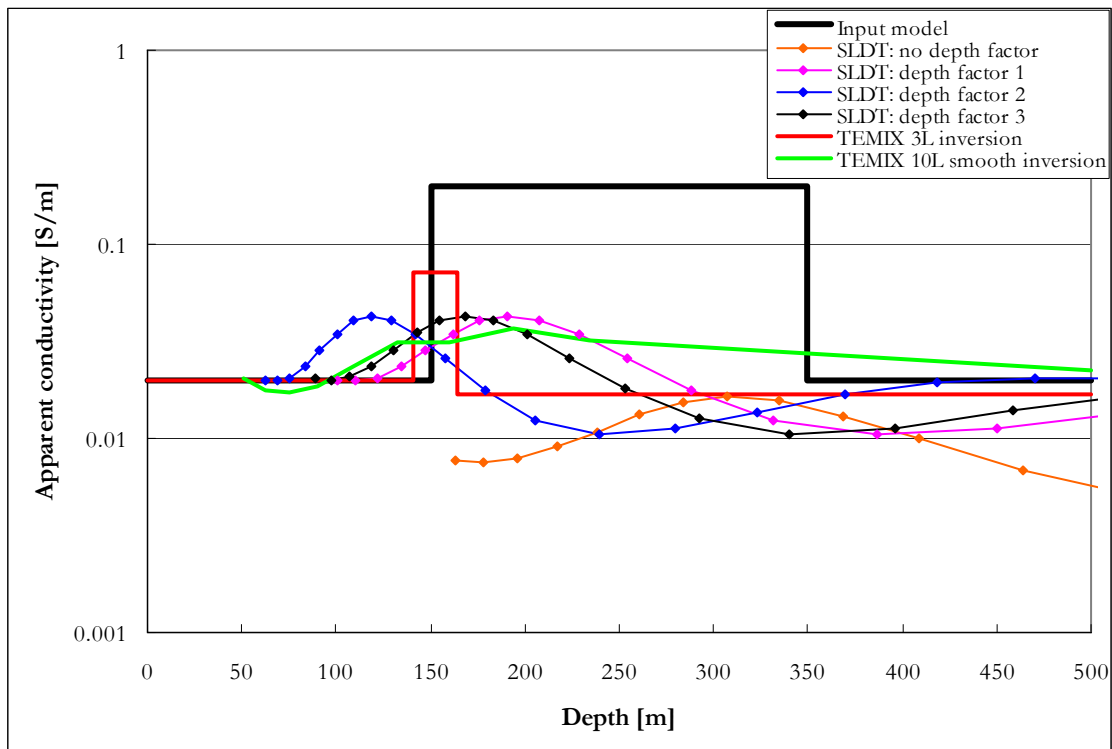


Figure 4-23: Comparison of S-layer differential transform (SLDT) solutions using different depth factors and layered earth inversions of synthetic data for a conductive prism in a resistive half space.

The depth to top of a conductive prism is well defined by the layered earth inversion as well as the correction factor 3 results.

In conclusion, the third scenario for correction correlates best with the actual model depths on synthetic data and was implemented in the software.

4.5.3 Behaviour of the S-layer transform when applied to synthetic data

In order to test (and develop a better understanding of the method) the conductivity-depth results of the improved S-layer transform a number of synthetic models are presented with their corresponding transformed results. Both the cumulative conductance [S] and conductivity [σ] curves are given for each model. The influence of noise added to the data is also investigated. The software used for the forward models is MARCO developed by AMIRA. The following system parameters were used for modelling:

Receiver area:	1 m ²
Receiver time channels:	0.08813 ms (Ch. 1) to 6.978 ms (Ch. 20) logarithmically spaced, i.e. the H range of the Geonics EM37.
Transmitter loop:	50 m X 50 m
Transmitter turn-off time:	40 μ s
Transmitter current:	1 A
Configuration:	Central loop sounding

4.5.3.1 Half space with conductivity of 0.02 S/m (50 ohm.m)

Figures 4-24 and 4-25 show the results from the S-layer transform for the case of a 50 ohm.m half space. The cumulative conductance curve (Figure 4-24) rises smoothly and the imaged conductivity versus depth levels out close to the expected value of 0.02 S/m when the late time approximation as validated.

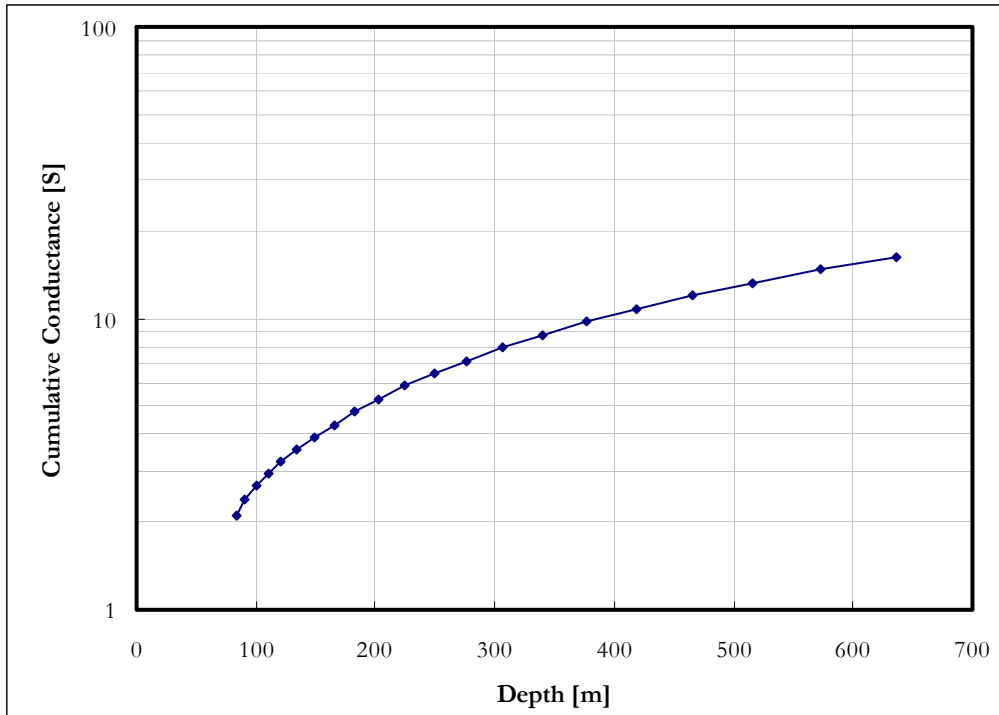


Figure 4-24 Cumulative conductance versus depth, 0.02 S/m (50 Ω.m) half space

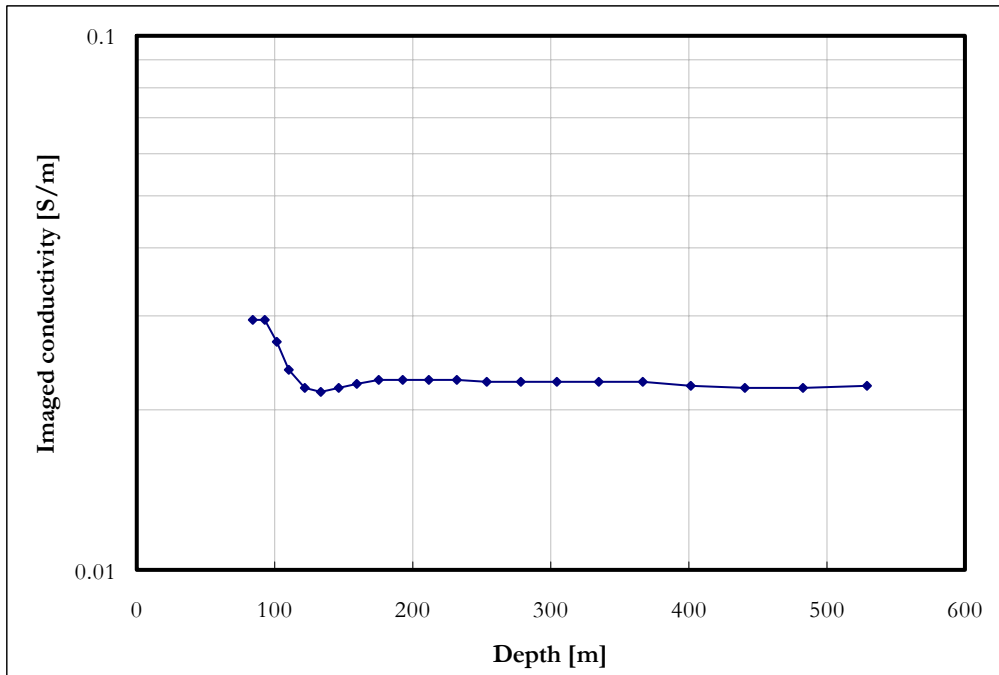


Figure 4-25 Conductivity versus depth, 0.02 S/m (50 Ω.m) half space.

4.5.3.2 Two layer earth with decreasing conductivity ($\sigma_1 > \sigma_2$)

Two models with different contrasts are presented in Figures 4-26 and 4-27. The first layer has a conductivity of 0.02 S/m and is 200 m thick in each instance while the second layer conductivity is changed from 0.002 S/m to 0.0002 S/m. The cumulative conductances rise smoothly with increasing depth and the conductivities approach the true values of the layers, although not a hundred percent accurate. However, the distinct nature of two layers with decreasing conductivity is clearly recognizable. The boundary (at 200 m) between the layers is not that easy to distinguish because of the gradual change in values on both curves, however it is easy to see that the different model curves start to diverge at this point when the second layer is starting to take effect.

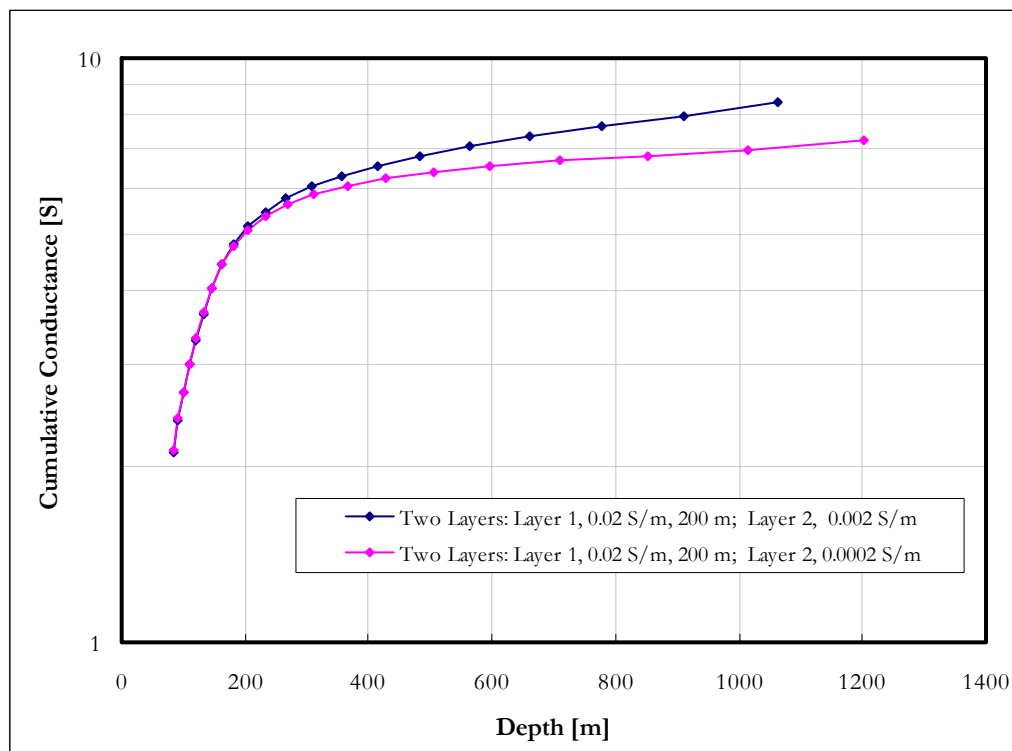


Figure 4-26: Cumulative conductance versus depth for two layers of decreasing conductivity; first layer thickness 200m.

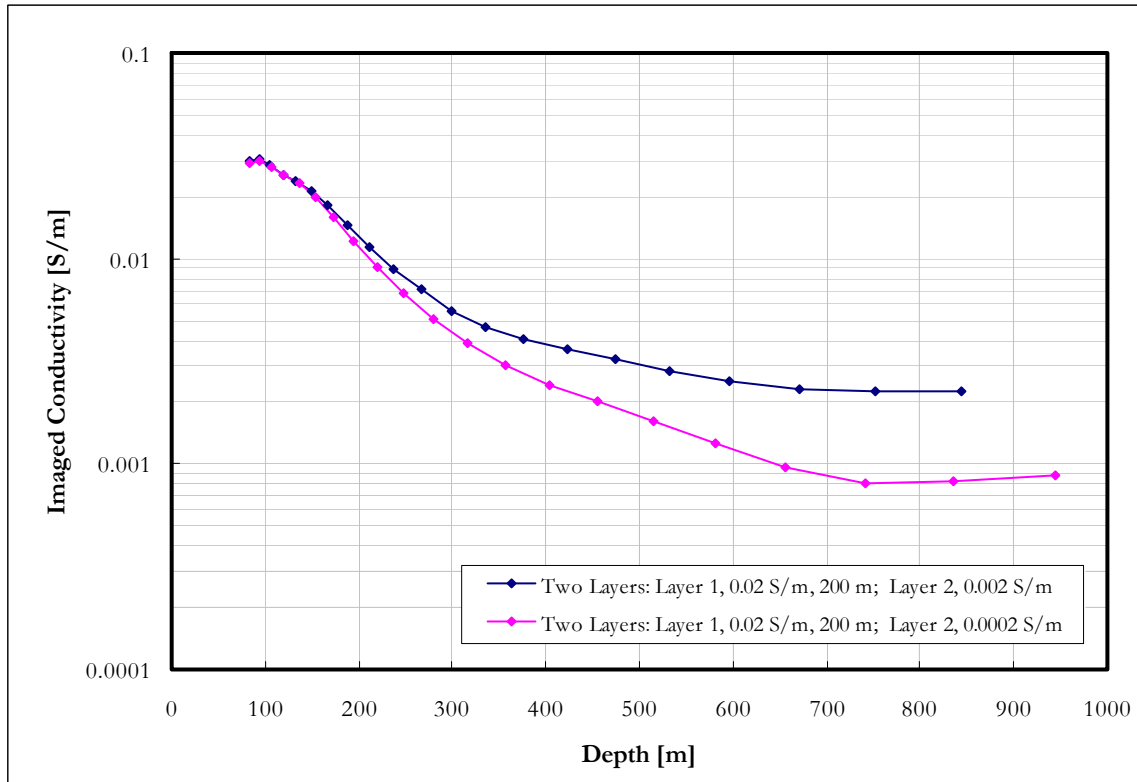


Figure 4-27: Imaged conductivity versus depth for two layers of decreasing conductivity; first layer thickness 200m.

4.5.3.3 Two layer earth with increasing conductivity ($\sigma_1 < \sigma_2$)

Once again two models with different contrasts are presented (Figures 4-28 to 4-30). The first layer still has the same parameters of 0.02 S/m and 200 m. The second layer conductivity is now changed from 0.2 S/m to 2 S/m. In this case the effect of the second layer is already visible before the 200 m mark. This method approximates a set of current distributions with one single filament and it can be expected that the transition would not be sharp and also that more conductive layers will influence the single filament even if its position is not indicated as inside the conductive layer itself. For the low contrast case (second layer conductivity = 0.2 S/m) the behaviour of the cumulative conductance and conductivity curves follow the expected pattern of increasing smoothly with depth and approximating the second layer conductivity ever closer after an initial overshoot. However, the high contrast case produces a very interesting phenomenon. Instead of yielding cumulative conductance and conductivity values at increasing depths with increasing time, a turning point is reached at some stage (300m depth for this case) after which time the equivalent S-layer filament is mapped with drastically increasing conductivity but decreasing depths. This type of unexpected behaviour contradicts the

assumption made in this method that cumulative conductance will always increase with increasing depth and the standard algorithm only calculates the derivatives for points until the depths start decreasing. For this specific case the slope of the curve was calculated in an alternate manner to investigate the conductivity behaviour.

The negative “conductivity” values and dramatic overshoot of the last positive slopes (Figure 4-28) show no relation to the true conductivities and does not add much value to the process. At first sight this might seem as a failure of the S-layer method, but the very distinctive pattern can easily be recognised on the cumulative conductance curves and will indicate the existence of a very conductive layer. The exact position of the boundary is not well defined, but can best be described from the conductivity curves as the first rise in conductivity. This transition is easier distinguished on graphs with linear scale (Figure 4-30).

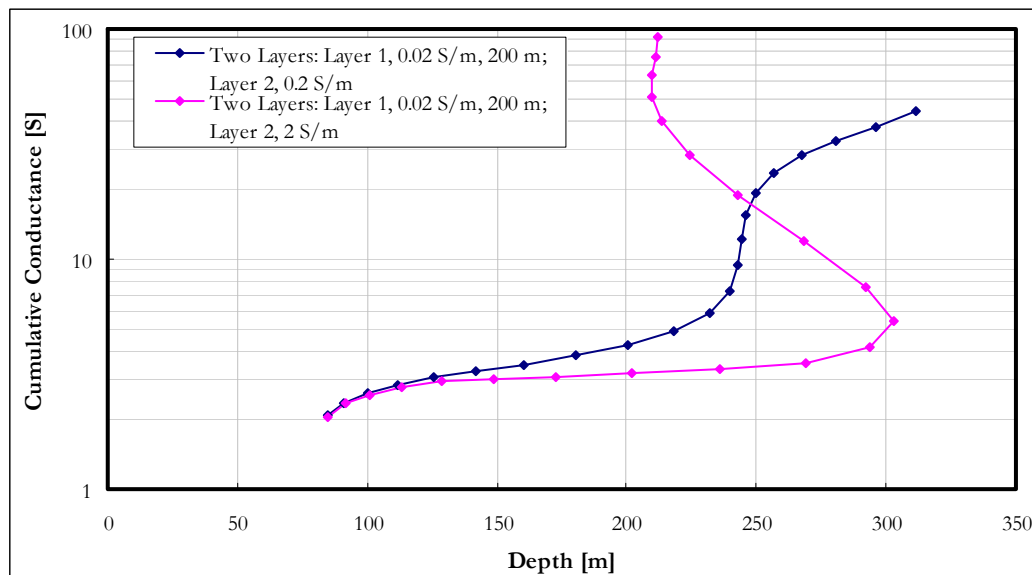


Figure 4-28: Cumulative conductance versus depth for two layers of increasing conductivity; first layer thickness 200m.

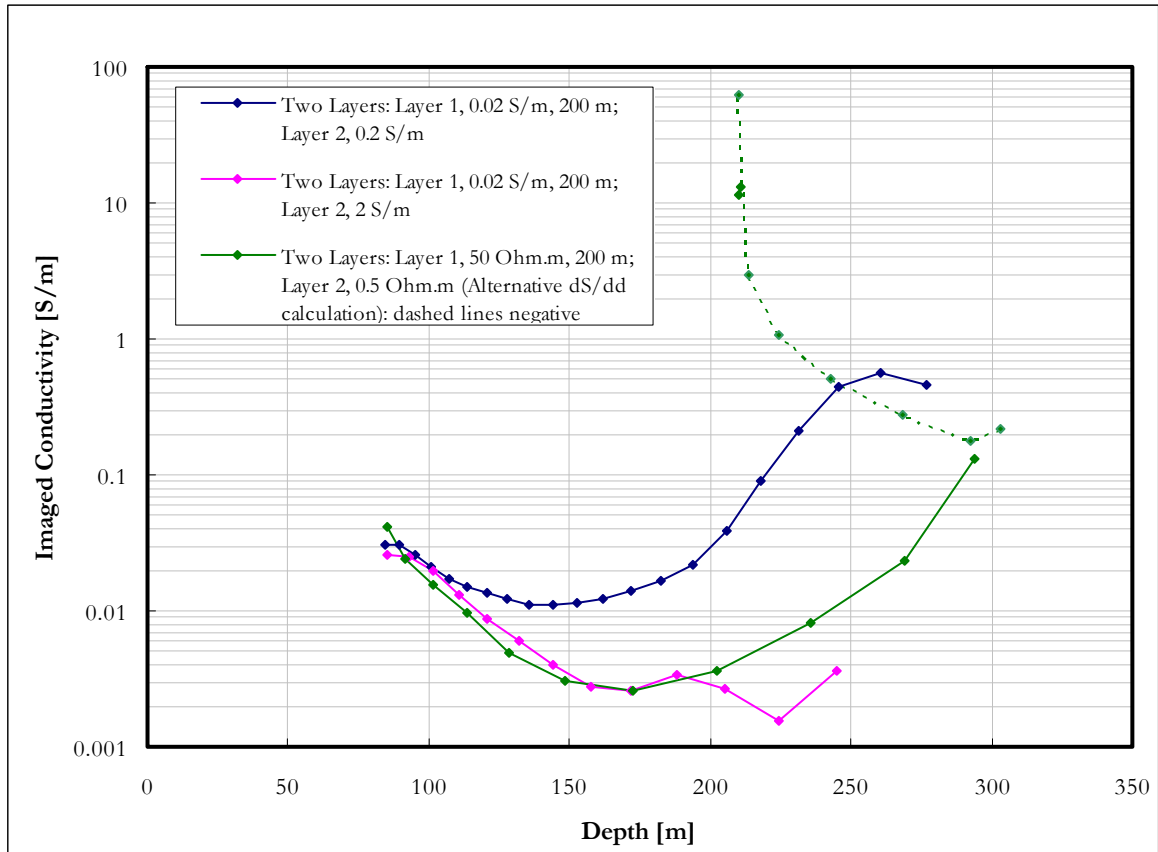


Figure 4-29: Imaged conductivity versus depth for two layers of increasing conductivity; first layer thickness 200m.

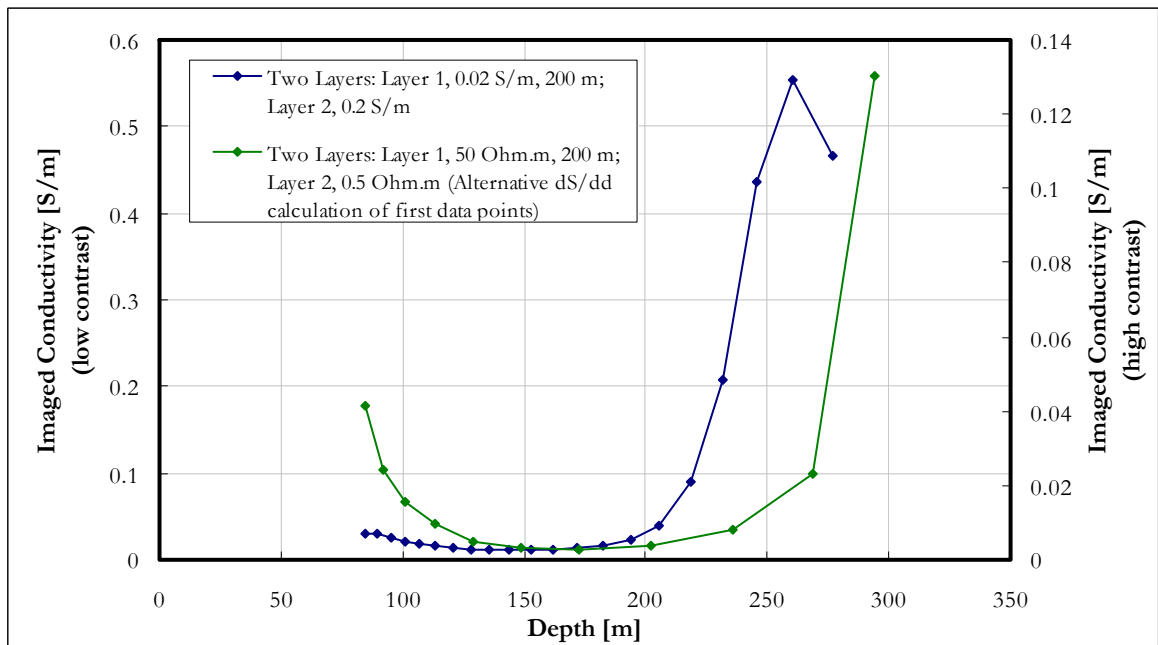


Figure 4-30: Imaged conductivity versus depth for two layers of increasing conductivity; first layer thickness 200m – linear scale.

The physical implication of this phenomenon can possibly be explained by a reflection of the equivalent S-layer filament at the very conductive high contrast boundary. As currents are induced into the second layer it can act as a secondary source and induce currents in the first layer again, diffusing away from this source, i.e. upwards. These currents are closer to the receiver than the ones in the second layer itself, diffuse quickly in the more resistive layer (implying large $\partial B_z / \partial t$) and will therefore dominate the measured signal for a certain time. At this point the assumptions made in developing the S-layer transform are clearly not valid anymore and the calculated conductivities and depths have to be filtered out from any future presentation of data.

4.5.3.4 Conductive layer in half space

Firstly, the influence of contrast in conductivity is investigated and secondly the thickness of the layer is changed. Four different contrasts and thicknesses were modelled and analysed for a conductive layer 150m deep in a 0.02 S/m half space. The results for conductivity contrasts are shown in Figures 4.31-4.33.

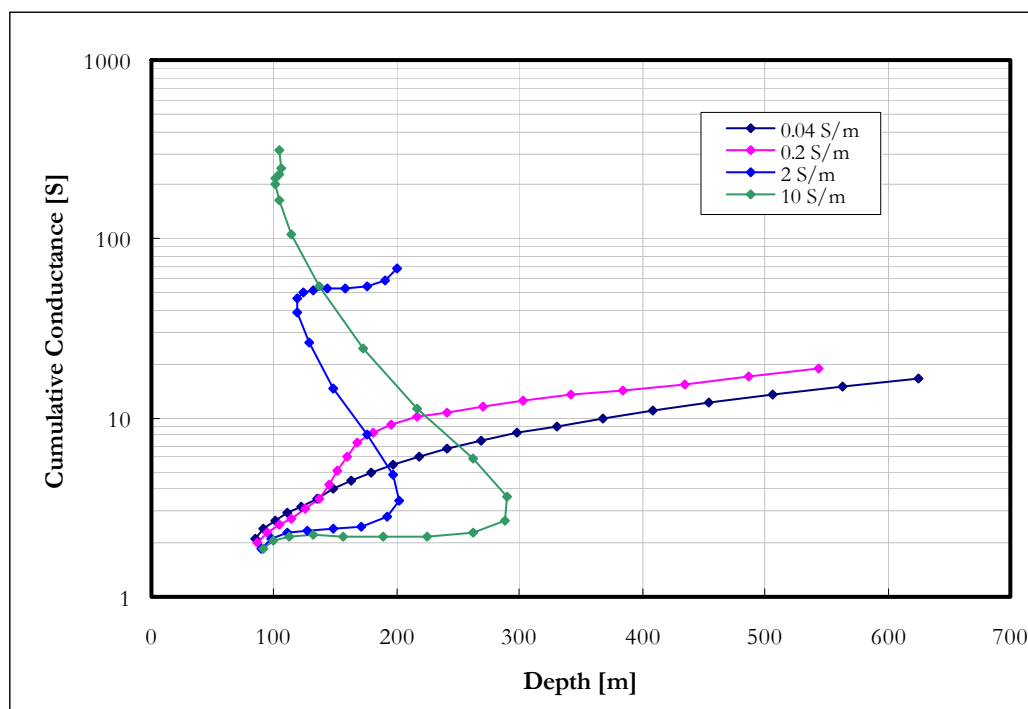


Figure 4-31: Cumulative conductance for a 15m thick layer of varying conductivity at 150m depth in a 0.02 S/m half space.

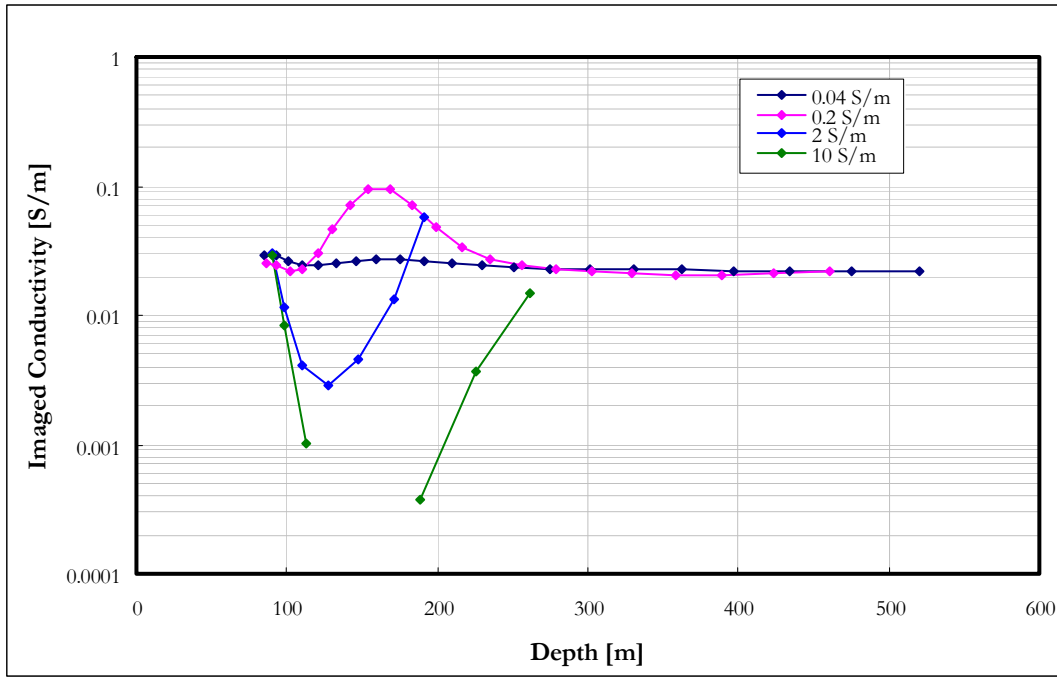


Figure 4-32: Imaged conductivity versus depth for a 15m thick layer of varying conductivity at 150m depth in a 0.02 S/m half space.

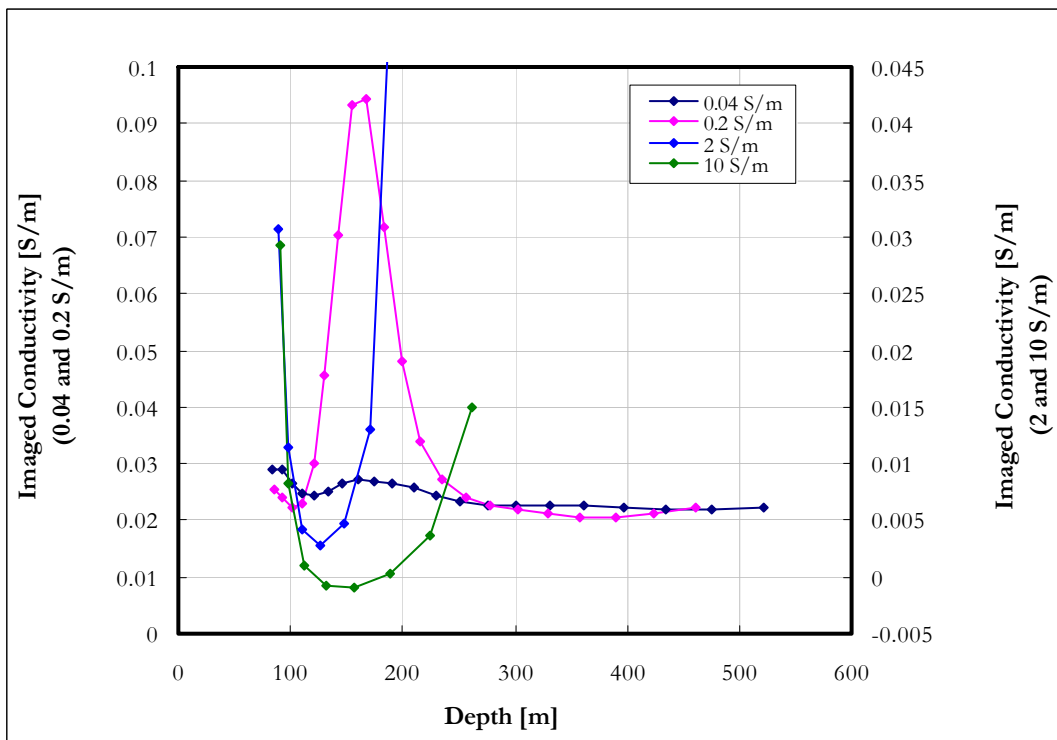


Figure 4-33: Imaged conductivity versus depth for a 15m thick layer of varying conductivity at 150m depth in a 0.02 S/m half space; linear scale.

The S-layer transform is clearly very sensitive to conductive layers and even with a conductivity contrast of 1:2 (0.02:0.04) is still able to resolve the layer. Depths for the low

contrast cases are predicted accurately although the high contrasts are not accurately mapped. The two most conductive layers generate underestimated values for conductivity (Figures 4-32 and 4-33) and might be interpreted to be more resistive than the half space if the conductivity sections are consulted without reference to the distinctive cumulative conductance signature.

Next, the effect of layer thickness for the low conductivity contrast scenario is investigated. Thicknesses of 2 m, 5 m, 10 m, 15 m, 20 m, 50 m and 100m are used (Figures 4-34 to 4-36). It is important to notice that the anomaly widths remain the same until a critical thickness is reached and only an increase in amplitude with increasing layer thickness is seen. Although the top of the layers are well defined, the true thickness and conductivity are not uniquely determined. Very important, though, is that the high contrast behaviour of decreasing depths with time is not seen here, no matter how large the conductivity-thickness product becomes.

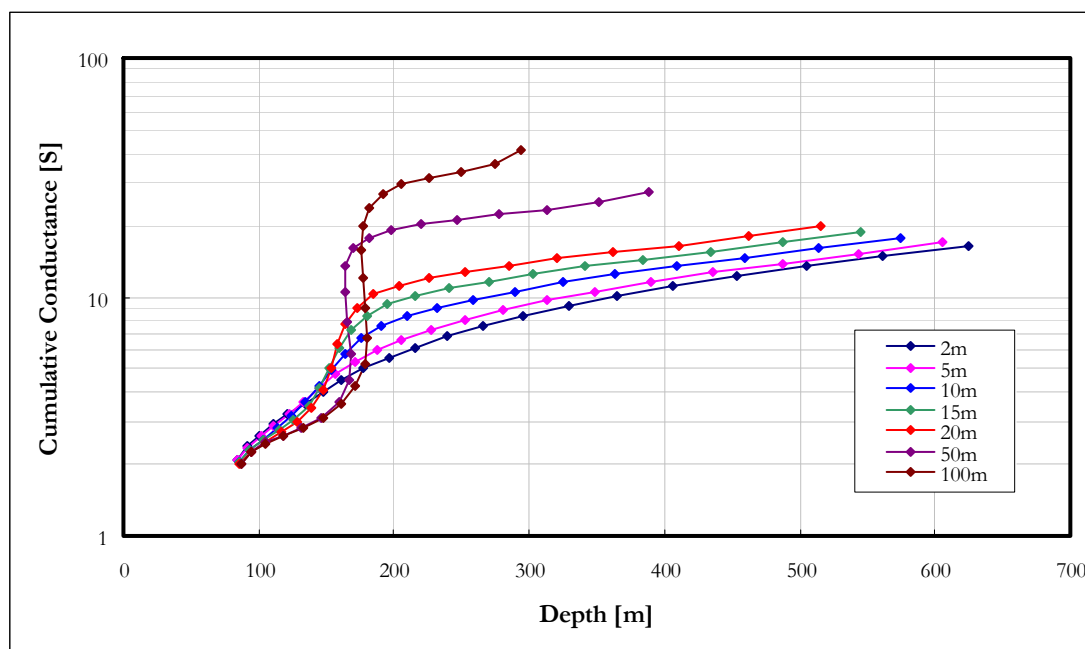


Figure 4-34: Cumulative conductance for a 0.2 S/m layer of varying thickness at 150m depth in a 0.02 S/m half space.

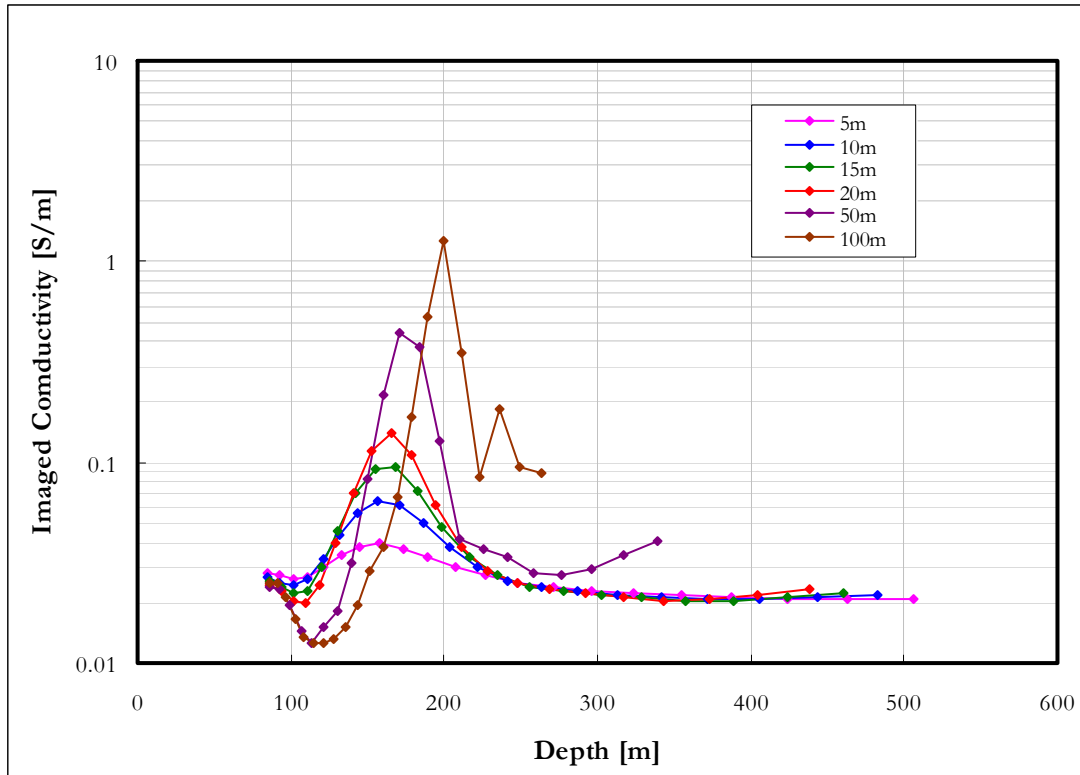


Figure 4-35: Imaged conductivity for a 0.2 S/m layer of varying thickness at 150m depth in a 0.02 S/m half space.

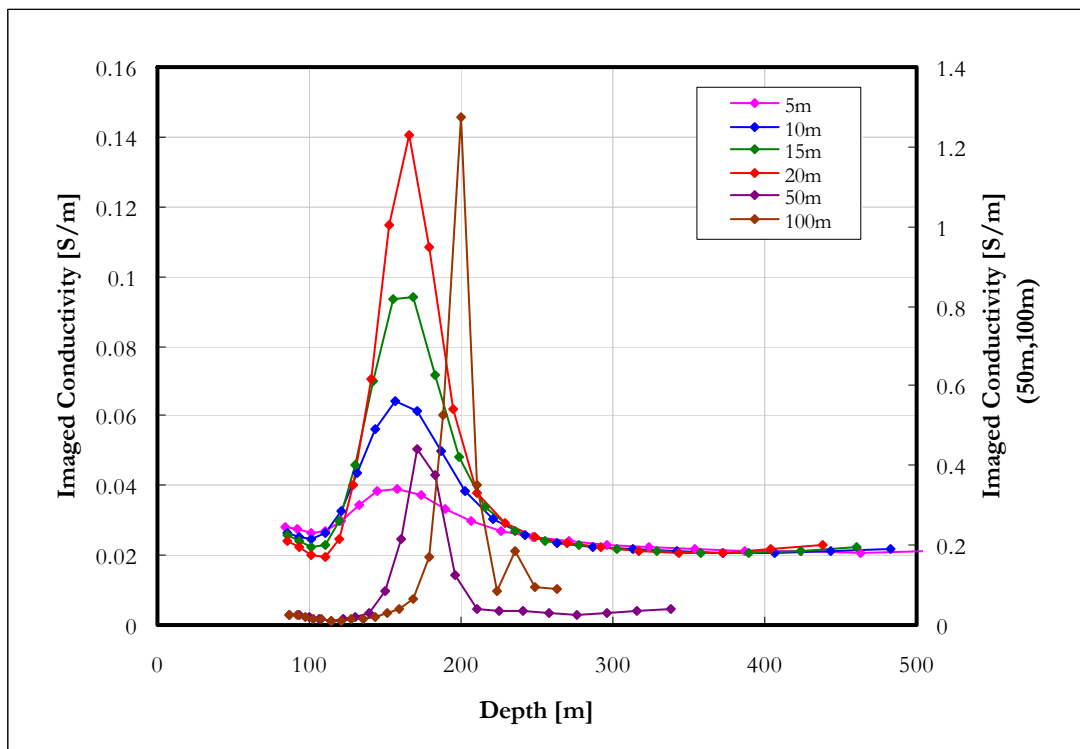


Figure 4-36: Imaged conductivity for a 0.2 S/m layer of varying thickness at 150m depth in a 0.02 S/m half space; linear scale.

The effect of layer thickness for the high contrast scenario is presented in figures 4-37 – 4-39.

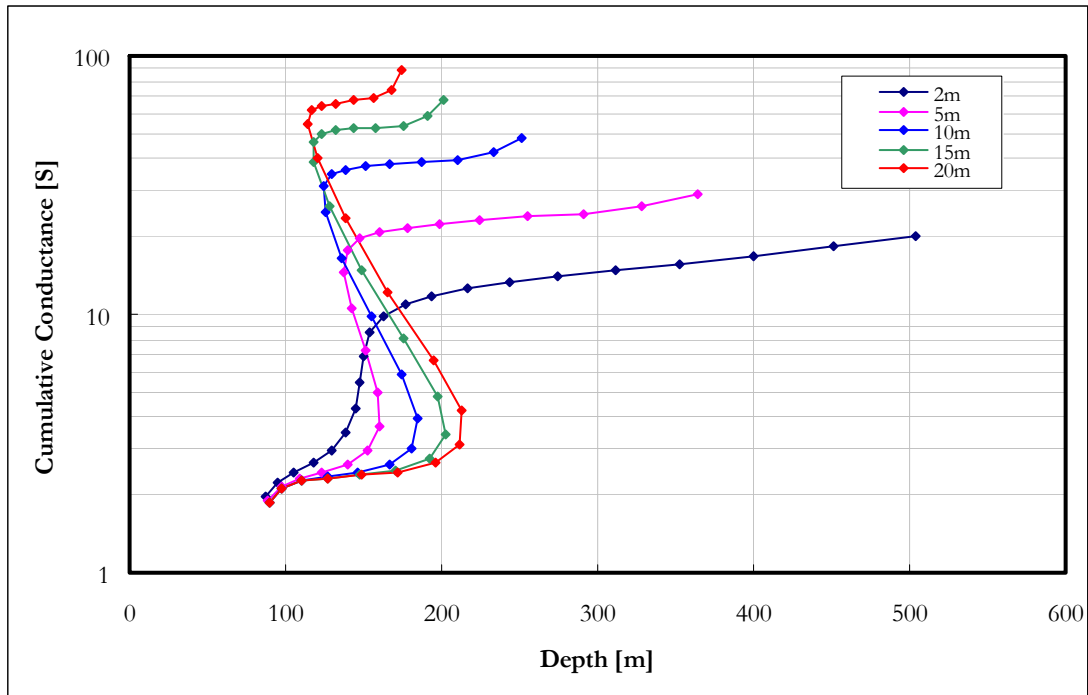


Figure 4-37: Cumulative conductance for a 2 S/m layer of varying thickness at 150m depth in a 0.02 S/m half space.

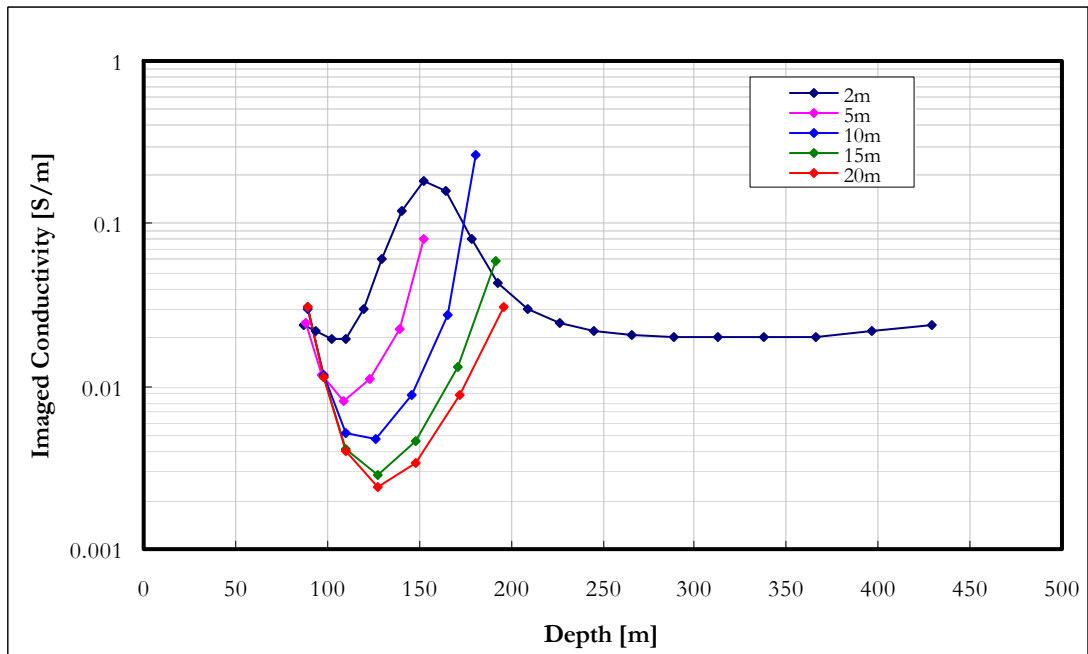


Figure 4-38: Imaged conductivity for a 2 S/m layer of varying thickness at 150m depth in a 0.02 S/m half space.

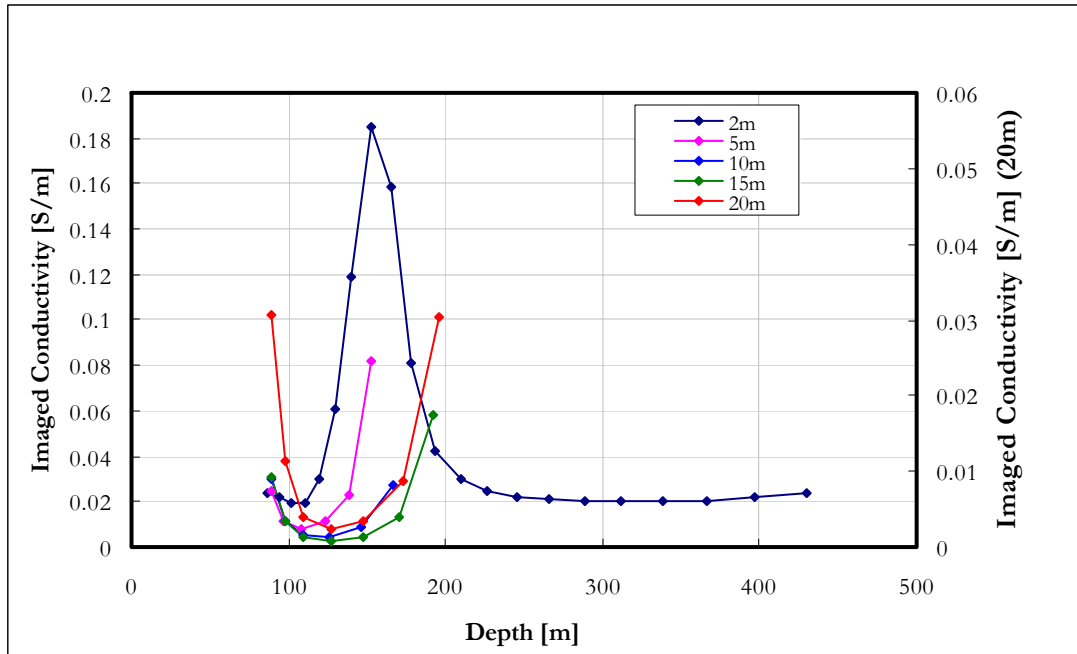


Figure 4-39: Imaged conductivity for a 2 S/m layer of varying thickness at 150m depth in a 0.02 S/m half space – linear scale.

Except for the 2 m layer, all the curves exhibit the high contrast behaviour. The thicker the layer becomes, the closer the curves resemble the two layer case with very little or no influence from the earth below the conductive layer contributing to the signal.

The effect of varying depth of a conductive layer is shown in Figures 4-40 – 4-42. The width of the anomaly increases with depth to top of the conductive layer while the amplitude decreases. One case of special interest is the layer at 50m depth. For the host rock conductivity of 0.02 S/m and the chosen system parameters, the shallowest depth of investigation is in the order of 100 m. However, if there is a conductive layer shallower than this, the depth of investigation is adapted to that. The curve is distorted compared to those of the deeper layers in the sense that there is no rise from the host rock response into the conductive layer. It actually takes a shape more indicative of a two layered earth.

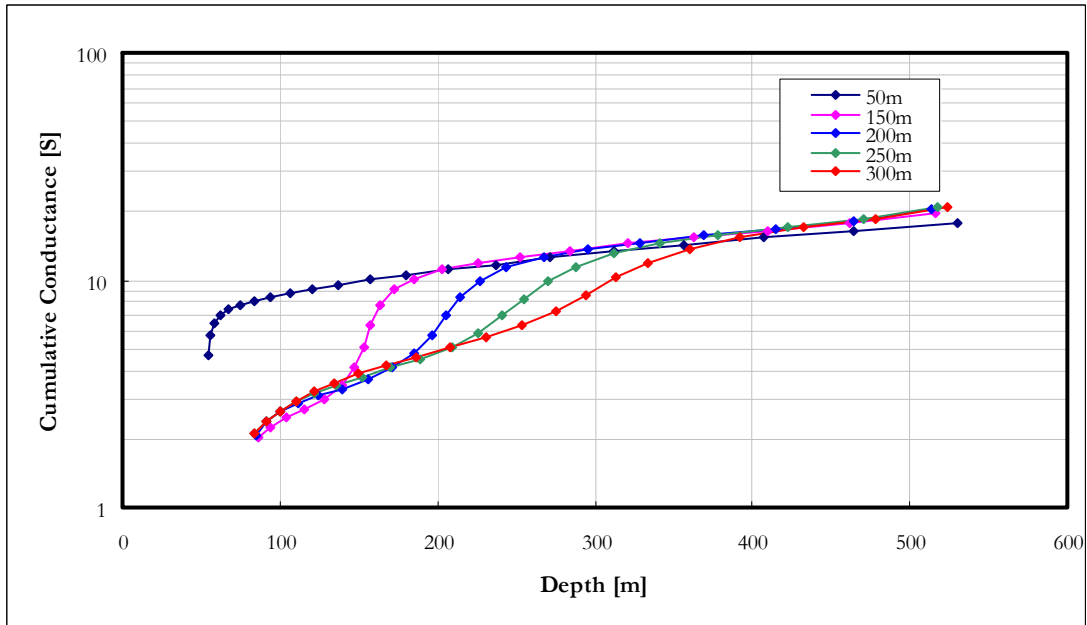


Figure 4-40: Cumulative conductance for a 0.2 S/m layer of 20 m thickness at various depths in a 0.02 S/m half space.

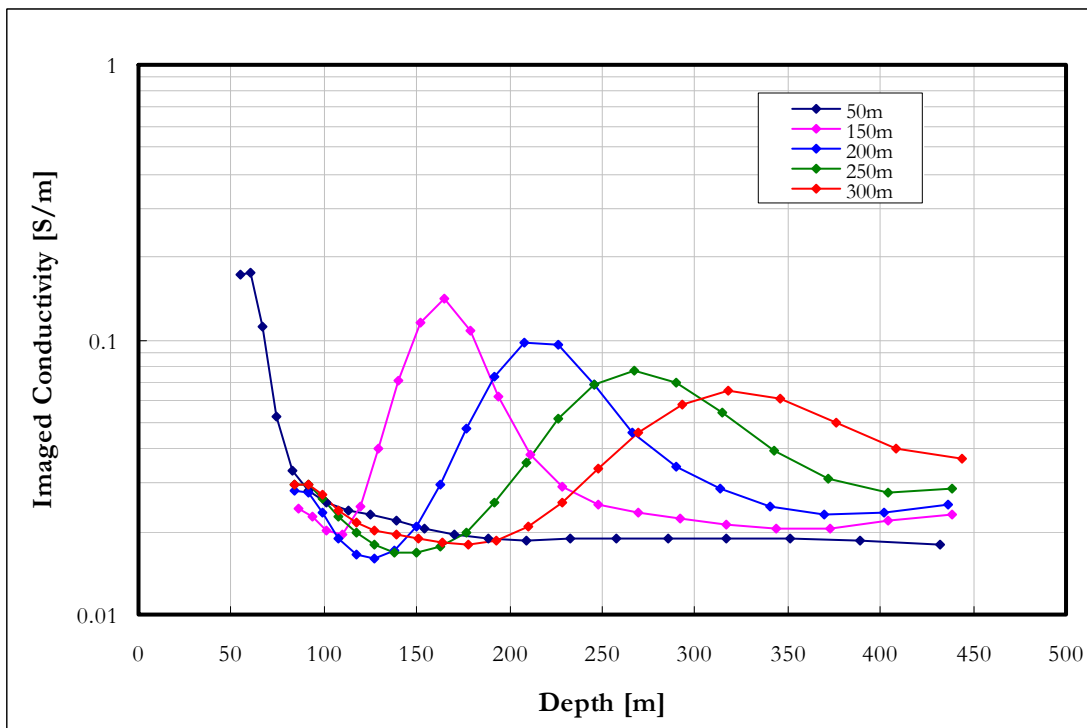


Figure 4-41: Imaged conductivity for a 0.2 S/m layer of 20 m thickness at various depths in a 0.02 S/m half space.

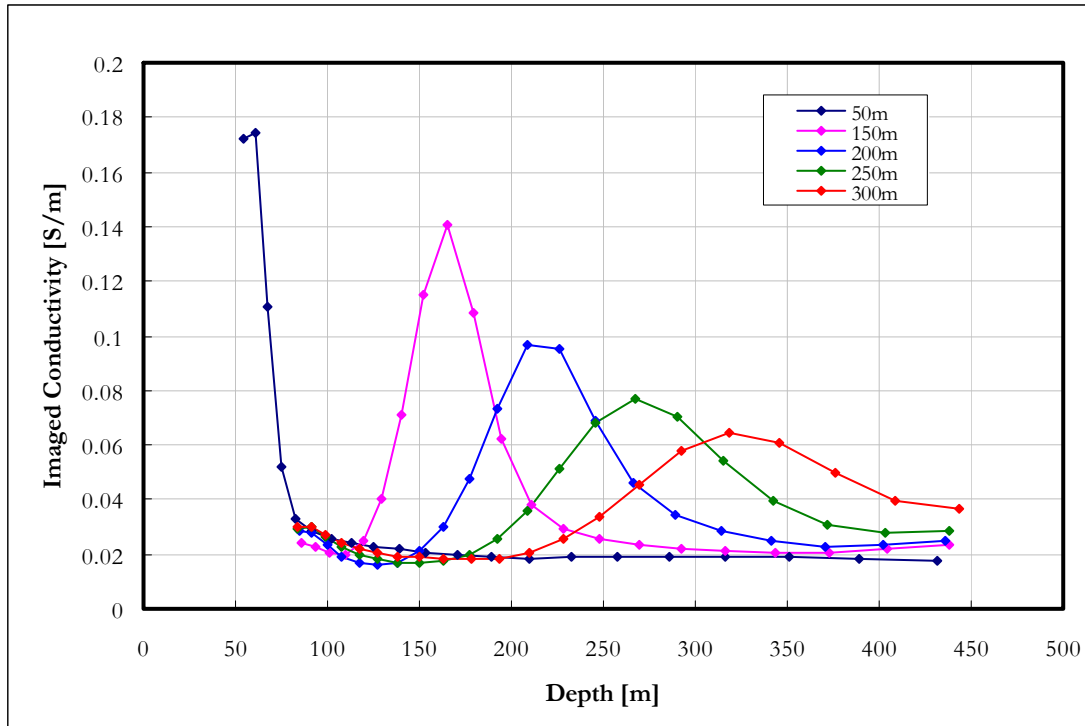


Figure 4-42: Imaged conductivity for a 0.2 S/m layer of 20 m thickness at various depths in a 0.02 S/m half space – linear scale.

The last factor contributing to the thin layer anomaly investigated is the host rock conductivity. A 20 m thick plate having conductivity of 0.2 S/m is modelled at 150 m depth in different host rock environments (Figures 4-43 – 4-45). The behaviour of all the curves is as expected from the previous experiments. High host rock conductivities (resulting in low contrasts) give the bell shaped conductivity function of depth while the high contrast (low host rock conductivity) results in the depth reversal of cumulative conductance plots, although the extent of this reversal is less than for the same contrast in a more conductive host rock. The depth of investigation decrease with increase in host rock conductivity, except for when a conductive layer is situated shallower than the “first channel depth” at which point the depth of investigation is governed by the depth of the conductor (0.01 S/m and less in this case). The imaged conductivities in these examples were calculated after the high contrast effects dissipated, yielding the correct host rock response.

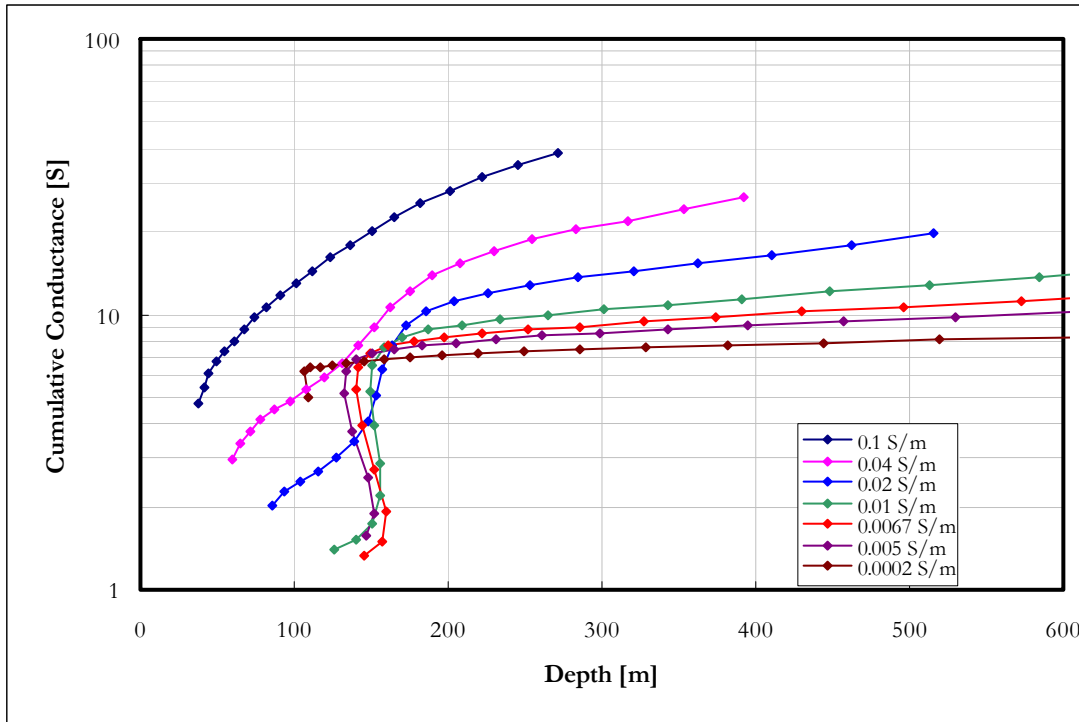


Figure 4-43: Cumulative conductance for a 0.2 S/m layer of 20 m thickness at 150 m depth in various host rock conductivities.

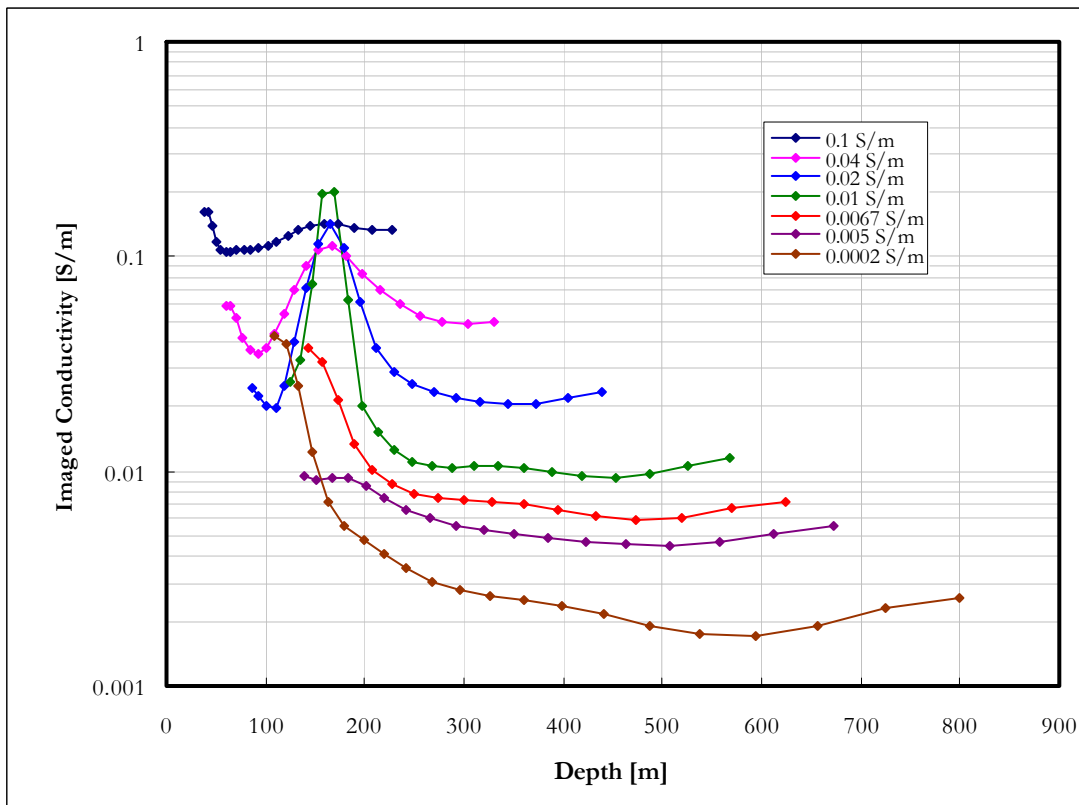


Figure 4-44: Imaged conductivity for a 0.2 S/m layer of 20 m thickness at 150 m depth in various host rock conductivities.

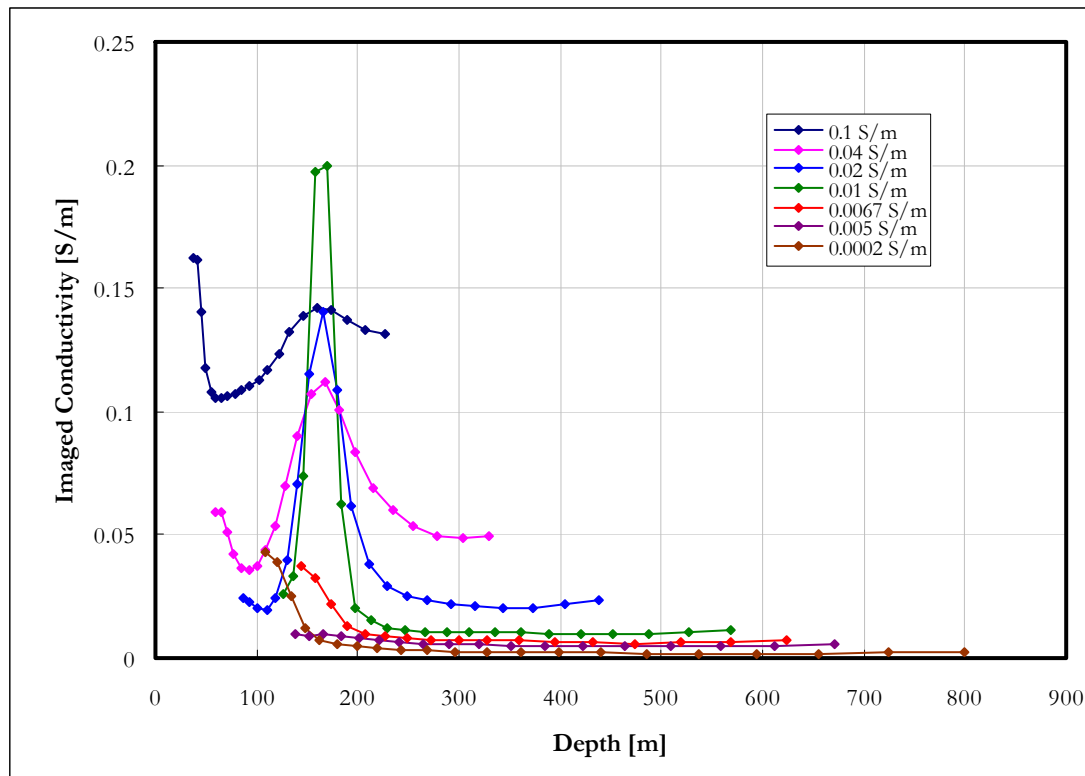


Figure 4-45: Imaged conductivity for a 0.2 S/m layer of 20 m thickness at 150 m depth in various host rock conductivities - linear scale.

Examining the S-layer transform performance in delineating a layered earth provides important insights into the characteristic behaviour and effectiveness of the technique. However, in order to map the subsurface accurately the study has to be extended to bodies with finite dimensions. Conductive, horizontal plates and prisms are modelled and their S-layer transform responses analysed in the following two sections.

4.5.3.5 Conductive, horizontal plates in a half space

The S-layer transform response of conductive horizontal plates with a thickness of 20 m and varying horizontal dimensions are compared to that of the infinite layer. This is done for both the low and high contrast scenarios. The side lengths of the square plates were chosen as 100 m, 200 m, 300 m and 400 m respectively and conductivities of 0.2 S/m and 2 S/m were used in a 0.02 S/m host rock. The low contrast results are shown in Figures 4-46 to 4-48 and the high contrast results in Figures 4-49 to 4-51.

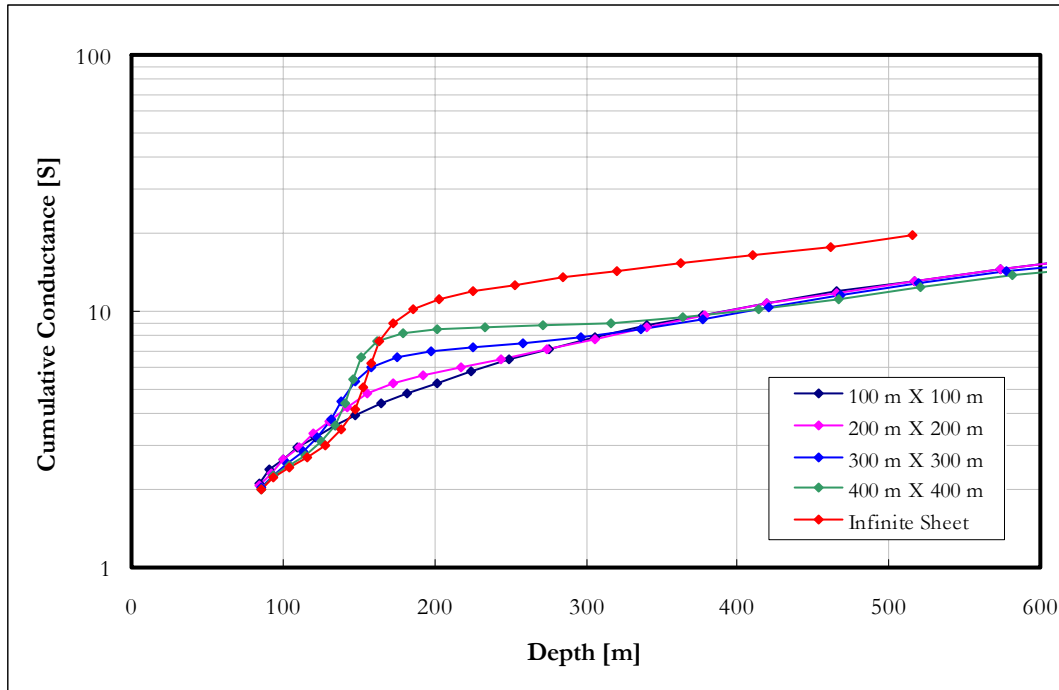


Figure 4-46: Cumulative conductance for a 0.2 S/m plate of 20 m thickness at 150 m depth in 0.02 S/m host rock. The horizontal dimensions vary from 100 m to infinite.

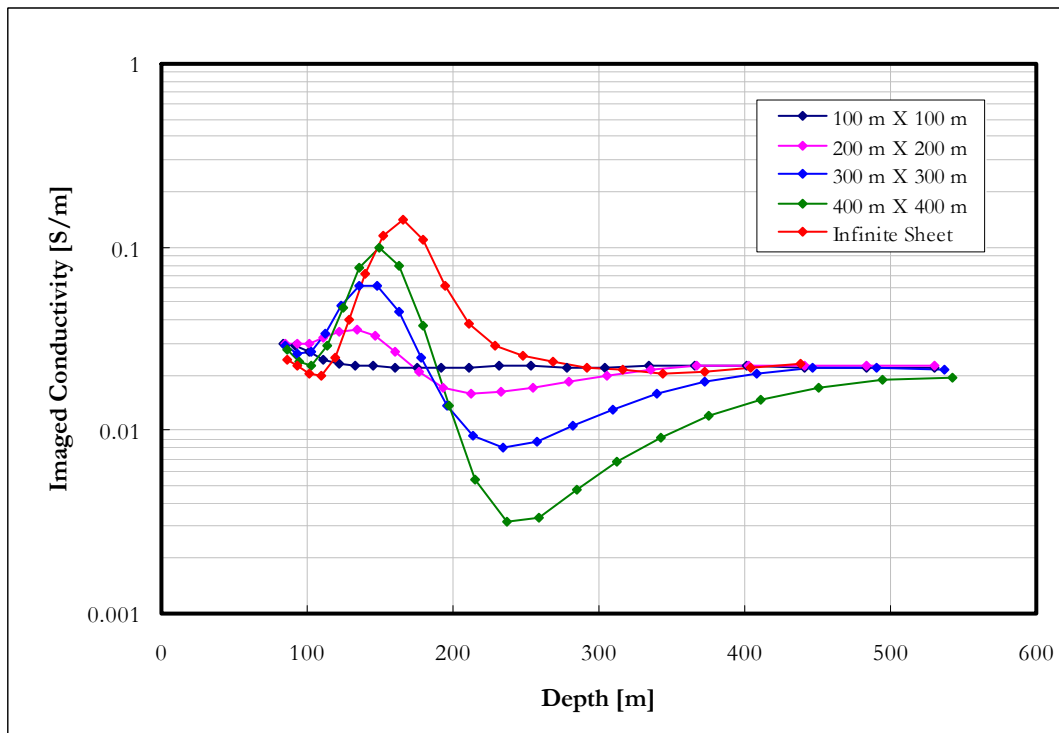


Figure 4-47: Imaged conductivity for a 0.2 S/m plate of 20 m thickness at 150 m depth in 0.02 S/m host rock. The horizontal dimensions vary from 100 m to infinite.

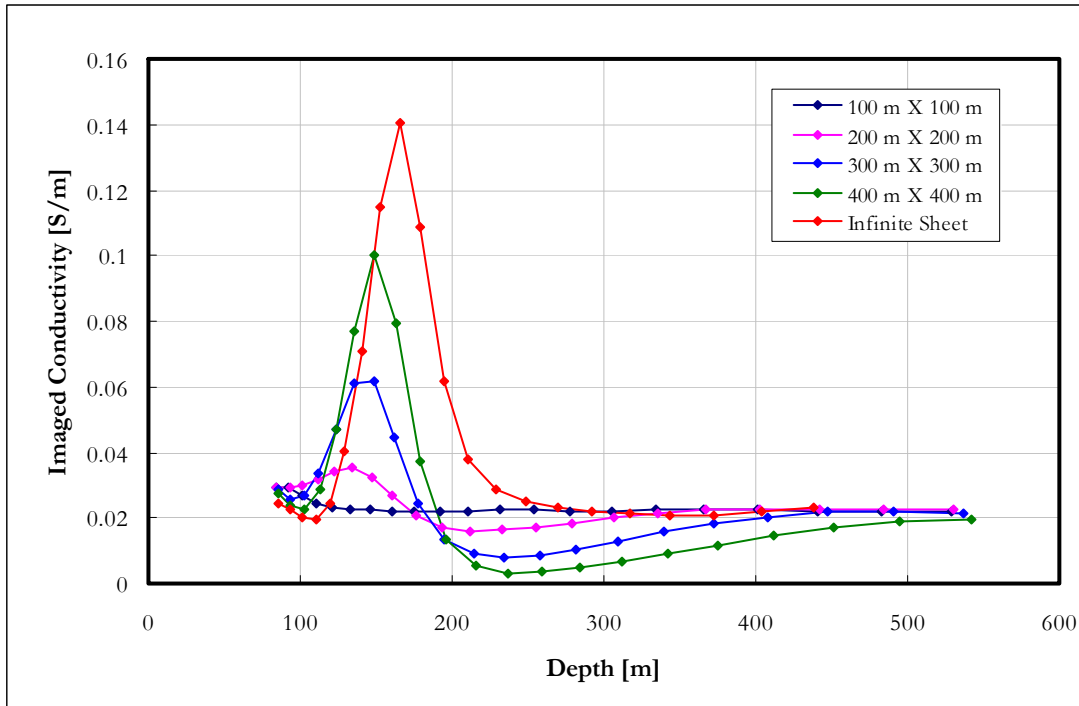


Figure 4-48: Imaged conductivity for a 0.2 S/m plate of 20 m thickness at 150 m depth in 0.02 S/m host rock. The horizontal dimensions vary from 100 m to infinite; linear scale.

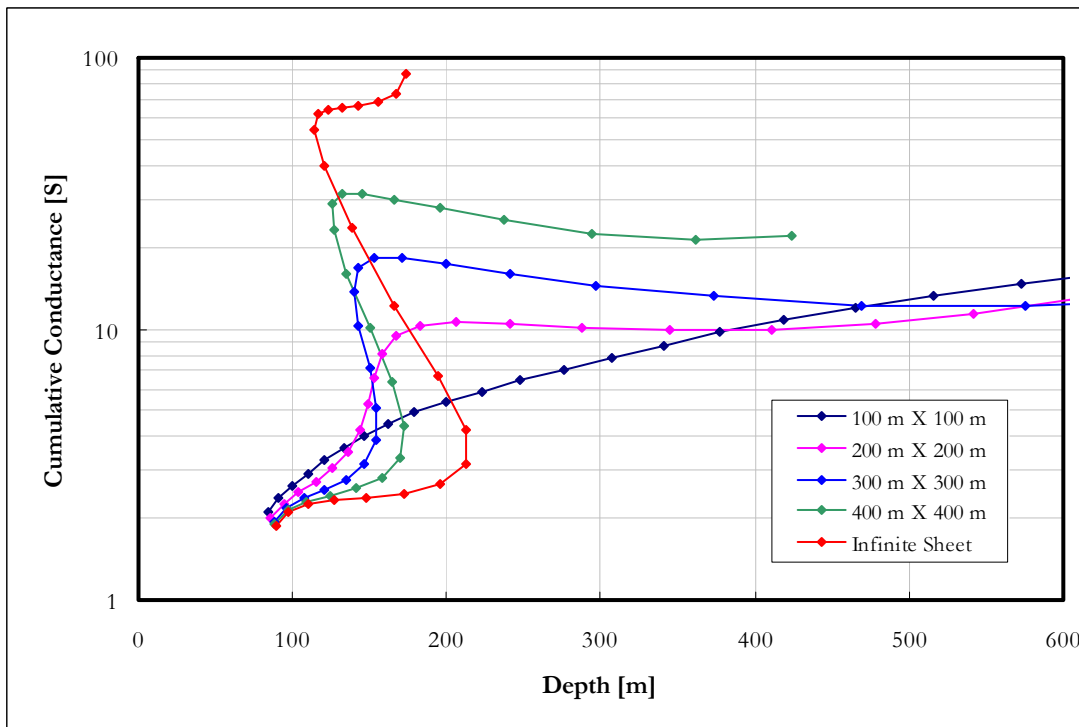


Figure 4-49: Cumulative conductance for a 2 S/m plate of 20 m thickness at 150 m depth in 0.02 S/m host rock. The horizontal dimensions vary from 100 m to infinite.

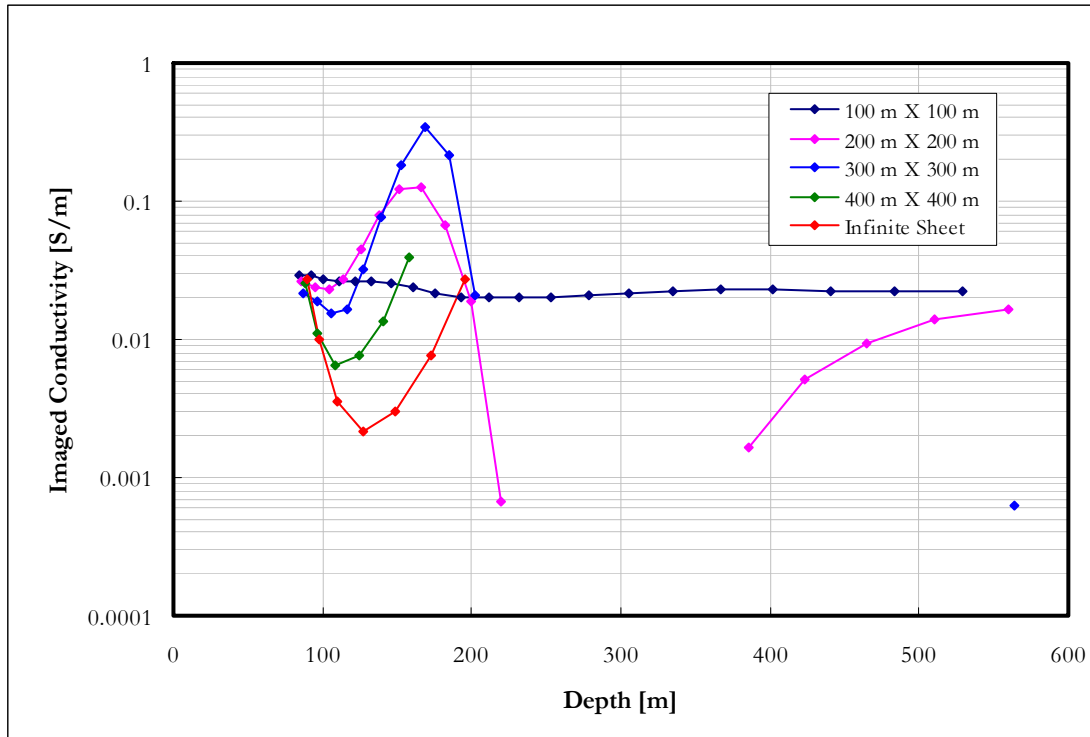


Figure 4-50: Imaged conductivity for a 2 S/m plate of 20 m thickness at 150 m depth in 0.02 S/m host rock. The horizontal dimensions vary from 100 m to infinite.

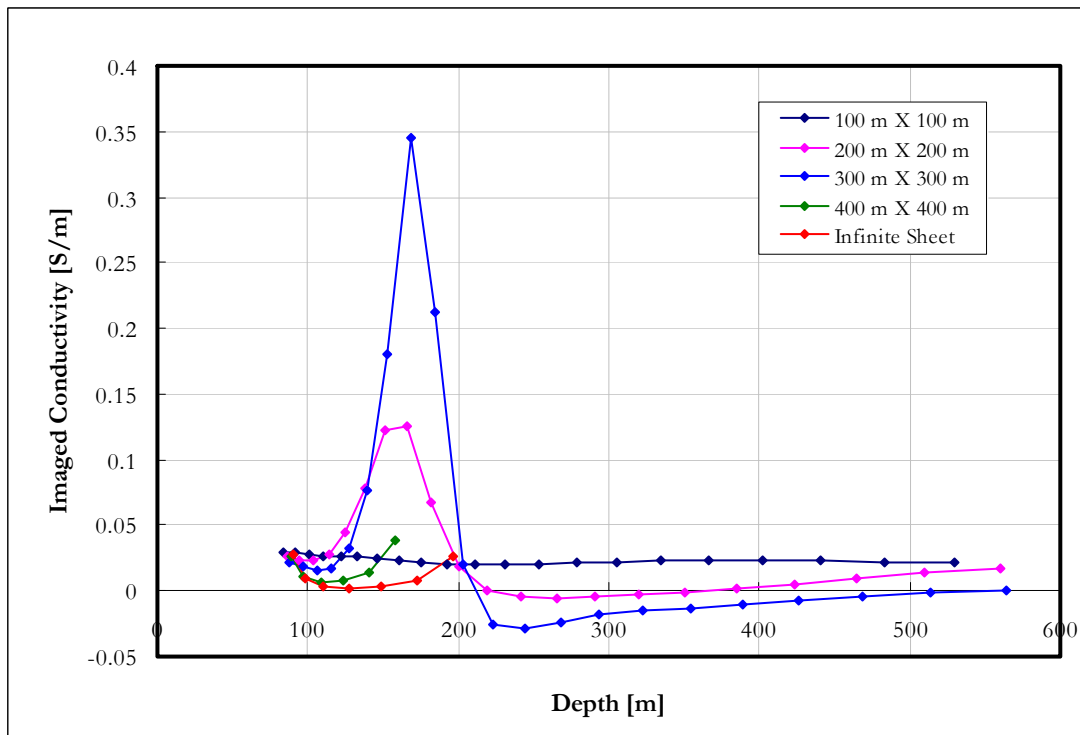


Figure 4-51: Imaged conductivity for a 2 S/m plate of 20 m thickness at 150 m depth in 0.02 S/m host rock. The horizontal dimensions vary from 100 m to infinite; linear scale.

The plates show very similar responses compared to that of the infinite layer. The main differences are that the depths would be underestimated slightly for the smaller plates if the same criteria are used as for the infinite layer and that the finite plates cause “lower than background” imaged conductivity anomalies after the peak values, reaching negative values in the high contrast cases. This behaviour is due to a reduction in cumulative conductance values and not a reduction in depth as was found for high contrast boundaries. It is therefore important to distinguish between the reasons causing negative imaged conductivities as these contain important information on the subsurface conductivity structure.

4.5.3.6 Conductive prisms in a half space

The effect of thicknesses in the same order as horizontal dimensions is investigated in this section. The same sizes and conductivities are used as for the horizontal plates. Results for the low contrast models are shown in Figures 4-52 to 4-54.

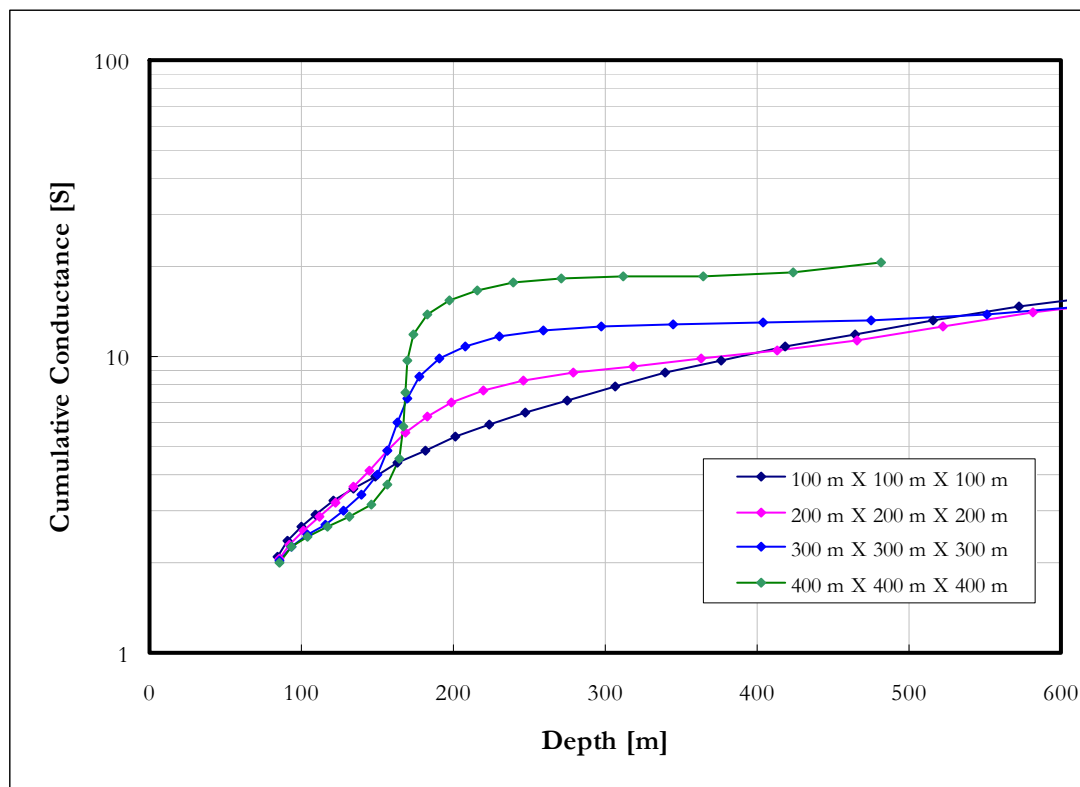


Figure 4-52: Cumulative conductance for a 0.2 S/m prism at 150 m depth in a 0.02 S/m host rock. The prism dimensions vary from 100 m to 400 m.

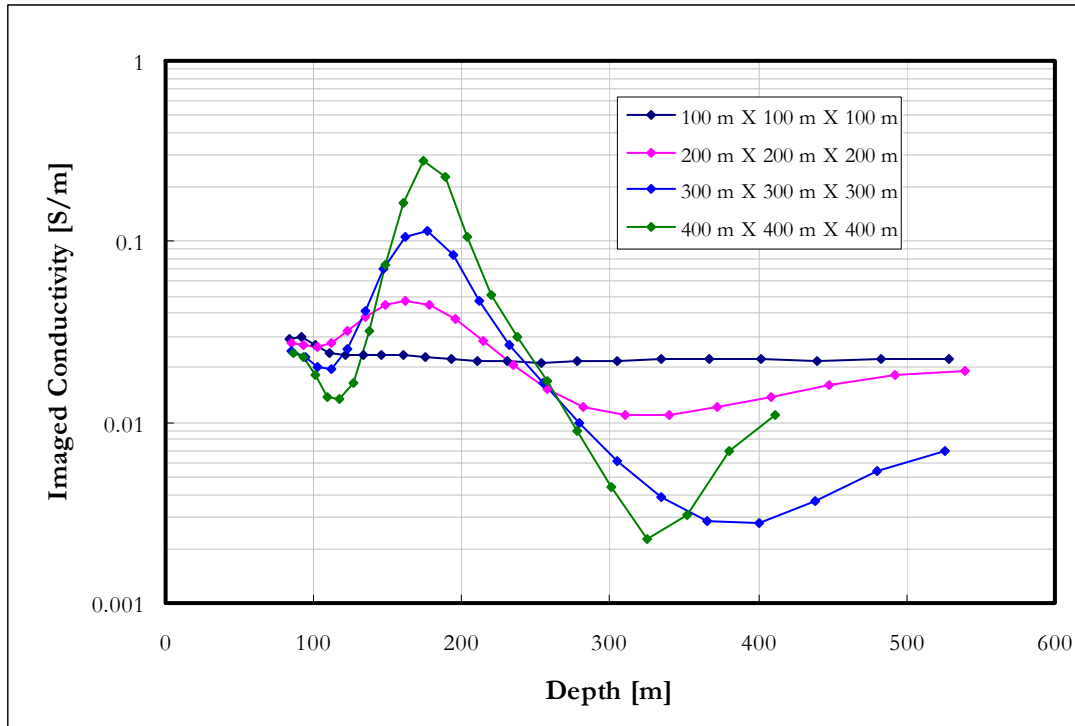


Figure 4-53: Imaged conductivity for a 0.2 S/m prism at 150 m depth in a 0.02 S/m host rock. The prism dimensions vary from 100 m to 400 m.

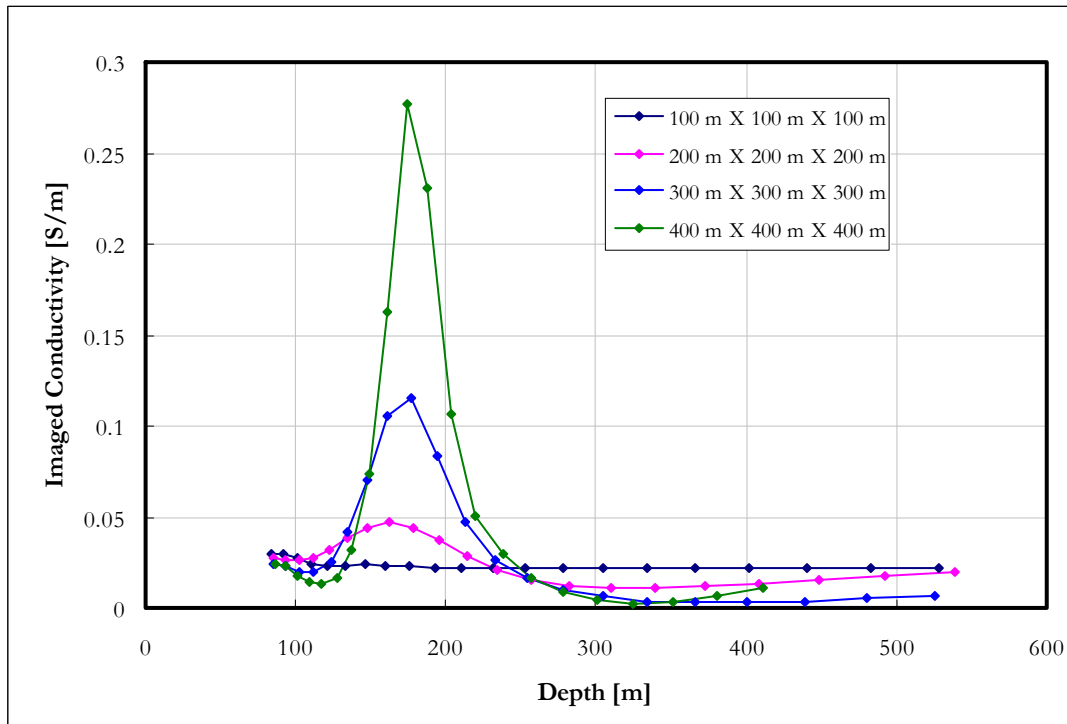


Figure 4-54: Imaged conductivity for a 0.2 S/m prism at 150 m depth in a 0.02 S/m host rock. The prism dimensions vary from 100 m to 400 m; linear scale.

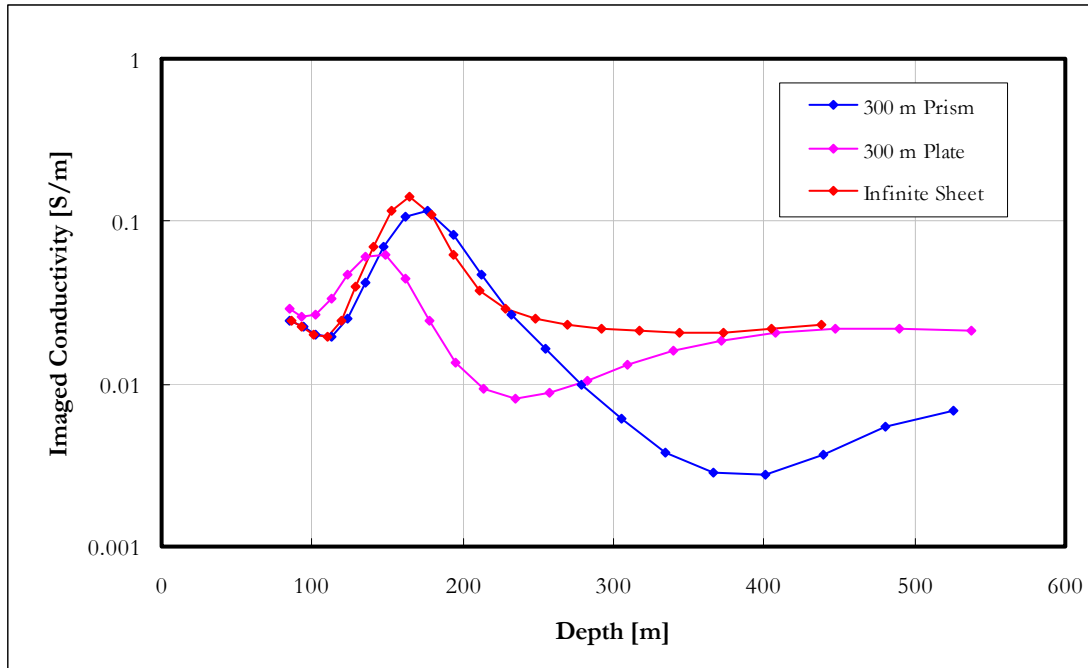


Figure 4-55: Comparison between imaged conductivities of a 0.2 S/m prism, 20 m thick plate and infinite sheet of 20 m thickness at 150 m depth in a 0.02 S/m host rock. Both the plate and prism have horizontal dimensions of 300 m.

Figure 4-55 shows a comparison of the infinite sheet, thin plate and prism responses. Compared to the plates, the prisms are imaged with higher conductivity values and depths and actually come very close to the infinite sheet model except for the lower conductivity values following the main positive peak. Responses obtained from prisms with a high conductivity contrast to the host rock are presented in Figures 4-56 to 4-59. Similar patterns are observed as with the low contrast case. However, the decreasing depth associated with high contrasts is visible on the 300 m prism but not the 300 m plate. Also, the high contrast prisms do not match the high contrast infinite sheet as closely as with the low contrast models.

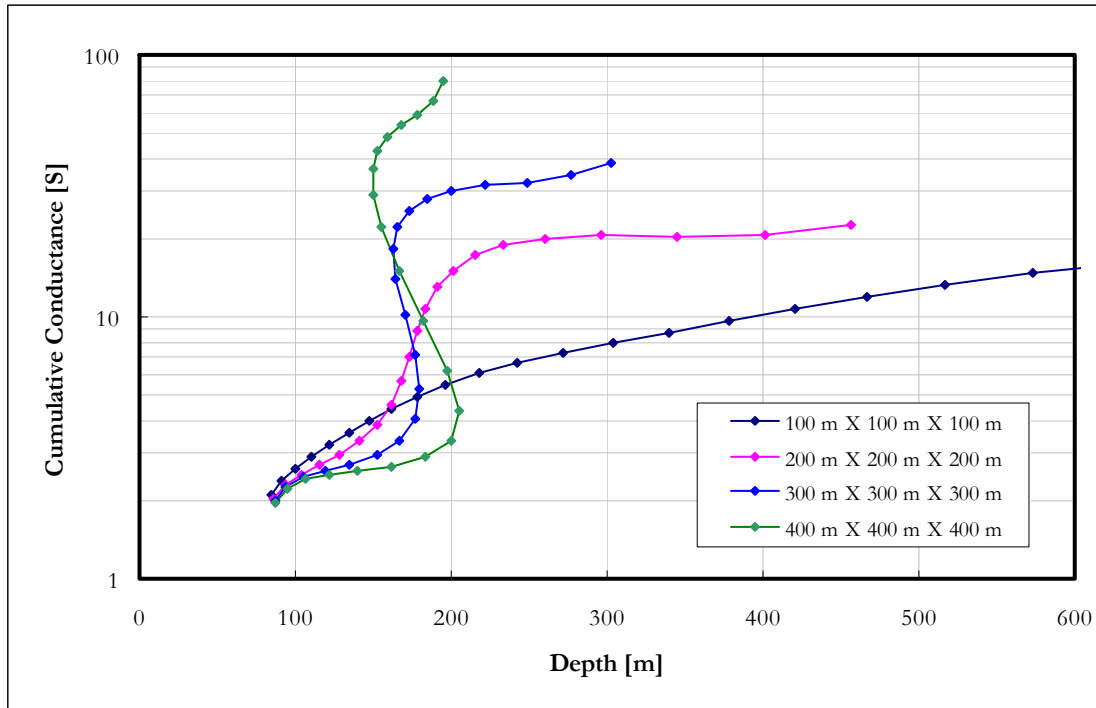


Figure 4-56: Cumulative conductance for 2 S/m prisms at 150 m depth in a 0.02 S/m host rock. The prism dimensions vary from 100 m to 400 m.

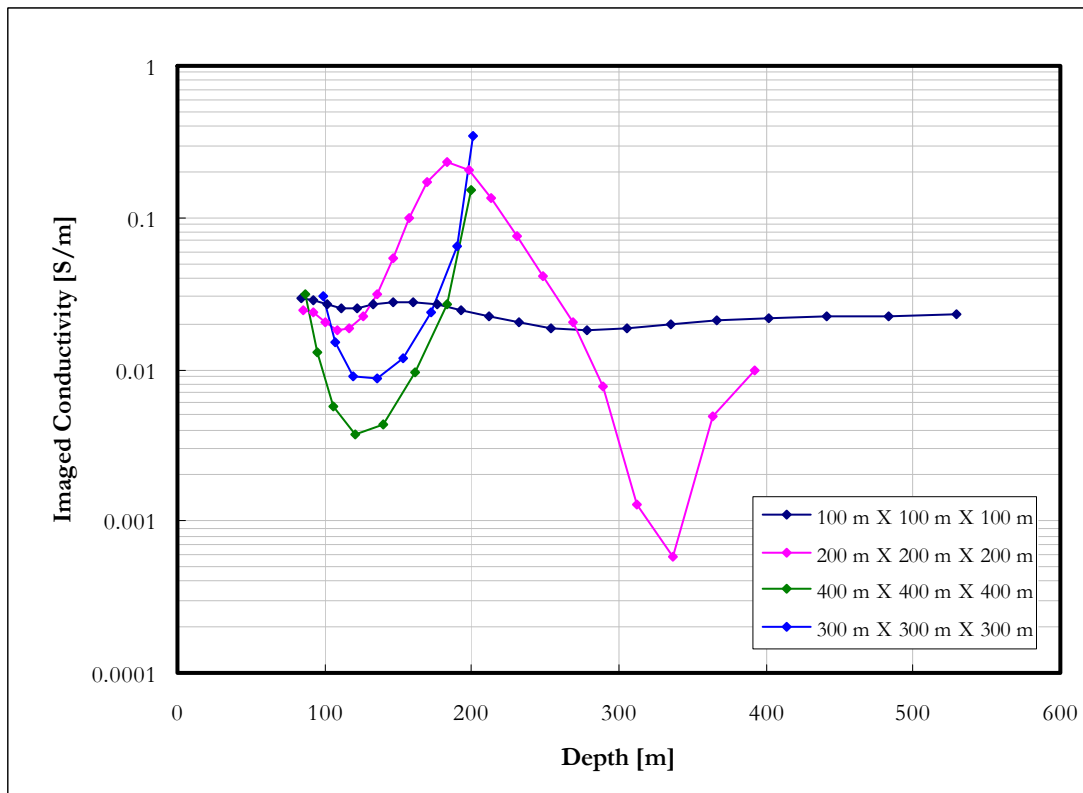


Figure 4-57: Imaged conductivity for 2 S/m prisms at 150 m depth in a 0.02 S/m host rock. The prism dimensions vary from 100 m to 400 m.

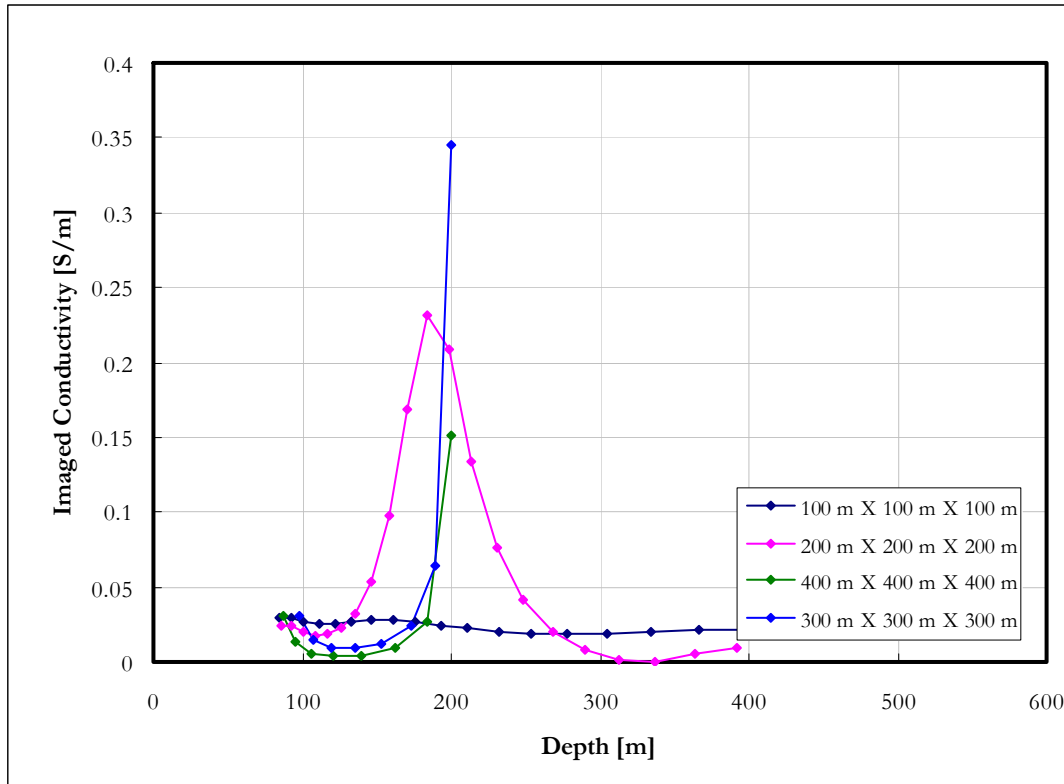


Figure 4-58: Imaged conductivity for 2 S/m prisms at 150 m depth in a 0.02 S/m host rock. The prism dimensions vary from 100 m to 400 m; linear scale.

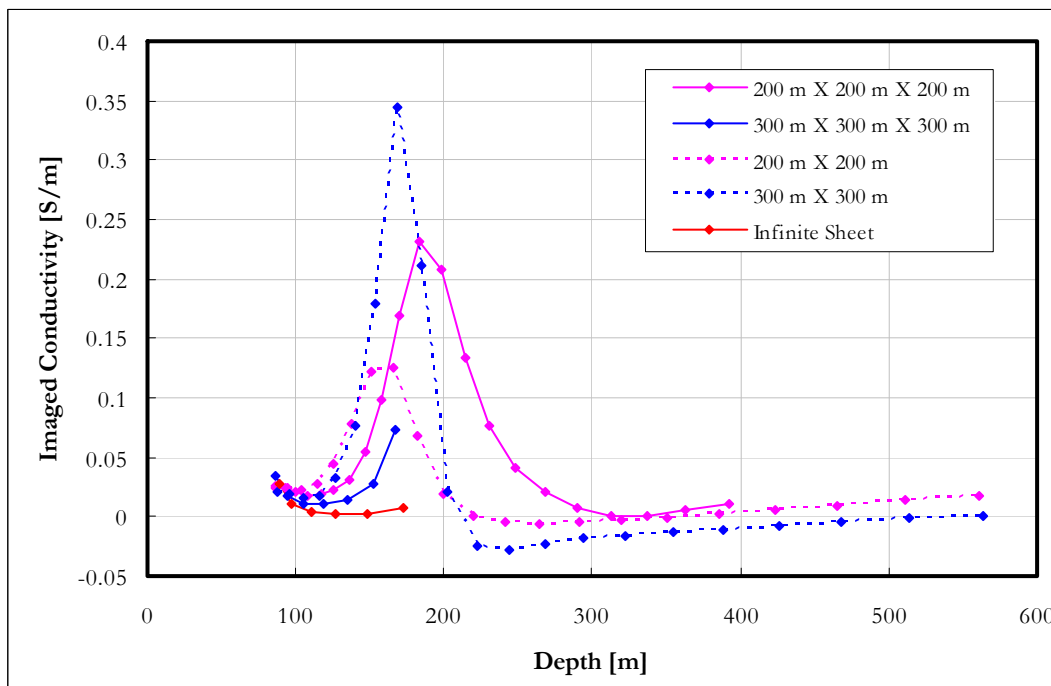


Figure 4-59: Comparison between imaged conductivities of 2 S/m prisms, 20 m thick plates and infinite sheet of 20 m thickness at 150 m depth in a 0.02 S/m host rock. Plates and prisms with horizontal dimensions of 200 m and 300 m are shown.

4.5.4 S-layer differential transform compatibility filter

The “returning smoke ring” behaviour illustrated in high conductivity contrast scenarios in 1.3 can also be observed in field data (Figure 4-60).

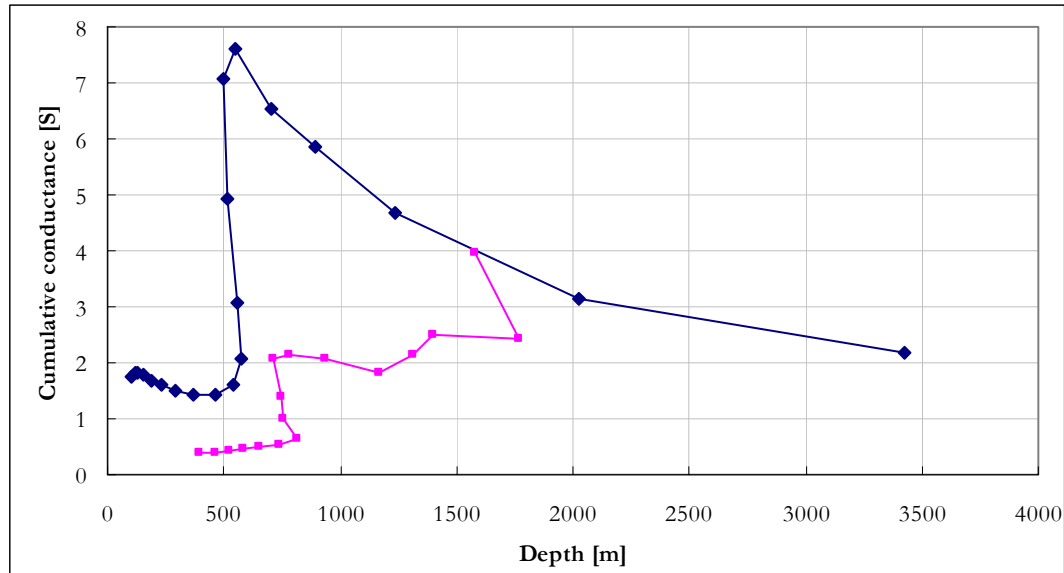


Figure 4-60: Examples of field data showing "returning smoke ring" behaviour (stations -1200 and -150 from line 4950, Rosh Pinah data set).

Only data conforming to the S-layer differential transform assumption of a monotonously increasing cumulative conductance curve can successfully be processed with this algorithm. A filter is therefore designed to only allow data compatible with the transform assumptions to be processed. This filter discards all data after the first point where a decrease in depth with an increase in channel number is observed. It also tests for unrealistic increases in conductance values which sometimes precedes the decreasing depth behaviour. Specifically, this is implemented as follows.

Step 1: Find the first data point conforming to S-layer late time behaviour.

For each sounding data values are analysed until the first three data points are found which conform to:

$$d[i-1] < d[i] < d[i+1] \quad \text{AND}$$

$$\text{abs}((S[i] - S[i-1]) / S[i]) < 1 \quad \text{AND}$$

$$\text{abs}((S[i] - S[i+1]) / S[i]) < 1.$$

The first data point passed through the filter is $(d[i-1], S[i-1])$.

Step 2: Find the first following data point not conforming to S-layer late time behaviour.

Apply the same conditions as in step 1, but look for the first point NOT satisfying these. The last point passed through the filter is then $(d[i], S[i])$.

The value of “1” chosen in conditions (b) and (c) is chosen based on empirical analysis of the case history 1 data set consisting of 1500 soundings over both resistive and conductive terrain. It is chosen to rather pass values that may be too high (resulting in excessively high conductivities) because these can always be filtered out at a later stage in the conductivity grids. Following this approach means that conductors will not be filtered out, and at worst will be assigned exaggerated conductivities. It has already been shown in the previous section that conductivities are normally underestimated by the algorithm and that the actual numeric values of conductivity should not be taken as the absolute truth especially for confined conductors. The value of this algorithm is in the identification and location of subsurface conductors and is not promoted as a complete and final interpretation tool.

4.5.5 Imaged conductivity depth sections generated from synthetic data

The final product of the algorithm as described in this chapter is illustrated in Figures 4-61 and 4-62 for six synthetic models. In Figure 4-61 it is important to note the migration effects similar to seismic data for vertical plates and low contrast conductors. It is produced for the same reason of applying one-dimensional assumptions to three-dimensional data; i.e. plotting all data below the point where it was measured. Migration routines similar to those found in seismic processing can be developed to correct for this but falls outside the scope of this study. High conductivity contrasts of the horizontal plate and prism result in data not conforming to the S-layer differential transform assumptions and are filtered out – resulting in white areas underneath these conductors. It is clear from the low contrast data as well that the lower boundaries of confined conductors are not resolved by this algorithm and that the apparent loss of data underneath conductors is in fact a useful tool indicating high conductivity contrasts.

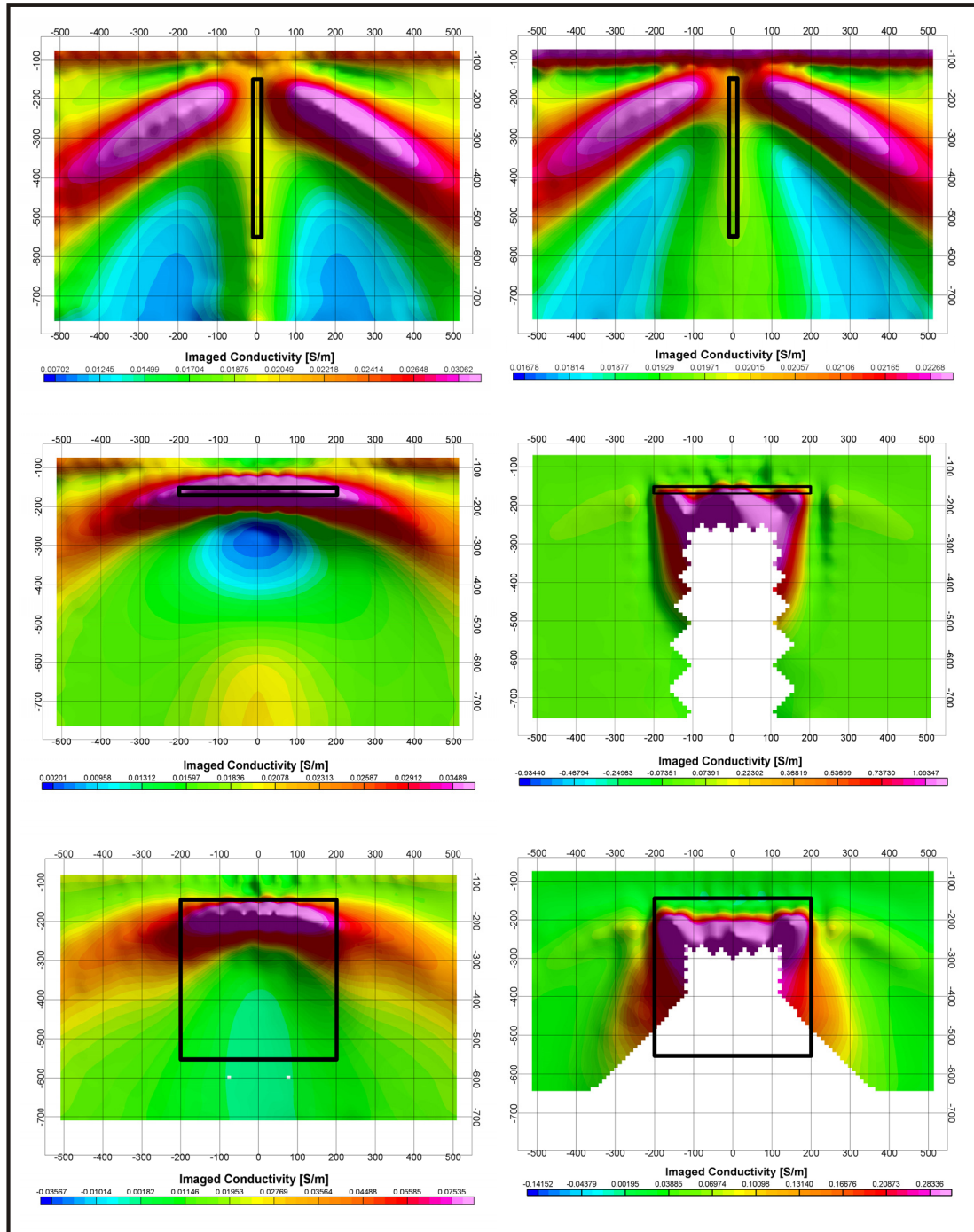


Figure 4-61: S-layer differential transform results (conductivity depth section) on synthetic data.
Top: Thin vertical plate (400m X 400m X 20m)
Middle: Thin horizontal plate (400m X 400m X 20m)
Bottom: Prism (400m X 400m X 400m).
Left hand side are low contrast scenarios (0.2 S.m⁻¹ conductor in 0.02 S.m⁻¹ half space). Right hand side are high contrast scenarios (2 S.m⁻¹ conductor in 0.02 S.m⁻¹ half space).

In Figure 4-62 the decay curve analyses are superimposed on the conductivity-depth sections. Each dot represents a channel which shows the indicated decay behaviour.

Channels are scaled so that channel 1 corresponds with the top of the section and channel 20 to the bottom. Note the half space (-2.5) decay that is observed on all models at some stage. Although conductors are present the conductive nature of the half space itself causes the dominant decay to be that of -2.5 as mentioned by Singh (1973) and discussed in 2.3.4. Only the high contrast horizontal plate shows finite conductor decay in the late time. Automated decay constant analyses should be applied with great care if the half space response has not been removed from data in a conductive host rock environment. It is clear that under these conditions the S-layer differential transform is a more effective way of determining the presence and locality of conductive bodies

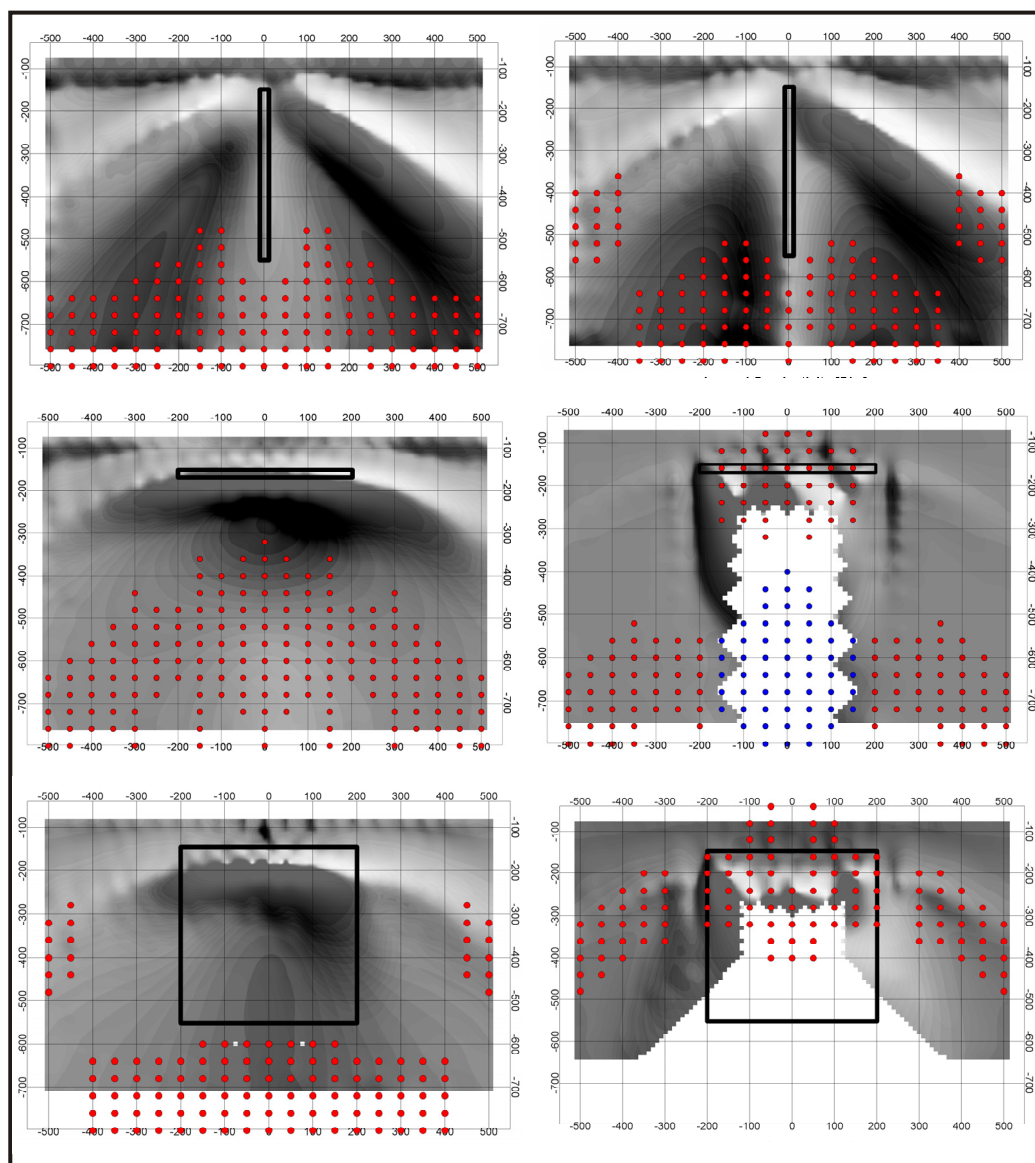


Figure 4-62: Same models as in Figure 4-63. Red dots indicate half space decay behaviour and blue dots indicate conductor in “free air” decay.

Table 2: Summary of S-layer differential transform performance on synthetic models. (h = thickness, d =depth, l= side length of square plate and prisms)

Model	Cumulative Conductance vs depth	Imaged Conductivity vs depth	Comments
Half space $\sigma = 0.02 \text{ S/m}$	Smoothly increasing with depth	Good approximation (12% error) to true conductivity in “late time”	
Two Layers $\sigma_1 = 0.02 \text{ S/m}$ $\sigma_2 = 0.002 \text{ S/m}$ $h_1 = 200 \text{ m}$	Smoothly increasing with depth, layer boundary clearly defined	Show decreasing trend with depth; values close to true conductivity; layer boundary not clearly defined	Decreasing conductivity, low contrast
Two Layers $\sigma_1 = 0.02 \text{ S/m}$ $\sigma_2 = 0.0002 \text{ S/m}$ $h_1 = 200 \text{ m}$	Smoothly increasing with depth, layer boundary clearly defined	Show decreasing trend with depth; second layer values not close to true conductivity; layer boundary not clearly defined	Decreasing conductivity, high contrast
Two Layers $\sigma_1 = 0.02 \text{ S/m}$ $\sigma_2 = 0.2 \text{ S/m}$ $h_1 = 200 \text{ m}$	Smoothly increasing with depth, layer boundary not clearly defined	Show increasing trend with depth (except for early time); values close to true conductivity for first layer only; layer boundary defined as “first increase” in conductivity, especially on linear scale	Increasing conductivity, low contrast
Two Layers $\sigma_1 = 0.02 \text{ S/m}$ $\sigma_2 = 2 \text{ S/m}$ $h_1 = 200 \text{ m}$	Decreasing depths with increasing times, layer boundary not clearly defined	Show increasing trend with depth (except for early time); values close to true conductivity for first layer only; layer boundary defined as “first increase” in conductivity, especially on linear scale; negative conductivities calculated	Increasing conductivity, high contrast “Reflecting smoke-ring” behaviour
Conductive layer in half space (varying σ contrast) $\sigma_{\text{HS}} = 0.02 \text{ S/m}$ $\sigma_{\text{Layer}} = 0.04 \text{ S/m}$ and	Smoothly increasing with depth	Resolve layer position well but with underestimation of conductivity values.	Low contrast

$\sigma_{\text{Layer}} = 0.2 \text{ S/m}$ $d_{\text{Layer}} = 150 \text{ m}$ $h_{\text{Layer}} = 15 \text{ m}$			
Conductive layer in half space (varying σ contrast) $\sigma_{\text{HS}} = 0.02 \text{ S/m}$ $\sigma_{\text{Layer}} = 2 \text{ S/m}$ and $\sigma_{\text{Layer}} = 10 \text{ S/m}$ $d_{\text{Layer}} = 150 \text{ m}$ $h_{\text{Layer}} = 15 \text{ m}$	Decreasing depths with increasing times	Layer depth overestimated proportional to contrast; initial decrease of conductivity before increasing to sometimes erroneously high values.	High contrast
Conductive layer in half space (varying thickness) $\sigma_{\text{HS}} = 0.02 \text{ S/m}$ $\sigma_{\text{Layer}} = 0.2 \text{ S/m}$ $d_{\text{Layer}} = 150 \text{ m}$ $h_{\text{Layer}} = 2 \text{ m}, 5 \text{ m}, 10 \text{ m}, 15 \text{ m}, 20 \text{ m}, 50 \text{ m}$ and 100 m	Change in curve characteristic for 50m and 100m thickness.	2m to 20m see similar graphs except for increase in maximum conductivity values with well defined top of layer; 50m and 100m thickness gives overestimation of depth proportional to thickness.	Low contrast behaviour (increasing depths mapped with increasing time) remains even if conductivity-thickness product becomes very large
Conductive layer in half space (varying thickness) $\sigma_{\text{HS}} = 0.02 \text{ S/m}$ $\sigma_{\text{Layer}} = 2 \text{ S/m}$ $d_{\text{Layer}} = 150 \text{ m}$ $h_{\text{Layer}} = 2 \text{ m}, 5 \text{ m}, 10 \text{ m}, 15 \text{ m}, 20 \text{ m}$	Thicknesses more than 2m exhibit decreasing depths with increasing time.	Overestimation of depths for 10m and thicker proportional to thickness.	High contrast. The thicker the layer becomes, the closer the curves resemble the two layer case with very little or no influence from the earth below the conductive layer contributing to the signal.
Conductive layer in half space (varying depth) $\sigma_{\text{HS}} = 0.02 \text{ S/m}$ $\sigma_{\text{Layer}} = 0.2 \text{ S/m}$ $d_{\text{Layer}} = 50 \text{ m}, 150 \text{ m},$	Smoothly increasing with depth. 50m shows anomalous behaviour (see comment)	Width of the anomaly increases proportional to depth while the amplitude decreases. Maxima slightly deeper than layer top boundary.	Low contrast. Conductive layers shallower than “first channel expected depth for host rock” maps at correct depth but with slightly distorted curves –

200 m, 250 m, 300 m $h_{\text{Layer}} = 20 \text{ m}$			can be mistaken for two layer earth.
Conductive layer in half space (varying host rock cond.) $\sigma_{\text{HS}} = 0.0002 \text{ S/m}, 0.005 \text{ S/m}, 0.0067 \text{ S/m}, 0.01 \text{ S/m}, 0.02 \text{ S/m}, 0.04 \text{ S/m}$ and 0.1 S/m . $\sigma_{\text{Layer}} = 0.2 \text{ S/m}$ $d_{\text{Layer}} = 150 \text{ m}$ $h_{\text{Layer}} = 20 \text{ m}$	Host rock conductivities $< 0.01 \text{ S/m}$ results in the depths decreasing with time of cumulative conductance plots, although the extent of this reversal is less than for the same contrast in a more conductive host rock.	Depth of investigation determined by host rock conductivity or shallower-than-first-channel-depth	Higher host rock conductivities cause more severe “non-late-time” distortions in early channels.
Conductive horizontal plate in half space (varying hor. dimensions) $\sigma_{\text{HS}} = 0.02 \text{ S/m}$ $\sigma_{\text{Plate}} = 0.2 \text{ S/m}$ $l_{\text{Plate}} = 100 \text{ m}, 200 \text{ m}, 300 \text{ m}, 400 \text{ m}$ $d_{\text{Plate}} = 150 \text{ m}$ $h_{\text{Plate}} = 20 \text{ m}$	Smoothly increasing with depth. 100m too small to resolve with current parameters.	Depths are slightly underestimated proportional to side length of plates; underestimation of conductivities just below plates.	Low contrast.
Conductive horizontal plate in half space (varying hor. dimensions) $\sigma_{\text{HS}} = 0.02 \text{ S/m}$ $\sigma_{\text{Plate}} = 2 \text{ S/m}$ $l_{\text{Plate}} = 100 \text{ m}, 200 \text{ m}, 300 \text{ m}, 400 \text{ m}$ $d_{\text{Plate}} = 150 \text{ m}$ $h_{\text{Plate}} = 20 \text{ m}$	300m and larger side lengths produce decreasing depths with increasing times. 100m too small to resolve.	100m and 200m side lengths give negative conductivities below plates.	High contrast. Second instance when negative conductivities can be calculated.
Conductive prism in half space (varying dimensions) $\sigma_{\text{HS}} = 0.02 \text{ S/m}$	Smoothly increasing with depth. 100m too small to resolve.	Depth to top and conductivity values resolved better than thin plates.	Low contrast. 300m and larger dimensions resemble infinite layer apart from underestimation of

$\sigma_{\text{Plate}} = 0.2 \text{ S/m}$ $l_{\text{Plate}} = 100 \text{ m}, 200 \text{ m}, 300 \text{ m}, 400 \text{ m}$ $d_{\text{Plate}} = 150 \text{ m}$			conductivities below prism.
Conductive prism in half space (varying hor. dimensions) $\sigma_{\text{HS}} = 0.02 \text{ S/m}$ $\sigma_{\text{Plate}} = 2 \text{ S/m}$ $l_{\text{Plate}} = 100 \text{ m}, 200 \text{ m}, 300 \text{ m}, 400 \text{ m}$ $d_{\text{Plate}} = 150 \text{ m}$	100m still not resolved. Decreasing depth with increasing time for 300m and 400m prisms.	Behaviour similar to infinite high contrast plates with overestimation of depths and negative conductivities below prisms.	High contrast.

In general the S-layer differential transform performs more reliably in low contrast environments although the “decreasing depth with increasing time” behaviour serves as a very important indicator of high contrast conductors. Keeping in mind that depths will be overestimated in this event (and underestimated for conductors with dimensions less than 300m) still allows the results to be interpreted accurately for the presence of a conductor even if there are constraints on the accuracy of depth to top in some cases. The depth to bottom cannot be determined from this algorithm. Imaged conductivities approach true conductivities for very thick layers (half space and two layer case) but this is not the case for confined conductors. However, the imaged conductivity behaviour can be used successfully to indicate “lower”, “higher” and “much higher” conductivities. Negative conductivities should not be just be discarded as invalid as it can be indicative of small confined conductors at shallower depths as well as the presence of high contrast conductors. In fact, the exact cause of negative conductivities for every instance can be found by inspection of the cumulative conductance curves if needed.

Chapter 5

5 APPLICATION TO FIELD DATA

"The bitterness of low quality remains long after the sweetness of low price is long forgotten."

(Benjamin Franklin, 1706-1790)

5.1 Introduction

This chapter contains results of S-layer differential transform applied to two data sets, one from a ground survey and one from an airborne survey. The ground survey covers an area of roughly 2km by 6km at low resolution (50m or 100m station spacing) with the intent to identify locations of conductors for follow-up work. The airborne data consists of a very high resolution (3m station spacing on average) line over an easily recognizable conductor and the purpose is to determine the depth and orientation of this body. Both survey geometries conformed to the central loop sounding configuration.

5.2 Ground survey

5.2.1 Data acquisition and system parameters

The data used were acquired in a sedimentary environment which has undergone various metamorphic events resulting in complex structural features. A TDEM in-loop survey was done across a mountain (Figure 5-1). The data acquisition was done under extreme field conditions. The station- and line-spacing varied across the survey area (mostly 100m line- and 50m station spacing). The grid that was surveyed is given in Figure 5-2. A total of 1543 stations were surveyed. At each station both the high and medium frequencies were utilized on the transmitter. The survey was done using a GEONICS EM57 transmitter and PROTEM receiver with a single component receiver coil. Parameters used for the survey are:

Frequency: 25 and 6.25Hz

Transmitter Loop Area: Single Turn 100x100m

Transmitter current: 14.5 A

Component: Vertical (z)

Synchronization: Reference cable.

Power Supply: 1,000W 110/220V, 50/60 (Hz single-phase motor-generator)

Current Waveform: Bipolar rectangular current with 50% duty cycle

Effective surface area of receiver coil: 100m²

Receiver Size: 34 x 38 x 27 cm



Figure 5-1: Mountain with TDEM survey team.

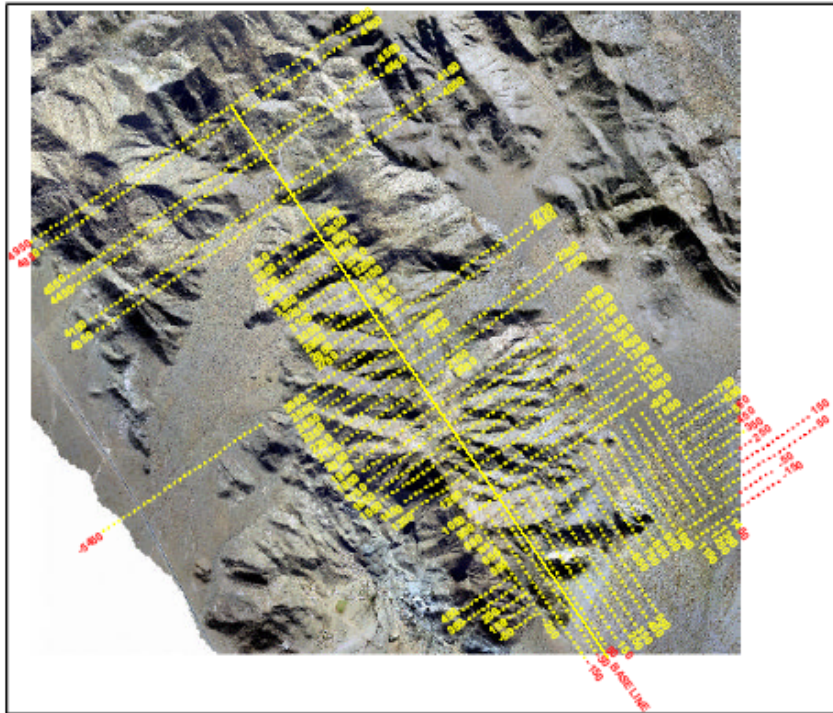


Figure 5-2: Grid locality and layout.

5.2.2 Objective

Based on the TDEM and other investigations (including geochemical and structural geological interpretations) some exploration boreholes were drilled and follow-up borehole TDEM surveys were done. This chapter is not intended to be a discussion of the exploration program or to propose a geological model for the area. The TDEM data acquired during this project are used to illustrate the performance of the S-layer differential transform under extremely challenging geological and topographical conditions.

5.2.3 Application of S-layer differential transform

The main challenge of applying an automated processing sequence to field data is noise. Even though system parameters can be chosen (McNeill, 1995) to optimise the signal to noise ratio, there will always be some stations in a large data set not conforming to the ideal TDEM decay behaviour. This can be due to random atmospheric noise, cultural

noise or geological noise. Whatever the cause, noise in data will produce noise in the processed product and in extreme cases may even cause a technique to fail. The S-layer differential transform is especially sensitive to noise because of the numerical differentiations performed. In addition to the optimal smoothing of data (chapter 4) a filter is also applied to *remove* noisy data points from each sounding before the transform is applied. Noise in a sounding curve is easily recognised through visual inspection of data, especially if presented in the logarithmic domain, by the sometimes random decay behaviour of the later time channels. A filter mimicking this visual inspection is achieved by computing the straight line regression coefficients for trios of data points starting from the last three channels and working back to the front. When the regression coefficient is larger than a specified value (0.997 default) it means that data conform to late time decay behaviour. (This test is performed in both the logarithmic and semi-logarithmic domains.) All data points after this channel are discarded as noise. Supplementary to that, the first appropriate positive data value is chosen as the first point for each sounding. This is done to negate the effect of sign changes sometimes manifesting in the early channels. Examples of the application of this filter as well as the “S-layer differential transform compatibility” (SDTC) filter (section 4.4.4) are shown in Figures 5-3 to 5-7.

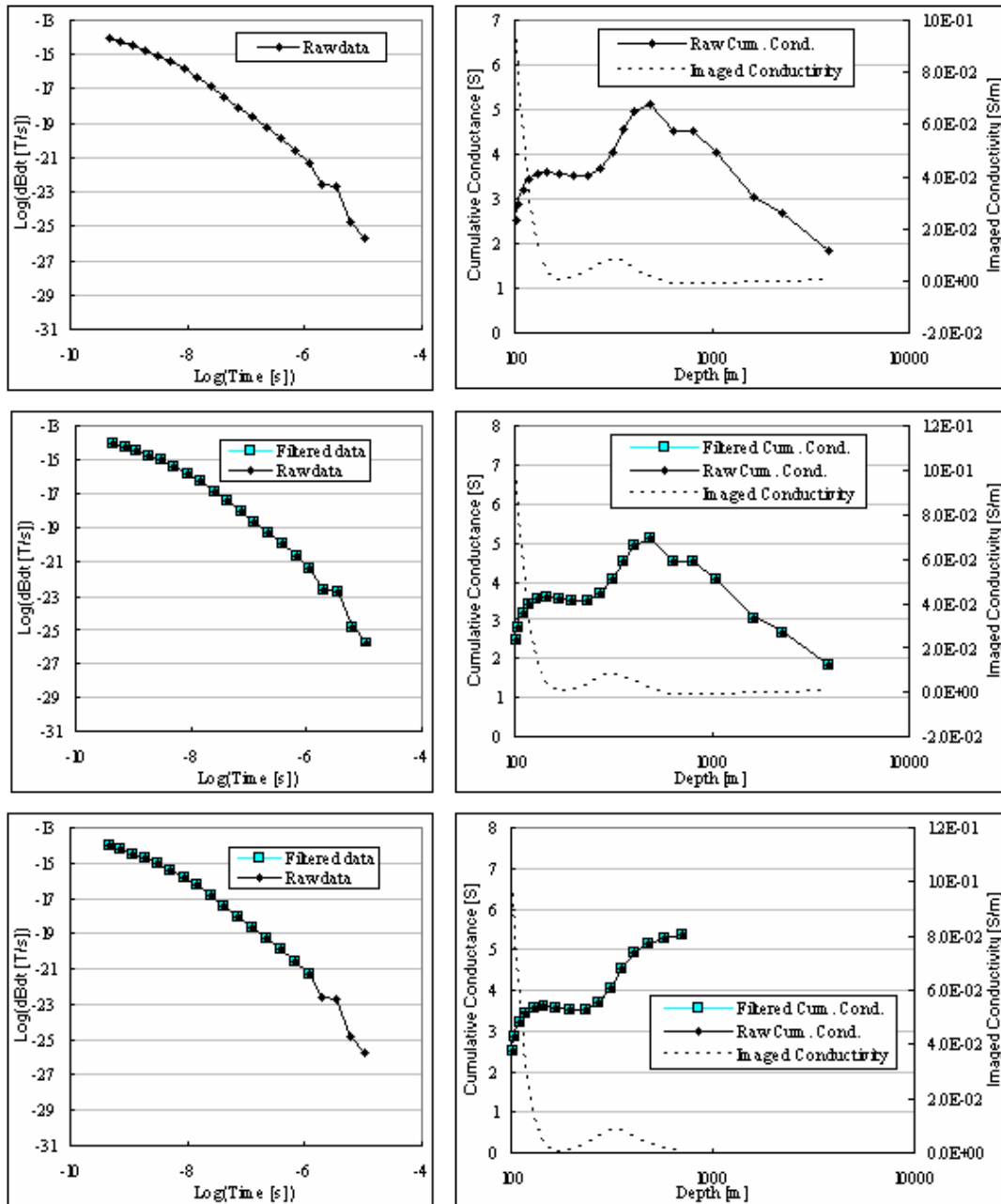


Figure 5-3: Line 4950, Station 100. *Top*: Raw data with calculated cumulative conductance and imaged conductivity. *Middle*: No filter effect on input data values, only on cumulative conductance curve with imaged conductivity of filtered conductance values. *Bottom*: Input data filtered for late channel erratic behaviour and filtered cumulative conductance values.

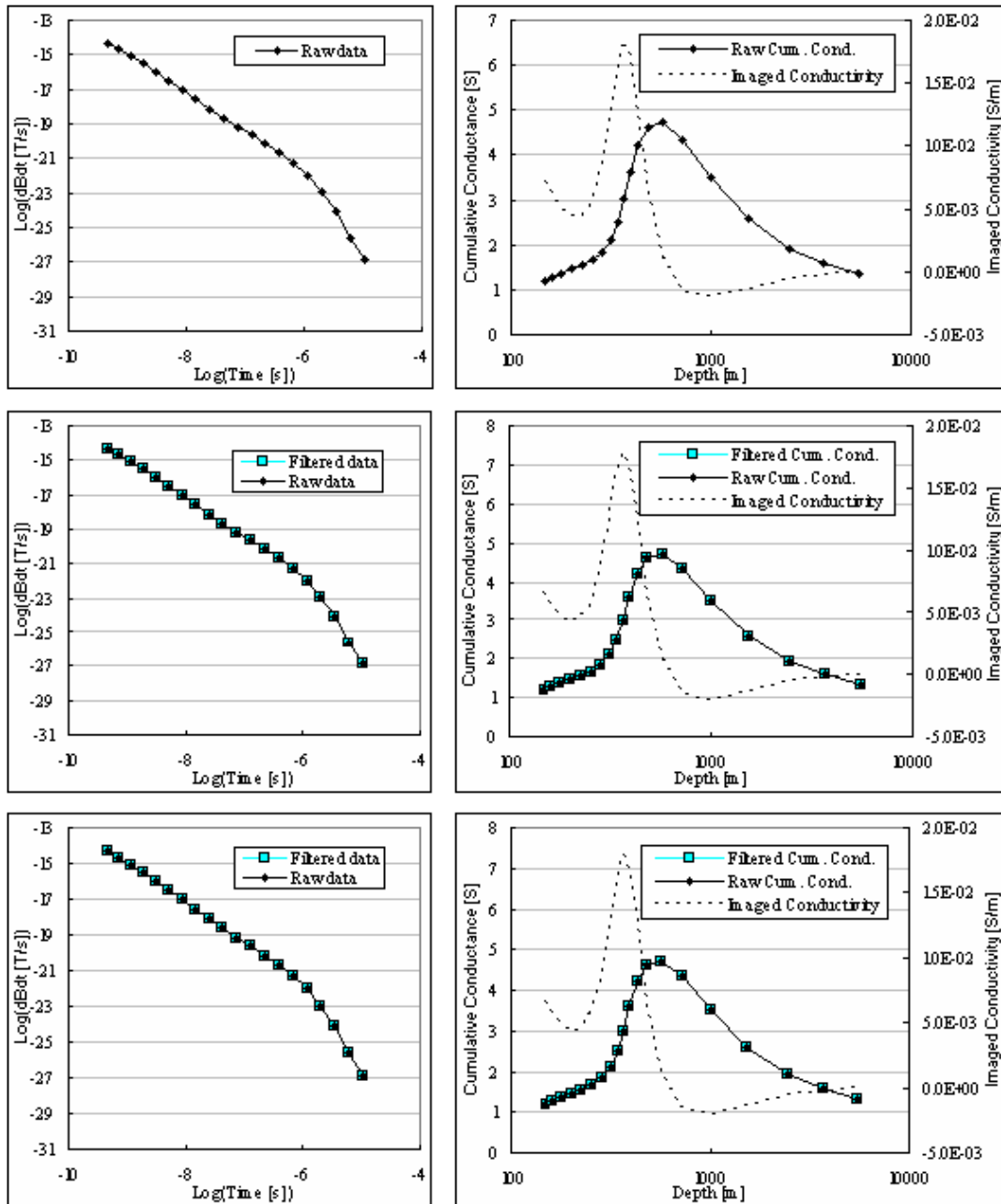


Figure 5-4: Line 4950, Station 300. *Top*: Raw data with calculated cumulative conductance and imaged conductivity. *Middle*: No filter effect on input data values, only on cumulative conductance curve with imaged conductivity of filtered conductance values. *Bottom*: Input data filtered for late channel erratic behaviour and filtered cumulative conductance values.

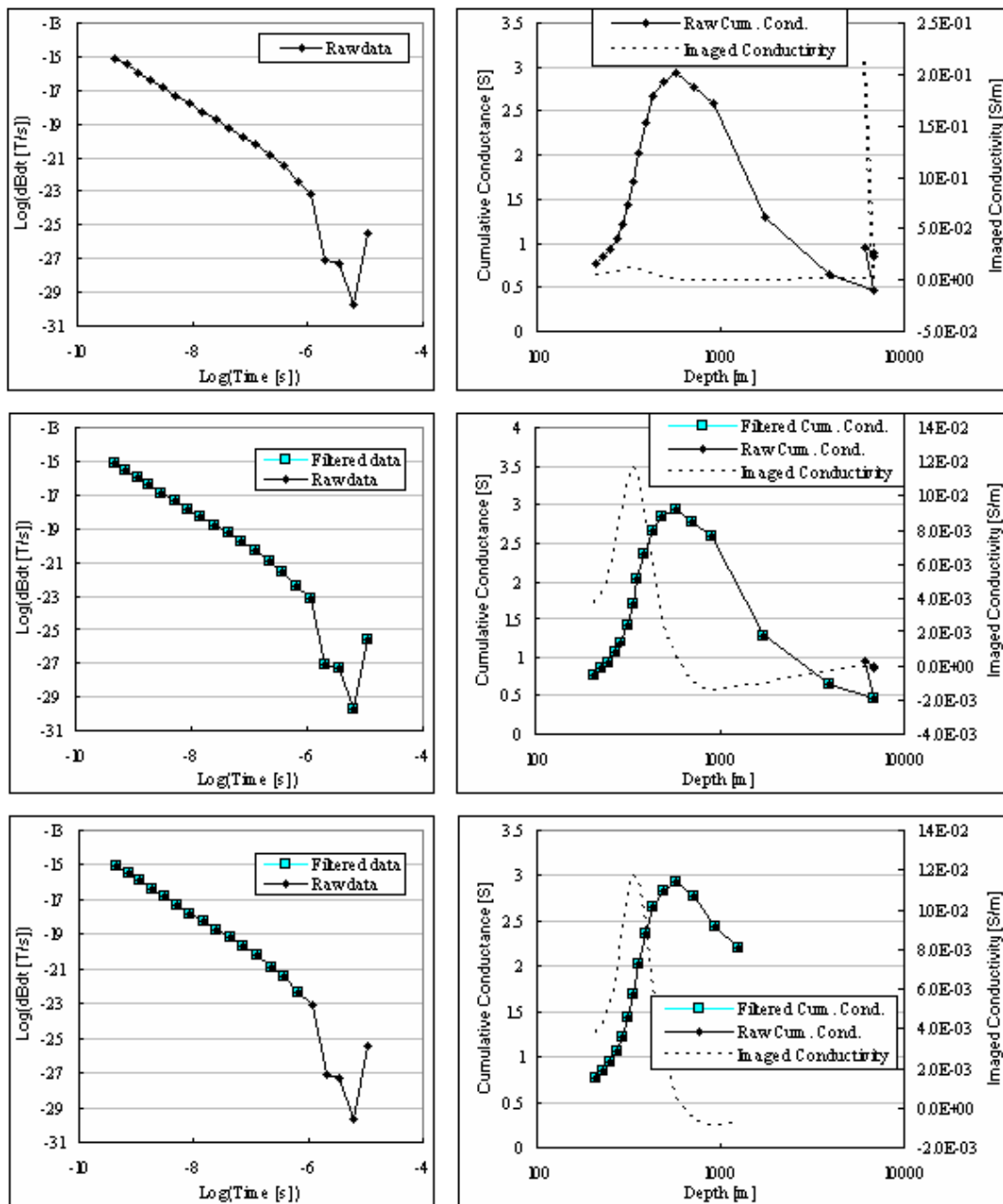


Figure 5-5: Line 4950, Station 400. *Top:* Raw data with calculated cumulative conductance and imaged conductivity. *Middle:* No filter effect on input data values, only on cumulative conductance curve with imaged conductivity of filtered conductance values. *Bottom:* Input data filtered for late channel erratic behaviour and filtered cumulative conductance values.

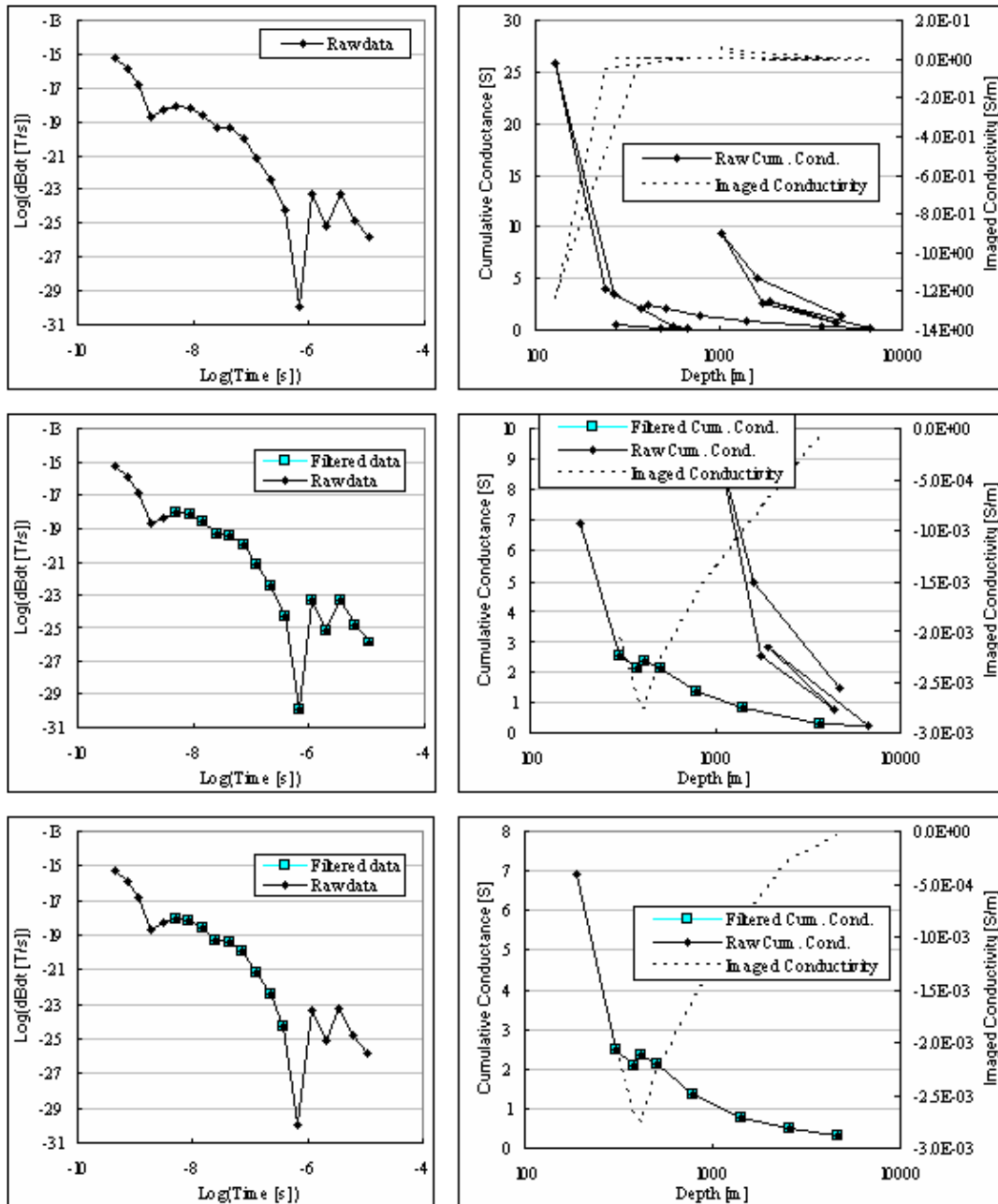


Figure 5-6: Line 4950, Station 450. *Top:* Raw data with calculated cumulative conductance and imaged conductivity. *Middle:* No filter effect on input data values, only on cumulative conductance curve with imaged conductivity of filtered conductance values. *Bottom:* Input data filtered for late channel erratic behaviour and filtered cumulative conductance values.

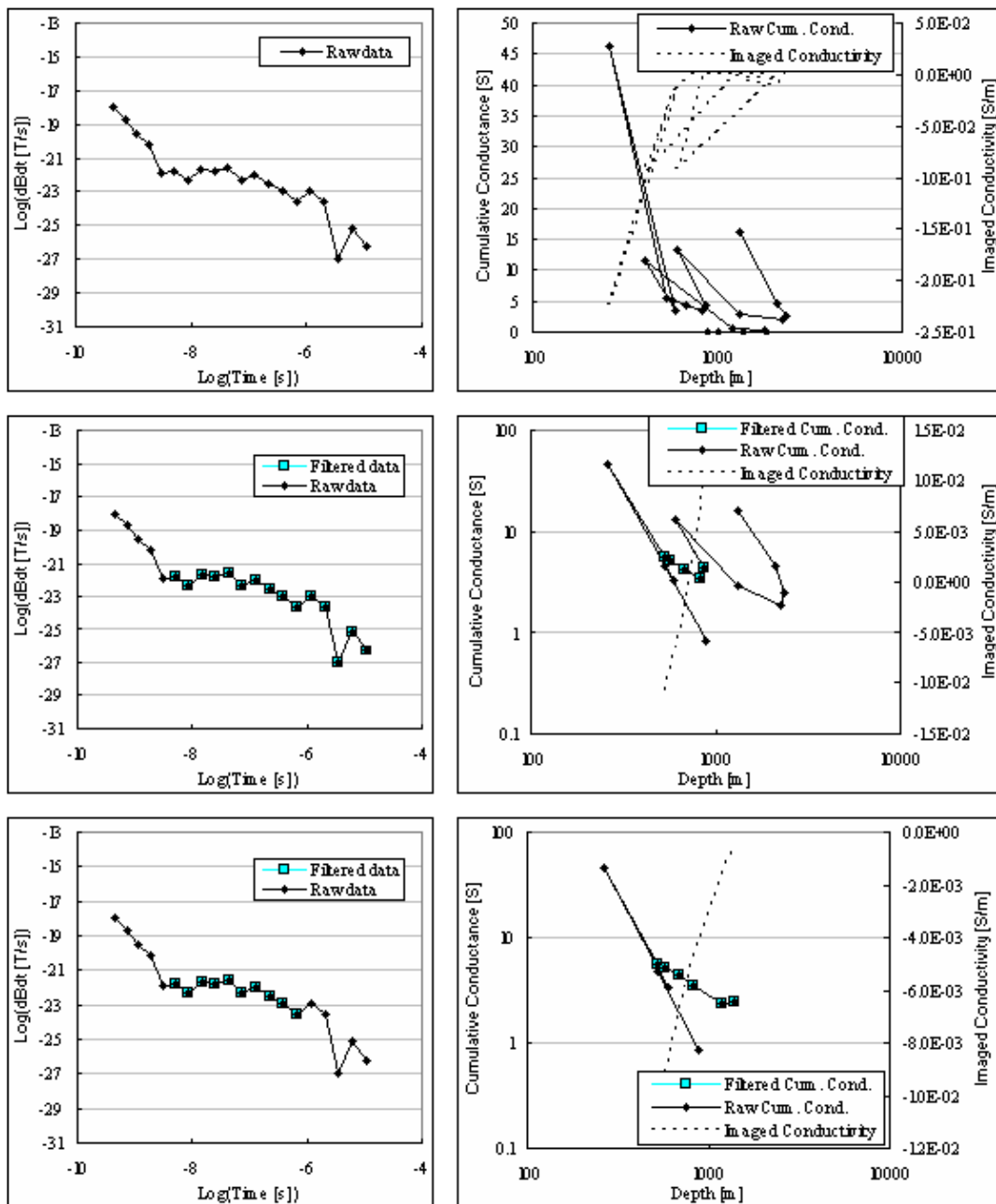


Figure 5-7: Line 4950, Station -1550. *Top:* Raw data with calculated cumulative conductance and imaged conductivity. *Middle:* No filter effect on input data values, only on cumulative conductance curve with imaged conductivity of filtered conductance values. *Bottom:* Input data filtered for late channel erratic behaviour and filtered cumulative conductance values.

Station 300 (Figure 5-4) has the smoothest input data, no data are filtered out and the final result (imaged conductivity) of the three processing options are identical. Station

100 (Figure 5-3) contains four data points at the end that are filtered out. No data are discarded by the SDTC filter and therefore the first two options yield identical results. The advantages of filtering out the last four points (17-20) are:

a more realistic maximum depth of investigation (706 m instead of 3943 m)

data points 15 and 16 still indicate high conductance values in the third case while in the first two cases they have been “contaminated” during smoothing by the consecutive noisy points to give lower than expected conductance values.

Similar results are observed for stations 400, 450 and -1550.

From these examples it is seen that the SDTC filter on its own also serves to discard some of the last erratic data points although it was not originally designed with this in mind. However, it is not as effective as removing the noisy points from the raw input data.

A final comparison of the second and third filter options are done by means of contoured imaged conductivity sections of line 4950. (*Note: This line has been chosen specifically because it contains stations with clean as well as noisy data.*) These sections are shown in Figure 5-8. Only imaged conductivities at depths of less than 800 m below the surface were contoured; deeper than that the data plot as individual, incoherent points and is not suitable for contouring. There is not much to choose between the two approaches when presented in this way. The only significant difference occurs between stations 400 to 600. Here the application of only the SDTC filter results in fairly high negative values (dark blue). The same feature is visible on the bottom section (SDTC plus noise filter) but it is less pronounced. Taking into account the fact that there are only three points on station 500, it is probably due to noisy data (see station 450, Figure 5-6) and the smoother, double filtered bottom section is preferable to the top one.

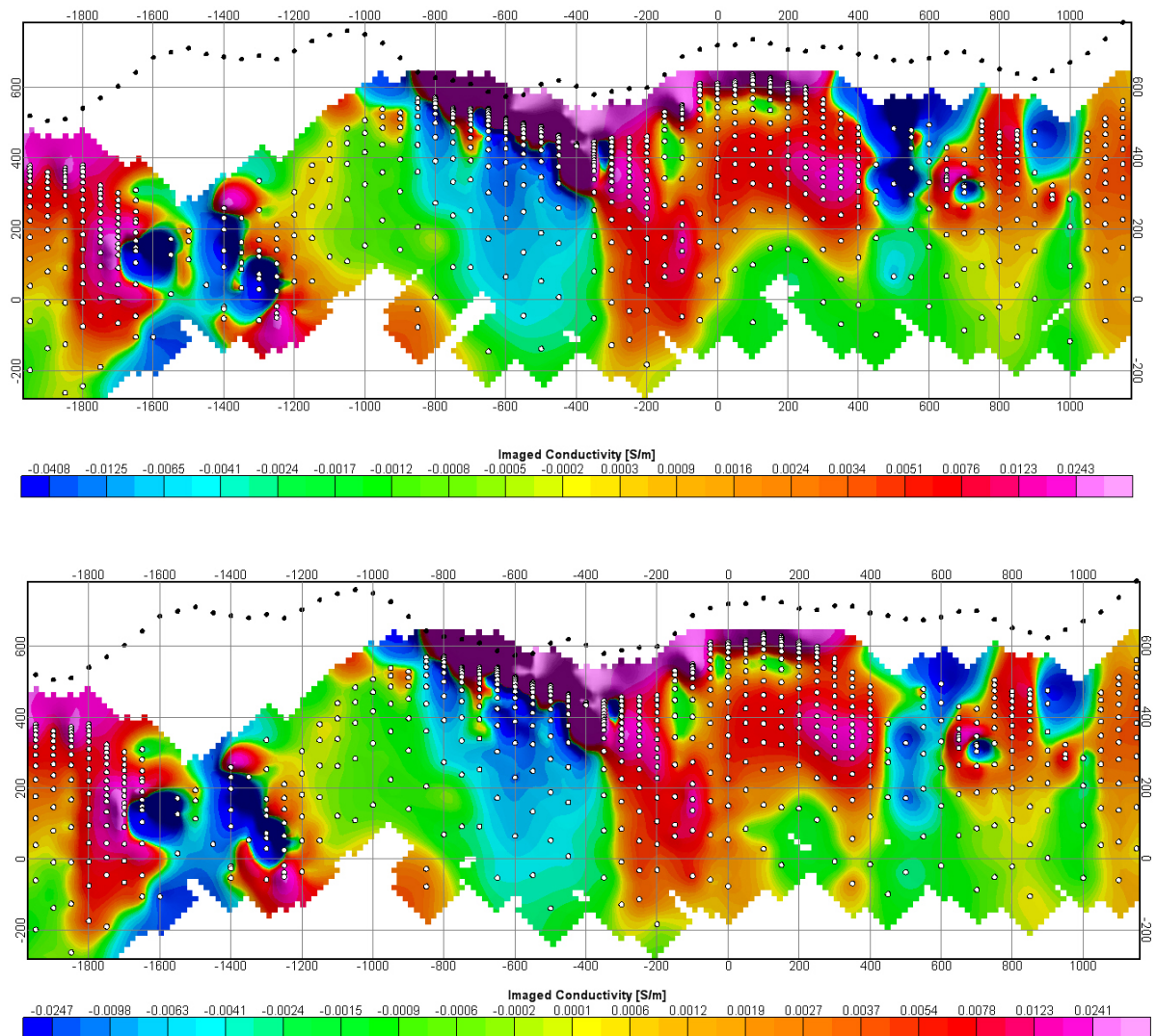


Figure 5-8: Comparison of SDTC filter only (top) and SDTC with additional noise filter (bottom). Black dots are station elevations (DTM) and white dots represent depths at which conductivities are calculated.

5.2.4 Comparison of 25Hz (high, H) and 6.25Hz (medium, M) base frequency data

The high frequency time channels range from 0.088ms to 6.978ms and the medium frequency channels from 0.35ms to 27.92ms. The first 14 channels of the medium frequency overlap with the last 13 of the high frequency. Measuring at these two frequencies therefore increases the coverage of the decay curve in terms of time, but also provides a check on the quality of data in the overlapping region. Often one frequency

will be noisier than the other in the overlapping range. If data quality is good for both frequencies, the conductivity depth sections obtained from the different frequencies should also overlap for intermediate depths with the high frequencies adding shallower data and the medium frequencies contributing to the deeper parts of the sections. Two lines are used to illustrate examples of poor and good correlations between these frequencies and to determine the reasons for discrepancies. Figure 5-9 is an example of good correlation between the sections obtained from the two frequencies. Three areas of interest are indicated by blocks A, B and C. In block A, a conductor is seen on both the high and medium frequencies.

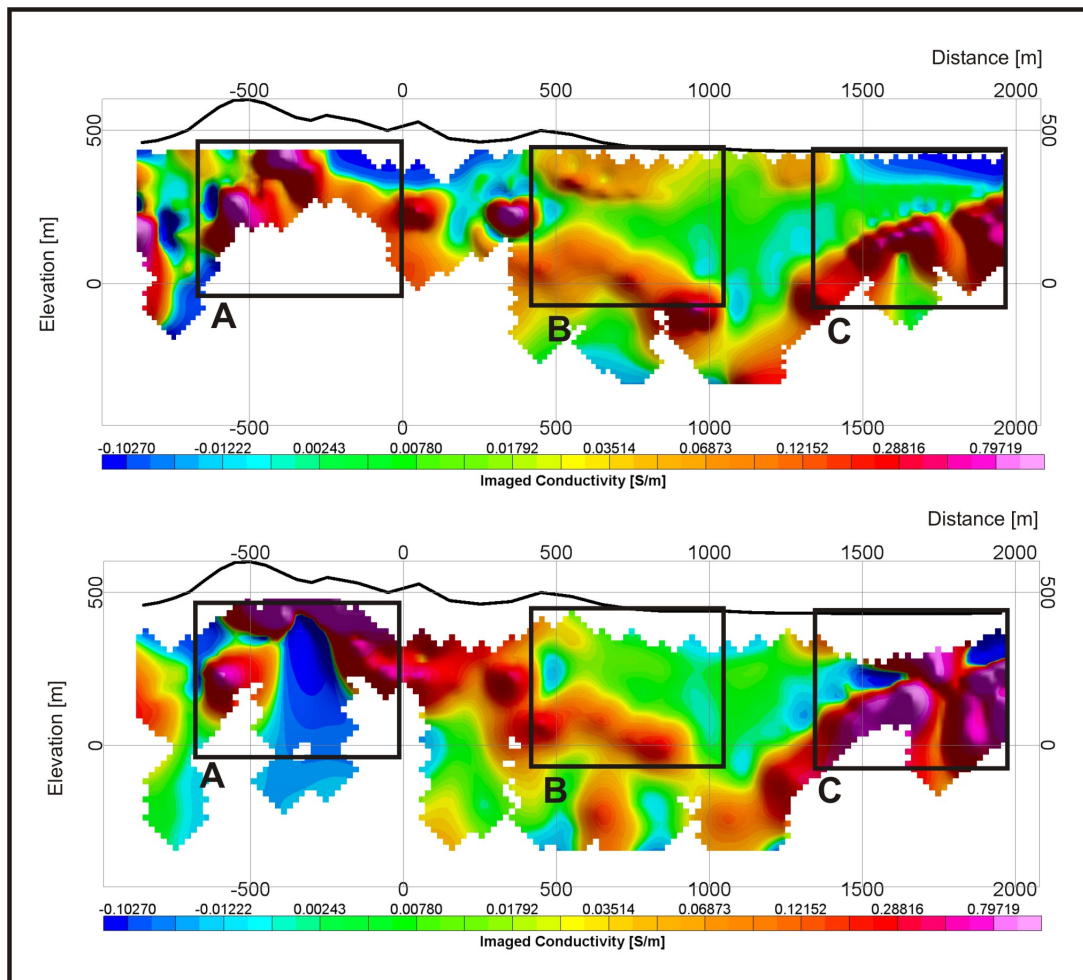


Figure 5-9: Line 450N showing good correlation between conductivity depth sections obtained from the high (top) and medium frequencies (bottom).

The top of the conductor is defined better by the high frequency. The medium frequency shows behaviour as in Figure 4-44 where it was found that when a conductor is shallower than the depth to where the 1st channel would plot in the surrounding half space (compare the depths of the first channel plots on the rest of the line), the cumulative conductance and conductivity curves are distorted. Block B indicates the capability of the method and the algorithm to map a deep conductor below a shallower one provided the right time channels are measured (two conductors on high frequency, only one visible on medium frequency). Block C indicates a good match between the frequencies with the medium frequency data containing some noise.

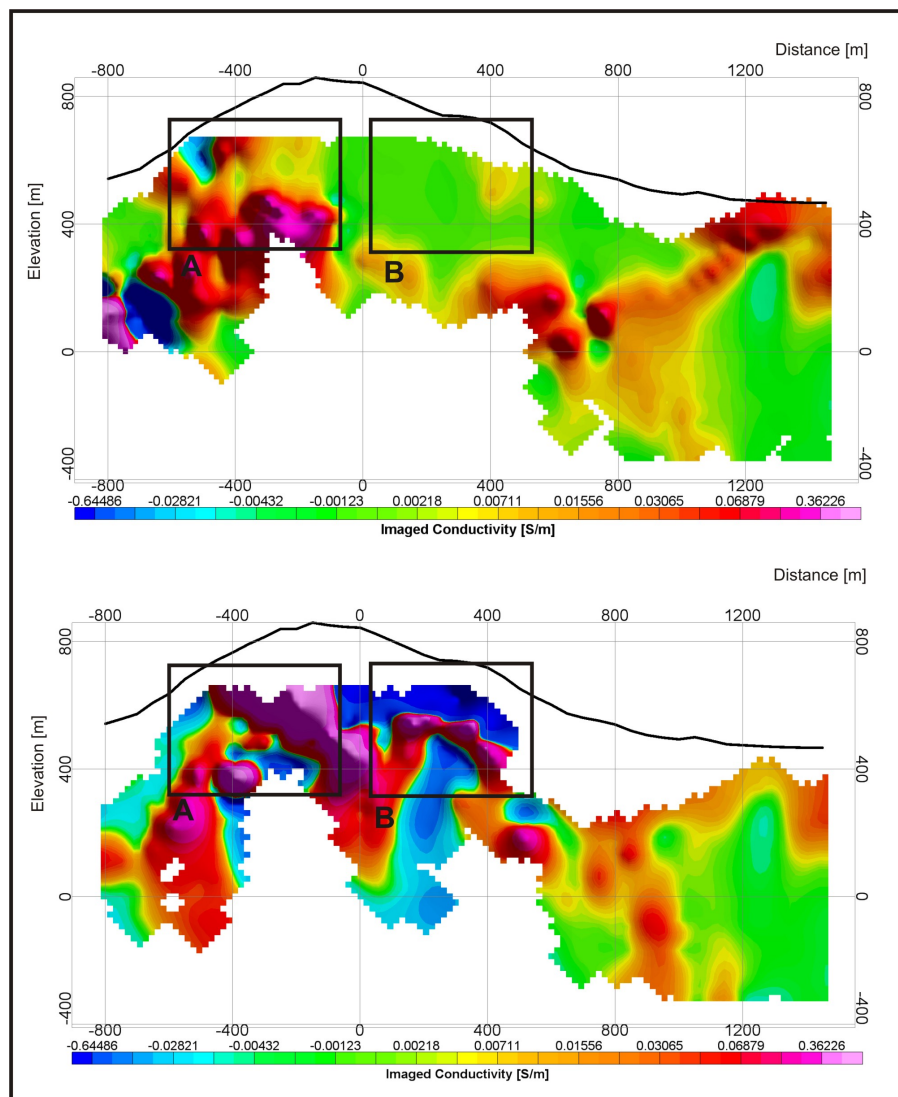


Figure 5-10: Line 1650N showing poor correlation between the high (top) and medium frequencies (bottom).

Figure 5-10 shows an example of poor correlation between conductivity depth sections for the two frequencies. In block A conductors are mapped on both frequencies but with more than 100m discrepancy in depth. In block B a conductor is mapped consistently over at least 4 stations on the medium frequency, but nothing is seen on the high frequency although this depth range is well covered. The question is where exactly these discrepancies originate. Figure 5-11 shows graphs of the measured data on line 450N for both frequencies and Figure 5-12 shows the same for line 1650N. It is clear that when the measured data correspond well (line 450N) the conductivity depth sections match. The reason for the discrepancies between dB/dt values for the medium and high frequencies of line 1650N is not known, but the behaviour of both frequencies is consistent over four adjacent stations (200m) implying a geological cause and not acquisition or processing error.

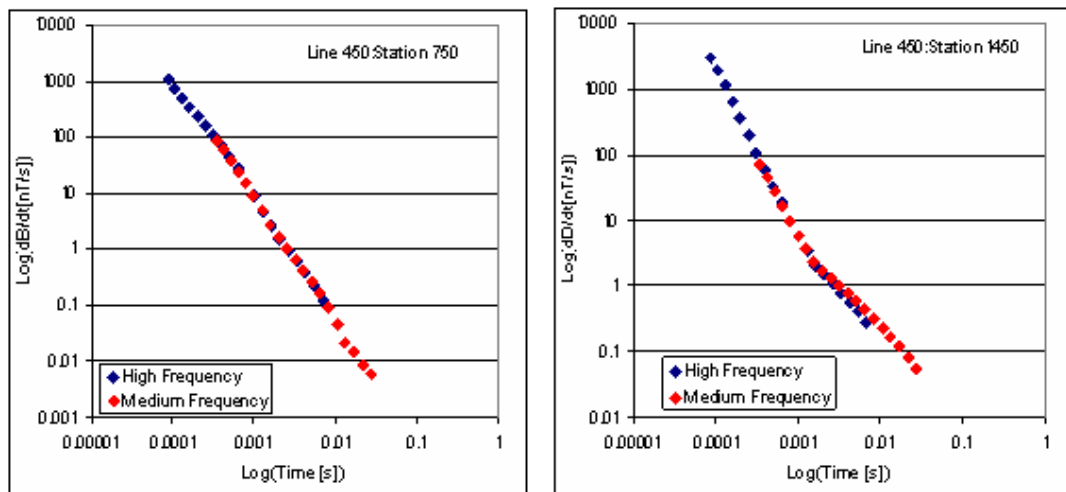


Figure 5-11: Line 450; Stations 750 and 1450; medium and high frequency measured data.

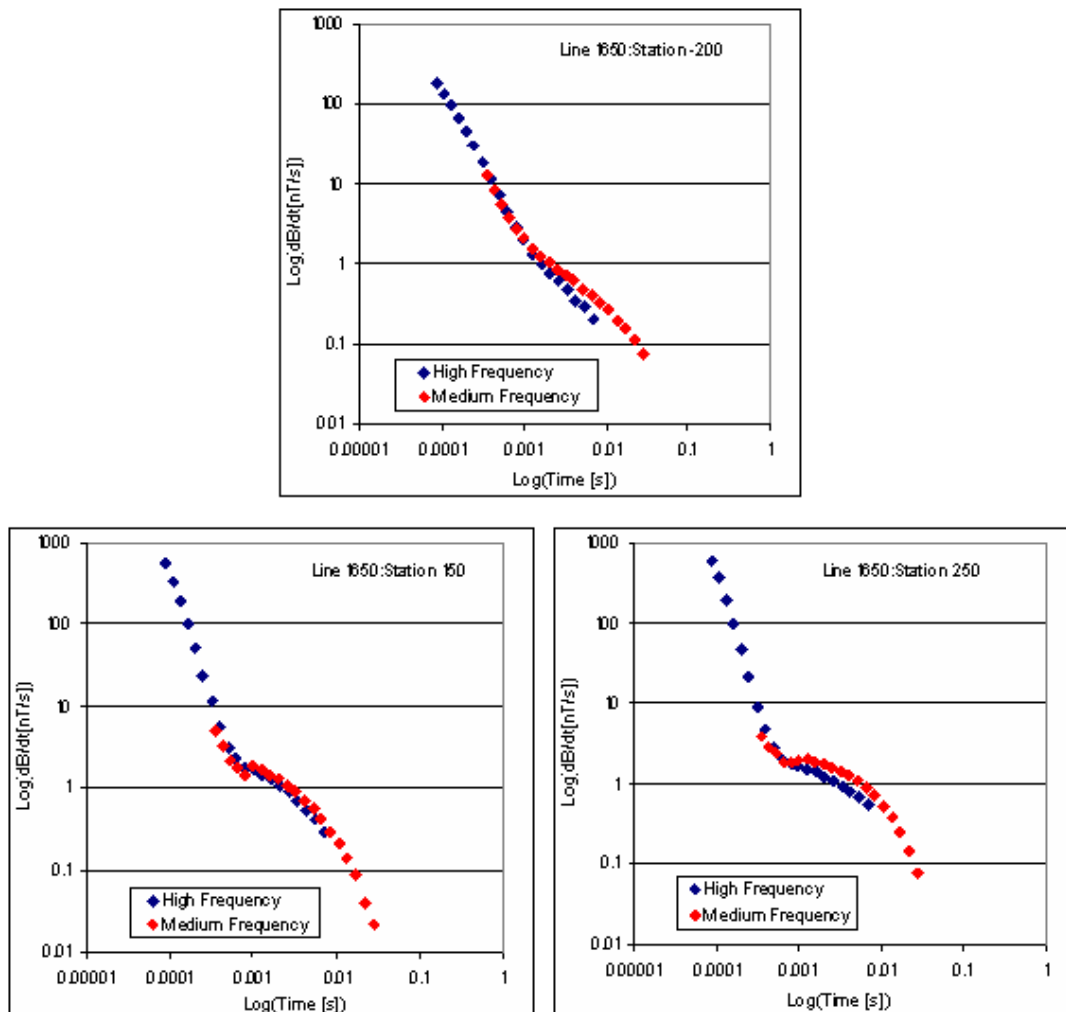


Figure 5-12: Line 1650; Stations -200, 150 and 250; medium and high frequency measured data.

5.2.5 *Imaged conductivity sections*

Figures 5-13 and 5-14 show screen dumps of a 3-D presentation of the complete data set as a series of imaged conductivity – depth sections plotted underneath the station positions which are draped over the DTM. The data set is attached in electronic format with Oasis Montaj Viewer where any combination of the sections can be displayed and viewed interactively in 3D. Also included is a colour contoured grid of the decay constant values determined as described in Chapter 4. Before contouring statistical inspection of the imaged conductivities still reveal a small number of erroneously high

values. A final filter is applied keeping only values between -5 and 5S/m to grid and contour. The contouring colour scheme is fixed for all sections and assigns dark blue to all negative values and a logarithmic scale from light blue (0S/m) to magenta (5S/m) for positive values. All negatives are grouped together as their presence can be used to help identify confined conductors and show instances where the assumptions of the S-layer differential transform were not completely satisfied, but there is little to be gained from the actual numerical value of these negative conductivities. It is therefore preferable to spread out the resolution of the colour contour scheme over the positive data range.

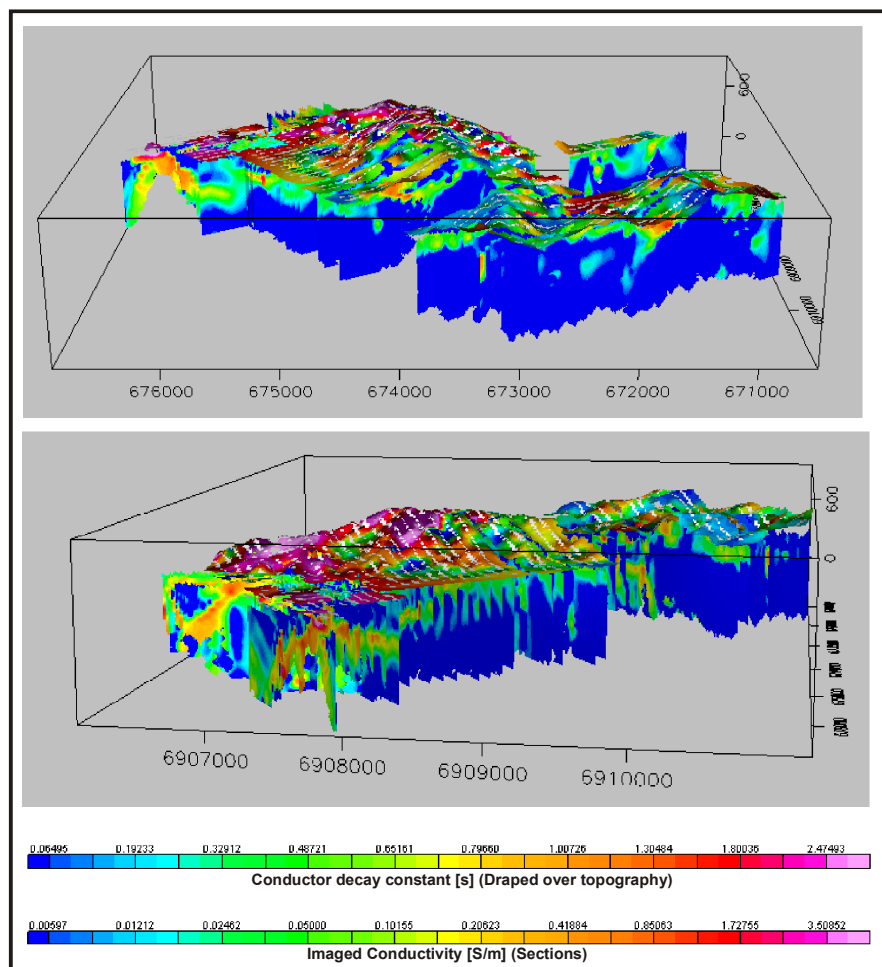


Figure 5-13: Contour map of conductor decay constants draped over topography and conductivity depth sections in 3D. Top viewpoint is from inclination 20°, declination 180° and 5km distance. Bottom viewpoint is inclination 10°, declination -100° and distance 5km. Axes are Northing, Easting and Elevation above sea level.

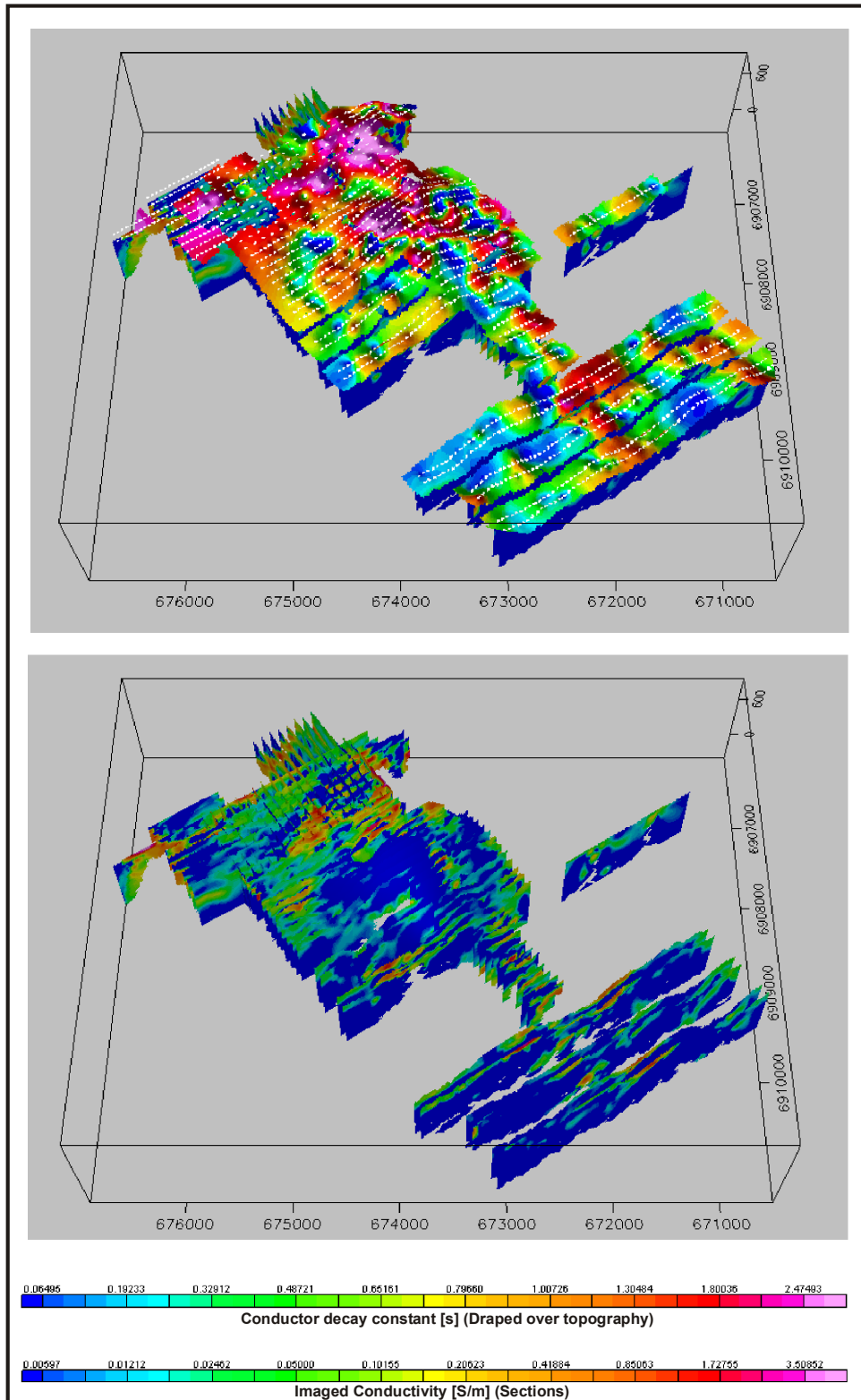


Figure 5-14: .3D view from inclination 60°, declination 180° and 5km distance with and without contour map of conductor decay constants.

In the following section one area of interest will be isolated and compared with plate modelling results.

5.2.6 *Comparison of automated conductor location with Maxwell plate model results*

The results of the automated processing and conductor location of line 4050 are presented in Figure 5-15. At the very top, the profile data are shown for channels 1-10 and channels 11-20 respectively. On the late time profiles (channels 11-20) two prominent conductors are recognised, centred at stations -800m and 200m. These can also be identified on the conductivity depth section (second from top) as two near-surface conductors. However, there is a prominent conductor (station -300m) at depth that is not immediately evident on the profile plots. The conductor decay constants (third from the top) are displayed at scaled channels positions on the vertical axis and are not indicative of depths of conductors. All three conductors are mapped by the calculated decay constants with the deep conductor exhibiting the largest values. Decay constants of less than 0.5s are calculated on many stations, sometimes overlapping with half space decay behaviour and may be indicative of restraints in the automated algorithm that are chosen too loosely. Decay constants in this range can be ignored or filtered out. The bottom section indicates channels exhibiting power-law decay conforming to half space and S layer behaviour. These are found on stations where conductors are absent. An exception is stations -450m to -550m where half space behaviour is found on the first 5 channels and is replaced by the exponential decay in the later channels confirming the presence of a deep conductor. Figure 5-16 gives the same information for adjacent line 4150 and the close correlation between the sections for these two lines provides an indication of the stability that can be expected from the automated techniques. Figures 5-17 and 5-18 compares the conductivity depth sections with plate models that were produced with the Maxwell software package. The profiles at the top are channels 10-17 for the field and modelled data. The plate models have well-known inherent weaknesses in areas of complex geology but the correlation found with the conductivity depth sections confirms the conductor locations.

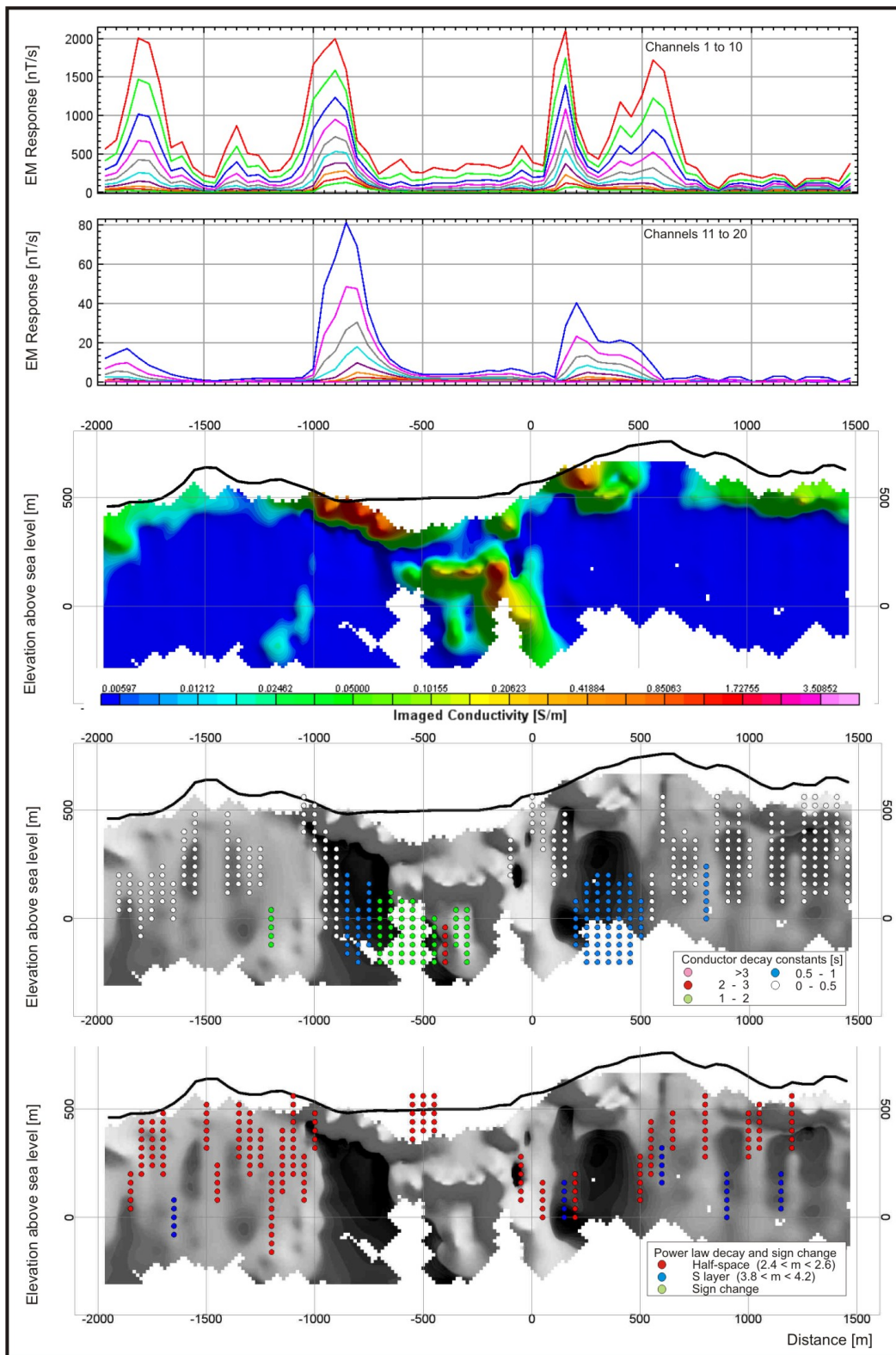


Figure 5-15: Line 4050. EM response profiles and sections from automated processing procedures.

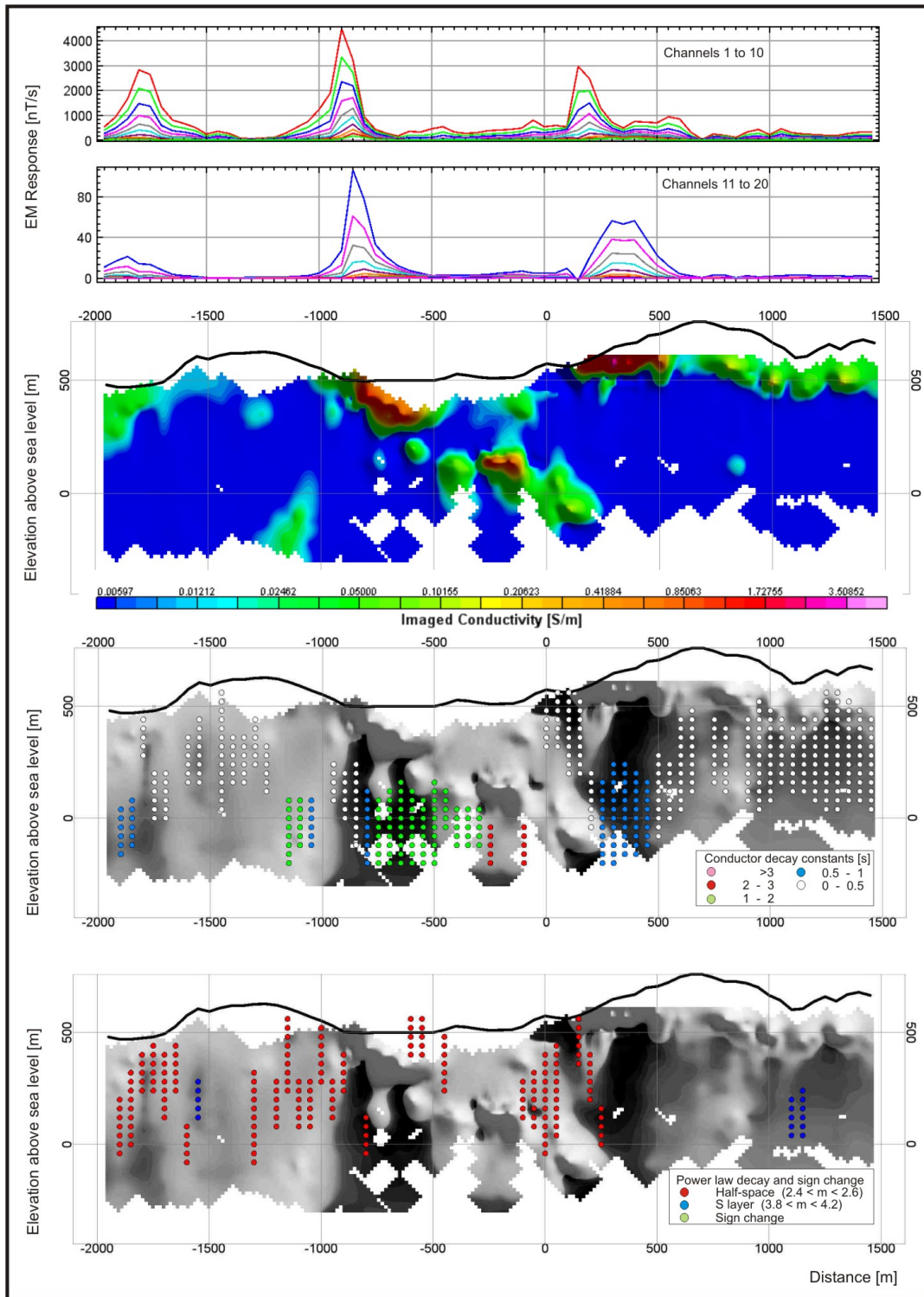


Figure 5-16: Line 4150. EM response profiles and sections from automated processing procedures.

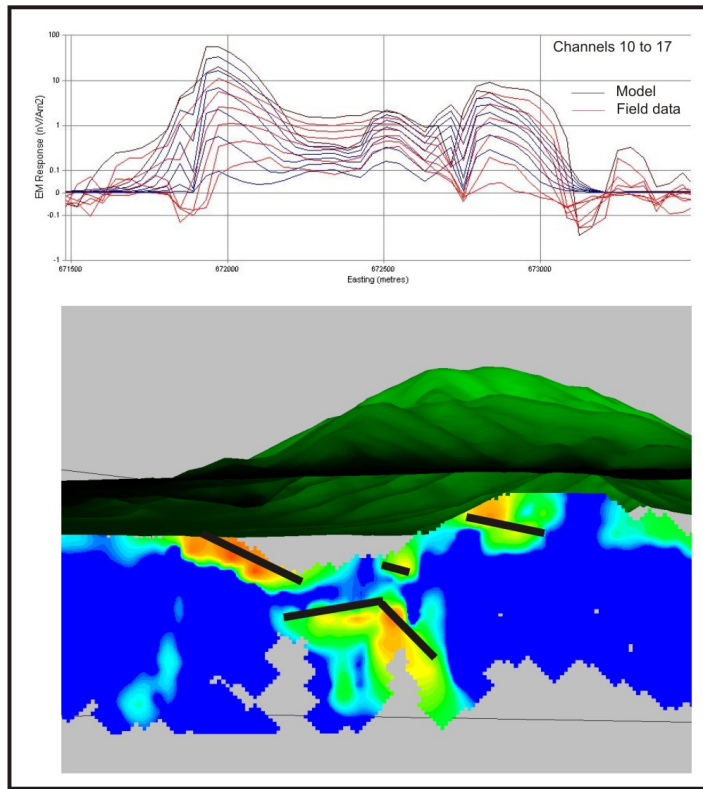


Figure 5-17: Line 4050. Comparison of Maxwell plate model and conductivity depth section.

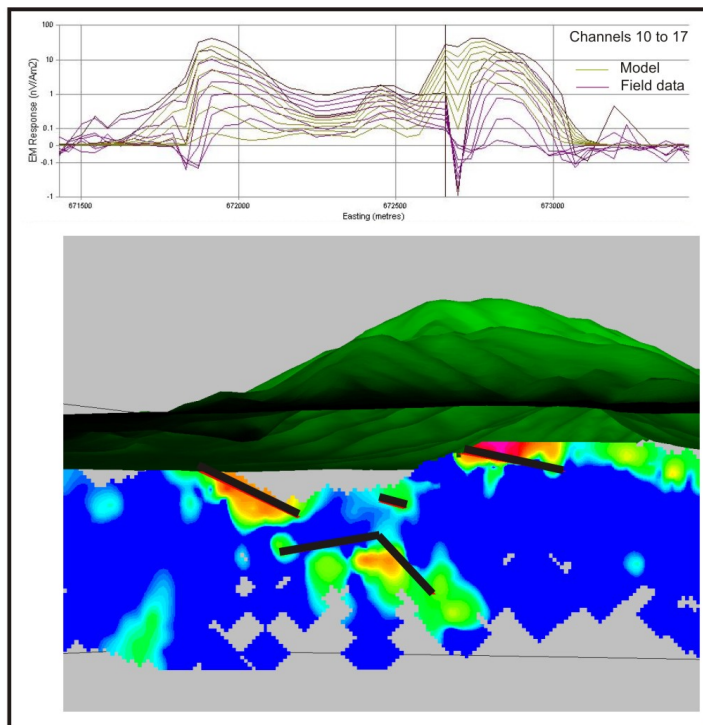


Figure 5-18: Line 4150. Comparison of Maxwell plate model and conductivity depth section.

5.3 Airborne survey

5.3.1 Data acquisition and system parameters

The airborne data were acquired with the VTEM system. The VTEM is a helicopter-borne TDEM system with central loop configuration developed by Geotech. One line is used to demonstrate the use of the S-layer transform. The data are presented here courtesy of BHP Billiton. Survey parameters are:

Transmitter Base Frequency Repetition Rate: 25

Transmitter Loop Diameter: 26m

Number of Turns: 4

Peak Current:: 170 A

Tx Dipole Moment: 361,000 NIA

Transmitter Wave Form: Trapezoid (with 40% duty cycle)

Receiver Loop Diameter: 1.1m

Rx Number of Turns: 60

Rx Time Gates: 27 ranging from 0.13ms to 8.9ms

Electromagnetic Receiver & serial number: Geotech VTEM 5

Electromagnetic Transmitter & serial number: Geotech VTEM 5

Length of cable for towed EM bird: 52

Height above ground for EM sensor: 80

The data is shown in Figure 5-19.

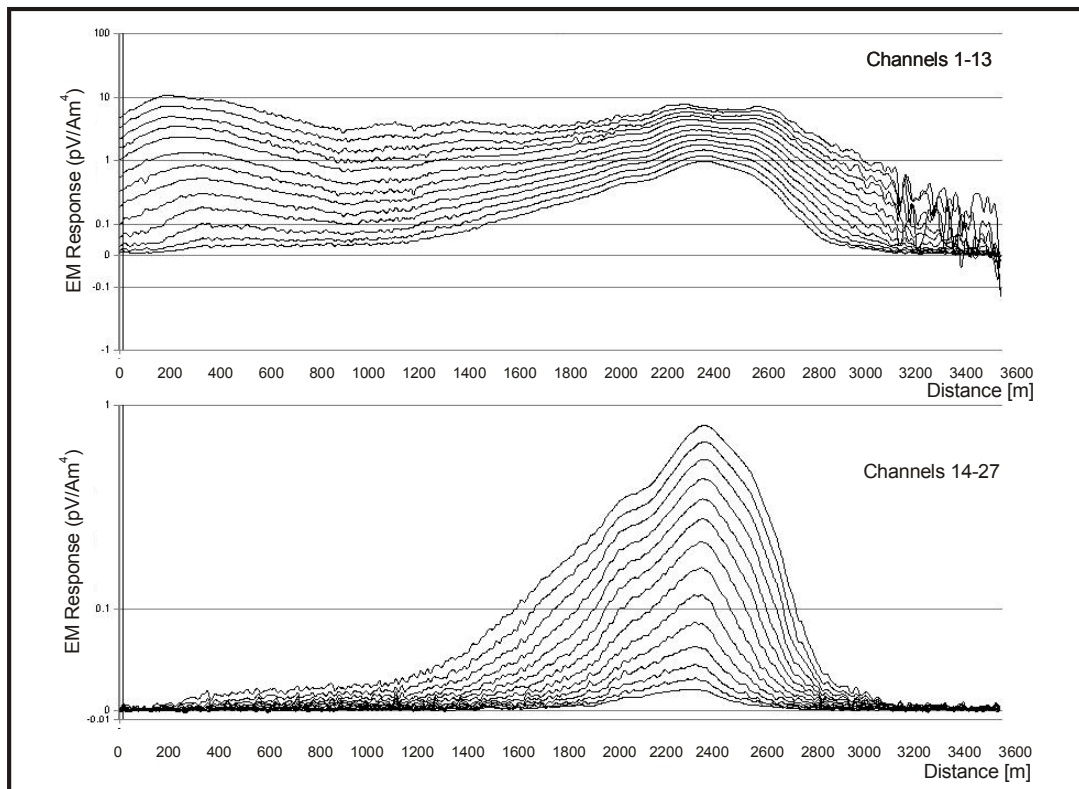


Figure 5-19: EM Response over conductor.

5.3.2 Automated processing

The conductivity depth section was calculated according to the same procedures set out in paragraph 5.2.3 and the conductor decay constants, half space decay behaviour and sign-changes determined as described in Chapter 4. The results are shown in Figures 5-20 to 5-23. The horizontal extent of the conductor is estimated to be from station 1700m to 2300m. The apparent extension of the conductor on either side can be explained in the same way as diffraction hyperbola phenomena on seismic sections. Stations not directly above the conductor will still measure its response, but data are plotted directly below the stations where it was measured, resulting in side “tails” on the conductivity depth sections. These effects are much more pronounced for dipping and vertical bodies. In this case it can be distinguished clearly based on the hyperbolic nature of the tail (station 2300m to 2800m), the corresponding drop in amplitude, and especially the “decrease of depth with increase of time” behaviour manifested as the white space

underneath the conductor where data not complying to the S-layer transform assumptions were filtered out (indicating high conductivity contrasts).

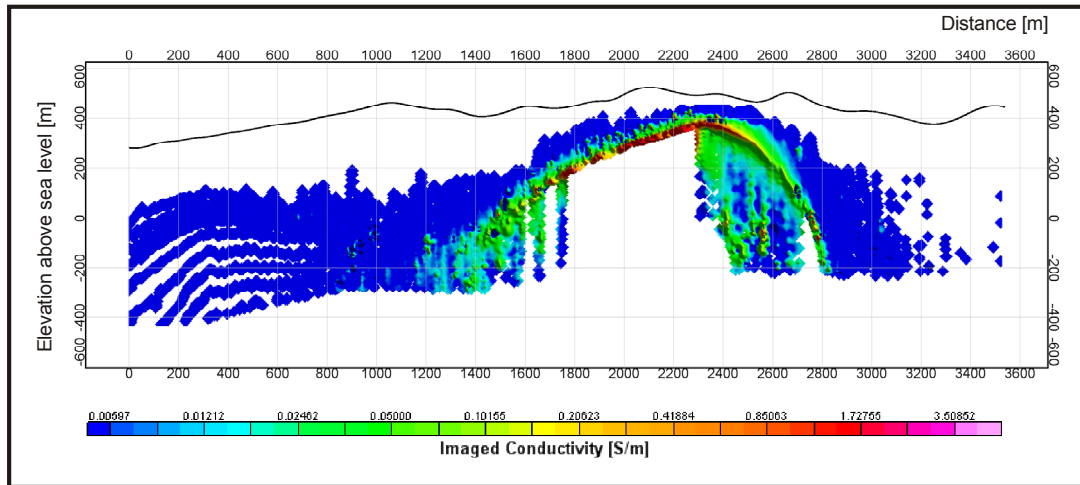


Figure 5-20: Conductivity depth section from S-layer transform, showing dipping conductor.

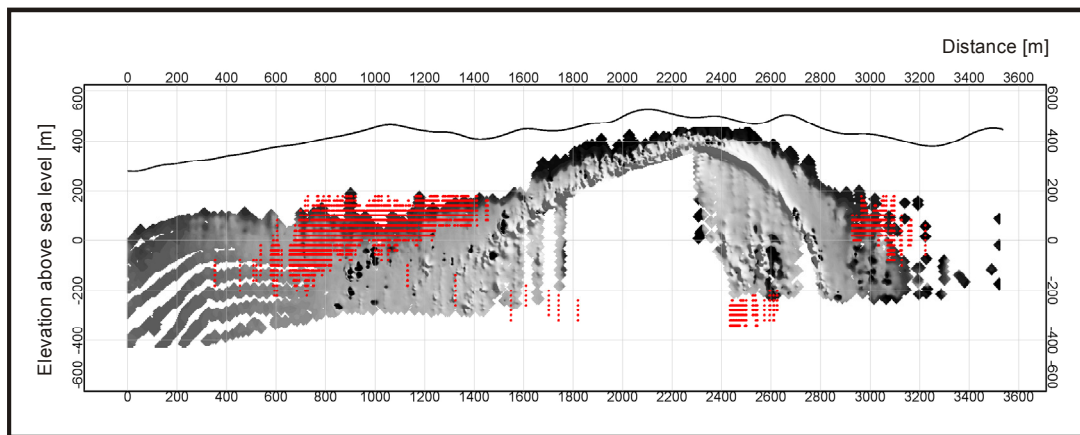


Figure 5-21: Conductivity depth section in greyscale with channels corresponding to half space power law decay indicated in red.

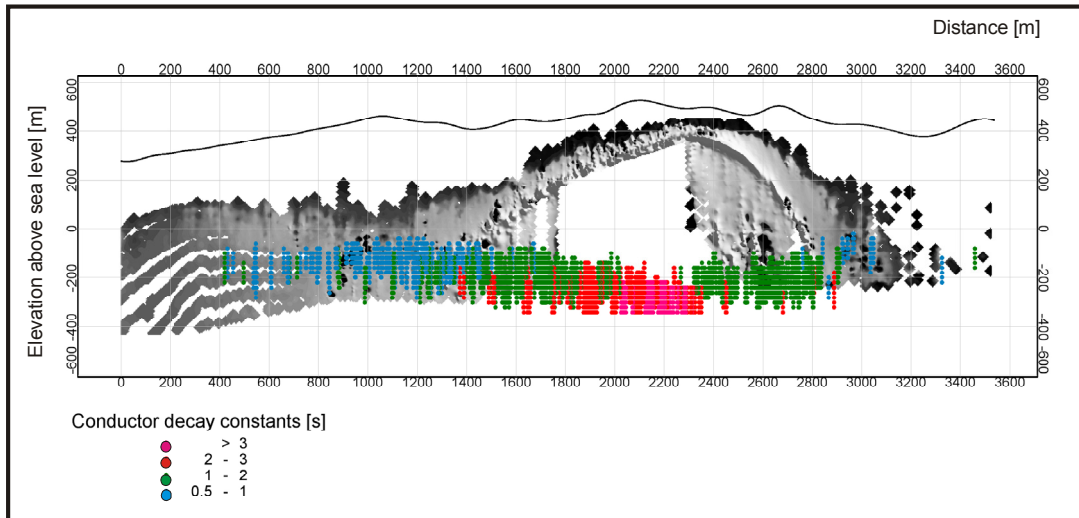


Figure 5-22: Conductivity depth section in greyscale with conductor decay constants plotted at scaled channel positions.

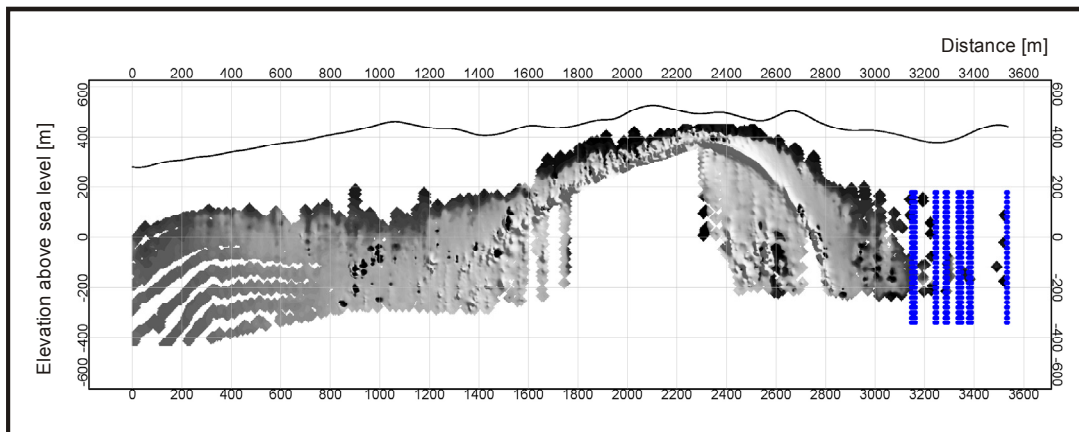


Figure 5-23: Conductivity depth section in greyscale with channels on stations showing sign changes indicated in blue.

The conductor decay constants plotted in Figure 5-22 also indicate maximum values on stations 1900m to 2400m, and if contoured the maximum of these values would correspond to the conductor location viewed in plan.

5.4 Conclusions and recommendations

The automated procedures outlined in chapter 4 can be implemented on both ground and airborne central loop configuration TDEM data. Filters to remove noise *as well as* clean data not conforming to the assumptions made in the S-layer differential transform can be applied efficiently in the time and spatial domains retaining the main advantage of the transform compared to inversion algorithms, namely speed. A combination of decay curve analysis and the S-layer differential transform allows sensitivity to both high conductivity contrast (well defined by exponential decay) and low contrast models (well defined by the S-layer transform). Care has to be taken when interpreting conductivity depth images, especially in the case of non-horizontal and especially near-vertical conductors as these will cause migration effects similar to that found in seismic sections. The procedures outlined in this work are considered to be completely automated since no starting model or information other than survey configuration and parameters are needed. Although the automated product is not considered to be a final interpretation it does provide very useful first phase identification of the subsurface conductivity.

Recommendations for further work are to:

- develop conductivity-depth section migration algorithms to correct for these effects
- test the effectiveness of the noise and SDTC filters on the more generalised inversion procedure described by Tartaras et. al. (2000)
- have borehole or other geological feedback in order to quantify the accuracy of the conductivity depth sections
- implement these, or similar algorithms, in TDEM instruments (such as a new generation metal detector) with the potential of real time imaging of data.

REFERENCES

- Barnett, C. T., 1984, Simple inversion of time-domain electromagnetic data. *Geophysics*, 49: 925-933
- Burden, R. L., and Faires, J. D., 1993, *Numerical Analysis –5th Ed.* PWS Publishing Company: 156-164
- Butler, D. K. 2003, Implications of magnetic backgrounds for unexploded ordnance detection. *Journal of Applied Geophysics*, 54:111 – 125
- Cooper, G. J., 2004. The stable downward continuation of potential field data. *Exploration Geophysics*, 35: 260-265
- Eaton, P. A., and Hohmann, G. W., 1987, An evaluation of electromagnetic methods in the presence of geologic noise. *Geophysics*, 52: 1106-1126
- Eaton, P. A., and Hohmann, G. W., 1989, A rapid inversion technique for transient electromagnetic soundings. *Phys. Earth Planet. Int.*, 53: 538-404
- James, B. A., 1988, Detection of tunnels by transient electromagnetic subsurface imaging. *U. S. Geol. Surv. Open-file Rep.* 87-76.
- Kaufman, A. A., and Keller, G. V., 1983, *Frequency and Transient Soundings: Methods in Geochemistry and Geophysics 16.* Elsevier Science Publishers, Amsterdam.
- Kaufman, A. A., and Keller, G. W., 1985, *Inductive Mining Prospecting, Part 1: Theory.* Elsevier Science Publishers, Amsterdam.
- Marquardt, D. W., 1963, An algorithm for least-squares estimation of non-linear parameters: *J. SAIM*, 11: 431-441.
- Macnae, J., and Lamontagne, Y., 1987, Imaging quasi-layered conductive structures by simple processing of transient electromagnetic data. *Geophysics*, 52: 545-554
- McNeill, J. D., 1980, Applications of Transient Electromagnetic Techniques. *Geonics Technical Note TN-7.* Geonics Limited, Toronto.
- Nabighian, M. N., 1971, Quasi-static transient response of a conducting permeable two-layer sphere in a dipolar field. *Geophysics*, 36: 25-37
- Nabighian, M. N., 1979, Quasi-static transient response of a conducting half space- An approximate representation. *Geophysics*, 44: 1700-1705
- Nabighian, M. N., and Macnae, J.C., 1991, Time Domain Electromagnetic prospecting Methods; in Nabighian, Misac N., Ed., *Electromagnetic Methods in Applied Geophysics, Volume 2,* Application: Soc. of Expl. Geophysicists: 427-520
- Nekut, A. G., 1987, Direct inversion of time-domain electromagnetic data. *Geophysics*, 52: 1431-1435

- Newman, G. A., Hohmann, G. W., and Anderson, W. L., 1986, Transient electromagnetic response of a three-dimensional body in a layered earth. *Geophysics*, 51: 1608-1627
- Newman, G. A., and Hohmann, G. W., 1988, Transient electromagnetic responses of high contrast prisms in a layered earth. *Geophysics*, 53: 691-706
- Pavlov, D. A., and Zhdanov, M. S., 2001, Analysis and interpretation of anomalous conductivity and magnetic permeability effects in time domain electromagnetic data. Part I: Numerical modelling: *J. Appl. Geophys.*, 46: 217-233
- Reitz, J.R., Milford, F.J., and Christy, R.W., 1992, *Foundations of Electromagnetic Theory - 4th edition*. Addison-Wesley Publishing Company.
- Singh, S. K., 1973, Electromagnetic transient response of a conducting sphere embedded in a conductive medium. *Geophysics*, 38: 864-893
- Sidorov, V. A., and Tikshaev, V. V., 1969, Electrical prospecting with transient field in near zone: Saratov University (in Russian).
- Smith, R. S., Edwards, R. N., and Buselli, G., 1994, An automatic technique for presentation of coincident-loop, impulse-response, transient, electromagnetic data: *Geophysics*, 59: 1542-1550
- Spies, B. R., 1980, Interpretation and design of time-domain EM surveys in areas of conductive overburden, in D. M. Emerson, Ed., *The geophysics of the Elura orebody*: Sydney, Austral. Soc. Expl. Geophys.: 130-139
- Spies, B. R., and Frischknecht, F. C., 1991, Electromagnetic Sounding; in Nabighian, Misac N., Ed., *Electromagnetic Methods in Applied Geophysics, Volume 2*, Application: Soc. of Expl. Geophysicists: 285-425
- Tartaras, E., Zhdanov, M. S., Wada, K., Saito, A., and Hara, T., 2000, Fast imaging of TDEM data based on S-inversion: *J. Appl. Geophys.*, 43: 15-32.
- Wang, T., and Hohmann, G. W., 1993, A finite-difference, time-domain solution for three-dimensional electromagnetic modelling. *Geophysics*, 58: 797-809
- Ward, S. M., and Hohmann, G. W., 1988, Electromagnetic Theory for Geophysical Applications; in Nabighian, Misac N., Ed., *Electromagnetic Methods in Applied Geophysics, Volume 1*, Theory: Soc. of Expl. Geophysicists: 131-148.
- Wolgram, P., Hyde, M., and Thomson, S., 1998, How to find localised conductors in GEOTEM data. *Exploration Geophysics*, 29: 665-670
- Xiong, Z., 1992, Electromagnetic modelling of 3-D structures by the method of system iteration using integral equations. *Geophysics*, 57: 1556-1561
- Zhdanov, M. S., and Pavlov, D. A., 2001, Analysis and interpretation of anomalous conductivity and magnetic permeability effects in time domain electromagnetic data. Part II: Su

inversion: *J. Appl. Geophys.*, 46: 235-
248

APPENDIX A

Derivation of Simpson's rule for unequally spaced data values (centre points).

A Lagrange polynomial $p(x)$ is obtained such that $p(x_i) = f(x_i)$ for $i=1,2,3$ and integrated over the interval $x_1 < x < x_3$.

$$p(x) = f(x_1) \frac{(x-x_2)(x-x_3)}{(x_1-x_2)(x_1-x_3)} + f(x_2) \frac{(x-x_1)(x-x_3)}{(x_2-x_1)(x_2-x_3)} + f(x_3) \frac{(x-x_1)(x-x_2)}{(x_3-x_1)(x_3-x_2)} \quad (\text{B.1})$$

So

$$\begin{aligned} \int_{x_1}^{x_3} f(x) dx &\approx \int_{x_1}^{x_3} f(x_1) \frac{(x-x_2)(x-x_3)}{(x_1-x_2)(x_1-x_3)} + f(x_2) \frac{(x-x_1)(x-x_3)}{(x_2-x_1)(x_2-x_3)} + f(x_3) \frac{(x-x_1)(x-x_2)}{(x_3-x_1)(x_3-x_2)} dx \quad (\text{B.2}) \\ &= \frac{f(x_1)}{(x_1-x_2)(x_1-x_3)} \int_{x_1}^{x_3} (x-x_2)(x-x_3) dx \\ &\quad + \frac{f(x_2)}{(x_2-x_1)(x_2-x_3)} \int_{x_1}^{x_3} (x-x_1)(x-x_3) dx \\ &\quad + \frac{f(x_3)}{(x_3-x_1)(x_3-x_2)} \int_{x_1}^{x_3} (x-x_1)(x-x_2) dx \\ &= \frac{f(x_1)}{(x_1-x_2)(x_1-x_3)} \int_{x_1}^{x_3} [x^2 - (x_2+x_3)x + x_2x_3] dx \\ &\quad + \frac{f(x_2)}{(x_2-x_1)(x_2-x_3)} \int_{x_1}^{x_3} [x^2 - (x_1+x_3)x + x_1x_3] dx \\ &\quad + \frac{f(x_3)}{(x_3-x_1)(x_3-x_2)} \int_{x_1}^{x_3} [x^2 - (x_1+x_2)x + x_1x_2] dx \\ &= \frac{f(x_1)}{(x_1-x_2)(x_1-x_3)} \left[\frac{1}{3} (x_3^3 - x_1^3) - (x_2+x_3) \frac{1}{2} (x_3^2 - x_1^2) + x_2x_3(x_3 - x_1) \right] \\ &\quad + \frac{f(x_2)}{(x_2-x_1)(x_2-x_3)} \left[\frac{1}{3} (x_3^3 - x_1^3) - (x_1+x_3) \frac{1}{2} (x_3^2 - x_1^2) + x_1x_3(x_3 - x_1) \right] \\ &\quad + \frac{f(x_3)}{(x_3-x_1)(x_3-x_2)} \left[\frac{1}{3} (x_3^3 - x_1^3) - (x_1+x_2) \frac{1}{2} (x_3^2 - x_1^2) + x_1x_2(x_3 - x_1) \right] \end{aligned}$$

$$\begin{aligned}
&= f(x_1) \left[\frac{\frac{1}{3}(x_3^3 - x_1^3) - (x_2 + x_3) \frac{1}{2}(x_3^2 - x_1^2) + x_2 x_3 (x_3 - x_1)}{(x_1 - x_2)(x_1 - x_3)} \right] \\
&\quad + f(x_2) \left[\frac{\frac{1}{3}(x_3^3 - x_1^3) - (x_1 + x_3) \frac{1}{2}(x_3^2 - x_1^2) + x_1 x_3 (x_3 - x_1)}{(x_2 - x_1)(x_2 - x_3)} \right] \\
&\quad + f(x_3) \left[\frac{\frac{1}{3}(x_3^3 - x_1^3) - (x_1 + x_2) \frac{1}{2}(x_3^2 - x_1^2) + x_1 x_2 (x_3 - x_1)}{(x_3 - x_1)(x_3 - x_2)} \right] \\
&= f(x_1)W_1 + f(x_2)W_2 + f(x_3)W_3
\end{aligned}$$

Derivation of Simpson's rule for unequally spaced data values (end points).

A Lagrange polynomial $p(x)$ is obtained such that $p(x_i)=f(x_i)$ for $i=1,2,3$ and integrated over the intervals $x_1 < x < x_2$ and $x_2 < x < x_3$ respectively.

Now,

$$\begin{aligned}
\int_{x_1}^{x_2} f(x) dx &\approx \int_{x_1}^{x_2} f(x_1) \frac{(x - x_2)(x - x_3)}{(x_1 - x_2)(x_1 - x_3)} + f(x_2) \frac{(x - x_1)(x - x_3)}{(x_2 - x_1)(x_2 - x_3)} + f(x_3) \frac{(x - x_1)(x - x_2)}{(x_3 - x_1)(x_3 - x_2)} dx \quad (B.3) \\
&= f(x_1) \left[\frac{\frac{1}{3}(x_2^3 - x_1^3) - (x_2 + x_3) \frac{1}{2}(x_2^2 - x_1^2) + x_2 x_3 (x_2 - x_1)}{(x_1 - x_2)(x_1 - x_3)} \right] \\
&\quad + f(x_2) \left[\frac{\frac{1}{3}(x_2^3 - x_1^3) - (x_1 + x_3) \frac{1}{2}(x_2^2 - x_1^2) + x_1 x_3 (x_2 - x_1)}{(x_2 - x_1)(x_2 - x_3)} \right] \\
&\quad + f(x_3) \left[\frac{\frac{1}{3}(x_2^3 - x_1^3) - (x_1 + x_2) \frac{1}{2}(x_2^2 - x_1^2) + x_1 x_2 (x_2 - x_1)}{(x_3 - x_1)(x_3 - x_2)} \right] \\
&= f(x_1)W_1 + f(x_2)W_2 + f(x_3)W_3
\end{aligned}$$

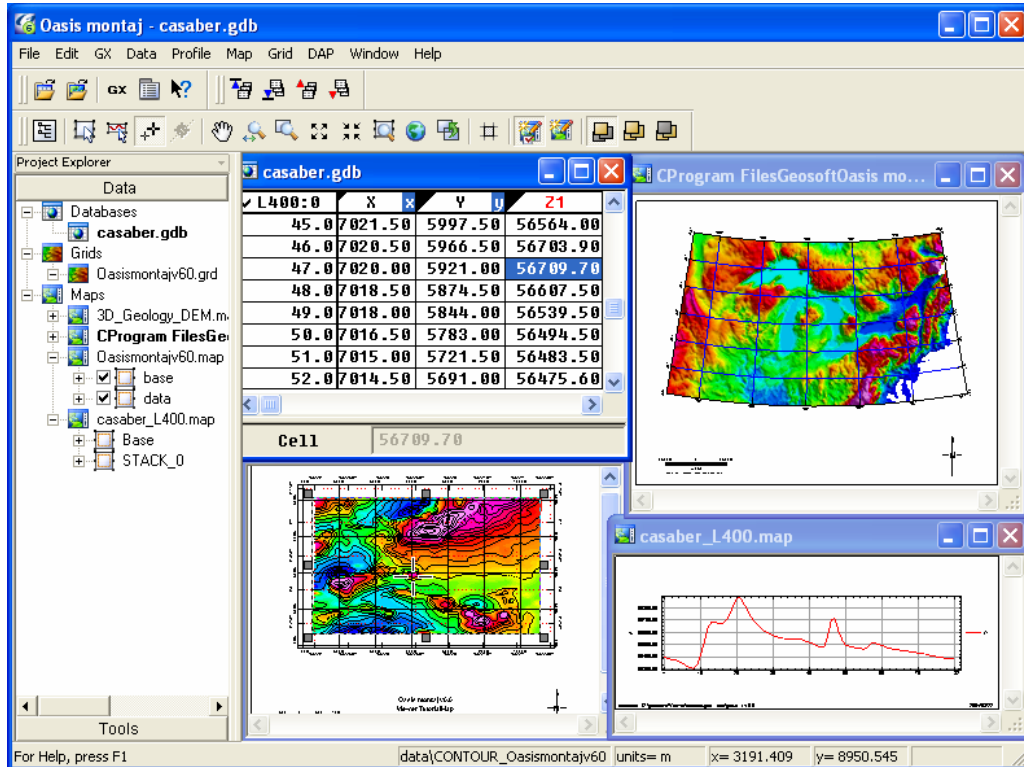
and

$$\begin{aligned}
 \int_{x_2}^{x_3} f(x) dx &\approx \int_{x_2}^{x_3} f(x_1) \frac{(x-x_2)(x-x_3)}{(x_1-x_2)(x_1-x_3)} + f(x_2) \frac{(x-x_1)(x-x_3)}{(x_2-x_1)(x_2-x_3)} + f(x_3) \frac{(x-x_1)(x-x_2)}{(x_3-x_1)(x_3-x_2)} dx \quad (\text{B.4}) \\
 &= f(x_1) \left[\frac{\frac{1}{3}(x_3^3 - x_2^3) - (x_2 + x_3) \frac{1}{2}(x_3^2 - x_2^2) + x_2 x_3 (x_3 - x_2)}{(x_1 - x_2)(x_1 - x_3)} \right] \\
 &\quad + f(x_2) \left[\frac{\frac{1}{3}(x_3^3 - x_2^3) - (x_1 + x_3) \frac{1}{2}(x_3^2 - x_2^2) + x_1 x_3 (x_3 - x_2)}{(x_2 - x_1)(x_2 - x_3)} \right] \\
 &\quad + f(x_3) \left[\frac{\frac{1}{3}(x_3^3 - x_2^3) - (x_1 + x_2) \frac{1}{2}(x_3^2 - x_2^2) + x_1 x_2 (x_3 - x_2)}{(x_3 - x_1)(x_3 - x_2)} \right] \\
 &= f(x_1)W_1 + f(x_2)W_2 + f(x_3)W_3
 \end{aligned}$$

Oasis montaj 6.3 Viewer

*The core software platform for working
with large volume spatial data*

QUICK START™ TUTORIAL



GEO SOFT
Knowledge from Data

www.geosoft.com

The software described in this manual is a completely free software environment that you can distribute freely to any recipient with whom you need to share your earth science results and ideas.

Manual release date: 26/04/2006.

Written by, Nancy Whitehead. Please send comments or questions to info@geosoft.com

Copyright © Geosoft Inc. 2006. All rights reserved. No part of this publication may be reproduced, stored in a retrieval system or transmitted, in any form, or by any means, electronic, mechanical, photo-copying, reading, or otherwise, without prior consent from Geosoft Inc.

Program Copyright© Geosoft Inc. 2006. All rights reserved.

Geosoft and Oasis montaj are registered trademarks of Geosoft Inc. GEOSOFT, Oasis are trademarks of Geosoft Inc.

Windows®, and Windows NT™ are either registered trademarks or trademarks of Microsoft Corporation.

Geosoft Incorporated
8th Floor
85 Richmond St. W.
Toronto, Ontario
M5H 2C9
Canada
Tel: (416) 369-0111
Fax: (416) 369-9599
Web Site: www.geosoft.com
E-mail: info@geosoft.com

Contents

Oasis montaj 6.3	1
Software and Hardware Requirements	1
Installing Oasis montaj <i>Viewer</i>	2
Install from the Oasis montaj <i>Viewer</i> CD ROM	2
Install from the Web	2
Authorizing Your Internet Communication Settings	3
Authorize Internet Communication Dialog	3
Internet Trust Relationship Dialog	3
Setting High-Resolution Graphics	4
Configuring Oasis montaj Settings	4
Finding More Help Information	5
Contacting Geosoft	5
Tutorial 1: Getting Ready to Work	7
Welcome to the Oasis montaj Environment	7
System Files	7
Creating a Working Directory	8
Before you Begin	8
Creating a Project	8
Changing Default Settings	10
Finding Help	13
Tutorial 2: Working with Data	15
Oasis montaj Databases	15

Opening a Database	15
Adding Compression to your Database	16
Displaying Data Files in an Oasis montaj Database	16
Displaying Channels (Columns) in the Spreadsheet	18
Displaying Basic Channel Statistics	20
Displaying Profiles in the Spreadsheet	21
DataBase Tool Bar	23
Profile Panel Options	23
Plotting Profile Windows	24
Metadata Tool	25
Data Types	25
Drag-n-Drop	27
Oasis montaj Maps	28
Displaying a Map	28
Adding Map Comments	28
Using the Map View/Group Manager Tool	28
Rendering Options	29
Other Tool Options	30
Using the Viewer Tool Bars	31
Standard Bar	31
Map Tools Bar	31
Navigation Tool Bar	32
Displaying Grids and Images on a Map	35
Data Access Protocol (DAP)	37
Using the Metadata Tool	42
3D Surface Tool	43
3D Rendering Memory Requirements	51
Copying and/or Converting Grid Files	52

Grid Report and Statistics	52
Sending E-maps	53
Unpacking an E-map	54
Exporting Data	54
Exporting Databases	55
Export Geosoft XYZ Data Format	55
Export CSV Format	56
Exporting Maps	56
Printing Maps in Oasis montaj	57
Printer Setup	58
Print a Map	58
Appendix 1: Geosoft Concepts	60
Oasis montaj Viewer	60
What is Oasis montaj?	61
Viewer Capabilities	61
Projects	61
Data and Profiles	62
Maps, Grids and Images	62
Online Help and Technical Support	62
Keeping you in touch with your data	63
Projects and the Project Explorer	64
What you need to know about Project files	65
Databases and high-volume data processing	66
Spreadsheets are the windows to your database	68
How the Spreadsheet Displays Project Data	69
Profiles and viewing your data graphically	70
Maps are more than printed sheets of information	71

Dynamically link data and information to knowledge	73
Geosoft Algorithms and Techniques	74
Process Maker technology links data processing	75
Appendix 2: Displaying Data Formats	76
Geosoft XYZ File Format	76
ASEG-GDF File Format	77
Geosoft GBN (Binary Data File) Format	78

Oasis montaj 6.3

Oasis montaj 6.3 is the latest release from Geosoft. **Oasis montaj** is available in two versions – a free *Viewer* and a licensed *Mapping and Processing System*.

The **Oasis montaj Viewer** is a free software product that enables you to view Geosoft databases, Geosoft grids and a variety of common image and data exchange formats. Specifically, this version provides you with the following capabilities:

- Access project data (Geosoft databases, grids and maps), tools (3D Tool and Project Explorer), and Geosoft toolbars (Database Tools, Map Tools, Standard Toolbar)
- Evaluate data, information and interpretations by viewing and performing specific tasks using Geosoft databases, profiles, maps, and grids as well as Geosoft and third-party images (including Geosoft PLT, AutoCAD DXF, MapInfo TAB, ArcView SHP and Microstation DGN files).
- Verify data quality, analyses and interpretations by tracking processes applied to databases and maps
- Perform selected processes made available through Geosoft menus or third-party GXs
- Share results and knowledge by viewing and/or sending E-maps to team members and other professional contacts
- Prepare reports using clipboard image copying capabilities

Software and Hardware Requirements

To run **Oasis montaj**, you require the following software and hardware:

Operating System	Windows XP recommended, Windows 2000 SP3 minimum. We do not support Windows 95, 98, Me or Windows NT
CPU	No requirement on a specific CPU type. An Intel Celeron processor is <u>not</u> recommended
RAM	512 MB or more of RAM recommended. 256 MB or more minimum (get as much RAM as you can afford)
Graphics	24-bit graphics card with 3D acceleration is recommended and required for full colour imaging. Recommend 64MB RAM on card
Printer/Plotter	Any Windows® supported colour printer. Hewlett Packard® large-format ink-jet plotters are recommended
Installation	Oasis montaj MUST be installed while logged on as Administrator
Installation Disk Space	1 GB or more of free space on the <i>Program Files</i> drive is required for the installation process
Data Disk Space	Data disk space depends on the volume of project data to be processed and the printer driver you are using, however 100 GB is recommended. This is largely based on your business and data

2 Oasis montaj

requirements.

Internet

To use the Internet capabilities in **Oasis montaj**, you will need to install [Internet Explorer 5.0](#) or later. This does not mean that you have to have Internet Explorer as your default browser; **Oasis montaj** just uses the Internet connection technology supplied in IE5

Installing Oasis montaj Viewer

The **Oasis montaj Viewer** can be installed from a CD-ROM or downloaded from the web and installed via an EXE file.

To use the Internet capabilities in **Oasis montaj**, you will need to install Internet Explorer 5.0 or later. This does not mean that you have to have Internet Explorer as your default browser; **Oasis montaj** just uses the Internet connection technology supplied in IE5 to connect to the web.

Install from the Oasis montaj Viewer CD ROM

Please note that your installation procedure will vary slightly depending on the operating system you are using. When installing **Oasis montaj** users **MUST** be logged on as **Administrator**.

1. Insert the **Oasis montaj** CD into your CD-ROM drive. The InstallShield Wizard Setup dialog is displayed and tells you that the system is preparing the installation.
2. When ready, the program displays the Geosoft **Oasis Montaj Viewer** – InstallShield Wizard Welcome screen. To continue, follow the directions on the screens that appear.
3. When the "Installation Completed" dialog is displayed, you can check the boxes provided to launch **Oasis Montaj Viewer** or view the release notes.
4. Click the [**Finish**] button to complete the installation process.

Install from the Web

The **Oasis montaj Viewer** can be downloaded from the Geosoft website at (www.geosoft.com/downloads/index.asp#free).

Please note that your installation procedure will vary slightly depending on the operating system you are using.

When installing **Oasis montaj** users **MUST** be logged on as **Administrator**.

1. Download the **Oasis montaj Viewer** (*.exe) file from the Geosoft website (www.geosoft.com/downloads/index.asp#free).
2. Run the self-extracting file (Oasis montaj Viewer.zip), the InstallShield Wizard Setup dialog is displayed and tells you that the system is preparing the installation.

3. When ready, the program displays the Geosoft **Oasis Montaj Viewer** – InstallShield Wizard Welcome screen. To continue, follow the directions on the screens that appear.
4. When the "Installation Completed" dialog is displayed, you can check the boxes provided to launch **Oasis Montaj Viewer** or view the release notes.
5. Click the [**Finish**] button to complete the installation process.

Authorizing Your Internet Communication Settings

The **Authorize Internet Communication** dialog box enables you to authorize what communication takes place between your **Oasis montaj** system and the Geosoft Internet Server. The **Internet Trust Relationship** dialog box enables you to select the default setting for authorizing all future communication with the server.

All communication with the Geosoft Server is encrypted for your privacy and security.

Authorize Internet Communication Dialog

This dialog box is displayed when **Oasis montaj** tries to communicate with an internet server. For example, when you try to download data from the Geosoft DAP server and your authorization is set to **Verify** (the default setting).

- Click the [**Authorize**] button to authorize the communication and connect to the server.
- Click [**Deny**] to cancel the communication. The server will not be accessed.
- Click [**Security**] to view the **Internet Trust Relationship** dialog box and change your default authorization setting (see below).

Internet Trust Relationship Dialog

This dialog box enables you to set the type of access you want when communicating with an internet or external server to download data.

You can select from three levels of access that will define how the Geosoft Server will communicate with your computer:



Trusted

This setting **will automatically authorize all communication** with the server. This means that you will not be prompted to verify everytime you connect with the Geosoft server. All communication with the server saved in a log file on your local computer so that you can check to see what information was sent and received.



Verify

This setting **will ask you to verify all communication** with the server before proceeding with a download. This means that whenever you access the server, the server will show you what is being downloaded and ask you to authorize it.

Click the [**Accept**] button to give permission and download the file(s) or click the [**Deny**] button if you do not want to download the file(s).

4 Oasis montaj

All communication with the server saved in a log file on your local computer so that you can check to see what information was sent and received. This is the default setting



Restricted

This setting **will not authorize any communication** with the server. This means that you do not want any communication with the server to take place. With this setting, you will not be able to download any data from the server.

Tip: You can modify your **Internet Trust Settings** at any time by clicking the **Settings/Internet** menu item from the **Edit** menu.

Setting High-Resolution Graphics

In order to view the colours in your maps and grids correctly, you may have to change your video card settings.

1. Click right mouse button on desktop screen.
2. On the *Properties* menu, click *Settings*.
3. Set the *colour palette* to High Colour 16-bit or True Colour 24-bit.

Configuring Oasis montaj Settings

Before you begin working with **Oasis montaj**, you may want to configure your other default settings. These settings can be accessed from the **Edit/Settings/General** menu item. For information on the different settings available in **Oasis montaj**, select the *Configuring Oasis montaj Settings* topic in the online help system.

Finding More Help Information

There are several other functions included in the basic **Oasis montaj** help system that may be useful to your work. The entire documentation for the system is available through the online help system. This electronic library of information enables us to constantly update the information and provide you with the most up-to-date information available.

The best way to find information in this system is to use the **Search** tab to perform a full-text search of all help topics. If you still can't find the information you're looking for, all of the Geosoft *Manuals and Tutorials* are available online, www.geosoft.com/resources/tutorials/

Contacting Geosoft

The list below provides contact information for Geosoft offices around the world. Note that, technical support is for **Licensed Users Only**.

North America

Geosoft Inc.,
85 Richmond St. W., 8th Floor
Toronto, Ont.,
Canada
M5H 2C9
Tel. (416) 369-0111
Fax (416) 369-9599
Email: info@geosoft.com

South America

Geosoft Latinoamerica Ltda.
Praça Floriano 51 / 19º Andar
CEP: 20031-050, Centro
Rio de Janeiro, RJ, Brasil
Tel: (55-21) 2532-0140
Fax: (55-21) 2532-7197
Email: info@geosoft.com

South and Central Africa

Geosoft Africa Ltd.
Buren Building, Second Floor
Kasteelpark Office Park
c/o Nossob & Jochemus Streets
Erasmuskloof X3, Pretoria
Tel: 27 12 347 4519
Fax: 27 12 347 6936
Email: info@geosoft.com

Europe and North Africa

Geosoft Europe Ltd.
20/21 Market Place, First Floor
Wallingford, Oxfordshire
OX10 OAD United Kingdom
Tel: +44 1491 835 231
Fax: +44 1491 835 281
Email: info@geosoft.com

Australia and Southeast Asia

Geosoft Australia Pty. Ltd
350 Hay Street
Subiaco WA 6008
Australia
Tel 61 (8) 9382 1900
Fax 61 (8) 9382-1911
Email: info@geosoft.com

Tutorial 1: Getting Ready to Work

In this tutorial, we will guide you through the steps you need to know to start working with your new software. At this point you should have already installed **Oasis montaj**. You should begin by starting **Oasis montaj**.

TO START USING OASIS MONTAJ

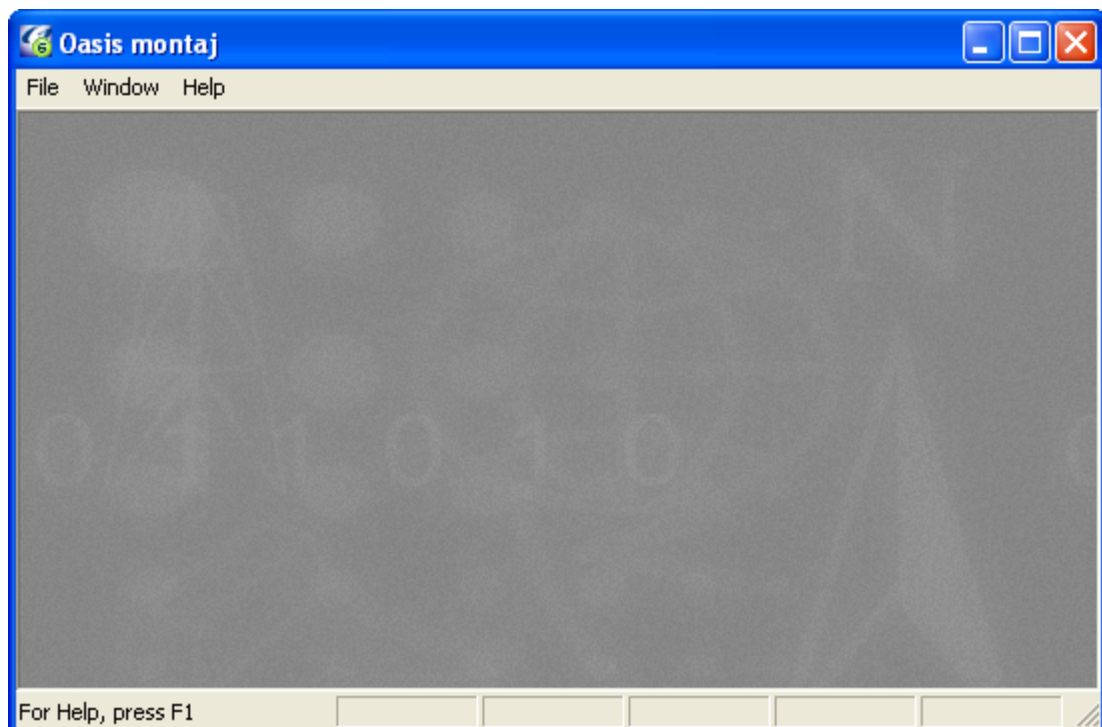
1. On the *Start* menu bar click *Programs* and then click *Geosoft* and then click *Oasis montaj Viewer/Oasis montaj Viewer*.

or

2. Double click on the **Oasis montaj Viewer** icon in Windows Explorer or File manager or the icon located on you desktop screen.

Welcome to the Oasis montaj Environment

When you run **Oasis montaj**, the system opens the **Oasis montaj** interface window.



System Files

As you work with the system, you will become familiar with a variety of standard files used for specific functions. The following list provides a short summary of the more important files.

Oasis montaj System Files

Geosoft database file

System File Extensions

*.GDB

8 Tutorial 1: Getting Ready to Work

Map file, including plots and grids	*.MAP
Geosoft grid file	*.GRD
Colour information for grids/images	*.AGG
Geosoft eXecutable	*.GX
Geosoft Script file	*.GS
Oasis Menu, Oasis sub-menu	*.OMN, * .SMN
Geosoft Project file	*.GPF
Geosoft projection information file	*.GI
Geosoft Map file (used in the MapInfo software to distinguish a Geosoft map file from a MapInfo (*.map) file)	*.GM

Creating a Working Directory

The system enables you to access files anywhere but it is a good strategy to carefully organize your data (project information and files) before carrying out any processing.

To start this tutorial, please create a working directory called **D:\Tutorial**. A general rule to follow in working with Geosoft applications is to avoid working in the directory where **Oasis montaj** was installed. In this tutorial, we will follow this rule by keeping all the working data files in **D:\Tutorial**.

Before you Begin

This tutorial uses sample data (**casaber.gdb**, **casaber.grd**, **xyz_format.xyz**, and **Oasis montaj v61.map**) which is available on the Geosoft website <http://www.geosoft.com/free/downloadfree.html>. Before you begin the tutorial, download and copy the data files to your working directory **D:\Tutorial**.

Creating a Project

To work in **Oasis montaj** requires an open Project. An **Oasis montaj** "Project" encompasses every item in your working project; from the data files in your project (databases, maps, and grids), to the tools used (including 3D tool and the Project Explorer), to the project setup including the menus you have displayed and whether you are working on a map or profile and the state in which you left it the last time you used it.

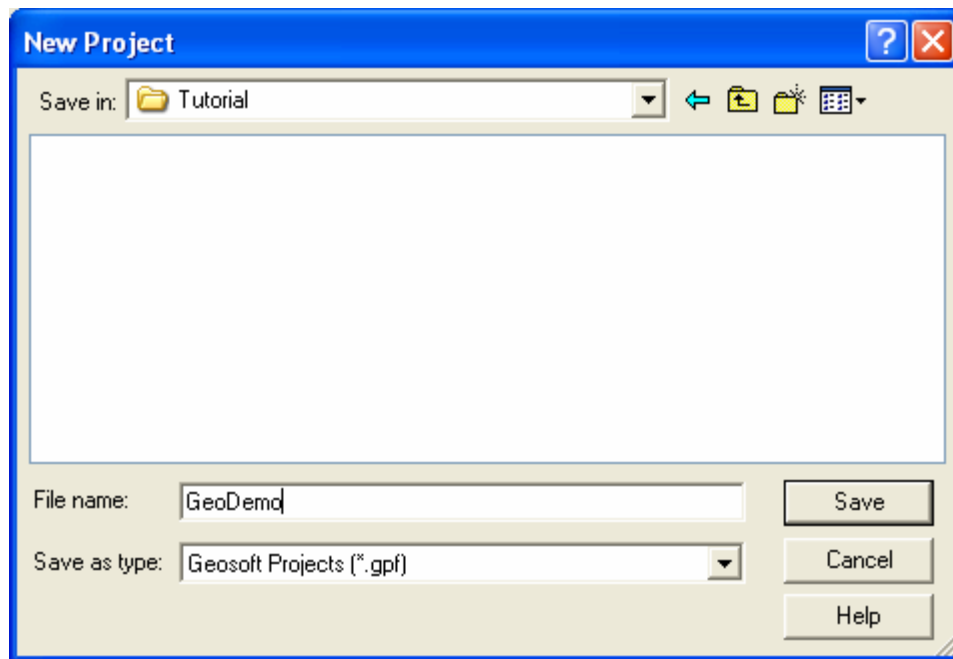
The project also controls your working directory. Projects are saved as (*.gpf) files. If you open an existing project from a directory, the system assumes that all your project files are located in the same directory. To streamline your work, as well as keep it organized, you may wish to make sure that your project file is in the same directory as the other files you want to use. We recommend that each project you work on have its own project (*.gpf) file.

The *Project Explorer* tool enables you to browse as well as open any project item. The Project Explorer has two windows, the *Data* window that includes all data files included in the project and the *Tools* window that organizes and maintains the project tools. To

access the Tools window click the Tools bar on the bottom of the Project Explorer. To return to the Data window, click the Data bar on the top the Project Explorer.

To CREATE A PROJECT:

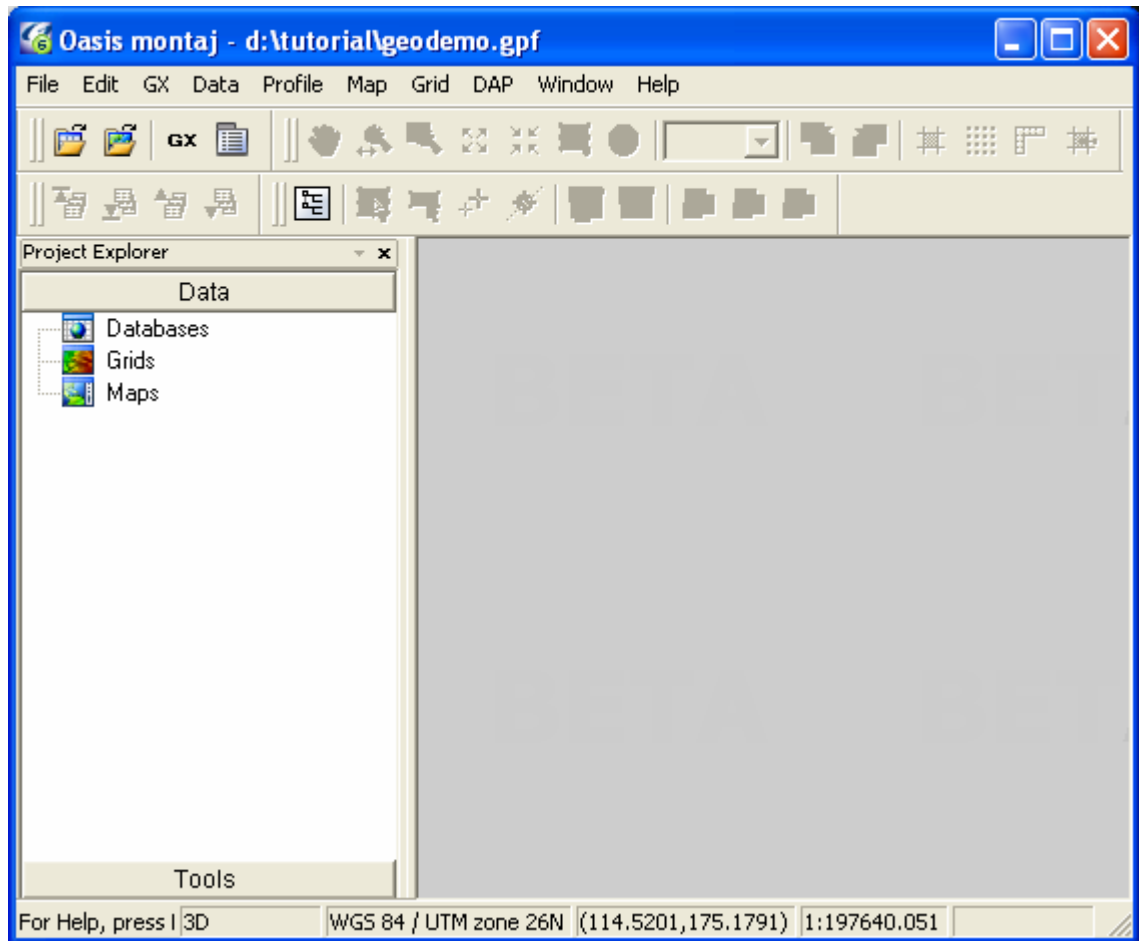
1. Start **Oasis montaj**.
2. On the *File* menu, click *Project* and then click *New*. The *New Project* dialog is displayed.



Note: **Oasis montaj** assumes that your data is in the directory containing this project

3. Specify a name and directory for the project. For example, name the project **GeoDemo** and specify the working directory as **D:\Tutorial**
4. Click the [**Save**] button. The system saves the project and indicates it is open by adding menus to the menu bar, adding buttons to the *Standard*, *Database*, *Map Tools* and *Navigation* short-cut toolbars and by displaying the *Project Explorer* window. These are visual clues indicating that you are ready to start working with the system.

10 Tutorial 1: Getting Ready to Work



5. To close a project, click *File/Project* and then click *Close*.

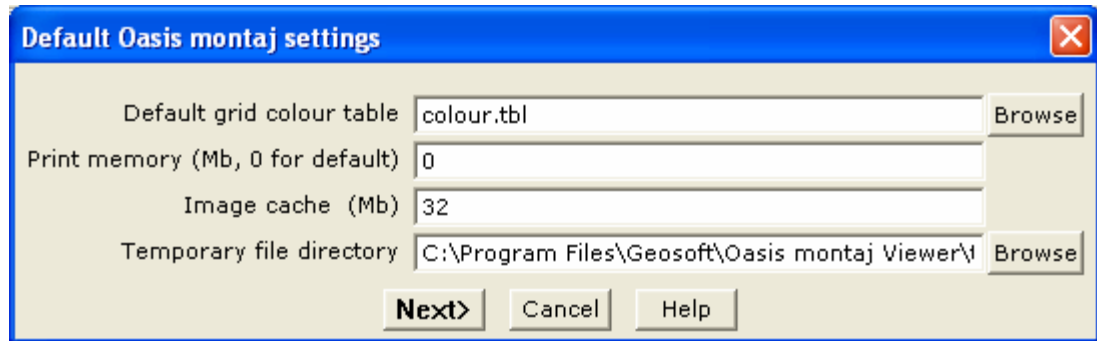
Changing Default Settings

The program will work correctly with all of the standard default settings; however these may be changed to reflect your personal requirements or those of your computer. The default settings are the selections made for many of the programs where there is no user input and are designed to yield logical results.

You may overwrite some of these intelligent defaults in normal use but this should not create any problems since the defaults are only intended to get you started with the system and should change as your knowledge of the system increases.

TO CHANGE THE DEFAULT SETTINGS OF THE OASIS MONTAJ ENVIRONMENT

1. On the *Edit* menu, click *Settings* and then click *General*. The *Default settings* dialog is displayed.
2. Select the desired choices from the available selections. You need not change any selections at this time. Once you are more familiar with Geosoft, you may come back to alter the settings.



The following list summarizes the default settings:

- | | |
|----------------------------------|---|
| Default grid colour table | Select the default colour table to use for displaying grids |
| Print memory (megabytes) | <p>Select the amount of RAM you would like the Geosoft print driver to use when printing. This only effects print configurations that use the Geosoft drivers. Enter 0 to use the default, which is 33% of the total physical RAM available on the system.</p> <p>The Geosoft print driver will slice each print job into bands of this size. The more RAM you use for printing, the faster printing will be. If you specify too much RAM, it is possible to significantly diminish the performance of other tasks on the computer. This amount should normally not exceed 50% of the installed RAM on your system, although we will allow the value to be up to 75% of the available RAM.</p> <p>This setting is not used by the Windows driver. If you use the Windows print driver, the printing process will use virtual memory up to the size required by the print. This can be up to 600 MB for A0 (E) size plots. We recommend that you use the Geosoft drivers when working with large plotters.</p> |
| Image Cache | <p>Select the amount of virtual RAM you would like to reserve for the image cache. As images are displayed in Oasis Montaj, an efficient access version of the image will be stored in the cache if there is room. The cache copy of the image greatly improves the performance of rendering the image when zoom/pan/redraw operations are performed. If there is insufficient room in the cache, the image will always be rendered from the DAT interface, which is slower.</p> <p>We recommend that you should set the image cache size to about 4 times the largest images that you routinely work with. Note that the image cache will be created in the GEOTEMP</p> |

12 Tutorial 1: Getting Ready to Work

directory, and there must be sufficient room to hold the cache plus other Geosoft temporary files. The image cache should not be more than 50% of the available room in GEOTEMP.

Temporary file directory

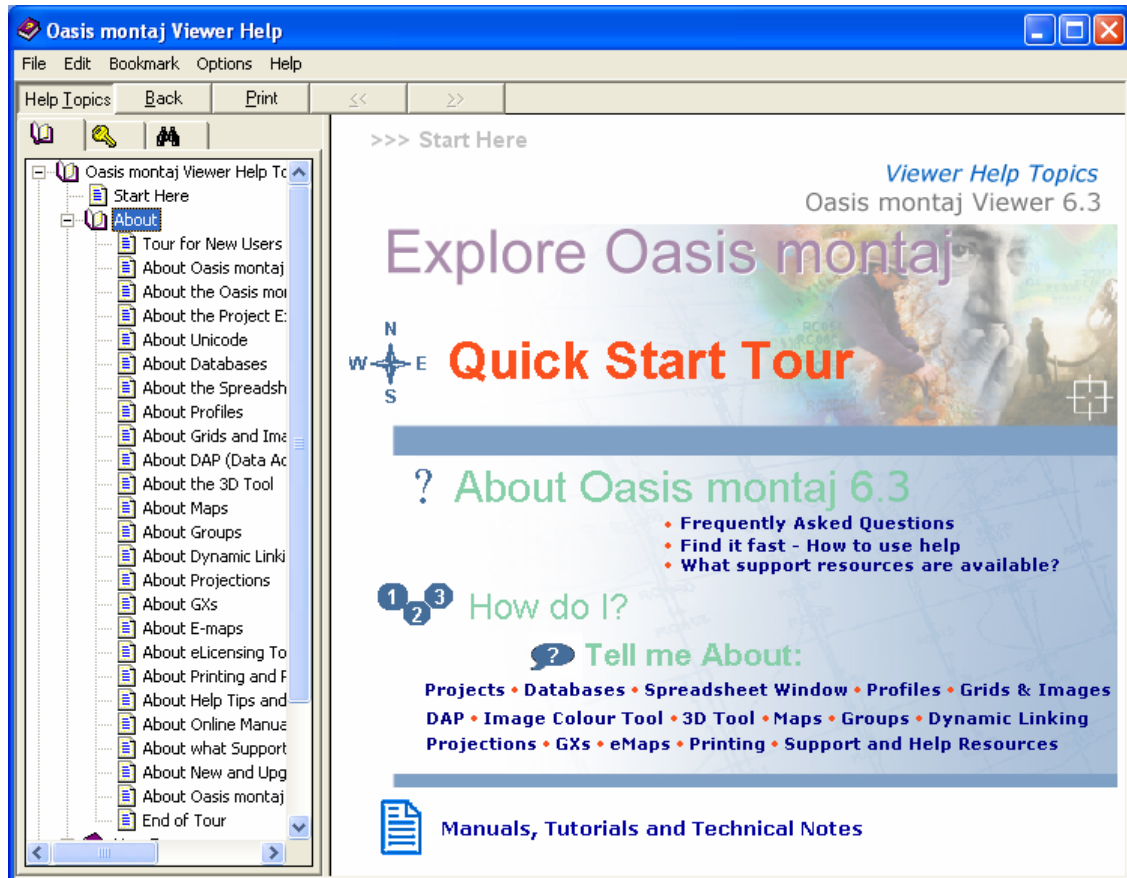
This directory is used by **Oasis montaj** to store temporary files. Depending on the application, the requirements for storage in this directory can be VERY large (from 10 megabytes to gigabytes). We recommend setting this parameter to a very FAST drive. This will improve performance of all large data operations (magmap, gridding, etc).

Oasis montaj cannot start if this drive is invalid or if it is set to a drive in which it cannot create files (CD ROM). Please ensure that the directory is always valid.

Note that in previous versions of **Oasis montaj** the GEOTEMP environment variable determined where this directory was stored. This variable is no longer used and the setting is controlled through the Windows registry.

Finding Help

Oasis montaj provides help information through two different interfaces. The **Online Help system** can be used to locate quick information using contents, index and find search tools. For new users we recommend that you take the online tour included in the *About* topics, which will introduce you to **Oasis montaj**. The **Manuals, Tutorials, and Technical Notes** system (using Acrobat Reader 4.0) contains full-length documents that you can download from the Geosoft website (www.geosoft.com/resources/tutorials/) and print.



Tutorial 2: Working with Data

To use **Oasis montaj** effectively, you will need to understand a bit about databases, spreadsheets, profiles and maps. The “window” to the database in **Oasis montaj** is a specialized earth science spreadsheet that appears automatically when you open a database. This spreadsheet provides access to a wide range of data management and profile viewing capabilities. Maps have special properties that you will learn about in later tutorials.

The purpose of this tutorial is to provide you with an overview of how you can use this data management system effectively.

Oasis montaj Databases

One of the fundamental technologies in **Oasis montaj** is its unique database architecture. This architecture is designed to let you display many kinds of data formats (ASCII and binary) in high-performance **Oasis montaj** databases.

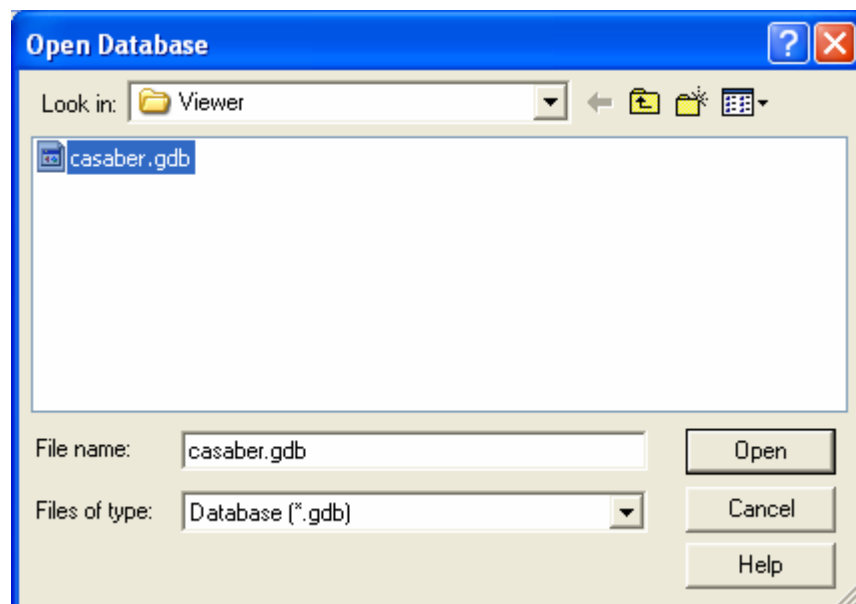
Oasis montaj provides the ability to add compression to a database. You can choose to compress for speed, size or use no compression at all. The type of compression you use depends on which type better suits your needs. We recommend that you use speed, as it provides the fastest access to your data with a good compression rate.

Opening a Database

Geosoft databases store and organize your survey data. Databases are displayed and organized in **Oasis montaj** in the Spreadsheet Window.

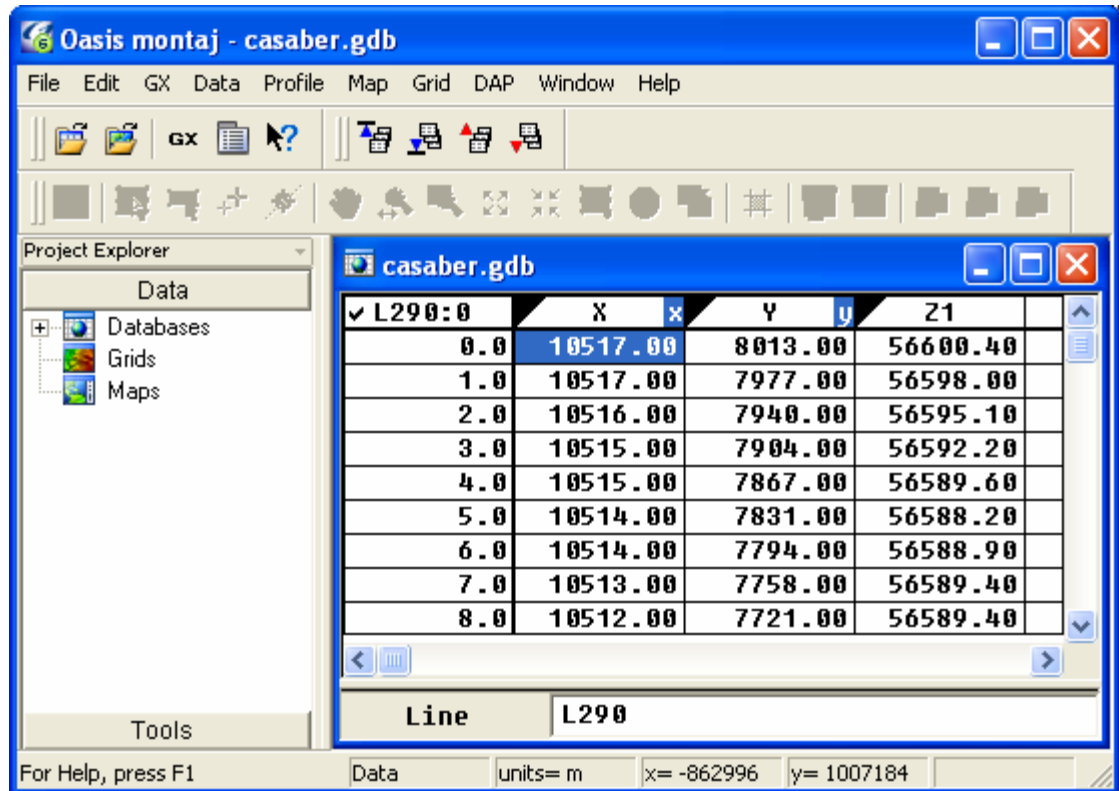
TO OPEN A DATABASE

3. On the *Data* menu, click *Open*, and then click *Open database*. The *Open Database* dialog is displayed.



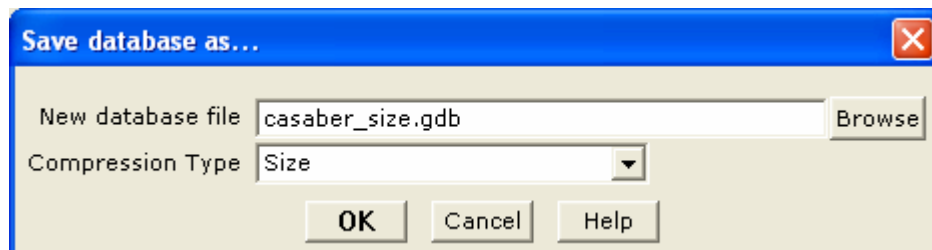
16 Tutorial 2: Working with Data

4. Select the tutorial database (**casaber.gdb**) and click **[Open]**. The **casaber.gdb** is displayed in your project.



Adding Compression to your Database

1. On the *Data* menu, click *Save database as*. The *Save database as* dialog is displayed.



2. Specify a new database name (**casaber_size.gdb**). From the *Compression Type* dropdown list select (**Size**) click the **[OK]** button to continue.
3. The new database (**casaber_size.gdb**) is displayed in your project.

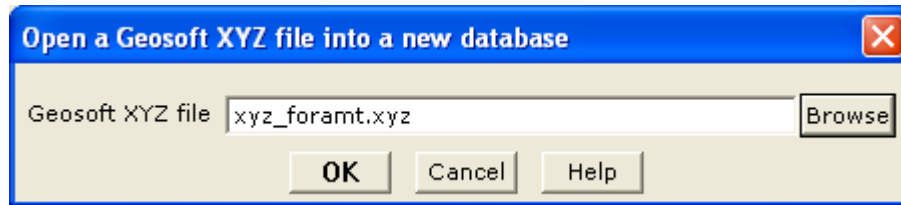
Displaying Data Files in an Oasis montaj Database

There are a number of options for displaying Geosoft and third-party formatted data files in an **Oasis montaj** database. In this tutorial, you will display a standard Geosoft XYZ

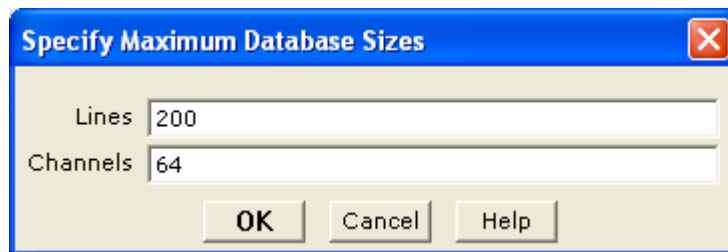
file. For more information about the Geosoft XYZ format and other file formats that can be displayed in an **Oasis montaj** database see *Appendix 2: Displaying Data Formats*.

DISPLAYING AN XYZ FORMAT FILE IN A DATABASE

1. On the *Data* menu, click *Open*, and then click *Geosoft XYZ*.
2. The *Open a Geosoft XYZ file into a new database* dialog is displayed.

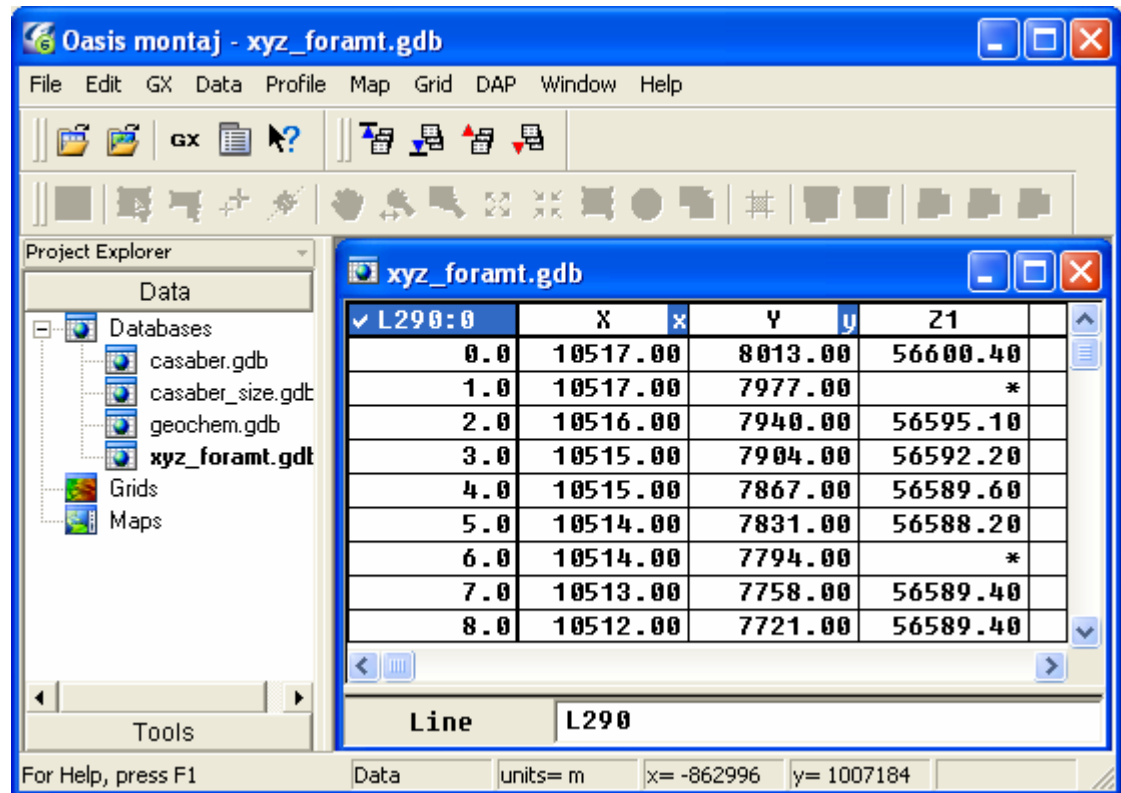


3. Using the [**Browse**] button locate the *Geosoft XYZ file* (**xyz_format.xyz**) in your project directory.
- Tip:** The [**Browse**] buttons allows you to browse and select files from anywhere on your computer or network drives.
4. Click the [**OK**] button. The system displays the *Specify Maximum Database Sizes* dialog.



5. This dialog enables you to specify the maximum size of the database in which the file will be displayed. You can accept the intelligent defaults and click the [**OK**] button. The file will be displayed in a Geosoft database with the same name as the XYZ file, but with a (*.gdb) extension (**xyz_format.gdb**).

18 Tutorial 2: Working with Data



Note: The default placeholder for missing or blank data (i.e. dummy value) in an XYZ file is “*”.

Displaying Channels (Columns) in the Spreadsheet

Unlike traditional spreadsheets, the **Oasis montaj** Spreadsheet windows provide a *view* of your database instead of the actual data in the database. This design enables you to customize the spreadsheet to display data to your specifications.

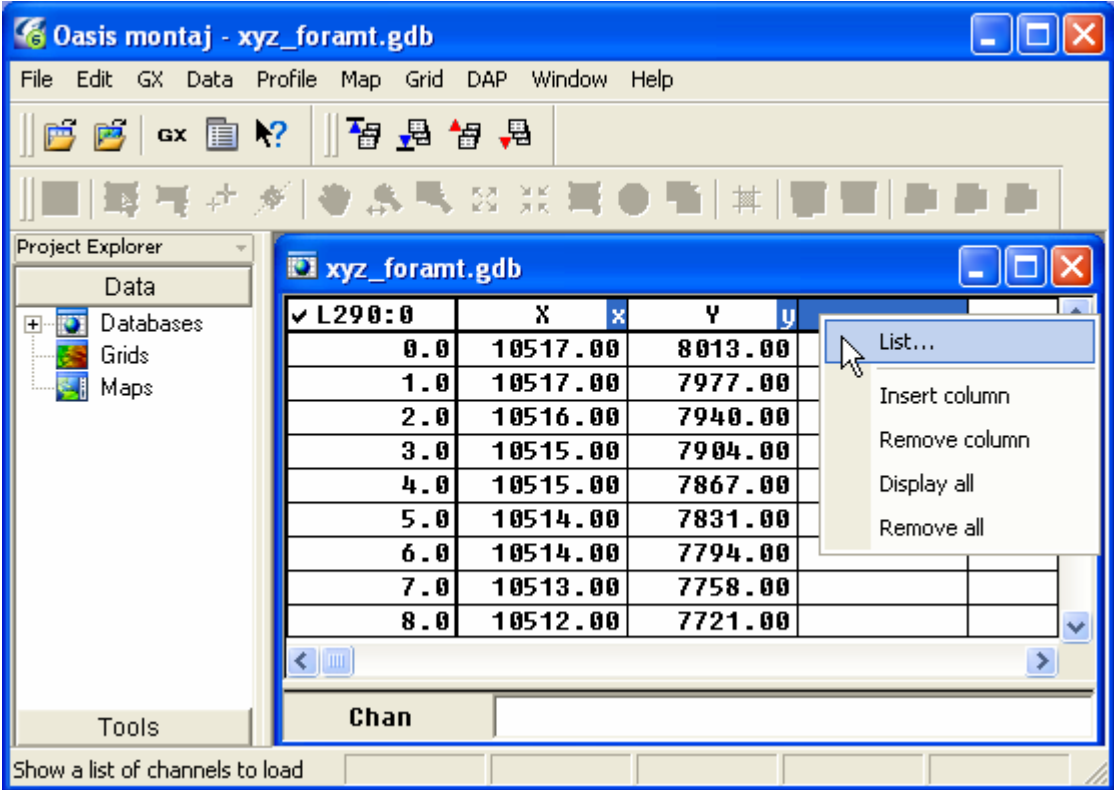
To REMOVE A CHANNEL (COLUMN)

1. Click once on the channel header cell labelled **Z1** to select it. Press the [**space bar**] key on the keyboard or click on the right mouse button and select *Remove column* from the popup menu. The channel is removed from the Spreadsheet view

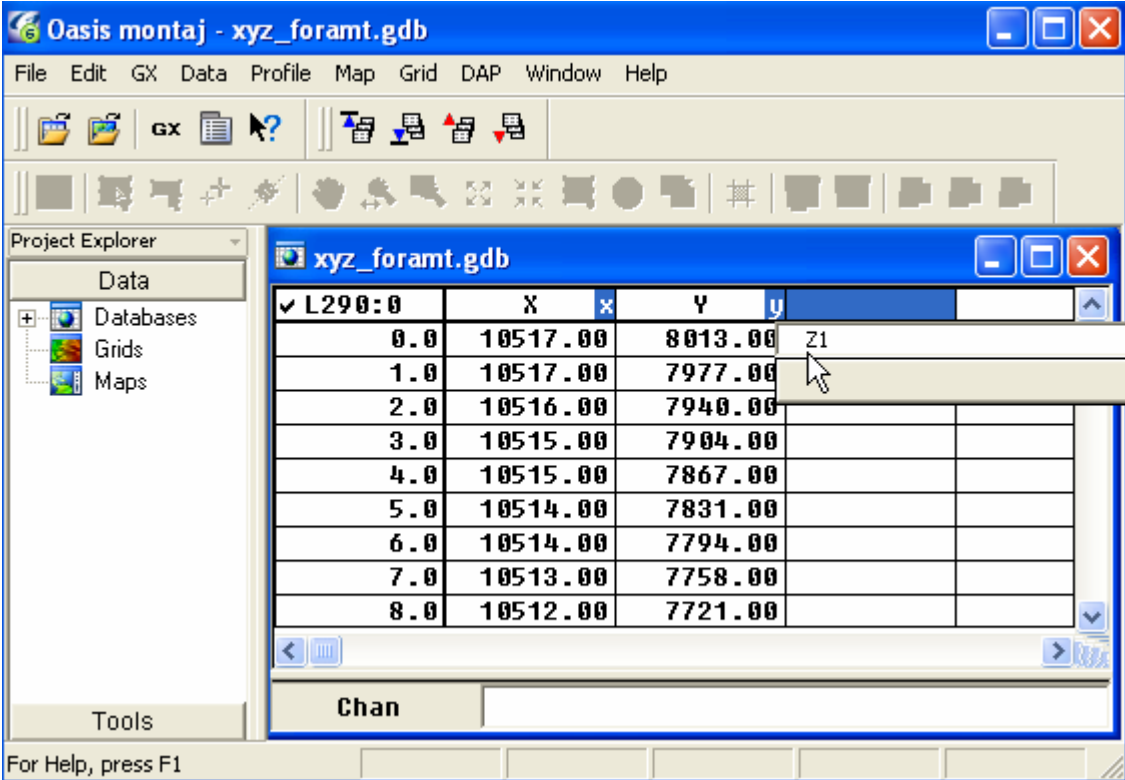
Note: The database (*.gdb) file still contains all the data. The Spreadsheet is only used to provide a view of selected channels.

To DISPLAY A CHANNEL

1. Move to the top of the first empty channel header and click right mouse button and select *List* from the popup menu.



- 2. A box will appear beneath the empty channel header listing all the available channels that are not currently being viewed in the Spreadsheet window.



20 Tutorial 2: Working with Data

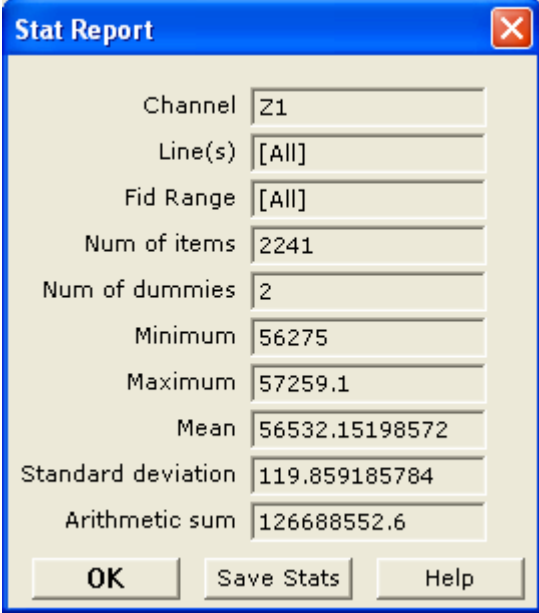
3. Select **Z1** and click the **[OK]** button, to display the channel in the Spreadsheet.
- Tip:** If you know the name of the data channel already, you can simply position the cursor on a specific Channel Header Cell, type the name and press the **[Enter]** key.
- Note:** The symbol ‘**’ in a channel cell indicates that the data are too wide for the spreadsheet column. To change the width of a column, place the cursor on the dividing line between the column headers. The cursor changes to a double arrow. Holding the left mouse button, drag the line to the right to increase the column width. Release the mouse button when done.

Displaying Basic Channel Statistics

After you open a Spreadsheet and display one or more channels, you can display and save the channel statistics.

TO CALCULATE BASIC STATISTICS ON A CHANNEL:

4. Click three times on the channel header cell labelled **Z1** to select (highlight) the channel header and all of the lines in the database. The selected data is the data the system will calculate the statistics on.
5. Click the right mouse button and select *Statistics* from the popup menu.

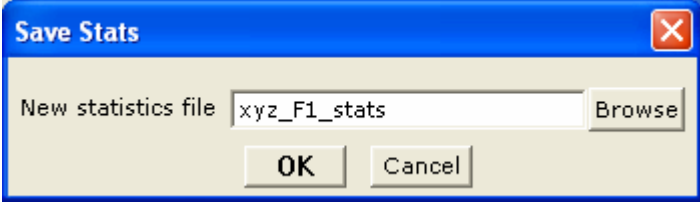


The 'Stat Report' dialog box displays the following statistics for channel Z1:

Field	Value
Channel	Z1
Line(s)	[All]
Fid Range	[All]
Num of items	2241
Num of dummies	2
Minimum	56275
Maximum	57259.1
Mean	56532.15198572
Standard deviation	119.859185784
Arithmetic sum	126688552.6

Buttons: OK, Save Stats, Help

6. You can save a copy of the statistical report by clicking the **[Save Stats]** button. The *Save Stats* dialog is displayed.



The 'Save Stats' dialog box shows the following information:

New statistics file: xyz_F1_stats

Buttons: OK, Cancel

- In the *New statistics file* box, specify a file name (**xyz_F1_stats.txt**). Click the **[OK]** button to save the file to your project directory. Then, click the **[OK]** button to close the *Stat Report* dialog box.

The following list summarizes how to obtain results on specific parts of your database:

Click once on the channel header cell to highlight the header cell.	No statistics can be calculated.
Click twice (double click) on the channel header cell to highlight the data in the current line (group).	Statistics are calculated for that specific line of the database.
Click three times on the channel header cell to highlight the data in all of the selected lines (groups) in the database.	Channel statistics are calculated for all of the selected lines in the database.

Displaying Profiles in the Spreadsheet

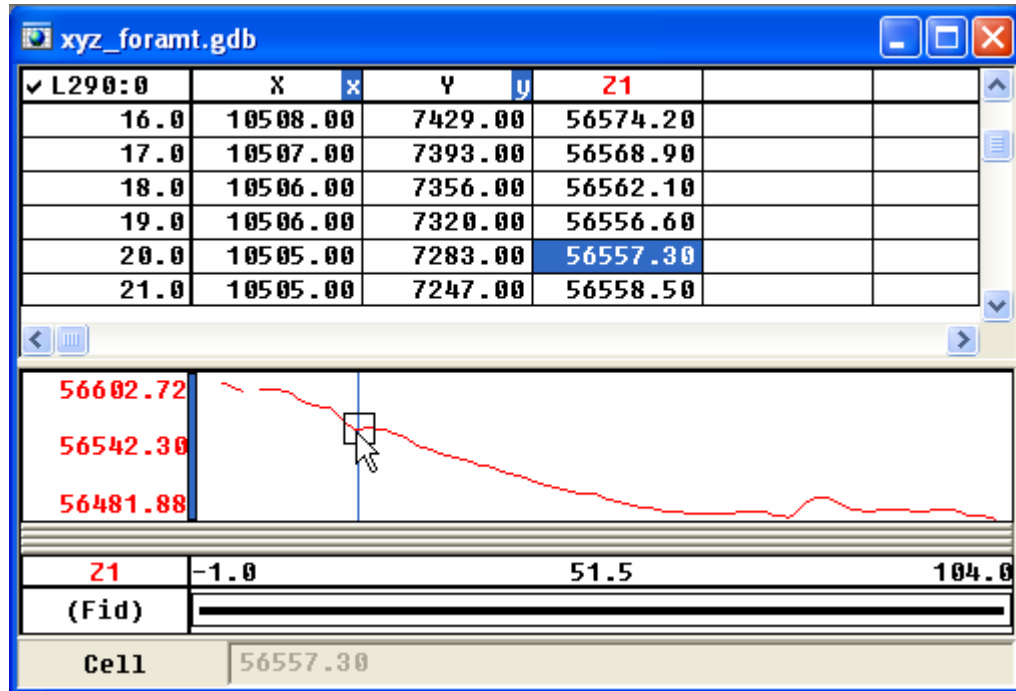
After you open a Spreadsheet and display one or more channels, you have the option of displaying them as a graphical profile line. You can display profiles for one or more channels in your database. The profile appears in the profile windows directly below the corresponding database. You can have up to five windows displayed, with a maximum of 32 channels displayed in each window. Profile windows are linked dynamically to their corresponding database. When you select a value or range of values in either the database or profile window respectively, they are also highlighted in the other window.

For more information about the Profile window, please refer to the Help system.

TO DISPLAY A PROFILE:

- Click the left mouse button on the channel header cell labelled **Z1** to highlight it. On the *Profile* menu, click *Show Profile*.
- The system displays a profile of the data in the *Profile Window* below the spreadsheet.

22 Tutorial 2: Working with Data

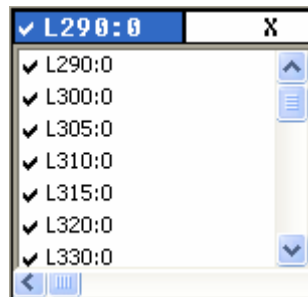


Tip: To see where the Z1 values are located on the profile line simply click on a value in the **Mag** channel and the system will show a box indicating the corresponding area on the profile.

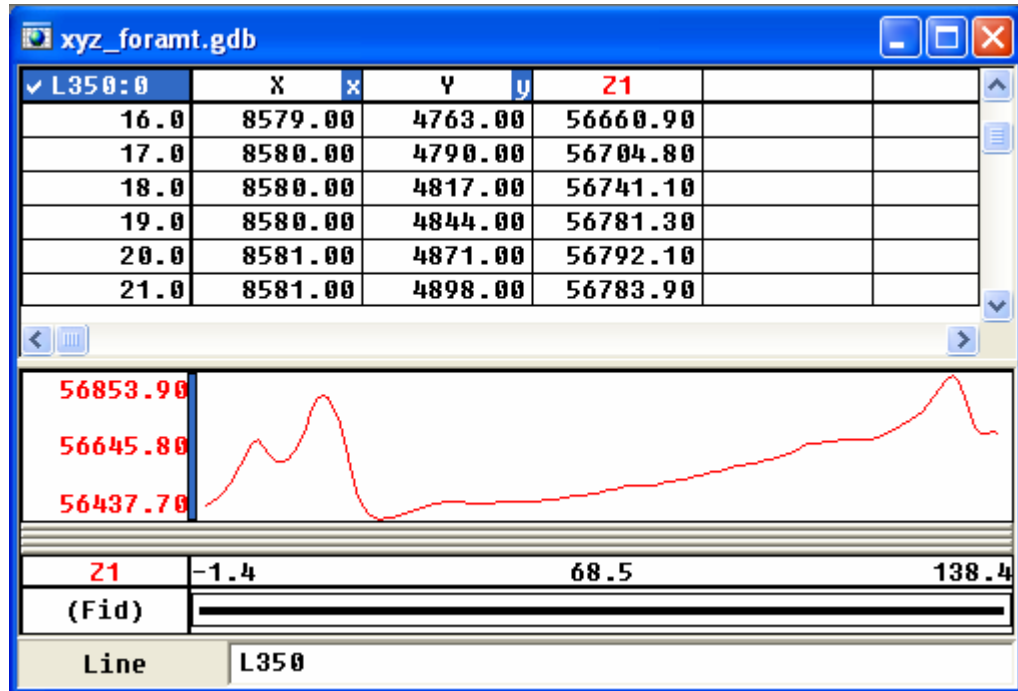
3. We recommend you experiment with the various options available for profile display, appearance, scaling and plotting etc. available via the *Profile* menu, under *Profile Options*.

TO DISPLAY A DIFFERENT PROFILE:

1. Move the cursor to the *Line Header Cell* in the top left corner of the spreadsheet. The currently displayed line in the worksheet is **L290:0**.
2. Click right mouse button on this cell and select the *List* option from the popup menu. A list of the line numbers is displayed. You can think of each line number as a worksheet in the spreadsheet window. When you view a new line number a new worksheet is opened in the spreadsheet window with corresponding line number information.



3. Click on **L350:0** from the list and display a profile for this line. The profile for **L350:0** is shown below:

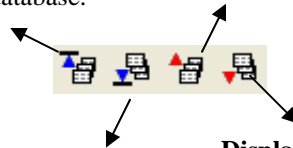


Tip: When the Line Number Cell is highlighted, you can use the **[Page Up]** and **[Page Down]** keys from your keyboard to scroll through lines. You can also use the *Database Tool Bar* to scroll through the lines. The figure below shows what each of these buttons do.

DATABASE TOOL BAR

Display First Line/Group. Click this button to show the data and profiles for the starting line in your database.

Display Previous Line/Group. Click this button to show the data and profiles for the previous line in your database.



Display Last Line/Group. Click this button to show the data and profiles for the final line in your database.

Display Next Line/Group. Click this button to show the data and profiles for the following line in your database.

Profile Panel Options

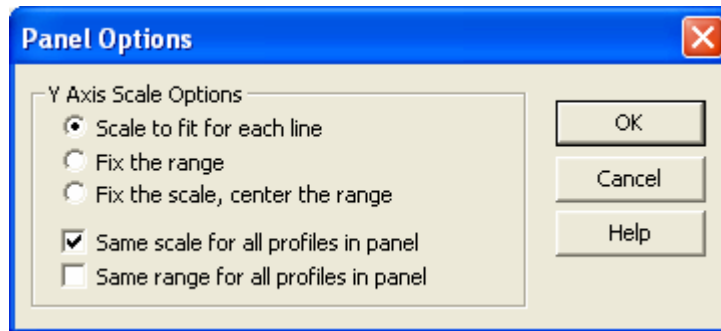
The *Panel Options* dialog box enables you to set scale options for the Y axis of the profiles in the profile window.

TO DISPLAY THE TWO PROFILES AT THE SAME SCALE:

1. Click the right mouse button on the profile window. On the *Profile* popup menu, click *Panel Options*.

24 Tutorial 2: Working with Data

- The system will display the *Panel Options* dialog box. Make sure the *Scale to fit for each line* option button is selected and there is a check mark in the *Same scale for all profiles in panel* option box.



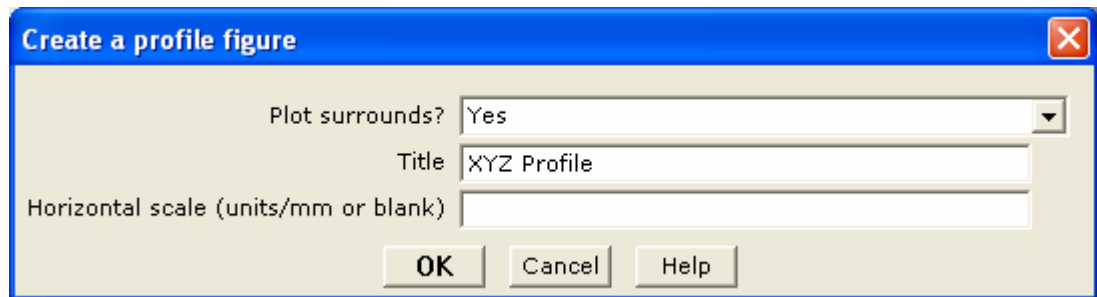
The following list summarizes the different scale options available to you:

Scale to fit for each line	Adjusts the scale in the profile box to fit each line that is displayed.
Fix the range	Uses the same range for all the profiles that are displayed..
Fix the scale, centre the range	Fixes the ranges and displays the line in the centre of the window.
Same scale for all profiles in panel	All profiles (including those from different channels) are set to the same scale.
Same range for all profiles in panel	All profiles are centred individually on their own mid-data value. Note: This is useful, for instance, in observing in-phase and quadrature values where there is a DC shift between the two levels.

Plotting Profile Windows

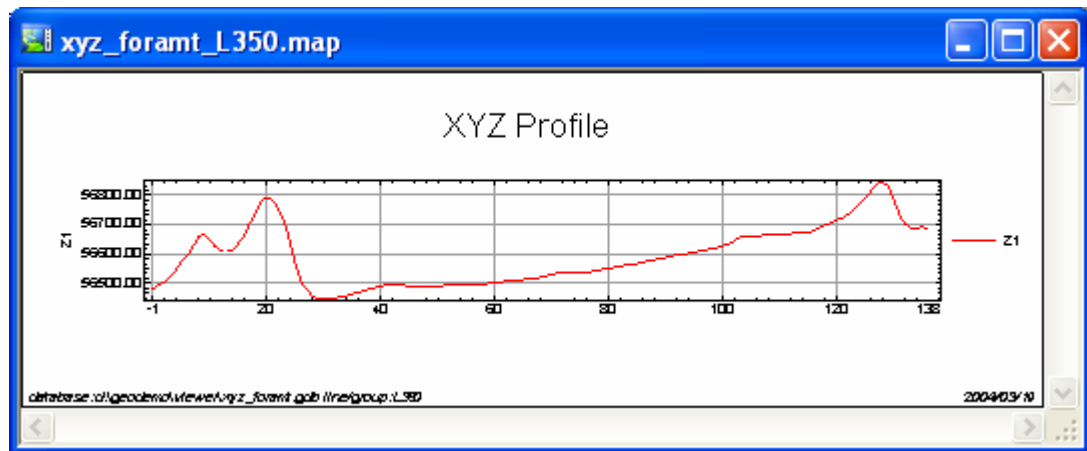
Oasis montaj enables you to quickly plot your displayed profile windows as an **Oasis montaj map** file. The map is named using the name of the current database and the profile line number.

- On the *Profile* menu, click *Plot profile figure* or click the right mouse button on the profile window and select *Plot Profile* from the popup menu.
- The *Create a profile plot* dialog is displayed.



- From the *Plot surrounds?* dropdown list select **Yes**. Then specify a *Title* and *Horizontal scale (units/mm or blank)*.

- Click [OK]. The profile plot map (**xyz_format_L350.map**) is displayed in your project.



Metadata Tool

The *Metadata Tool* is a context-oriented, interactive method for viewing and editing attributes assigned to Geosoft data.

Attributes (or metadata), information about data, can be simple or complex and the descriptive needs of different kinds of data are infinitely diverse. To allow for this and provide flexibility, Geosoft developed the *Metadata Tool* to help you organize your metadata.

Even though each Geosoft data type (database, map, point, polygon, etc) exhibits many different attributes, using the tool is simple. The current selection drives what exists inside the tool. For example, while in map edit mode, select a polygon to see that polygon’s attributes. As the context changes (i.e. database becomes current document or you select text on a map, etc.) so does the tool’s focus.

Data Types

The following table provides examples of the data types available to be stored and viewed using the *Metadata Tool*:

Databases	Displays mostly un-editable content including Name, numbers of Lines, Channels, and lists all Lines and Channels. Some editable content includes the projection and a description.
Grids	One of the most attribute-rich data type in the Geosoft world. Includes basic information including Name, Description, Location/Boundary Information, Origins, etc. Also could include a handy polygon file outlining the boundary region and a fully editable projection field.
Maps	Once a map has been selected into context, some basic information is shown. Maps are special, however, in that they

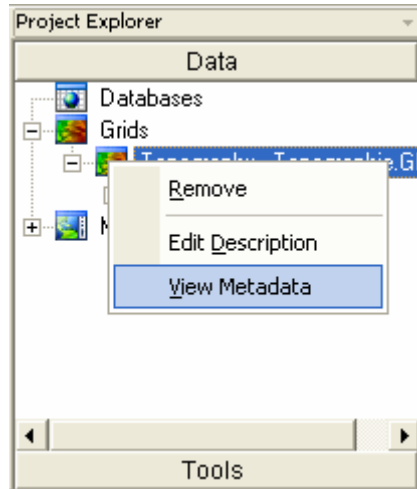
26 Tutorial 2: Working with Data

	can exhibit attribute information for specific map elements. For example, a polygon contains specific attributes which are displayed if a polygon is the current selection (only permitted in map edit mode). Map views and groups exhibit different characteristics and the tool is adjusted with each context change. Map elements (polygons, lines, points, etc.) exhibit their own attributes depending on the context chosen.
Global Settings	Contains all the information need to customize and drive Oasis montaj sessions.

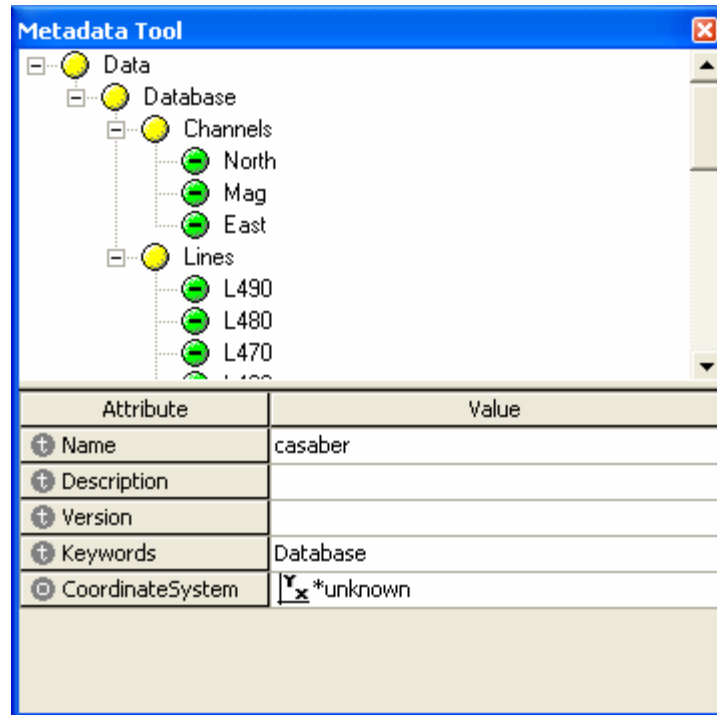
Note: Values displayed in a grey box cannot be edited. Values displayed in a white box may be edited.

To VIEW METADATA:

1. Select (highlight) a data item in the *Project Explorer* window (i.e. database (*.GDB), map (*.MAP), or grid (*.GRD) file. Right-click and from the popup menu, select *View Metadata*.



2. The *Metadata Tool* will be displayed.



3. The white letter in a grey circle to the left of the “Attribute” indicates the data value type; "i" for integers, "r" for real floating point numbers, "t" for text, and "o" for data objects.
4. Some information is contained in an object, which will normally display an object icon and object name as the Value. The *CoordinateSystem* attribute shown above is an example of an object. Objects can usually be edited or activated by double-clicking on the object value. For example, double-clicking on the *CoordinateSystem* will display the coordinate system in the Geosoft Coordinate System dialog.
5. Values displayed in a grey box cannot be changed. Values displayed in a white box may be changed.
6. To close the dialog, click the (X) on the top right corner.

Drag-n-Drop

The ability to drag XYZ files and drop them into an open database file (*.GDB) has been added to **Oasis montaj**. Note that, only default parameters are used and XYZ files must be in the correct format and the database must be large enough to hold the dropped XYZ file.

The ability to drag other file types directly from Windows Explorer and drop them into **Oasis montaj** for display is also available including; grid files (*.GRD), map files (*.MAP) and database files (*.GDB) files. Items on the Project Explorer bar may also be dragged and dropped.

Oasis montaj Maps

In **Oasis montaj**, a *Map* is more than a printed sheet of information. Maps are special items that serve a number of purposes in the system. The map window provides the basic mechanism for creating maps, displaying images, and linking to other maps and data. To work effectively with maps, you need to be familiar with the purposes of maps in the system as well as the role of *Views* and *Groups*.

Maps use *Views* to organize and display information. A *View* divides the information on a map into a Base view, (e.g. map surrounds, north arrows, and scale bars) which uses paper coordinates, and a Data view, (e.g. map coordinates, contours, and grids) which uses ground coordinates.

Maps use *Groups* to determine the order in which objects are displayed (rendered) on a map. *Groups* are layered on top of each other in a specific order determined by the *Map View/Group Manager Tool*.


Displaying a Map


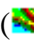


1. On the *Map* menu, click *Open map*. The *Open Map* dialog box is displayed.
2. Select the map file (**Oasismontaj.map**) and click [**Open**]. The map is opened in your project.

Adding Map Comments


1. On the *Map* menu, click *Map comments*.
2. The *Default Text Editor* (i.e. notepad) is displayed.
Note: If you have not specified your *Default Text Editor*, the *Select a default text editor* dialog is displayed. Using the [**Browse**] button, locate a text editor on your computer (notepad is recommended), and then click [**OK**].
3. Type your comments in the window, then save the file and exit the text editor. The comments are saved in the map file (*.map file).

Using the Map View/Group Manager Tool

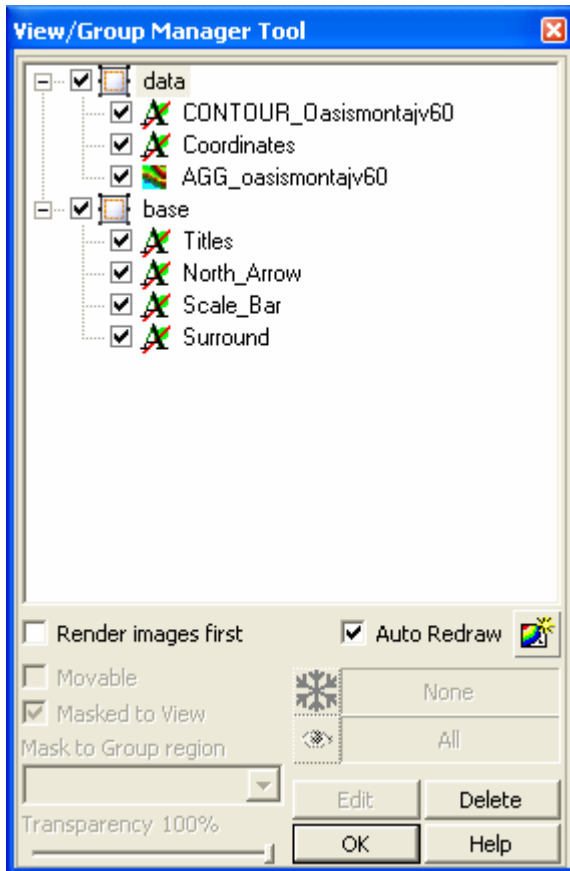
You can use the *Map View/Group Manager* tool () to display and edit the Views and Groups in a map. This tool consists of a 'tree' structure that contains two main branches representing the *Base* view and the *Data* view. Under each view, a number of groups are listed according to their layer on the map

Each group in a view shows an icon beside its name that identifies the group as either a map vector object () or an aggregate (). Views can either be normal *2D views* () or *3D views* (). The check boxes in the tree controls and indicates visibility of an item.


To select single items in the tree click on the item desired. Multiple selections of groups within a view can be achieved by holding the <Ctrl> key and clicking on the desired items. Changing the selection during group editing will end group editing without cancelling any current changes.

The effect of a double click on any item depends on the state of the map. If in shadow cursor mode the map will switch to either group or view selection mode and select the item that was clicked upon. If the map is already in either of these selection modes a double click has the same effect as hitting the  button or using the activate shortcut key (default <Enter> key).

The group on the top layer (closest to the front) is listed first, followed by the next layer behind it, followed by the rest of the layers to the bottom layer at the end of the list. It is possible to control the render order in the tree by using the *Drag n Drop* technology. The *Drag n Drop* capability enables you to move map groups up and down within Views and also to move Views relative to each other.



RENDERING OPTIONS

- Check the *Render images first* box to render (draw) the images groups first.
- Check the *Auto-Redraw* box to automatically redraw the map when a change is made to it.
-  Click the *Redraw* button to redraw the map when changes are made to the groups in the View/Group Manager and the Auto-Redraw option is off.

The *View/Group Manager Tool* is a “modeless” dialog, which means it can remain open while you work on your map. It can be toggled on or off using the “M” hot key and can even be docked on the side of your screen or at the top with the toolbars.

30 Tutorial 2: Working with Data

OTHER TOOL OPTIONS

The other Tool options include moving, masking, transparency settings, editing and deleting. All of the following properties require the licensed version of **Oasis montaj**.



Frozen Scale

Click this button to freeze the scale of the currently selected map group, independent of the view scale of the map. For example, when zooming in the text size in a group will not grow but remain the same size on the screen.



Visible Scale

Click this button to set a scale range in which the currently selected Group will be visible. For example, individual groups may be made visible only at specific scales. Then, while zooming, if the map scale is outside the range, the group is not drawn.



Moveable

Check the *Moveable* box to enable the movement of the selected group on the map using the cursor.



Masked to View

Check the *Masked to View* box to mask the selected view using the mask applied to the View (*Mapping/Masking/Apply mask to a view - VIEWCLIP.GX*).

This option enables you to apply a mask to selected groups within a View.



Mask to Group region

Using the *Mask to Group region* dropdown list, select the extended view mask applied to the View (*Mapping/Masking/Add/Replace group mask in view - VIEWEXTCLIP.GX*).

This option enables you to save the mask into the map and activate it on specific groups in the View.



Transparency

Check the *Transparency* box to enable the slider (Transparent - Opaque). Move the slider to the transparency level wanted for the selected group.

Edit

Edit


Click the button to edit (or activate) the selected item.

Note: Double click on a group or view in a map or using the activate shortcut key (default Enter-Key) will also activate the edit mode for that item. The edit mode depends on the item; group edit mode for vector groups, image color tool for images and color symbols and 3D Viewer for 3D views.

Delete

Delete

Click the *Delete* button to delete the selected View/Group.

Note: If you delete a group by mistake or make any other undesired changes, you can click the *Undo last map change* () button on the Standard Toolbar or use the shortcut (Default Ctrl-Z) at any time to undo any

changes and revert to the original map.

Using the Viewer Tool Bars

The following *Tool Bars* can be displayed in the **Oasis montaj Viewer**. Note that the **Database Tool Bar** can be found on page 23.

To *Show/Hide* tool bars, on the *Tools* tab of the *Project Explorer* select the tool bar of interest, right-click and select *Show/Hide* from the popup menu.

STANDARD BAR



Open Database

Use this command to open a previously defined Oasis montaj database.



Open Map

Use this command to open an existing Geosoft map.



Run GX

Use this command to run a GX from the GX directory.



Load Menu

Use this command to load a menu to the menu bar.

MAP TOOLS BAR



Map View/Group Manager

Click this button to open the **Map View/Group Manager** tool which enables you to display and edit the *Views* and *Groups* in a map. This tool consists of a 'tree' structure that contains two main branches representing the *Base* view and the *Data* view.

Under each view, a number of groups are listed according to their layer on the map.

For instructions on how to use the manager, please refer to the Online Help.



Select or Change the Current View

Click this button Switches between data (ground coordinate) and base (map coordinate) views.



Select a Group

Click this button to select the different groups in a Map (including image aggregates, contours, surrounds, and other graphics layers). Once selected, you can copy the group to the clipboard.



Shadow Cursors

Click this button to display a Shadow cursor (⌘) on a map for dynamic linking.

As you move the cursor around the map, the value for that same geographic location is highlighted or indicated in all linked databases, profiles and maps.

32 Tutorial 2: Working with Data



Shadow Cursors with Dynamic Link

Click this button to create a dynamic link between one or more maps and data (in Spreadsheet and Profile windows) to assist in locating and comparing data, profiles and maps.

If you have plotted flight lines on your map, you can use this button to dynamically link the map to the database and profiles.

When you move the Shadow cursor on the map, the database and profile views will update to show the corresponding data. If the corresponding data are in a different database line, then the spreadsheet window will automatically display this line. When you select a value in the database or a point on a profile, the Shadow cursor will update in the map view.



Toggle Auto-Redraw

Click this button to toggle the Auto-Redraw option on/off. The Auto-Redraw option refreshes/redraws a map automatically after changes are made to it. When this option is **ON** any changes made to the map contents will cause the map to be refreshed/redrawn. This includes editing changes, group selection changes, or changing the rendering order of a group.

- If the Auto-Redraw is OFF the map is only refreshed on zoom, pan, or if the refresh button is pressed.
- A refresh button has also been added to the **Map View/Group Manager** dialog to support this feature. If the Auto-Redraw option is off, and you make changes to the groups in the **Map View/Group Manager**, click this button to refresh and show your changes on the map. This is useful for displaying your changes when moving groups in front or behind each other. By default Auto-Redraw is initially ON.

You can also access this command by clicking the right mouse button on a map and selecting *Redraw* from the popup menu.



Redraw

Click this button to refresh/redraw a map in the Map window after making editing changes.

You can also access this command by clicking the right mouse button on a map and selecting *Redraw* from the popup menu.



This Map Only

Click this button to apply map commands to the currently selected map window only.



All Maps

Click this button to apply map commands to all the open map windows in the project.



Other Maps Only

Click this button to apply map commands to all maps other than the currently selected map.

***Pan (Default Shortcut: P-Key or Spacebar)***

Click this button to move around in the currently selected map. Click the left mouse button and while holding the button down, move the hand cursor to pan around the current map area.

You can also access this command by clicking the right mouse button on a map and selecting *Pan* from the popup menu.

***Interactive Zoom (Default Shortcut: Shift-Z)***

Click this button to activate the interactive zoom. Click on the area of the map you want to zoom (e.g. an anomalous location on a grid), then while holding down the left mouse button, move your cursor left to zoom out and right to zoom in on the selected area.

You can also access this command by clicking the right mouse button on a map and selecting *Interactive Zoom* from the popup menu.

***Zoom Box (Default Shortcut: B-Key)***

Click this button to activate the zoom box. Click on the map, then while holding down the left mouse button, move your cursor to box in the area of the map you want to zoom, click the left mouse button to select the area. Click the mouse button again to zoom to the area selected.

Note: Once the box has been defined, the cursor and the box are linked and by moving the cursor around the map you can move the box to another location, and then click the left mouse button to zoom to the boxed area.

You can also access this command by clicking the right mouse button on a map and selecting *Zoom Box* from the popup menu.

***Zoom Out (Default Shortcut: X-Key)***

Click this button to zoom out and shrink the displayed map features by 50%.

You can also access this command by clicking the right mouse button on a map and selecting *Zoom Out* from the popup menu.

***Zoom In (Default Shortcut: Z-Key)***

Click this button to zoom in and increase the displayed map features by 50%.

You can also access this command by clicking the right mouse button on a map and selecting *Zoom In* from the popup menu.

***Zoom to Selection (Default Shortcut: S-Key)***

Click this button to zoom to the selected map view or group.

You can also access this command by clicking the right mouse button on a map and selecting *Zoom to Selection* from the popup menu.

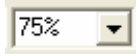
34 Tutorial 2: Working with Data



Full Map (Default Shortcut: F-Key)

Click this button to display the whole map area in the map window.

You can also access this command by clicking the right mouse button on a map and selecting *Full Map* from the popup menu.



Zoom Level Control

This option enables the user to specify an estimation percentage of print size on screen (100%) or various other levels (for example, 400%, 200%, 100%, 75%, 50% and 25%). The control also supports custom levels by typing a percentage in the control and pressing the <Enter> key.

The zoom level reported here is somewhat related to the scale reported in the status bar. The scale shown in the status bar depends on the view selected. For example, for a **50%** zoom reported or typed in the toolbar with a **1:500** scale data view with:

Base view Selected: Status bar shows **1:2**

Data view Selected: Status bar shows **1:1000**



Go Back to Previous Extent (Default Shortcut: L-Key)

Click this button to undo navigation changes that you have made recently. This command is useful for returning the view to any extents that was previously viewed after changing it by zooming and panning.



Go to Next Extent

Click this button to redo navigation changes that you have made recently.



Snap to grid during edit operations

Click this button to toggle the Snap to Grid option on/off. The snapping grid origin is at the lower left corner of a map or map template and the snapping distance can be controlled using the *Layout View Properties* button (licensed version only).



Show/hide snapping grid

Use this to toggle the visibility of the snapping grid. The units and snapping grid size are controlled by the *Layout View Properties* button (licensed version only).



Show/hide ruler

Use this to toggle the visibility of a ruler on the left and top sides of the view the snapping grid. The units displayed on the ruler are controlled by the *Layout View Properties* button (licensed version only).



Layout view properties

Click this button to set the resolution, units and other properties for snapping and rulers. The default is 5mm. The units set here controls the units that is used for layout of maps and map templates and also affects coordinates and measurements displayed in the status bar for Base view operations (licensed version only).

Displaying Grids and Images on a Map

In **Oasis montaj**, grids and images are always displayed on a map in the Map window. There are several types of grids and images you can display. For a complete list of the grid and image formats that are supported in **Oasis montaj** see the online help topic *Data Exchange formats*.

In **Oasis montaj**, a *Grid* is a visual representation of a survey area interpolated from a series of survey points. For example, magnetic survey data are collected as a series of point values organized using a number of lines and arranged in a grid pattern.

When you create a grid, **Oasis montaj** takes these point values from the database and interpolates between them, creating a visual representation similar to a contour map. However, instead of simple contour lines, colours and shading are used to represent the magnetic differences across the grid.

There are two types of images in **Oasis montaj**, **Raster** and **Vector** images.

Raster Images

Raster images or bitmap graphics (.bmp, .tif, and .jpg) are created from a series of pixels to represent graphics. Each pixel in a bitmap image has a specific location and colour value assigned to it.

Bitmap images are resolution dependent—that is, they represent a fixed number of pixels. As a result, they can appear jagged and lose detail if they are scaled on-screen or if they are printed at a higher resolution than they were created for.

Vector Images

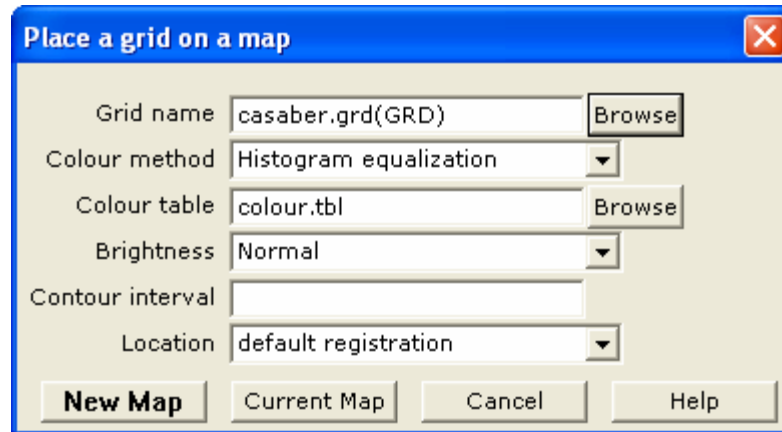
Drawing programs such as AutoCAD create vector graphics (.dxf, .eps, .wmf), made of lines and curves defined by mathematical objects called vectors. Vectors describe graphics according to their geometric characteristics. The **Oasis montaj** CAD drawing tools (licensed version) enable you to draw vector lines and shapes.

A vector graphic is resolution-independent—that is, it can be scaled to any size and printed on any output device at any resolution without losing its detail or clarity. As a result, vector graphics are the best choice for type (especially small type) and bold graphics that must retain crisp lines when scaled to various sizes—for example, logos.

Because computer monitors represent images by displaying them on a grid, both vector and bitmap images are displayed as pixels on-screen.

DISPLAYING A GRID ON A MAP

1. On the *Map* menu, click *Display*, and then click *Grid*. The *Place a grid on a map* dialog is displayed.



2. Select the *Grid name* (**casaber.grd**), *Colour method*, *Colour table*, *Brightness*, *Contour interval*, and the *Location*. For more information on these parameters click the [**Help**] button.

3. Click [**New Map**]. The grid is displayed on a new map.

Note: To display a grid on a current map, click the [**Current Map**] button.

DISPLAYING AN IMAGE ON A MAP

1. On the *Map* menu, click *Display*, and then click *Image (bmp, tiff, etc.)*. The *Place an image on a map* dialog is displayed.
2. Using the [**Browse**] button, display the *Image* dialog and select the image *File name* and *File type*.
3. Click [**Open**]. The *Place an image on a map* dialog is displayed again.
4. Select the image *Location* (*default registration* or *fit to an area*).
5. Click [**New Map**] the image is displayed on a new map.

Note: To display an image on a current map, click the [**Current Map**] button.

DISPLAYING A GEOSOFT PLOT FILE

1. On the *Map* menu, click *Display*, then click *Geosoft PLT files*. The *Display a Geosoft PLT file* dialog is displayed.
2. Select the *Plot file* name. Click [**New Map**]. The Geosoft plot file is displayed on a new map.

Note: To display a Geosoft plot file on a current map, click the [**Current Map**] button.

DISPLAYING AN AUTOCAD DXF FILE

1. On the *Map* menu, click *Display*, then click *AutoCAD DXF files*. The *Display a DXF file on a map* dialog is displayed.
2. Select the *New map?* name, *DXF file* name, *Maximum number of pen styles*, and *Colours?*. For more information on these parameters, click the [**Help**] button.
3. Click [**OK**]. The DXF file is displayed on a map.

Data Access Protocol (DAP)

DAP is a technology that enables efficient transfer of high volume spatial data from a designated DAP data server to a DAP client via the Internet or an Intranet. There are two types of DAP clients, a thick client (a desktop software application) and a thin client (web browser).

Oasis montaj, MapInfo and ArcGIS are thick DAP client software applications. Thick client applications enable you to download and save the actual data to your hard drive, so you can use the data in **Oasis montaj** or any other GIS or spatial data processing program.

Thin clients, like Geosoft's DAP Data Explorer use a web browser to browse, view and extract data from a DAP server. Visit www.geodap.com/map/ and see how it works!

Geosoft's DAP capability enables users of both the free Viewer and licensed applications to access Geosoft's public DAP server. This server contains global topographic, coastline and river data as well as magnetic and gravity data for North America and Australia.

These data sets (grid and point data) can be used to create sample maps in **Oasis montaj** and to learn about the newest technology for accessing high volume data via the Internet.

Additional public access DAP servers are expected to go online soon, for more information visit: www.geodap.com/map/

DAP's main features include:

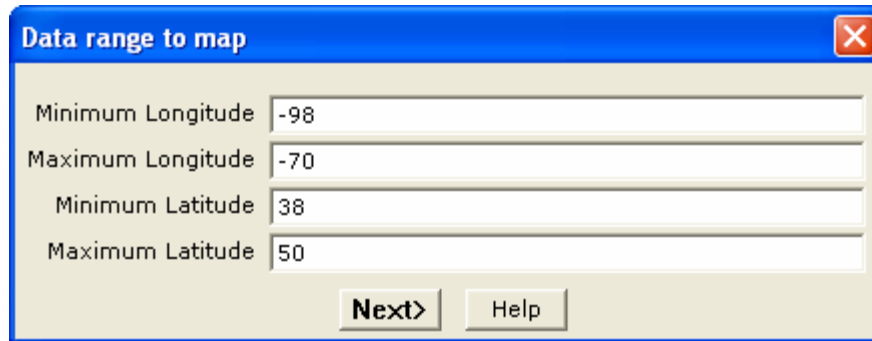
- **Large Volume Data Transfer:** DAP technology handles the efficient transfer of very high-volume data, and its associated metadata, through a streaming technology.
- **Spatially Aware:** DAP is spatially aware, enabling user-specified spatial querying and retrieval.
- **Ready-to-use Data:** DAP provides localized data that matches your current Oasis montaj map window and projection information.
- **Safe and Efficient Data Transfer:** DAP data transfer technology provides direct DAP client/server communication enabling the transfer of compressed data that maintains original data integrity.

TO ACCESS THE DAP SERVER:

Data on Geosoft's DAP server can be accessed through the **Oasis montaj DAP** menu. Once connection to a DAP server has been established the server will determine what grid data matches the data view of your map. You will then be presented with a list of data that is available to be downloaded and displayed on your map.

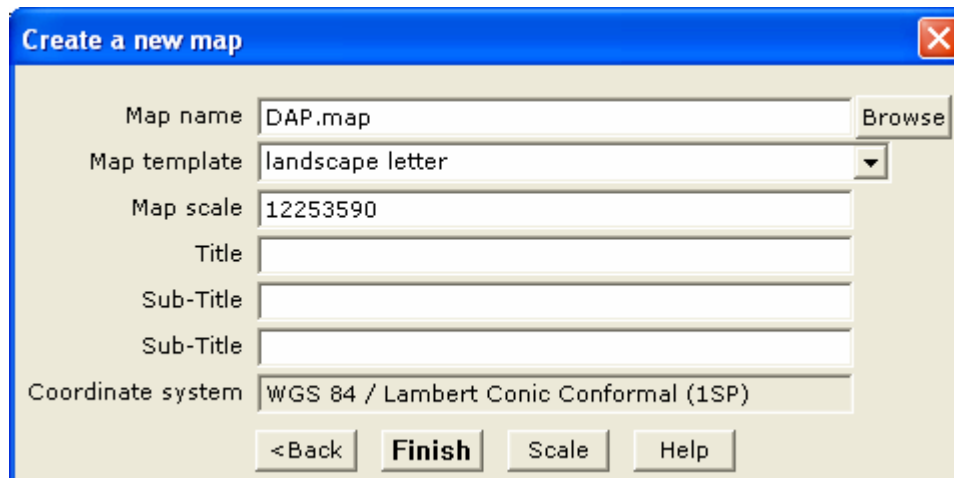
1. On the *DAP* menu, click *New Map*. The *Data range to map* dialog is displayed.

38 Tutorial 2: Working with Data



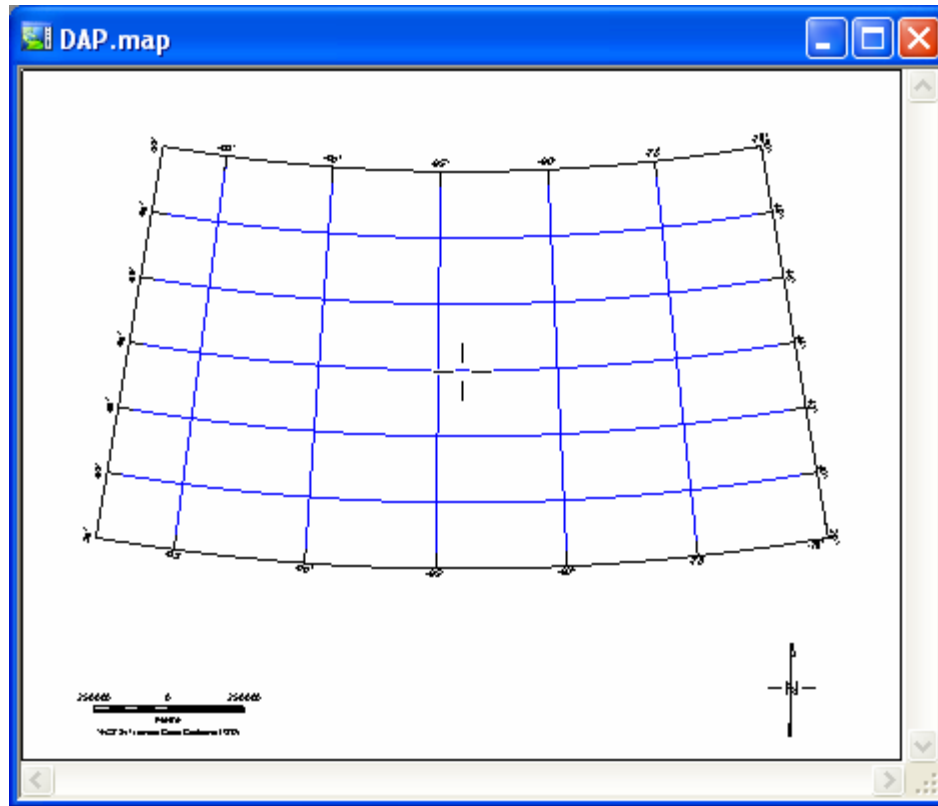
The 'Data range to map' dialog box has a blue title bar with a close button (X) on the right. It contains four text input fields: 'Minimum Longitude' with the value '-98', 'Maximum Longitude' with '-70', 'Minimum Latitude' with '38', and 'Maximum Latitude' with '50'. At the bottom, there are two buttons: 'Next>' and 'Help'.

2. Specify in *Longitude/Latitude* the data range you want to download and display. Click the [Next>] button. The *Create a new map* dialog is displayed.

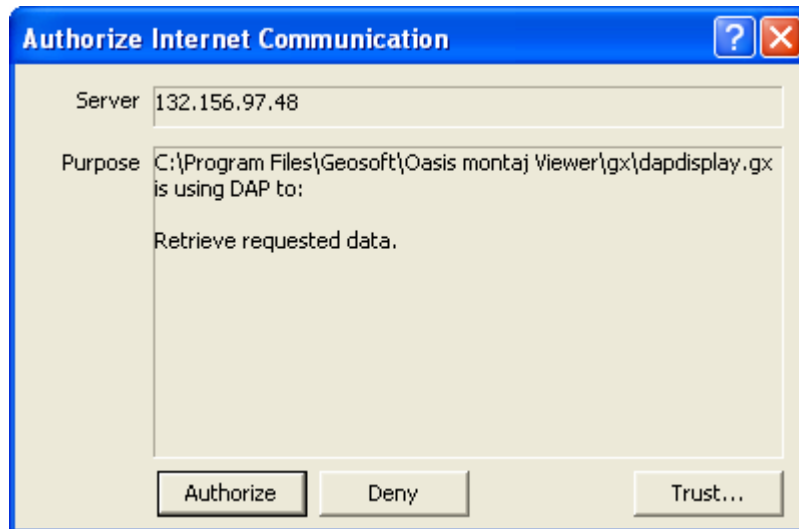


The 'Create a new map' dialog box has a blue title bar with a close button (X) on the right. It contains several fields: 'Map name' with 'DAP.map' and a 'Browse' button; 'Map template' with a dropdown menu showing 'landscape letter'; 'Map scale' with '12253590'; 'Title' (empty); 'Sub-Title' (empty); another 'Sub-Title' (empty); and 'Coordinate system' with 'WGS 84 / Lambert Conic Conformal (1SP)'. At the bottom, there are four buttons: '<Back', 'Finish', 'Scale', and 'Help'.

3. Specify the map parameters: *Map name*, *Map template*, *Map scale* (by clicking the [Scale] button the default map scale - based on the data range and map template - will be displayed), and *Map Titles*. Note that, the default map projection is displayed in the *Coordinate system* box.
4. Click the [OK] button to display the map. Note that, latitude/longitude surrounds are drawn on the map by default.

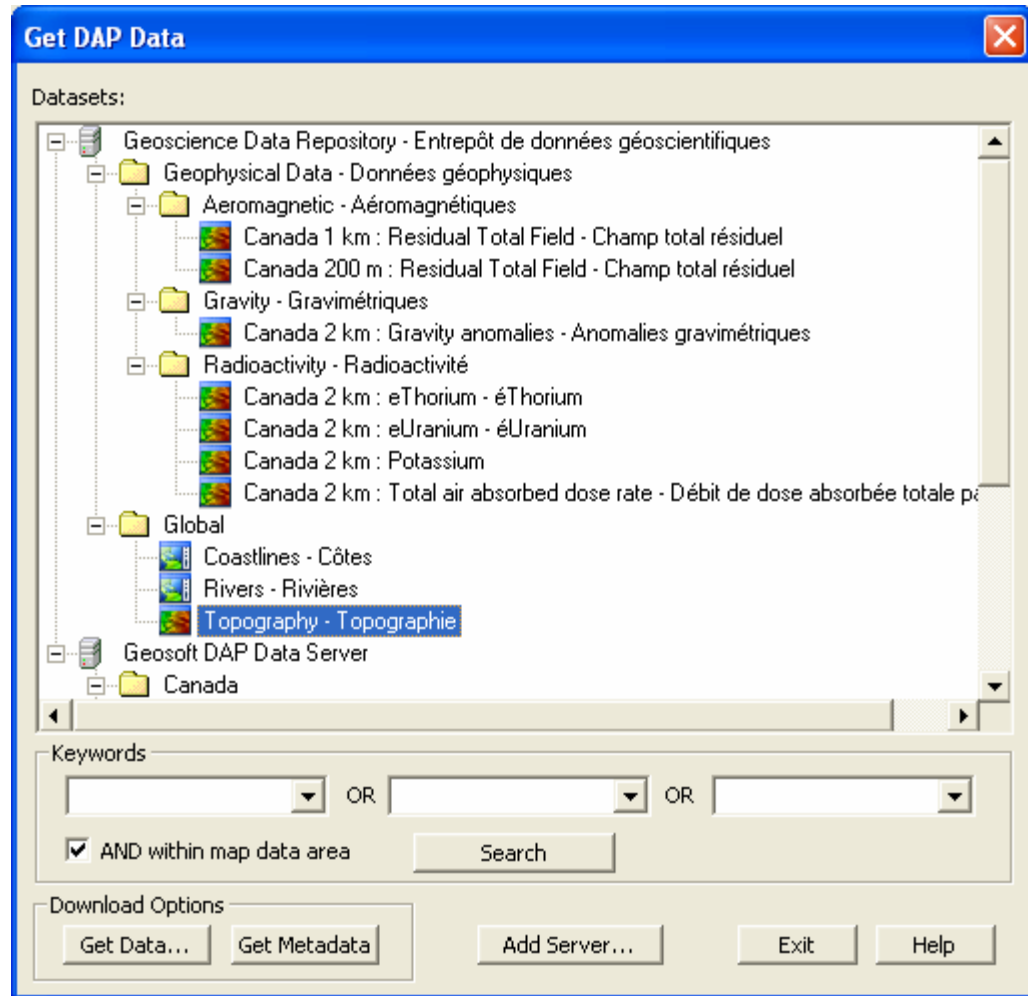


- On the *DAP* menu, click *Get DAP data*. The *Authorize Internet Communication* dialog is displayed (Note: If you Internet Trust Configuration is set to "Trusted" this dialog will not appear).

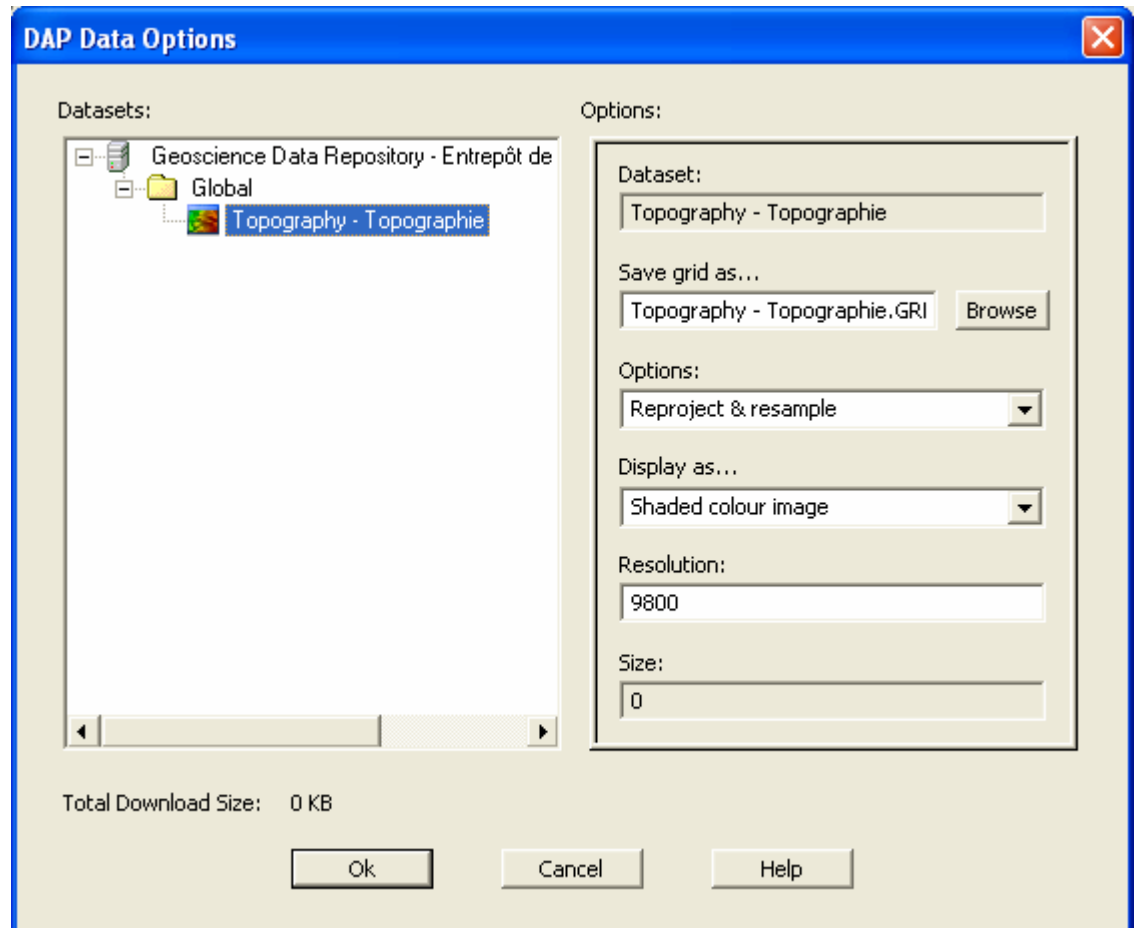


- Click the [**Authorize**] button to query the DAP server to determine what grid data the DAP server has that matches the data view of the current map. The *Get DAP Data* dialog will be displayed.

40 Tutorial 2: Working with Data

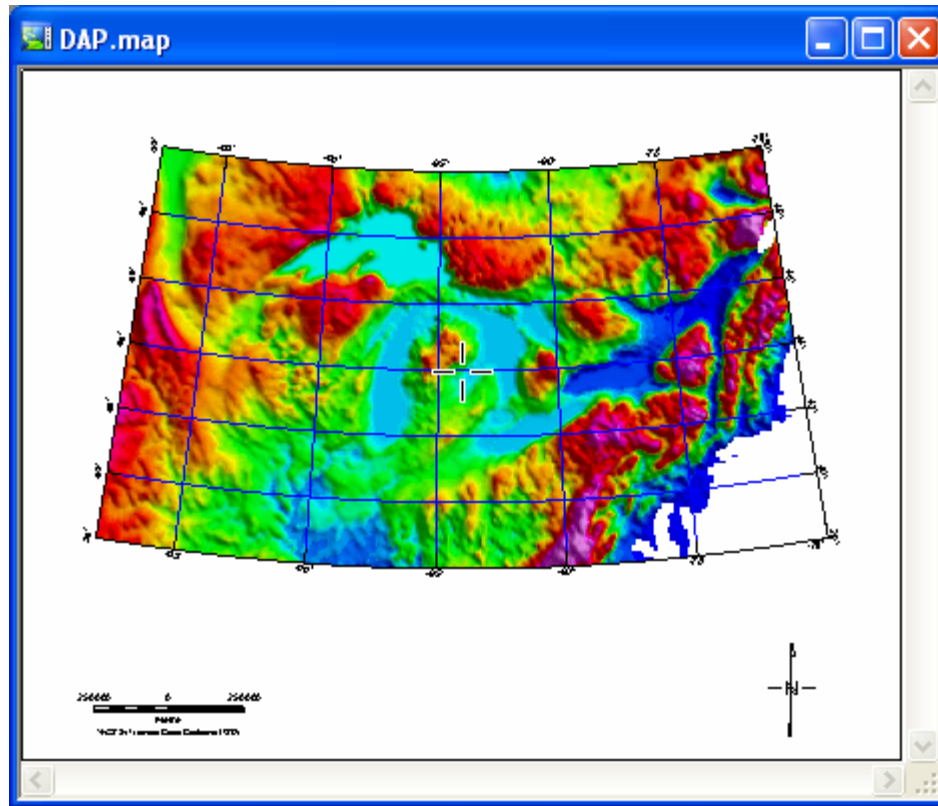


7. Select the data you wish to download (e.g. Topography) and click the **[Get Data]** button. The *DAP Data Options* dialog is displayed.



8. Use this dialog to specify the parameters for your data. For more information on the data options, click the **[Help]** button.
9. Once you have specified your data options, click the **[OK]** button to download and display the DAP data on your current map.
10. Once the download is complete, the *Get DAP Data* dialog will again be displayed. Click the **[Exit]** button to close the window. The gridded data will be displayed in your open map.

42 Tutorial 2: Working with Data

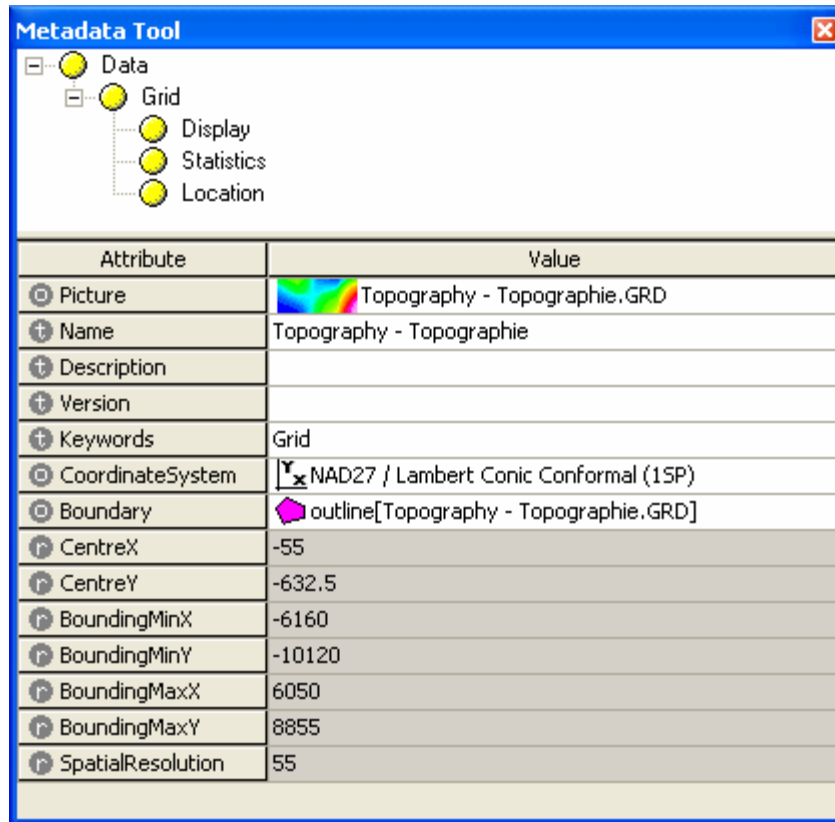


Note: Oasis montaj licensed users have access to a variety of DAP display technology features including; Re-project the grid to the projection of the current map view, Re-project and resample the grid to a specified resolution, Save the grid in the native projection format, Display the grid as a simple colour image, Display the grid as a shaded colour image, and Download and save only, do not display the grid.

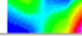

Using the Metadata Tool

The *Metadata Tool* is a context-oriented, interactive method for viewing and editing attributes assigned to Geosoft data. For more detailed information on the *Metadata Tool*, see page 25.

Following, is an example of the metadata included with the grid file previously downloaded from the DAP server (**Topography - Topographie.GRD**) and displayed in a map.



The screenshot shows the Metadata Tool window. The tree view on the left shows a hierarchy: Data (expanded) -> Grid (expanded) -> Display, Statistics, and Location. The table below lists the metadata attributes and their values.

Attribute	Value
Picture	 Topography - Topographie.GRD
Name	Topography - Topographie
Description	
Version	
Keywords	Grid
CoordinateSystem	NAD27 / Lambert Conic Conformal (15P)
Boundary	 outline[Topography - Topographie.GRD]
CentreX	-55
CentreY	-632.5
BoundingMinX	-6160
BoundingMinY	-10120
BoundingMaxX	6050
BoundingMaxY	8855
SpatialResolution	55

Data: The Data branch contains all metadata associated with any spatial data type. The information at the "Data" level is common to all types of spatial data.

Grid: This example describes a grid of data; hence there is a "Grid" branch, which contains metadata that is specific to grids.

Display: Grids may contain display information about the grid data set, which is stored in the "*Grid/Display*" branch.

Statistics: Grids may contain statistical information about the grid data set, which is stored in the "*Grid/Statistics*" branch.

Location: The information that locates a 2-D grid array within the "Data" coordinate system is stored in the "*Grid/Location*" branch.





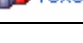
3D Surface Tool

The **3D Tool** enables you to modify the appearance of your 3D View in the **3D Viewer**. The 3D Tool is available in the *Tools* section of the *Project Explorer* and will appear whenever a 3D Viewer is open. If more than one 3D Viewer is open, the parameters of the 3D Tool will represent whichever Viewer currently has focus.

Note: To create an **Oasis montaj** 3D View requires the **Oasis montaj Mapping and Processing System** (licensed version).

The **3D Tool** consists of a dialog with five tabs and a **3D Viewer**. Each tab enables you to modify different aspects of the 3D View within the 3D Viewer.

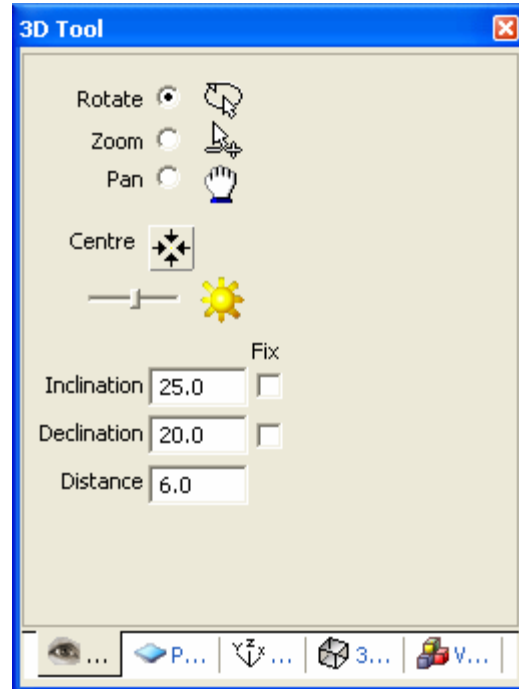
44 Tutorial 2: Working with Data

 View	- enables you to modify the overall view of the 3D View on a map
 Planes	- enables you to modify the individual planes within each 3D View
 Axis	- enables you to add labels, axis, and a box around the 3D View
 3DCon	- enables you to adjust the rendering resolution in the 3D tool
 Voxels	- enables you to modify the voxel display parameters in the 3D tool

View Tab


The **View** tab enables you to:

- **Rotate** your 3D View 360 degrees in all directions
- **Zoom** in and out of the displayed View
- Use the **Pan** tool
- **Centre** the displayed View (reset focus point of the View)
- Modify the **brightness** level
- Specify and fix the **inclination** of the View
- Specify and fix the **declination** of the View
- Specify the viewing **distance** from the central focal point of the View



TO ROTATE THE 3D GRID:

When you select the *Rotate* button the cursor changes to the rotate mode, and enables you to rotate the displayed grid 360 degrees in all directions.

1. Select the Rotate button. The cursor changes to rotate mode ()
2. Left click, and while holding down on the mouse key move right to left or up and down. The grid will rotate in the direction in which you move the mouse.

Note: Moving the mouse from left to right turns the grid in an anti-clockwise direction, and moving right to left turns the image in a clockwise direction.

TO ZOOM THE 3D GRID:


When you select the *Zoom* button the cursor changes to the zoom mode, and enables you to zoom in and out of the displayed grid.

1. Select the *Zoom* button. The cursor changes to zoom mode ().

2. Left click, and while holding down on the mouse key move to the right to zoom in and to the left to zoom out.

TO USE THE PAN TOOL:

When you select the *Pan* button the cursor changes to the pan mode, and enables you to move the entire displayed grid.

1. Select the Pan button. The cursor changes to pan mode ().
2. Left click, and while holding down on the mouse key move the grid right to left or up and down. The entire grid will move in the direction in which you move the mouse.

TO CENTRE THE GRID:

When you select the *Centre* button, the focus point of the grid is reset and the current displayed grid is centred in the 3D Surface Display Tool.

1. Select the Centre button. The displayed grid is centred.

TO MODIFY THE BRIGHTNESS LEVEL OF THE GRID:

When you select the *Brightness* bar, you can modify the brightness of the displayed grid.

1. Select the brightness bar.
2. Slide the bar to the left to increase the brightness level and to the right to decreases the brightness level of the displayed grid.

TO SPECIFY AND FIX THE INCLINATION OF THE GRID:

1. Click inside the *inclination* box and specify the inclination you want for the 3D grid.
2. Check the Fix box, and then click the OK button. The grid will be redrawn on your map with the new fixed inclination.

TO SPECIFY AND FIX THE DECLINATION OF THE GRID:

1. Click inside the *declination* box and specify the declination you want for the 3D grid.
2. Check the Fix box, and then click the OK button. The grid will be redrawn on your map with the new fixed inclination.

TO SPECIFY THE DISTANCE OF THE GRID:

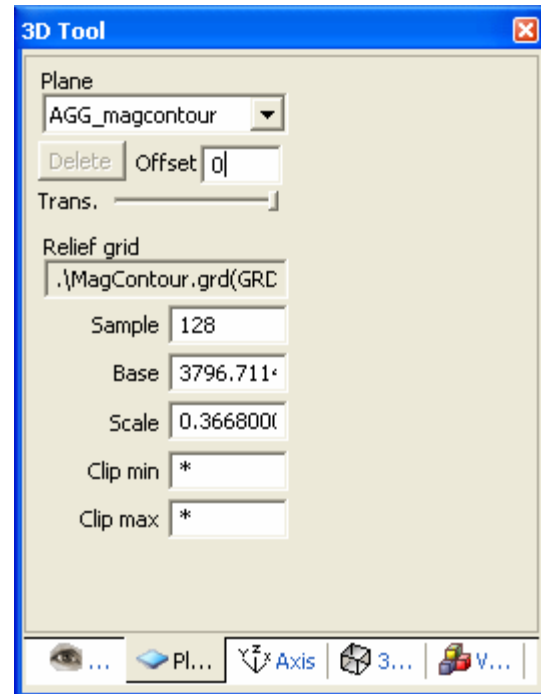
The *distance* specifies the distance away from the centre focal point relative to the longest displayed dimension. For example, a value of 5 will place the viewpoint 5 times the size of the grid away from the centre of the grid.

1. Click inside the distance box and specify the distance you want for the 3D grid.
2. Click the OK button. The grid will be redrawn on your map with the new distance.

Planes Tab

The **Plane** tab enables you to:

- Select the **Plane** to modify
- Select the plane **Offset** in Z units relative to the plane coordinates.
- Specify the **Transparency** of the plane
- Indicate the name of the **Relief grid** (if one is used for the selected plane)
- Specify the **Sample** resolution of the relief grid
- Specify the **Base** value of the relief grid
- Specify the vertical **Scale** of the relief grid
- Specify a **minimum clipped** value for the relief grid
- Specify a **maximum clipped** value for the relief grid

**TO SELECT THE PLANE TO MODIFY:**

1. From the *Plane* dropdown menu select the plane to modify.

TO SELECT THE PLANE OFFSET IN Z UNITS:

1. In the *Offsets* box, specify the offset value in ground units. Press the **[Enter]** key. The plane will be redrawn in the 3D viewer with the new offset.

TO SPECIFY THE TRANSPARENCY OF THE PLANE:

1. Move the *Trans.* Slider bar from left to right to increase the transparency.

Note: We use a “screen-door” dithering technique to make a plane transparent. This method is fast and robust, but may not always give you what you expect because the transparency screens will overlap in certain combinations. If you only need to make one plane transparent transparency should work as you expect. If you are displaying two planes and require both to be transparent, you should set the transparency of each plane to 50%. If you want to make 3 or 4 planes transparent at the same time, set all planes to 25% transparency. In the *Sample* box, specify the sample resolution.

TO SPECIFY THE RELIEF GRID SAMPLE RESOLUTION:

1. In the *Sample* box, set a sampling resolution that is reasonable for the detail required in the relief surface. Higher sample resolutions provide more relief

detail at the expense of performance. You can select a number up to 768 (you entry will be converted to an even multiple of 16). Press the **[Enter]** key. The relief grid will be redrawn in the 3D viewer with the new sample resolution.

TO SPECIFY THE BASE VALUE OF THE RELIEF GRID:

1. In the *Base* box, specify the base value of the relief grid. Press the **[Enter]** key. The relief grid will be redrawn in the 3D viewer with the new base value.

TO SPECIFY THE VERTICAL SCALE OF THE RELIEF GRID:

1. In the *Scale* box, specify the vertical scale of the relief grid. Press the **[Enter]** key. The relief grid will be redrawn in the 3D viewer with the new vertical scale.

TO SPECIFY A MINIMUM CLIPPED VALUE FOR THE RELIEF GRID:

The *Clip minimum* enables you to specify the minimum Z value of your relief grid. Grid values below this will be clipped.

1. Click inside the *Clip min* box and specify the minimum value you want for the Z data of the relief grid. Press the **[Enter]** key. The relief grid will be redrawn in the 3D viewer with the new minimum Z value.

TO SPECIFY A MAXIMUM CLIPPED VALUE FOR THE RELIEF GRID:

The *Clip maximum* enables you to specify the maximum Z value of your relief grid. Grid values above this will be clipped.

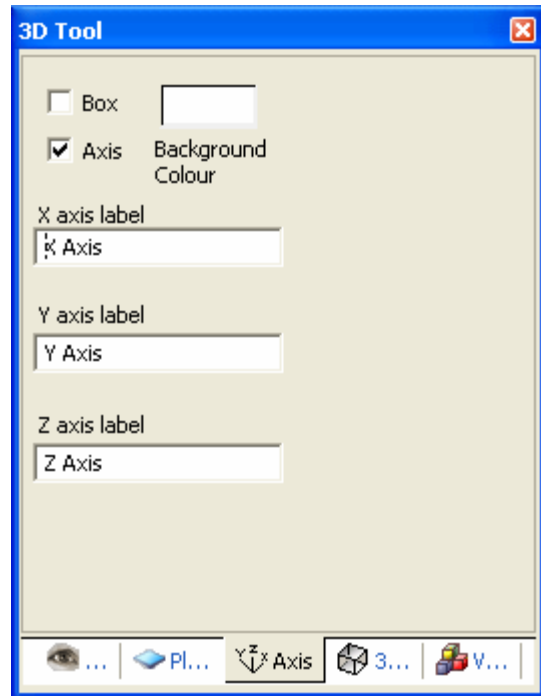
1. Click inside the *Clip max* box and specify the maximum value you want for the Z data of the relief grid. Press the **[Enter]** key. The relief grid will be redrawn in the 3D viewer with the new maximum Z value.

48 Tutorial 2: Working with Data

Axis Tab

The **Axis** tab enables you to:

- Add a **box** around the 3D View display
- Add an **axis** to the 3D View display
- Specify the **X axis label**
- Specify the **Y axis label**
- Specify the **Z axis label**



TO ADD OR REMOVE AN AXIS ON MY 3D VIEW:

The *Axis* check box enables you to draw an X, Y and Z axis on the View display.

1. Click the Axis check box to add or remove the X, Y, and Z axis on the View display.

TO ADD OR REMOVE A BOX AROUND MY 3D VIEW:

The *Box* check box enables you to draw rectangular box edges around the 3D volume being rendered

1. Click the Box check box to add or remove the rectangular box edges around the 3D volume being rendered.

TO SPECIFY LABELS FOR THE X, Y, AND Z AXIS OF MY 3D VIEW:

You can specify the *labels* for the X, Y, and Z axis, if the axis is selected.

1. Click inside the X, Y and Z axis label box, and specify the titles you want to display for your 3D grid image.
2. Press the **[Enter]** key. The axis labels will be redrawn on your map with the new axis titles.

3D Con Tab

Use the *3D Con* tab to adjust the rendering resolution in the 3D tool.

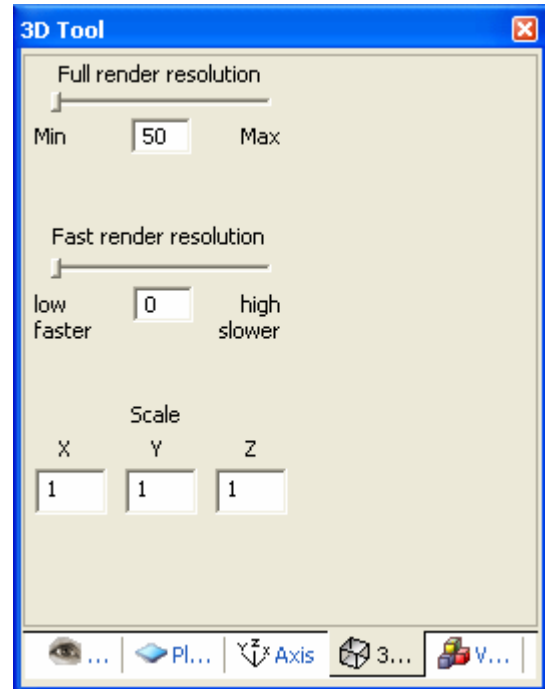
Important information about the 3D Con tab:

- The controls on the 3D Con tab are system controls and changes made to this tab will affect all 3D maps in your **Oasis Montaj** system.

- Full rendering occurs every time you modify the 3D view and the view is redrawn.
- Fast rendering occurs when the image is in constantly motion for example while rotating, zooming or panning.
- The 3D Views rendering process makes heavy use of the available memory on your video card, and performance will be substantially reduced if your limits are exceeded.

The **3D Con** tab enables you to:

- Adjust the "**full**" redraw rendering resolution
- Adjust the "**fast**" motion rendering resolution
- Independently adjust the **scale** of the three axis X, Y and Z



TO ADJUST THE FULL REDRAW RENDERING RESOLUTION:

The 'full' redraw rendering resolution occurs every time you modify the 3D view and the view is redrawn.

1. Move the *Full* render resolution slider bar from left to right to increase the resolution.

TO ADJUST THE FAST REDRAW RENDERING RESOLUTION:

The 'full' redraw rendering resolution occurs when the image is in constant motion, for example while rotating, zooming or panning.

1. Move the *Fast* render resolution slider bar from left to right to increase the resolution.

TO MODIFY THE SCALE OF X, Y AND Z COORDINATE:

The Scale option enables you to independently modify the X, Y and Z coordinates.


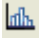



1. Specify the Scale for the X, Y and Z coordinates (note that, each coordinate can have its own scale factor). Press the <Enter> key and the scale will be updated in the 3D Viewer.


3D Voxel Tab

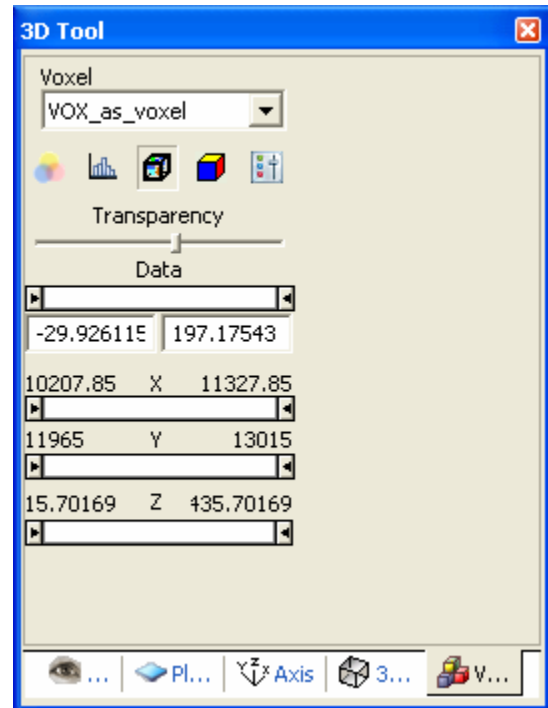
50 Tutorial 2: Working with Data

Use the 3D Voxel tab to modify the voxel display parameters in the 3D tool.

The **3D Voxel** tab enables you to:

- Select the voxel to modify
-  select **Color Tool**
-  select **Voxel statistics**
-  select add a **box around Voxel**
-  select display **Voxel grid lines**
-  select **Voxel Controls** dialog
- Specify the **Transparency** of the voxel
- Adjust the **Data** range using slider or data boxes
- Adjust the **X** range using slider
- Adjust the **Y** range using slider
- Adjust the **Z** range using slider


Note: To adjust the **X, Y** and/or **Z** ranges by specifying exact values, click the **Voxel Controls**  button.




TO SELECT A VOXEL TO MODIFY:

1. From the *Voxel* dropdown list select the voxel to modify.


TO ACCESS THE COLOR TOOL:

1. Click the *Color tool* () button and the *Color Symbol Tool* will be displayed.
2. The *Colour Symbol Tool* enables you to interactively edit/modify the colour zoning of your zone coloured symbols, store your custom colour configurations in specialized colour palette files (*.ITR, *.ZON, *.TBL and *.LUT) and apply the colour palette files to any of your zone symbols. For more information, click the **[Help]** button on the *color Symbol Tool*.
3. Click the **[OK]** button to close the *Color symbol tool* and return to the 3D Tool.

TO ACCESS THE VOXEL STATISTICS:


1. Click the *Voxel statistics* () button and the *Voxel statistics* dialog is displayed.
2. This dialog displays the *Voxel Name*, *Valid Data*, *Dummies*, *Volume*, *Minimum*, *Maximum*, *Mean Value* and *Standard Deviation*.
3. Click the **X** on the top right corner to close the dialog and return to the 3D tool.

TO ADD/REMOVE A BOX FROM AROUND THE VOXEL:


1. Click the *add box around Voxel* () button and a box will be added/removed to/from the Voxel.

2. This button works as a toggle you can toggle on or off the Voxel box.

TO DISPLAY VOXEL GRID LINES:

1. Click the display *Voxel grid lines* () button and the Voxel colour shading will be removed/added and the Voxel grid/Voxel colour fill will be displayed.
2. This button works as a toggle you can toggle on or off the Voxel grid lines or colour shading.

TO DISPLAY VOXEL CONTROLS DIALOG:

1. Click the *Voxel controls* () button and the *Voxel Controls* dialog will be displayed.
2. Using either the slider bars or the corresponding value boxes, specify the *Data Range*, *X Range*, *Y Range* and *Z Range* values for your Voxel display.
3. Click the [OK] button and the Voxel will be updated with the new data ranges.

TO SPECIFY THE TRANSPARENCY OF THE VOXEL:

1. Move the *Transparency* slider bar from right to left to increase the transparency.

TO INTERACTIVELY MODIFY DATA RANGE:

1. Using the slider bars specify the *Data* range and the Voxel will be updated simultaneously.

Note: If you specify new *Data* ranges by specifying values in the data boxes, you must press the <Enter> key to update the Voxel.

TO INTERACTIVELY MODIFY MY X, Y, Z RANGES:

1. Using the slider bars specify the *X*, *Y*, *Z* ranges and the Voxel displayed in the 3D Viewer will be updated simultaneously.

3D Rendering Memory Requirements

You can adjust the rendering resolution for 3D Views on the 3D Con tab. The controls on this tab are system controls and changes made to this tab will affect all 3D maps in your **Oasis Montaj** system.

The 3D Views rendering process makes heavy use of the available memory on your video card, and performance will be substantially reduced if your limits are exceeded.

Full render resolution:

When the full render resolution is set to maximum it can easily consume hundreds of megabytes of memory (200-600 Mb). If you do not have adequate memory available your computer will start to thrash, your hard drive light will turn on and stay on and the rendering will take a very long time. If you have less than 256 Mb of RAM, you should not increase this control.

52 Tutorial 2: Working with Data

Fast render resolution:

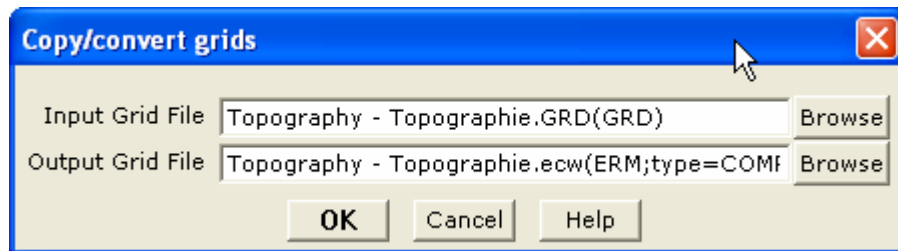
The fast render resolution moves 128k to the video card at the low range, 2 Mb at the middle range and 24 Mb at the high range. This means that every time you draw in FAST mode you move that much memory to the video card. Unfortunately, if your memory bandwidth is low or your video card is not very fast this slows down the rendering time.

Copying and/or Converting Grid Files

Oasis montaj enables you to copy and/or convert any supported grid format to any other supported grid format.

COPYING AND/OR CONVERTING GRID FILES

1. On the *Grid* menu, click *Copy/convert grids*. The *Copy/convert grids* dialog is displayed.
2. Using the [**Browse**] button, select the *Input Grid File*, and specify the *Output Grid File*.



3. Click the [**OK**] button. The grid is copied and/or converted as specified.
Note: For more information on copying and /or converting grid files, click the [**Help**] button. For information on the supported grid formats see the “Data Exchange Formats” help topic. (Hint: use the *Search* tab on the online Help system to locate topics of interest.)

Grid Report and Statistics

Basic grid information and statistics can be quickly displayed in **Oasis montaj**.

DISPLAYING GRID INFORMATION AND STATISTICS

1. On the *Grid* menu, click *Grid Information*. The *Grid Statistics* dialog is displayed.
2. Using the [**Browse**] button select the *Grid File* you want information about (**casaber.grd**). Click the [**Open**] button to return to the *Grid Statistics* dialog.
3. Click the [**Report**] button to view the *Basic grid report* dialog.

Field	Value
Grid file	.\casaber.grd(GRD)
Grid element type	FLOAT
Grid points in X direction	179
Grid points in Y direction	108
X point separation	35.754955
Y point separation	35.754955
Grid row orientation	Bottom left to right (KX= 1)
X location of bottom left point	4219.08468
Y location of bottom left point	4254.83964
Grid rotation angle	0
Coordinate system	WGS 84 / UTM zone 22N
Coordinate system units	metre
Compression Ratio	62.88%

Buttons: <Back, Stats, Docn, Meta, Exit, Help

- Click the [**Stats**] button to view the *Grid statistics report* dialog.

Field	Value
Grid File	.\casaber.grd(GRD)
Valid Items	18339
Dummies	993
Minimum Value	56260.2539
Maximum Value	57281.625
Mean Value	56524.1289
Standard Deviation	113.359059

Buttons: <Back, Re-Calc, Trend, Cancel

- Click the [**<Back**] button to return to the *Basic grid report* dialog. For more information on the *Basic Grid Report* and the *Statistics Report* click the [**Help**] button. Click the [**Exit**] button to exit the *Grid Information* dialogs.

Sending E-maps

E-maps, also called packed maps, enable you to pack all the files (grids, images, map objects) that are displayed on a map into a single file. This means that you don't have to worry about making sure all the files (such as *.GI or *.GRD files) associated with a map

54 Tutorial 2: Working with Data

are included in the e-mail. When you open an e-map in **Oasis montaj**, all the information can be read in this format by all related functions, such as grid statistics.

1. Select (highlight) the map you want to send.
2. On the *Map* menu, click *Send map to*.
3. A new e-mail is composed in your default e-mail program with an attached e-map file.

Unpacking an E-map

If you receive an e-map and you would like to for example, view the grid statistic of a displayed grid, you must first unpack the map and extract the grid file.

To UNPACK A MAP:

1. Select (highlight) the **Oasis montajv60.map**.
Note: The **Oasis montajv60.map** file is a packed map that contains 3 files (**Oasis montajv60.map**, **Oasis montajv60.grd**, and **Oasis montajv60.grd.gi**).
2. On the *Map* menu, click *Unpack map files*. The map is unpacked and the extracted associated grid files are placed in the current project directory.

Exporting Data

Oasis montaj Viewer provides a variety of exporting capabilities including exporting databases and maps.

Exporting Databases

- Marked Data
- Geosoft XYZ Data Files
- Geosoft GBN Data Files
- Subset GDB Data Files
- Microsoft Access Data Files
- ASEG-GDF Data Files
- Other Data File Formats such as CSV, ODDF, POST PC and POST UNIX

Exporting Maps

- Enhanced Metafile
- ArcView Shapefile
- CGM Plot
- Bitmap
- PCX
- PNG
- Encapsulated Post Script
- Geosoft COLOUR Grid
- ER Mapper RGB
- Geosoft Plot file
- DXF AutoCAD 12
- DXF AutoCAD 13
- JPEG
- JPEG High Quality
- TIFF
- GeoTIFF
- MapInfo TIFF
- ArcView TIFF

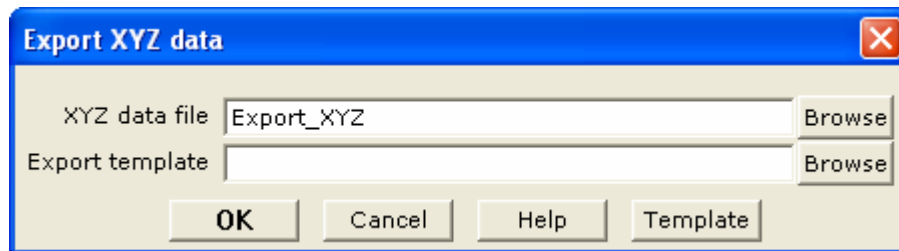
Exporting Databases

Oasis montaj Viewer enables you to export **Oasis** databases in a variety of data formats. This tutorial will describe how to export to a Geosoft XYZ and CSV Data format file.

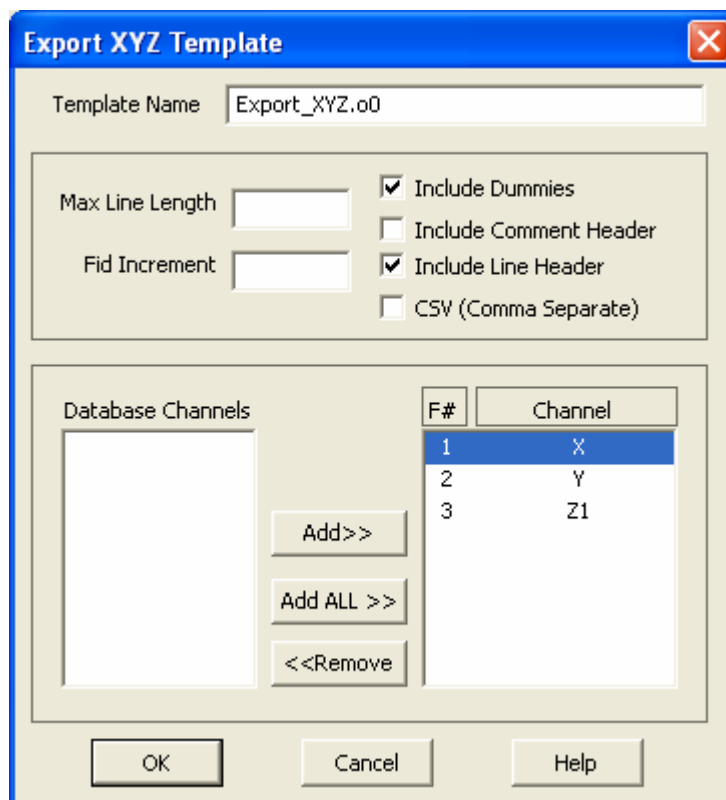
Export Geosoft XYZ Data Format

The directions below describe how to export a database as a Geosoft XYZ file.

1. Select the **Casaber.gdb** database in your current project.
2. On the *Data* menu, click *Export*, and then click *Geosoft XYZ*. The *Export XYZ data* dialog box is displayed.



3. Specify the XYZ data file name (**Export_XYZ**), and click the [**Template**] button. The *Export XYZ Template* wizard is displayed.



Note: The *Export XYZ Template* uses a wizard to determine which channels to export, the export parameter settings (maximum line length, fiducial

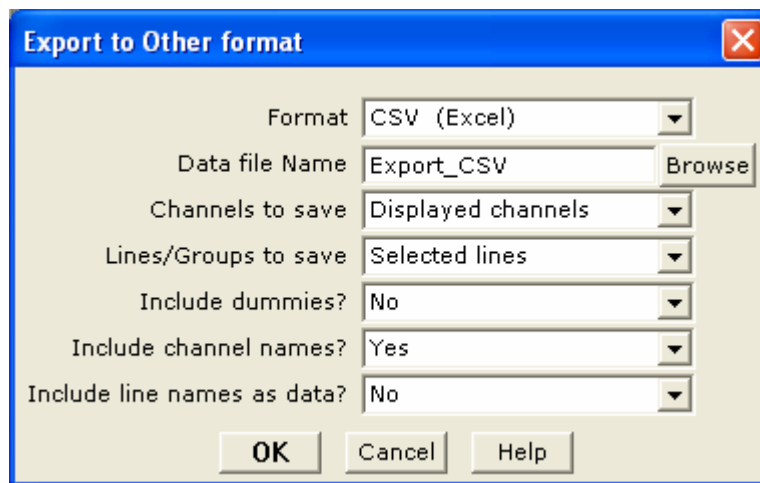
56 Tutorial 2: Working with Data

increment), and to include (or not include) dummies, comment headers, line headers, and CSV formatting.

4. You can specify a *Template name* (**Export_XYZ.o0**) or use the default (default.o0) template.
5. Click **[OK]** to return to the *Export XYZ data* dialog, click **[OK]** to export the data as **Export_XYZ.xyz**.

Export CSV Format

1. Select the **Casaber.gdb** database in your current project.
2. On the *Data* menu, click *Export*, then click *Other*. The *Export to Other format* dialog is displayed.



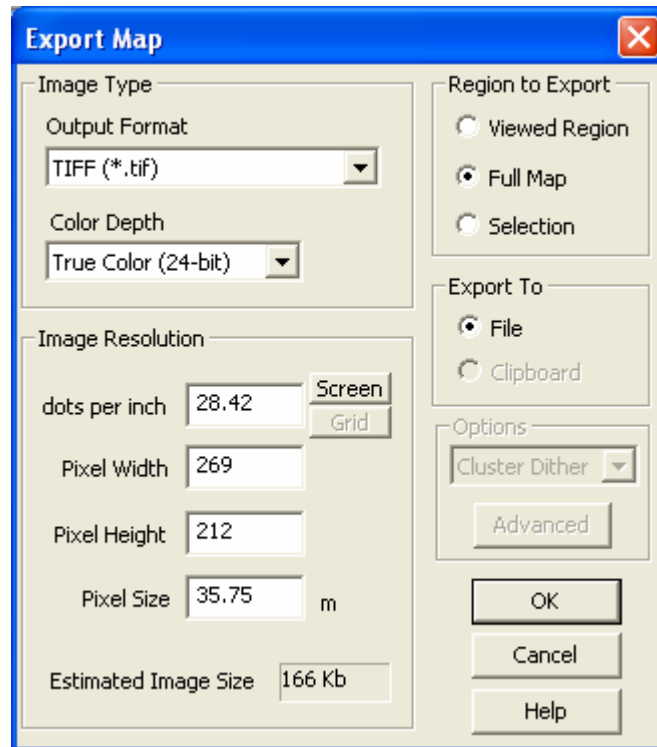
3. Specify the *Format* as **CSV** (Excel).
4. Provide the *Data file Name* (**Export_CSV**), and then specify the *Channels to save*, and the *Lines/Groups to save*. You can also specify to *Include dummies?*, and to *Include channel names?*.
5. Click the **[OK]** button. The system exports the data to the designated file name.

Exporting Maps

Oasis montaj Viewer enables you to export **Oasis** maps to a variety of grid and image formats. This tutorial will describe how to export a map to a tiff file format.

EXPORTING MAP

1. Select (highlight) the map you want to export (**Oasis montajv60.map**).
2. On the *Map* menu, click *Export*. The *Export Map* dialog is displayed.



3. In the *Image Type* box, choose the *Output Format* as (**TIFF (*.tif)**) and select the *Colour Depth* (**True Color (24-bit)**)
 4. In the *Region to Export* box click the (**Full Map**) option.
 5. In the *Image Resolution* box, change the *Pixel Size* to **35.75**.
- Note:** Pixel Size is the number of ground units each pixel in the image represents. In the example above, each pixel in the exported map represents **35.75** meters. You can set the pixel size to match the grid cell size *closely**. However, rounding error usually prevents the grid cell size from exactly equalling the pixel size.
6. In the *Export to* box click **File**.
 7. Click [**OK**] to export the **Oasis montajv60.map** in tiff format. The *Export file name* dialog is displayed.
 8. Specify a file name for the tiff file and click [**Save**]. The tiff file is saved in your project directory.

Printing Maps in Oasis montaj

Oasis montaj, by default, uses your Windows system drivers to create printer or plotter output. When you start printing maps for the first time, you will most likely accept the defaults. Depending on your driver's performance however, you may want to add a new configuration that uses more advanced printing options.

Geosoft provides a special printer setup capability that starts an internal rasterizing engine that performs most of the print/plot processing and passes it to the driver for final output.

58 Tutorial 2: Working with Data

If you are not satisfied with your driver's performance, you can try selecting; Geosoft bands, Geosoft bands and dither, HP-RTL or the Postscript printing option. Refer to the on-line help system for a complete discussion on the pros and cons of the different printing modes.

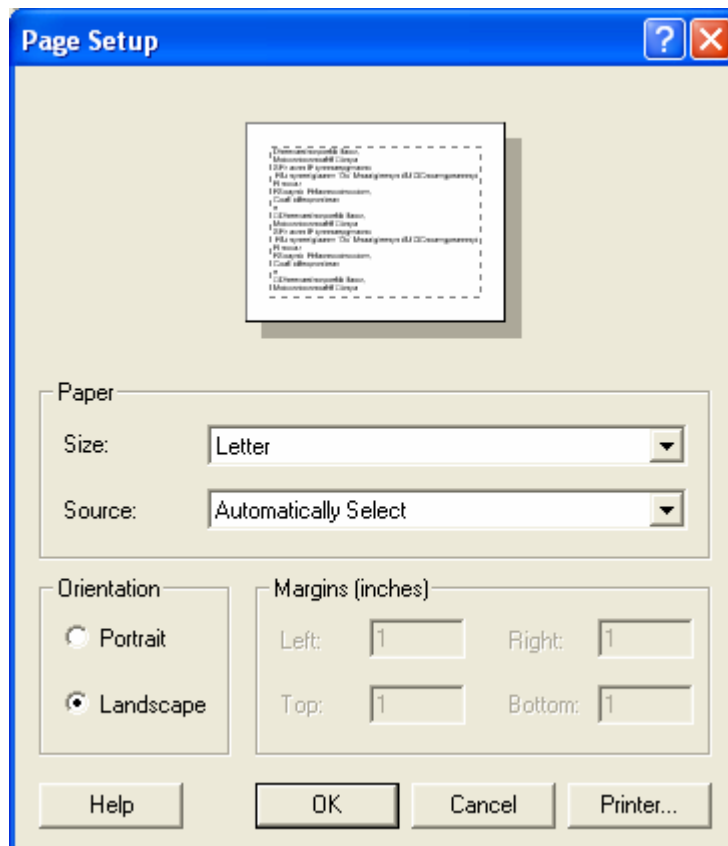
Printer Setup

The *Printer Setup* dialog box enables you to specify the part (displayed or entire area) of the currently selected map that you want to plot and specify scaling for the plot:

You can plot the currently visible part of the map (i.e. enlarged or reduced map) or the entire map. When plotting, you also have the option of scaling the visible or entire plot to cover the entire plot area or to scale the entire plot to a specific range.

SETTING UP THE PRINTER

1. On the *File* menu, click *Printer Setup*, the *Page Setup* dialog is displayed.



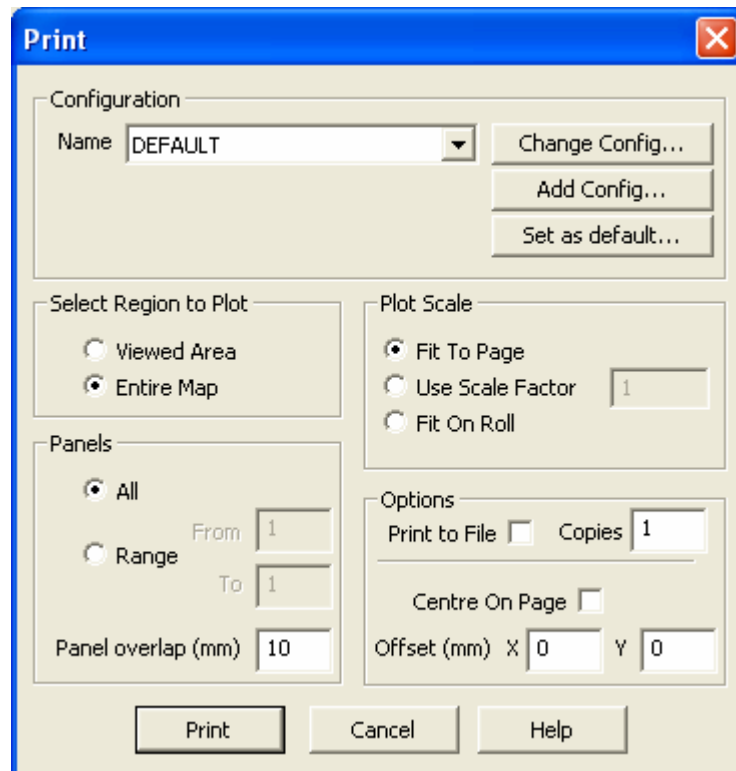
2. Change the paper *Orientation* to **Landscape** and click **[OK]**.

Note: For more information on printing setup parameters click the **[Help]** button on the *Page Setup* dialog box, or see the *Printing* topics in the **Oasis montaj** online help system.

Print a Map

1. Select (highlight) the map that you would like to print.

- On the *File* menu, click *Print*. The system displays the *Print* dialog box.



- In the *Select Region to Plot* box select **Entire Map**. In the *Plot Scale* box select **Fit To Page**.

Note: Map may not be plotted to scale. To maintain the map scale, select the **Use Scale Factor** option and specify a value, (**1 = 100%**). If you use this option, the map may require more than one page depending on the media to which you are printing or plotting.

- In the *Panels* box, select **All**.

Note: *Panel overlap (mm)* If you are printing multiple panels, you can specify an overlap in mm. This helps you to match panels later.

- In the *Options* box, select **1** copy.

- Click the [**Print**] button to send the map or plot to the currently configured printer or plotter.

Note: For more information on print parameters click the [**Help**] button on the *Print* dialog box, or see the *Printing* topics in the **Oasis montaj** online help system.

Appendix 1: Geosoft Concepts

This chapter contains information about the components included in **Oasis montaj**[™] and describes the concepts you will need to know to use the system. A quick overview of the concepts described in this chapter are available in the **Oasis montaj Viewer** help system in the **About** directory called *Tour for New Users*.

Oasis montaj is Geosoft's core software platform for working with large volume spatial data. The core software platform consists of a free **Viewer** and a licensed **Mapping and Processing System**. For more information on the **Oasis montaj Mapping and Processing System** visit www.geosoft.com/pinfo/oasis_montaj.html

Oasis montaj Viewer

The **Oasis montaj Viewer** is a free software product that enables you to view Geosoft databases, Geosoft Grids and a variety of common image and data exchange formats. Specifically, this version provides you with the following capabilities:

- Access project data (Geosoft databases, grids and maps), tools (3D Tool, Project Explorer, Undo/Redo Tool), and Geosoft toolbars (Database Tools, Map Tools, Standard Toolbar)
- Evaluate data, information and interpretations by viewing and performing specific tasks using Geosoft databases, profiles, maps, and grids as well as Geosoft and third-party images (including PLT and DXF).
- Verify data quality, analyses and interpretations by tracking processes applied to databases and maps
- Perform selected processes made available through Geosoft menus or third-party GXs
- Share results and knowledge by viewing and/or sending E-maps to team members and other professional contacts
- Prepare reports using clipboard image copying capabilities

The **Oasis montaj** environment provides direct access to data contained in Oasis databases through a spreadsheet window and an integrated profile display window. The Oasis database is a high-performance database that provides efficient storage and access for very large spatial data sets.

The **Viewer** provides visual data links that enable you to dynamically connect data in the spreadsheet, profile and map views. DAT technology (for accessing grids and images) enables the **Viewer** to display a variety of grid and image formats in **Oasis montaj**.

The **Oasis montaj** core platform provides the basic resources for all Geosoft Applications and Tools. Geosoft provides a variety of systems that address specific applications in exploration geophysics, drillhole geology, exploration geochemistry and other areas. These systems consist of menus and corresponding Geosoft eXecutables (GXs) that run on the core platform.

What is Oasis montaj?

The concept of an integrated environment for earth science data emerged from over two decades of software development at Geosoft and is now implemented in the **Oasis montaj** software platform. Geosoft's vision reflects the fast pace of today's professional work environment and the significant changes in data processing over the past twenty years:

- An order of magnitude increase in data volumes
- Increasing digital data availability and connectivity
- Shift in processing from office to *in situ* (or field) environments
- Replacement of proprietary software with commercial solutions

By design, Geosoft's **Oasis montaj Viewer** meets specific needs including:

- Project Explorer Tool enables users to browse as well as open any 'project' item
- Enhanced metadata capabilities provide access to the "Properties" (or meta) of the data displayed in the Project Explorer using the Metadata tool
- File locations are displayed in a popup dialog when you mouse over an item in the Project Explorer
- Description tool enable users to add descriptive text to the items displayed in the Project Explorer
- Geosoft's DAP (Data Access Protocol) technology enables users to access very large spatial datasets residing on an Internet Server (or locally on a Personal Computer).
- Connecting you to your data and information via dynamic linking – a unique technology for graphically connecting data, profiles and maps in a single desktop environment
- Addressing high-volume data storage and access requirements for very large spatial data sets
- Delivering focused solutions to specific Earth Science problems
- Free **Oasis montaj Viewer** for Data and Information Sharing

Viewer Capabilities

The **Oasis montaj Viewer** is a free software product for accessing and sharing data and images in native Geosoft and standard PC formats. The **Viewer** is available for download at www.geosoft.com. The **Viewer** can be freely distributed by anyone who wants to enable other geoscientists to share data and maps in a Geosoft environment. Some of the **Viewer's** capabilities are listed below.

PROJECTS

- Open and display projects and display/edit project comments
- Browse and open any project item in the Project Explorer
- Add or modify "descriptions" of all data items displayed in the Project Explorer
- View and edit project data "Properties" (or meta) using the Metadata Browser

62 Appendix 1: Geosoft Concepts

DATA AND PROFILES

- Open new databases imported from Geosoft GDB, Geosoft GBN, Geosoft XYZ and ASEG-GDF formats
- Export databases as Geosoft GDB, Geosoft GBN, Geosoft XYZ, ASEG-GDF, CSV (Excel), ODDF (USGS), POST PC (USGS) and POST UNIX (USGS)
- Show and plot data profiles in upto five database profile windows
- View data projected coordinate system information
- View data statistics and historical processing logs
- Dynamically link data between spreadsheet, profile window and maps

MAPS, GRIDS AND IMAGES

- Display a wide variety of grid and image files (for a detailed list see the *Data Exchange Format* online help topic)
- Import and display Geosoft PLT, AutoCAD DXF, MapInfo TAB, ArcView SHP and Microstation DGN files
- Open and display maps, and display/edit map comments
- Pan, zoom, and cursor-link map views
- View map view projected coordinate system information
- Copy and paste database data and maps to other Windows applications
- Export maps to a variety of formats
- Plot maps to Windows printers and large-format plotters
- Send and receive E-Maps

ONLINE HELP AND TECHNICAL SUPPORT

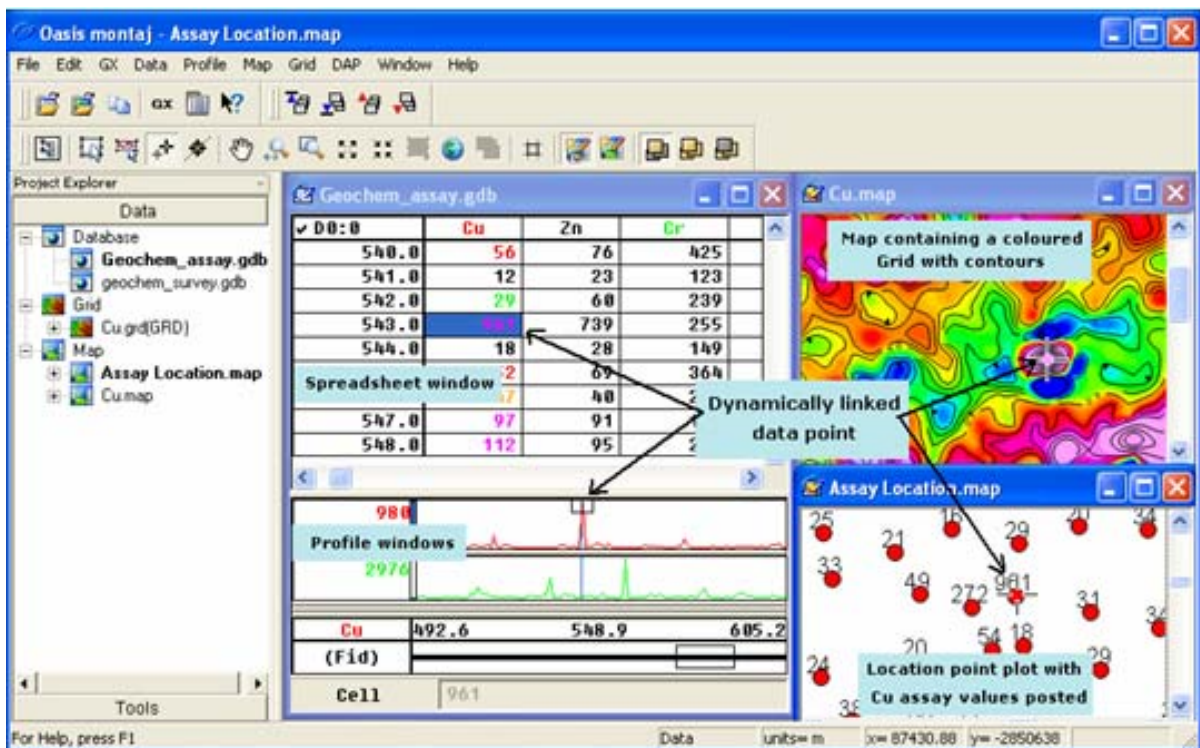
- Full on-line help system with links to Geosoft Web Server.
- Access to Geosoft [**geonet**] support list and Geosoft Web Site resources.

Keeping you in touch with your data

An important design strategy in **Oasis montaj** was to keep you in touch with your data. In fact, the system is intended to connect you with your data and information in several unique ways:

- By providing an integrated environment that holds all of your project information
- By enabling quick and easy access all your project data via the Project Explorer including; databases, grids, maps, tools and metadata information
- By providing unique views of data (spreadsheet, profile and map)
- By connecting you to data and information in these views (through a specialized dynamic linking technology)
- By delivering a wide variety of algorithms and techniques
- By “memorizing” the processing you apply to data and maps by means of a proprietary process “maker” technology. This capability is especially useful for quickly testing and optimizing processing parameters. It also keeps a record of processing so that you can remember your settings if you stop working on your project and later return to it.

Geosoft’s approach is intended to give you a means of keeping in close contact with your original and processed data and information — from start to finish. As you use the system, you will find your own ways to take advantage of these capabilities.



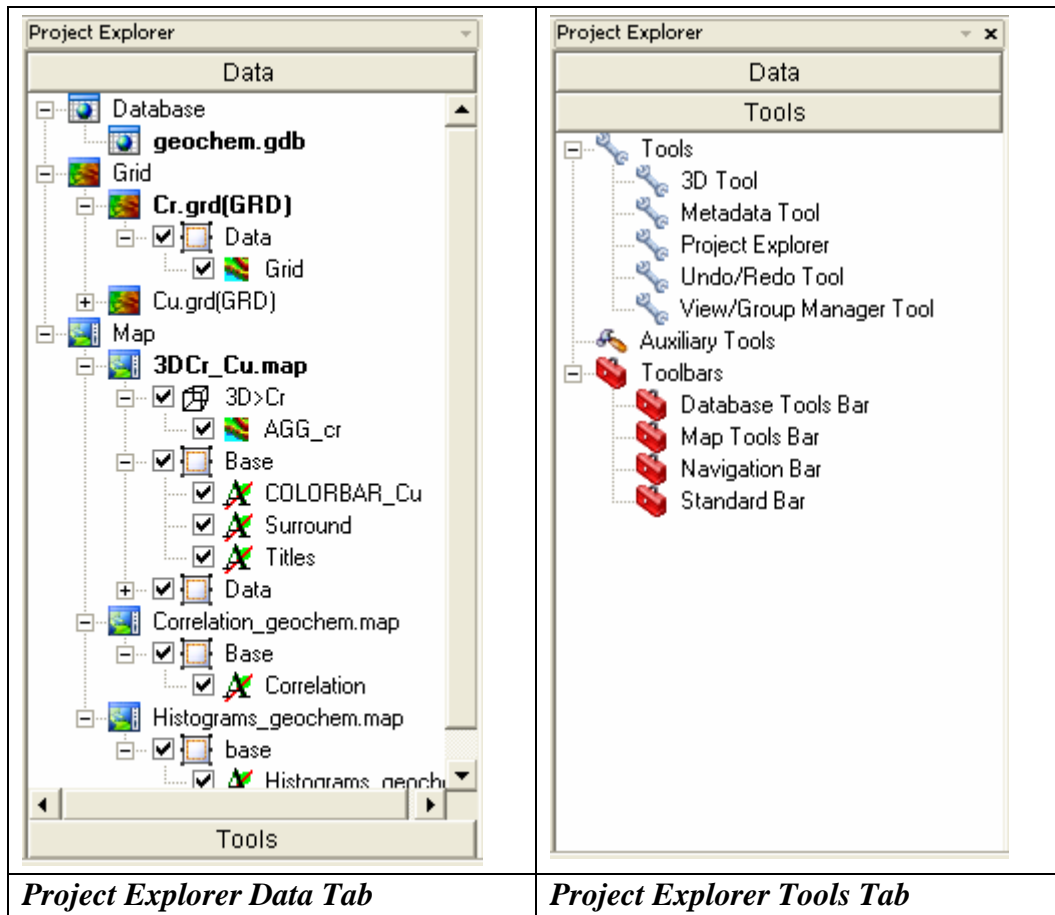
The remainder of this section provides some brief details about projects, databases, maps, views, dynamic links and process makers.

Projects and the Project Explorer

To work in **Oasis montaj** requires an open Project. An **Oasis montaj** "Project" encompasses every item in your working project; from the data files in your project (databases, maps, and grids), to the tools used (including auxiliary tools such as histograms, scatter plots etc. - licensed version only), to the project setup including the menus you have displayed and whether you are working on a map or profile and the state in which you left it the last time you used it.

The **Project Explorer** enables you to browse as well as open any project item. The project file (*.gpf) is used to keep track of all information related to a working project.

The Project Explorer has two windows, the *Data* window that includes all data files included in the project and the *Tools* window that organizes and maintains the project tools.



Some of the capabilities of the Project Explorer are:

- Keeps track of all files and using the description and metadata tools enables you to keep track of project information. Note that, in previous versions, file information was maintained in the file system and the user had to keep track of what the files were.
- Explorer tools including; Tools, Toolbars and Auxiliary Tools (licensed version only)

- **Tools;** 3D Tool, Metadata Tool, Project Explorer and Undo/Redo Tool and the View/Group Manager Tool.
 - **Toolbars;** Database Tools Bar, Map Tools Bar, Navigation Bar and Standard Toolbar. Also available with the licensed version, Map Edit Tools Bar, Polygon Tools Bar and Script Bar.
 - **Auxiliary Tools:** Histograms, Scatter plots, Probability plots and Triplots (licensed version only).
 - File locations displayed in popup dialog when you mouse over item in the Project Explorer
 - Data Description Tool enable users to add description to project items
 - Enhanced metadata capabilities enable access to the "Properties" of all items displayed in the Project Explorer
 - Recent Projects & recent Geosoft data files available under File menu
- Note:** Grids appear in the Project Explorer under "Grids". Opening a grid opens a view of the grid in its own internal "map". A grid map view is just like a real map and can accept any graphics that a map can. It can also be saved as a map, in which case the map will appear in the "Map" section of the project explorer.

What you need to know about Project files

You require an open project to do any work in **Oasis montaj**. The project also controls your working directory. Projects are saved as (*.gpf) files. If you open an existing project from a directory, the system assumes that your files are located in the specified directory. To streamline your work, as well as keep it organized, you may want to make sure that your project is in the same directory as the other files you want to use.

We recommend that each project you work on have its own project (*.gpf) file. If you use a number of applications or add-on tools in **Oasis montaj** that have different menus, you can use the project to display only the menus you require.

Important Note: Workspace files (*.gws) used in **Oasis montaj** prior to version 6.0 can be easily converted to Project files (*.gpf) simply by opening them in **Oasis montaj**. On the *Open Project* dialog (*File|Project|Open*) select *File of Type* as "Workspaces (*.gws)" and when asked if you want to convert the old workspace into a new **Oasis montaj** project file, select "Yes". The workspace file will be converted to a project file and all associated workspace information will be transferred to the new project file. In addition, the workspace file will remain untouched so that it can be opened in previous versions.

Databases and high-volume data processing

Many commercial and governmental groups currently use **Oasis montaj** for routine processing of high volume datasets (tested up to 10 gigabytes) and also for relatively low volume processing in a variety of mapping and other applications. One key to the system’s capabilities is the proprietary 3-dimensional database architecture, which enables the rapid processing and analysis of high volume data. This object-oriented database structure stores data in a form that enables rapid access and efficient storage of your data.

Databases are displayed and organized in **Oasis Montaj** in the Spreadsheet Window.

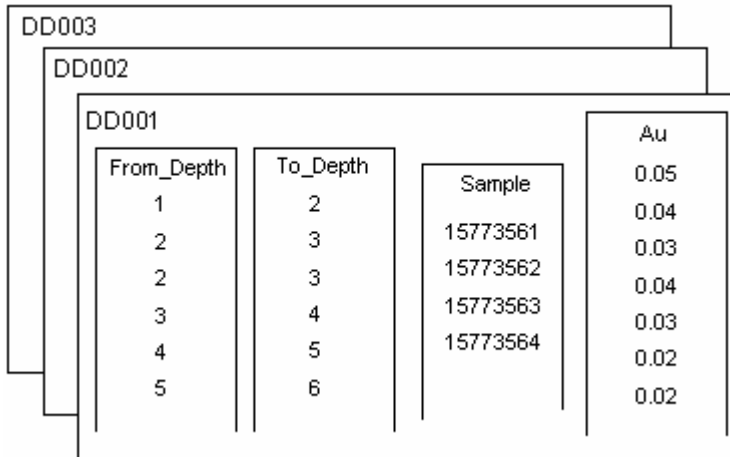
The spreadsheet window organizes and displays data differently than conventional (relational) spreadsheet and database programs. Conventional databases organize data as tables, records and fields, as shown below:

Hole_ID	From_Dep	To_Depth	Sample	Au ppm	As ppm
DD001	0	1	15773561	0.05	13
DD001	1	2	15773562	0.04	11
DD001	2	3	15773563	0.03	19
DD001	2	3	15773564	0.04	19
*	*	*	*	*	*
DD003	98	99	15767021	0.4	-0.5
DD003	99	100	15767022	0.22	-0.5
DD004	0	5	15766457	0.04	-0.5

Conventional databases organize data as tables, records and fields. This is effective for querying and searching type applications but limits it as a data processing engine because:

- Programs must read an entire record to access a single field
- It is computationally intensive to change record structures
- Data sampled at different intervals and starting points are difficult to store

Oasis montaj is based on a proprietary 3-dimensional-file format architecture that overcomes these limitations, as shown below:



Organized in lines (or groups), columns and elements, the database stores all data values of a particular type in individual columns or channels. This enables stand-alone processing of columns and eliminates the need to write results to interim storage areas and then re-write them after processing. The result is a significant increase in processing efficiency. This Geosoft file structure provides additional advantages including:

- Ability to process any number of lines/groups
- Ability to handle lines/groups with unlimited columns
- Ability to handle very large datasets

In addition, since columns are stored separately, this file format is capable of storing and manipulating data with different end point and sample intervals.

Spreadsheets are the windows to your database

When you create or open a database, you see a spreadsheet. The Spreadsheet view is your “window” to the **Oasis montaj** database and it also provides you with flexibility in setting up your working environment. All data is stored securely in the underlying database — you simply decide which data you want to display in the spreadsheet and keep all other data in the background, hidden from view.

The spreadsheet is organized in rows, channels (columns) and lines (also called groups in other applications such as drillhole plotting). Rows and columns work similar to standard spreadsheets in that you can edit and delete them as needed. The system also enables multiple “worksheets” in your database – depending on the type of data you are working with (line, random line or drillhole); the worksheets have different names. To see what type of name is used, look at the Line Header Cell located at the top left corner of the spreadsheet. An “L” for example, indicates that you are working with line data. An “L” for example, indicates that you are working with line data.

The screenshot shows a spreadsheet window titled "testing.gdb". The spreadsheet has a header row with the following labels: "Line Number", "Column", "Channel Header Cell", and "Protected Channel". The first row of data is highlighted in green and contains the values: "L40013:0", "Y", "X", and "Z1". The subsequent rows contain numerical data. A red box highlights the first column of data, labeled "Fiducial Cells". A red box highlights the last column of data, labeled "Data Cell". A red box highlights the "Channel Header Cell" area, which contains a diagonal line. A red box highlights the "Protected Channel" area, which contains a diagonal line. A red box highlights the "Line Number" area, which contains a checkmark and the text "L40013:0".

Line Number	Column	Channel Header Cell	Protected Channel
✓ L40013:0	Y	X	Z1
411.0	1021025.50	79724.40	194.40
412.0	1021030.00	79723.20	195.20
413.0	1021035.10	79721.90	196.80
414.0	1021040.00	79720.70	196.50
415.0	1021044.60	79719.20	196.80
416.0	1021049.50	79718.00	196.60
417.0	1021054.10	79716.70	196.00
418.0	1021060.20	79715.30	197.60
419.0	1021064.10	79713.80	198.60
420.0	1021068.20	79712.50	198.20
421.0	1021072.20	79711.30	196.30
422.0	1021077.70	79709.80	196.50
423.0	1021084.20	79708.40	197.60
424.0	1021088.20	79707.00	197.50
425.0	1021091.30	79705.50	202.00
426.0	1021096.30	79704.20	202.00
427.0	1021100.80	79702.80	203.00
428.0	1021108.30	79701.40	202.30

General spreadsheet capabilities include:

- The ability to display data from your database through a spreadsheet window
- Handling of any sample interval
- Supports full editing and mathematical processing capabilities

- The ability to process selected samples, selected channels and selected lines or groups

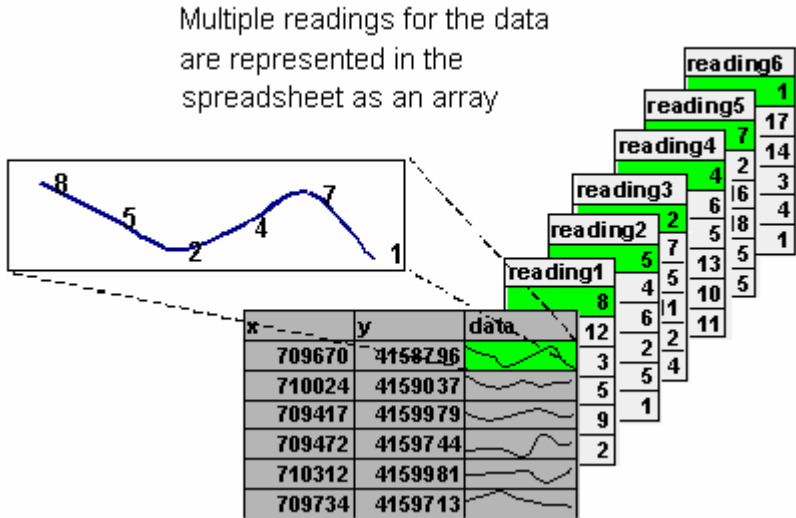
How the Spreadsheet Displays Project Data

The spreadsheet does not display your actual data, but rather a view of the data. Depending on your type of project, the spreadsheet will display your data as either values or arrays.

For surveys where a single value is recorded at each station, for example an assay survey, each data cell will contain a single value.

x	y	data
709670	4158796	8
710024	4159037	12
709417	4159979	3
709472	4159744	5
710312	4159981	9
709734	4159713	2

For surveys where a multiple readings were recorded at each station, for example an Induced Polarization survey, each data cell will contain multiple values.



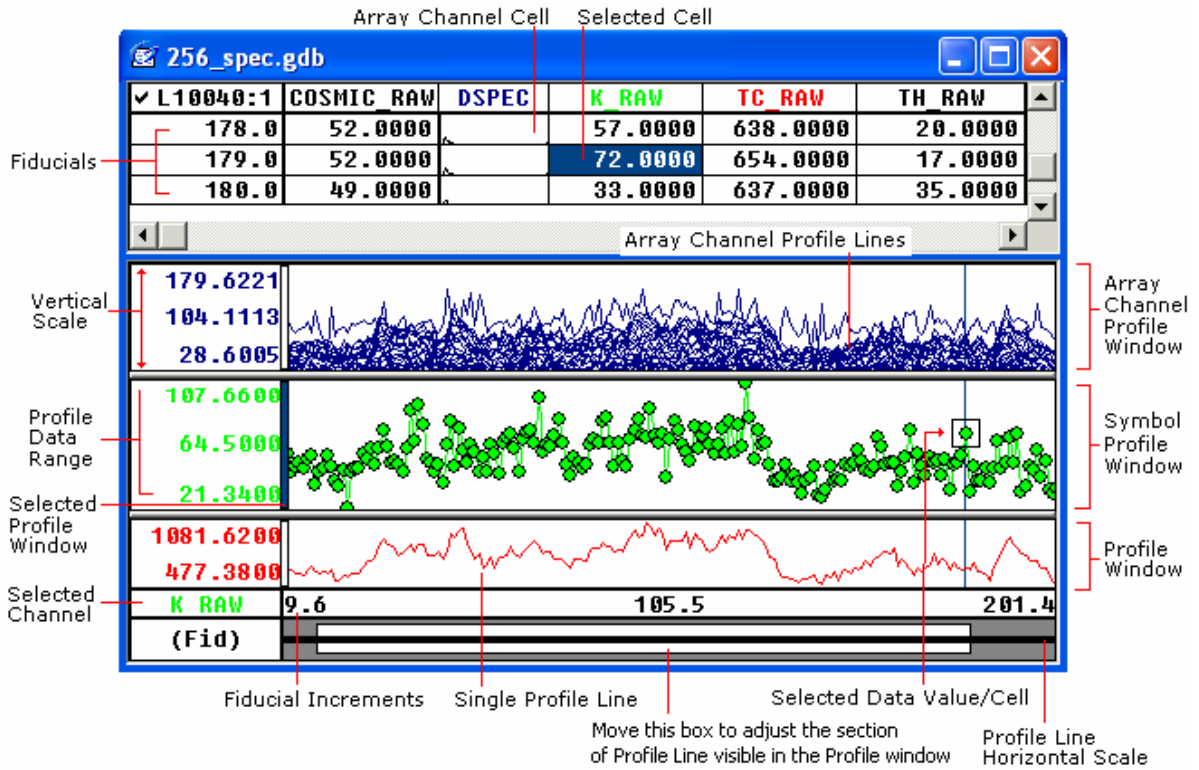
The spreadsheet represents these values as a profile line in an array channel.

Profiles and viewing your data graphically

The Profile view is your “graphical window” to the **Oasis montaj** database. You can display profiles of one or more variables in your database simply by selecting the channel and selecting a simple menu item. The profile appears directly below its corresponding database in a profile window. You can have up to five “panes” with 32 variables in each pane.

A key point to note about profile windows is that they are linked dynamically to their corresponding database. When you select a value or range of values in either the database or profile window respectively, they are also highlighted in the other window.

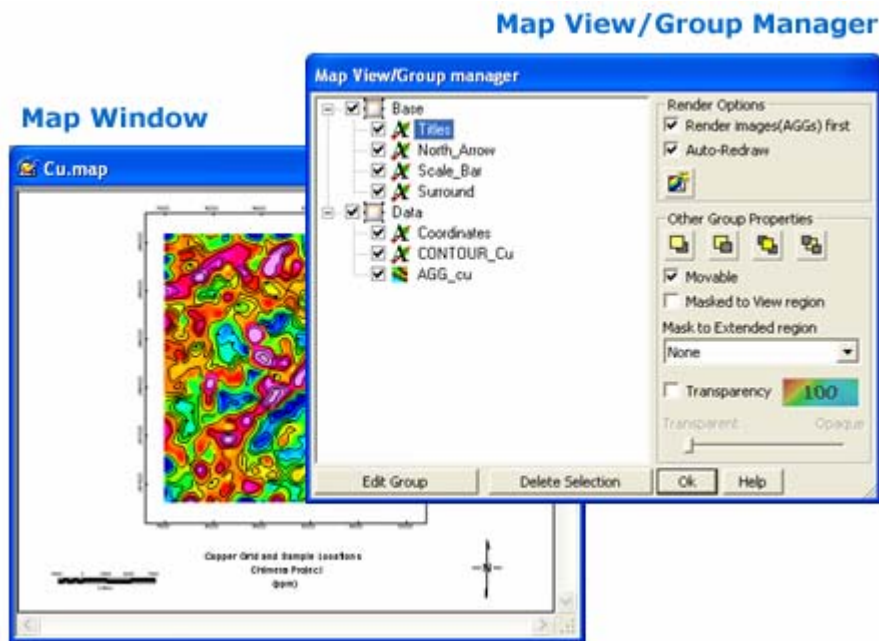
This capability keeps you in touch with your data and gives you an interactive means of accomplishing quality control or analysis tasks.



Maps are more than printed sheets of information

Geosoft's mapping capabilities are the result of more than a decade of programming development, and the options for producing and editing maps — as well as the quality of output — reflect this level of experience. You can use the system to produce a variety of professional presentations quickly and easily.

However, you should also be aware that a map is more than a printed sheet of information in **Oasis montaj**; the Map view gives you an electronic area for analyzing, visualizing and editing your data and information.



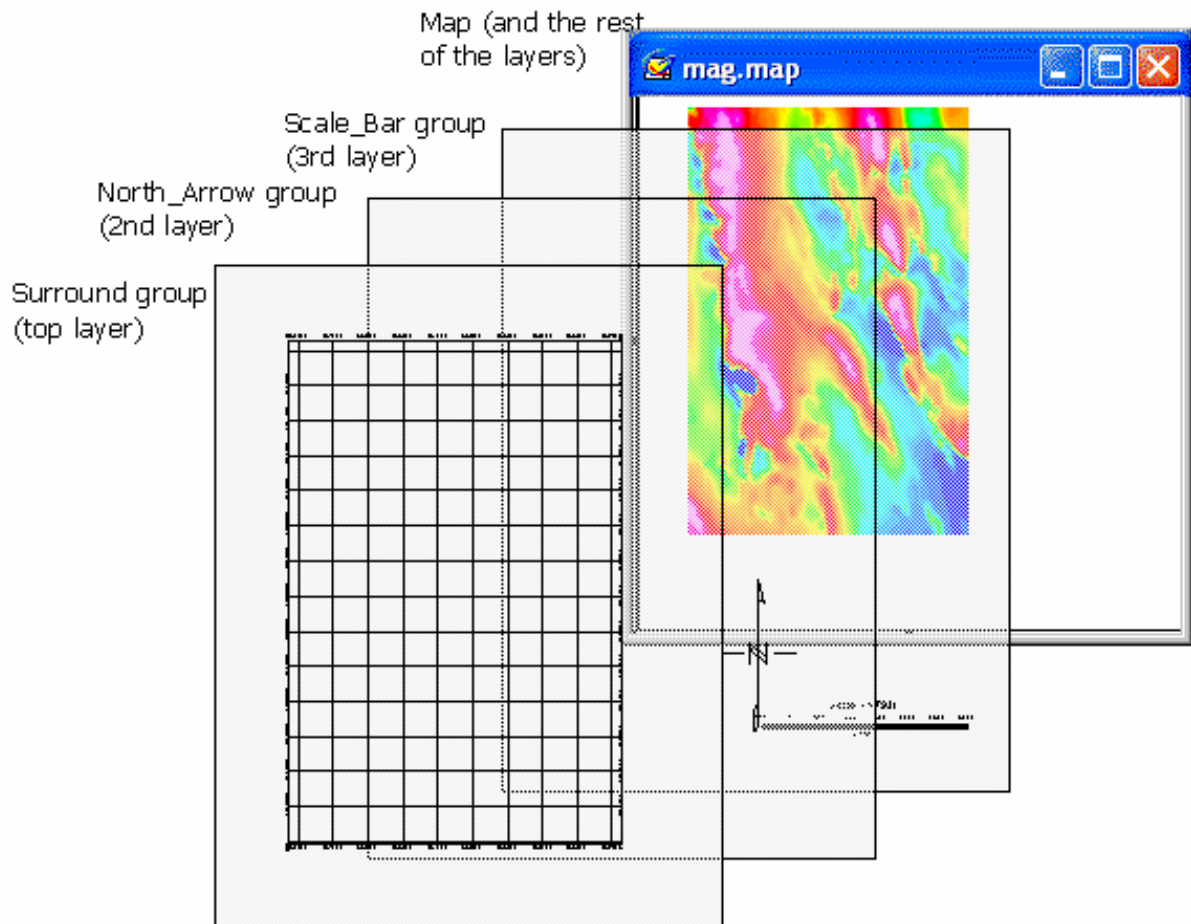
When you create a new map the system opens up a new blank *Map Window*. After a *Map Window* is open, you can add a wide variety of data- and base map-related information. **Oasis montaj** Maps use *Views* to organize and display information. A *View* divides the information on a map into a *Base* view, which uses paper coordinates, and a *Data* view, which uses ground coordinates. Map surrounds, north arrows, and scale bars are examples of map groups plotted in the *Base* view. Map coordinates, contours, and grids are examples of map groups that are plotted in the *Data* view.

Groups are a fundamental part of maps. **Oasis montaj** uses *Groups* to determine the order in which objects are displayed (rendered) on a map. Groups are layered on top of each other in a specific order determined by the *Map View/Group Manager Tool*. You can create, edit, move, hide, and mask groups. You can also move groups in front and behind each other. Any new object you add to a map, such as a polygon or line, is added to the current group.

The 'Light table' display technology is based on a new generation of rendering capabilities. Each group or layer in a map has individual transparency settings, controlled

72 Appendix 1: Geosoft Concepts

from the *Map View/Group manager*. These transparency settings affect both 2D raster images and vector line work.

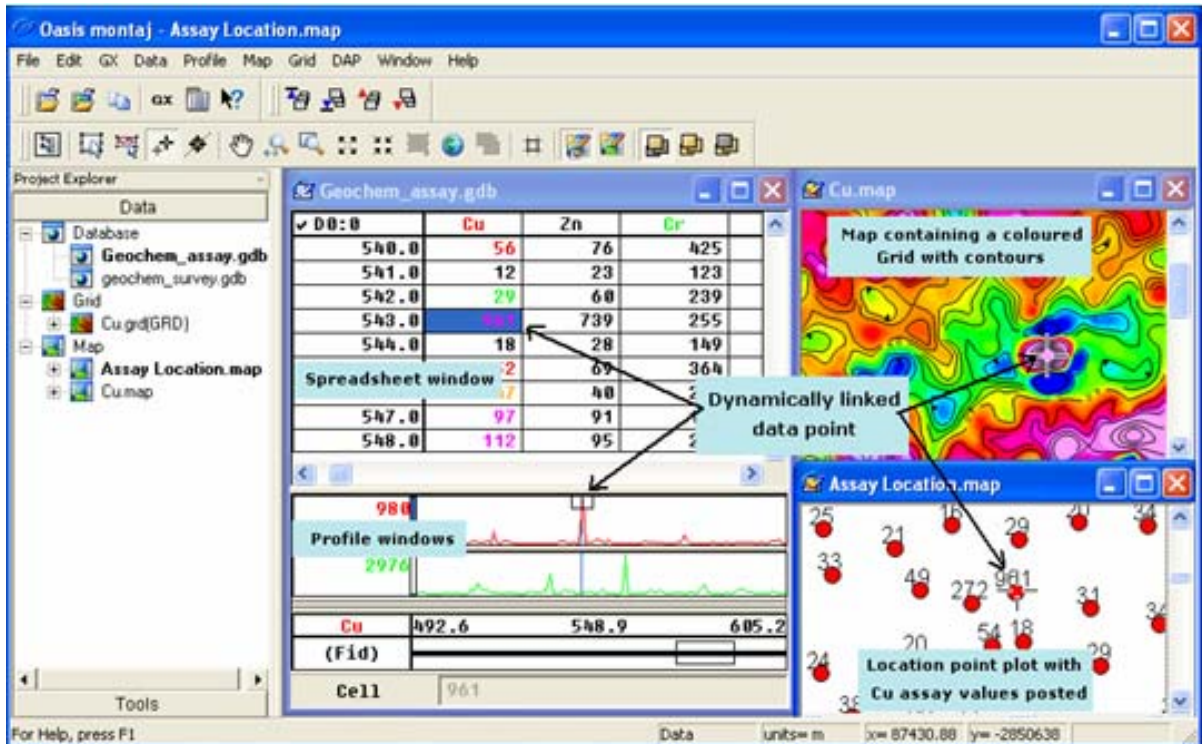


As you use the system, you will become familiar with the information that is stored in each type of *View* and how to manipulate them (for example, by turning off a map layer for plotting purposes). And as shown in the next section, you will also learn to activate dynamic links between databases, profiles and maps so that you can perform advanced processing (selection of parameters) as well as interactive analysis and visualization.

Dynamically link data and information to knowledge

Dynamic links are a key part of Geosoft’s strategy of helping professional’s stay in close touch with their data—from import to processing to analysis. By definition, dynamic links are interactive graphical connections that you can activate between databases, profiles and any number of maps in your project. When you activate links and select any item or position in a database, profile or map, a cursor automatically connects the item or point in all items.

This capability gives you an important means of visualizing original or processed results in any view and seeing the corresponding representation in another view. The practical benefit is that you can quickly perform quality control, processing or analysis using all available data and information. Applying dynamic linking is also a highly efficient approach to building knowledge and making informed decisions.



Geosoft Algorithms and Techniques

The Geosoft eXecutable (GX) is the basic mechanism through which Geosoft provides the basic resources for all Geosoft Applications and Tools. GXs are programmed processes that are attached to the main menus in the system and to the special menus used in application suites. GXs run interactively in the graphical user interface but many GXs can also run in batch mode (using script commands).

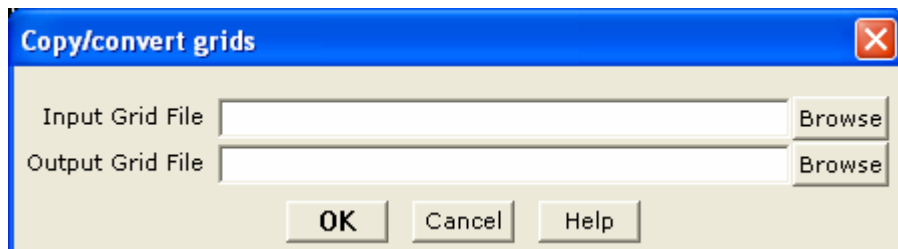


All Geosoft GXs are signed. A Geosoft signed GX is a GX written and tested by Geosoft. It contains no viruses or code that can harm your system. As a user you can trust that this GX works and is safe to use. Non-signed GXs will generate a report warning the user that there could be a problem with the GX or its contents and that Geosoft did not test or create this GX.

Individual users can create GXs using the GX Developer Toolkit. Geosoft's own developers also use this product to develop applications. The GX Developer is designed for users who consider themselves to be computer-oriented scientists (i.e. you do not have to be a computer scientist to use it effectively). If you encounter a non-Geosoft GX a report warning will be displayed notifying you that this is not a Geosoft signed GX.

Third party developers are also creating GXs and the product offers many opportunities for integrating other products into the system either via DLLs or by directly accessing Geosoft's database and function library. For more information, please contact your Geosoft representative.

The following dialog box shows a standard GX dialog box. Geosoft now supports Visual Basic programming so that users can create even more advanced dialog boxes as required for their specific applications.



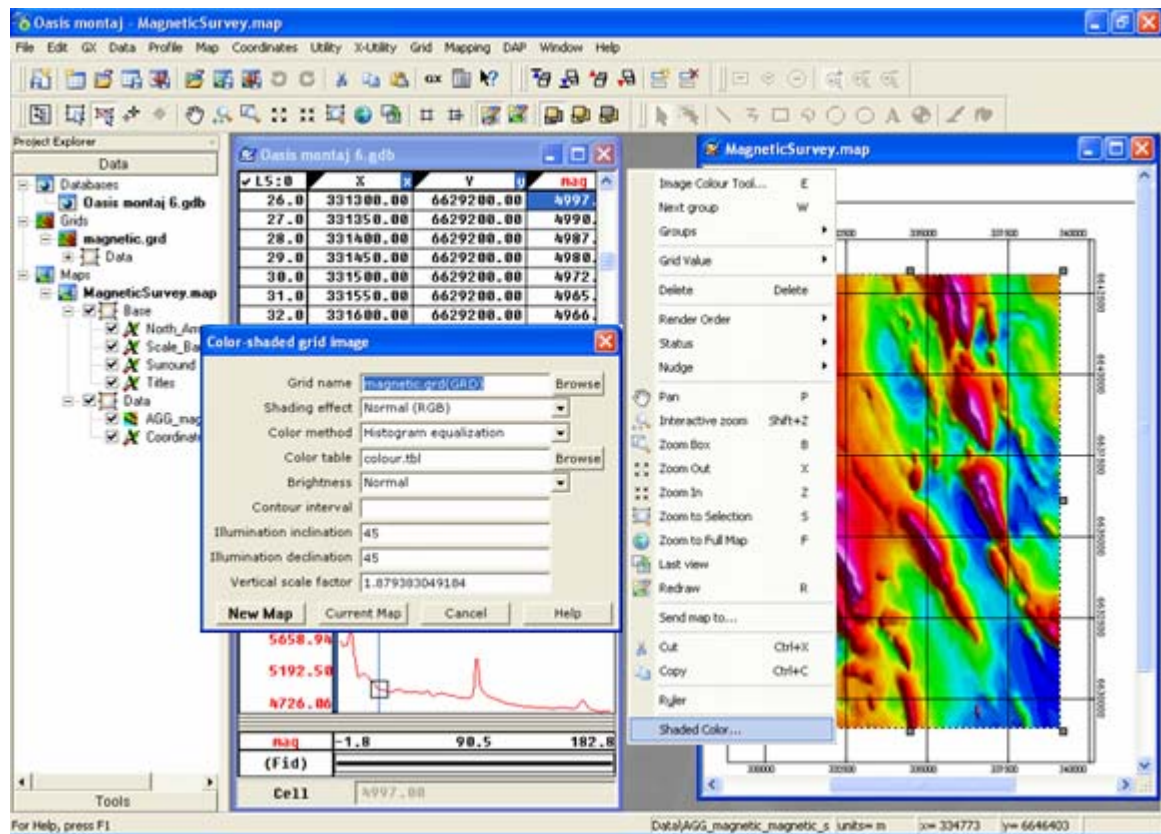
Process Maker technology links data processing

A dynamic process link is a built-in feature that remembers the processing parameters associated with a specific object such as a channel, grid or map and that enables you to quickly rerun the process using different settings.

A quick tool for reprocessing data, the process link is also useful for remembering processing settings. This latter capability is particularly effective if you are away from your project for any length of time and want to recall the settings you were using.

To access the maker popup menu is the maker associated with the object. Select this option and you will see the corresponding dialog box and settings. You can either change settings and re-process, or exit from the dialog as required.

Process Maker technology brings dynamic linking to data processing



Appendix 2: Displaying Data Formats

Oasis montaj Viewer enables users to display various file formats (Geosoft XYZ, Geosoft GBN, and ASEG-GDF) in an **Oasis montaj** database.

Geosoft XYZ File Format

The following is an example of a Geosoft XYZ file format:

```

Line 290.0
 10517.0    8013.0    56600.4
 10517.0    7977.0
 10516.0    7940.0    56595.1
 10515.0    7904.0    56592.2
 10515.0    7867.0    56589.6
 10514.0    7831.0    56588.2
 10514.0    7794.0
 10513.0    7758.0    56589.4
 10512.0    7721.0    56589.4
 10512.0    7685.0    56590.0

Line 300.0
 10209.0    8013.0    56648.7
 10209.5    7973.0    56641.0
 10210.0    7933.0    56633.2
 10210.0    7893.5    56623.0
 10210.0    7854.0    56616.5
 10210.5    7814.0    56607.5
 10210.5    7776.5    56598.4
 10209.5    7741.5    56596.6
 10208.5    7706.5    56599.5

Line 305.0
 10012.0    5318.0    56492.4
 10012.5    5239.0    56489.4
 10013.0    5160.0    56488.4
 10013.5    5112.0    56487.5
 10014.0    5080.5    56485.4
 10014.0    5033.0    56487.5
 10014.5    4985.5    56491.5
 10015.5    4858.5    56492.9
 10016.0    4763.5    56493.3
 10017.0    4684.0    56501.3
 10017.0    4636.5    56509.1
 10017.0    4589.0    56518.0

Line 310.0
 9883.5    4329.5    56510.7
 9884.0    4356.5    56514.0
 9884.0    4384.0    56516.8
 9884.0    4411.5    56519.2
 9884.0    4438.5    56522.2
 9884.5    4465.5    56524.5

```

ASEG-GDF File Format

Following is an example of an ASEG-GDF import template:

```
[IMPORT ASEG-GDF]
DEFN BOOTHILL.dfn
DATA BOOTHILL.dat
FLC FLTLINE
IMPORT FLIGHT,FLIGHT,SHORT
IMPORT DATE,DATE,LONG
IMPORT TIME,TIME,FLOAT
IMPORT FIDUCIAL,FIDUCIAL,FLOAT
IMPORT ALTITUDE,ALTITUDE,FLOAT
IMPORT TMAGRAW,TMAGRAW,FLOAT
ALIAS L20440,L20440
ALIAS L20450,L20450
```

The template file is searched for the line [IMPORT ASEG-GDF], and the IMPORT and ALIAS lines that follow are read to determine what data to import and the channels in which to place the data. You may add any comment line you wish before the [IMPORT ASEG-GDF] line.

DEFN syntax:

```
DEFN file_name
where file_name is the name of the ASEG-GDF DEFN file to
import.
```

FLC syntax:

```
FLC flight_line_channel
where flight_line_channel is the name of the ASEG-GDF channel
containing the flight line information.
```

IMPORT syntax:

```
IMPORT name, channel, type
The name is the name used in the ASEG-GDF DEFN file to indicate
the data name. The channel is a mapping to the channel that will
be created in the database. And the data type (one of BYTE,
UBYTE, SHORT, LONG, FLOAT or DOUBLE) which should correspond to
the type in the DEFN file.
```

ALIAS syntax:

```
ALIAS aseg_line_name,new_line_name
As the ASEG-GDF lines are imported, if a line-channel already
exists in the database, it will be replaced. The ALIAS statement
in the import template can be used to re-name lines of the ASEG-
GDF data file during import. If the new_line_name is blank, the
line will not be imported.
```

If ALIAS is used, ALL lines contained in the ASEG-GDF file must be defined by an ALIAS line in the same order that the lines appear in the file. The SCANASEG GX can be used to construct a default template that includes ALIAS lines for all lines of a file. This file can be edited as required by the system.

For example, if a file contains line L90, two sections of line L100 and a tie line L30, the following ALIAS lines can be used to import the data into properly named lines:

```
ALIAS L90,L90
ALIAS L100,L100.0
ALIAS L100,L100.1
ALIAS L30,T30
```


Geosoft GBN (Binary Data File) Format

The following is an example of a Geosoft GBN file format:

```

A Geosoft Binary Data file (.GBN) contains survey data in a binary
format that can be imported directly into an Oasis montaj™
database.
The format is intended for programmers who wish to design output
data files that can be easily imported into an Oasis montaj
database.
//-----
//
// gbn.fh   Geosoft Oasis montaj binary file structure.
//
//-----
//
// An Oasis montaj database is an object oriented data structure
that is too
// complex to create without the use of the Geosoft object
libraries.
// If you would like to access the database directly, this can be
done
// from a GX using GX Developer, which also provides a mechanism
for
// calling Geosoft libraries from your own DLLs.
//
// The Oasis montaj binary file is a simple file structure that is
intended
// to be used by programmers as a convenient way to import data
into
// an Oasis montaj database.  The Oasis montaj GBN GX will import
Oasis montaj binary files
// into an Oasis montaj database.
//
// A Oasis montaj binary data file consists of an ASCII comment
header
// followed by an ASCII 26 (hex <1A>), followed by binary data.
//
// Binary data consists of a series of variable length binary
records.
// Each record begins with a single byte value that identifies the
// record type, followed by the record data and data in the case
of
// data records.
//
// Record type are:
//
//   <01> simple channel record (GBN_Channels)
//   <02> line record (GBN_Line)
//   <03> data record (GBN_Data)
//
// Version 2 GBN record types (Oasis montaj v4.2 and later):
//
//   <04> array channel record (GBN_ArrayChannels)
//   <05> parameter (GBN_Parameter)
//
// The length of each record depends on the record type.
// The length of a data record will be the length of the data
record
// structure plus the length of the data.
//
// IEEE numbers and Intel byte order is required.
//

```

```

// The first 17 characters of the comment header must be:
//
//   "Oasis BINARY DATA"
//
// Any amount of ASCII text may follow.  Oasis montaj will start
reading
// binary data at the first byte after the first <1A> byte.
//
// The file structure is as follows:
//
//   Oasis BINARY DATA           // required first 17
bytes.                             //
//   comment text                 // As much ASCII text as
//   .                             // desired can be placed
//   .                             // in the comment
header.                             //
//   .                             //
//   <1A>                         // end of ASCII
comments.                          //
//   <01> 80 byte simple channel record // GBN_ChanRec
structure.                          //
//   <05> 192 byte parameter record    // optional parameter
settings                            //
//   .                               //
//   <04> 84 byte array channel record // GBN_ArrayChanRec
structure.                          //
//   .                               // <01> or <04> repeated
//   for                           //
//   .                               // each channel of data.
//   <05> 192 byte parameter record    // optional parameter
settings                            //
//   .                               //
//   .                               //
//   <02> 28 byte line record         // GBN_LineRec
structure.                          //
//   <05> 192 byte parameter record    // optional parameter
settings                            //
//   .                               //
//   <03> data record                 // GBN_Data structure +
data                                //
//   <03> data record                 // GBN_Data structure +
data                                //
//   .                               //
//   .                               //
//   <02> 28 byte line record         // GBN_LineRec
structure.                          //
//   <05> 192 byte parameter record    // optional parameter
settings                            //
//   .                               //
//   <03> data record                 // GBN_Data structure +
data                                //
//   <03> data record                 // GBN_Data structure +
data                                //
//   .                               //
//   .                               //
//   <00>                             // end of data.
//
// Notes:
//
//   Data records are related to the channels by channel number.
If

```


80 Appendix 2: Displaying Data Formats

```
// you have defined three channels, they will be numbered 0, 1
and
// 2. Channel data records can be in any order(i.e. 0,1,2 or
1,0,2)
// and you do not need to specify all channels on every line.
//
// If the channels already exist in the database, the channel
// parameters are ignored.
//
//-----
//
// Example:
//
// Hex values are in <hex>, other binary values are in (value,
// value,...).
//
// The binary type of each value can be determined from the
record
// structures. For example, a channel data record
(1,5,4610.0,0.1,
// 42150) in binary would be:
//
//             lChanNumber   = 1;           // long, 4 bytes
//             lBinaryType   = 5;           // long, 4 bytes
//             dFidStart     = 4610.0;      // double, 8 bytes
//             dFidIncrement = 0.1;        // double, 8 bytes
//             lLength       = 42150;      // long, 4 bytes
//
// In this example, 42150 double (8-byte) values must
immediately
// follow the channel data record.
//
// A carriage-return line-feed <0D0A> is assumed at the end of
each
// comment header line for the purpose of calculating offsets.
//
// Channel names are null terminated in a 64 character field.
//
// byte
// offset  data
comments
// ----- [-----]-----
//      0 [Oasis BINARY DATA ]
required
//      19 [ ]
//      21 [ This is a sample Oasis montaj binary data file which
]
//      69 [ contains two lines, 100 and 110, from flight 10 flown]
//      119 [ on January 19, 1995. The data includes X, Y, GPS ]
comments
//      170 [ time and 256-channel spectrometer sampled once a ]
//      222 [ second and in-phase (EM-I) and quadrature (EM-Q) ]
//      272 [ data sampled 10 times per second. ]
//      315 [ ]
//      317 [<1A> ]
end comments
//      318 [<01> ("Time",4,2,10,1) ]
Time channel
//      399 [<01> ("X",5,0,12,1) ]
X channel
//      480 [<01> ("Y",5,0,12,1) ]
Y channel
//      561 [<01> ("Mag",4,0,10,1) ]
Mag channel
```

```

//      642 [<01> ("EM_I",4,0,10,0) ]
EM inphase
//      723 [<01> ("EM_Q",4,0,10,0) ]
EM quadrature
//      808 [<04> ("Spec",1,256,0,6,0) ]
256-channel spec.
//      804 [<02> (100,0,0,10,1995,1,19) ]
line 100
//      889 [<03> (0,4,1000.0,1.0,3610) (data,data, 3610 times) ]
Time data
//      15358 [<03> (1,5,1000.0,1.0,3610) (data,data, 3610 times) ]
X data
//      44267 [<03> (2,5,1000.0,1.0,3610) (data,data, 3610 times) ]
Y data
//      73176 [<03> (3,4,1000.0,0.1,36100) (data,data, 36100 times) ]
Mag data
//      217605 [<03> (4,4,1000.0,0.1,36100) (data,data, 36100 times) ]
EM I data
//      362034 [<03> (5,4,1000.0,0.1,36100) (data,data, 36100 times) ]
EM Q data
//      506463 [<03> (5,1,1000.0,1.0,924160) (data,data, 924160 times)]
spectrometer
//2354812 [<02> (110,0,0,10,1995,1,19) ]
line 110
//      etc. [<03> (0,4,4610.0,1.0,4215) (data,data, 4215 times) ]
Time data
//      [<03> (1,5,4610.0,1.0,4215) (data,data, 4215 times) ]
X data
//      [<03> (2,5,4610.0,1.0,4215) (data,data, 4215 times) ]
Y data
//      [<03> (3,4,4610.0,0.1,42150) (data,data, 42150 times) ]
Mag data
//      [<03> (4,4,4610.0,0.1,42150) (data,data, 42150 times) ]
EM I data
//      [<03> (4,4,4610.0,0.1,42150) (data,data, 42150 times) ]
EM Q data
//      [<03> (5,1,1000.0,1.0,924160) (data,data, 924160 times)]
spectrometer
//      [<00> ]
end of data
//-----
#ifndef GBN_FH
#define GBN_FH
// --- record byte headers ---
#define GBN_CHAN_REC      1
#define GBN_LINE_REC     2
#define GBN_DATA_REC     3
#define GBN_ARRAYCHAN_REC 4
#define GBN_PARAMETER_REC 5
#define GBN_EOF_REC      0
// --- establish Geosoft defines if not already set ---
#ifndef LINE_NORMAL
// --- line type defines ---
#define LINE_NORMAL      0
#define LINE_BASE       1
#define LINE_TIE        2
#define LINE_TEST       3
#define LINE_TREND      4
#define LINE_SPECIAL    5
#define LINE_RANDOM     6
// --- data types ---
#define GS_BYTE          0      // signed byte
#define GS_USHORT        1      // unsigned 2-byte integer
#define GS_SHORT         2      // signed 2-byte integer

```

82 Appendix 2: Displaying Data Formats

```
#define GS_LONG      3      // signed 4-byte integer
#define GS_FLOAT    4      // 4-byte floating point
#define GS_DOUBLE   5      // 8-byte floating point
// A string type is indicated by the negative string length. For
// example,
// a 10 byte string would be type -10. String data should be NULL
// terminated.
// --- dummy values ---
#define GS_U1DM (char      ) 255U
#define GS_S1DM (signed char) -127
#define GS_U2DM (unsigned short) 65535U
#define GS_S2DM (short      ) -32767
#define GS_S4DM (long       ) -2147483647L
#define GS_R8DM (double     ) -1.0E32
// --- 4-byte float dummies require a variable to prevent compiler
// problems ---
#ifndef GS_R4DM
float GBN_r4dm = (float) GS_R8DM
#define GS_R4DM (GBN_r4dm)
#endif
// --- display formats ---
#define GSF_NORMAL 0      // Normal decimal number format
#define GSF_EXP    1      // Exponential floating point
(1.2E+23)
#define GSF_TIME   2      // Time (HH:MM:SS.SSSS)
#define GSF_DATE   3      // Date (YYYY/MM/DD)
#define GSF_GGRAPH 4      // Geographical (DEG.MM.SS.SSS)
// --- end of defines ---

#endif
// --- simple channel record ---
typedef struct {char      szName[64];          // channel name,
case tolerant,
// NULL terminated
/ -----
/ If the channel does not already exist, the following 4
parameters
// are used to create the Oasis montaj channel structure. If the
channel
// exists, this information is ignored.
// -----
long      lChannelType;          // channel data type, one of GS_?
long      lDisplayFormat;       // one of GSF_?
long      lDisplayWidth;        // display width in characters
long      lDisplayDecimals;     // digits after decimal place
} GBN_ChanRec; // record type <01>
// --- Array channel record for array elements ---
typedef struct {
char      szName[64];          // channel name, case tolerant,
// NULL terminated
// -----
// If the channel does not already exist, the following 5
parameters
// are used to create the Oasis montaj channel structure. If the
channel
// exists, this information is ignored.
// -----
long      lChannelType;          // channel data type, one of GS_?
long      lArrayDepth;          // number of samples per element
long      lDisplayFormat;       // one of GSF_?
long      lDisplayWidth;        // display width in characters
long      lDisplayDecimals;     // digits after decimal place
} GBN_ArrayChanRec; // record type <04>
// --- line record ---
```

```

typedef struct {
long    lLineNumber;
long    lLineVersion;
long    lLineType;           // one of LINE_?
long    lFlight;
long    lYear;
long    lMonth;
long    lDay;
} GBN_LineRec; // record type <02>
// --- data record ---
typedef struct {
long    lChanNumber;        // number from channel list, 0 is
first
long    lBinaryType;       // incoming binary data type, one of
GS_?
double  dFidStart;         // start fiducial number
double  dFidIncrement;     // fiducial increment
long    lLength;           // number of data elements that
follow

                                // For type 2 channel records,
lLength                                // will be the number of elements
times                                // the lArrayDepth, and data must
be                                    // row ordered.
} GBN_Data; // record type <03>
// ---
// Named parameters.
//
// Database lines and channels may have associated named
information
// which is stored as named parameters and their text string
values.
// Any number of these records may immediately follow the <01>,
<02>
// or <04> records.
//
// ---
// Projection information.
//
// Coordinate map projections may be defined using named
parameters as
// follows:
//
// Name                               Usage
//
// "_PJ_x"                             name of the X channel
// "_PJ_y"                             name of the Y channel
// "_PJ_name"                          POSC projection name
// "_PJ_ellipsoid"                     ellipsoid name, major axis,
eccen., prime meridian
// "_PJ_projection"                   projection type, parameters (see
GXF rev. 3)
// "_PJ_datum_transform"              transform name,
dX,dY,dZ,rX,rY,rZ,Scale. If not
//                                     defined, no local datum is assumed.
// ---
typedef struct {
char szParm[64]; // parameter name, NULL
terminated
char szValue[128]; // parameter value, NULL
terminated

```

84 Appendix 2: Displaying Data Formats

```
} GBN_ParameterRec; // record type <05>
//-----
// BINARY TYPES
//
// Some of the data types in a GBN file have special usage in
Oasis
// montaj. These are:
//
//      GSF_TIME      2          // Time (HH:MM:SS.SSSS)
//      GSF_DATE      3          // Date (YYYY/MM/DD)
//      GSF_GGRAPH    4          // Geographical (DEG.MM.SS.SSS)
//
// They are stored as either GS_FLOAT or GS_DOUBLE in a channel
and can
// be display in Oasis montaj as a number of as their special
format (Time,Date).
//
// The following C functions can be used to create GEOSOFT dates
and times.
// Note that the GGRAPH format is just a TIME format with hours
between -360 and 360.
//
//-----
//
// long RoundLong(double a)
// {
//     if (a > 0.0)
//         return((long) (a + 0.5));
//     else
//         return((long) (a - 0.5));
// }
//
// void
// BreakTime(double dVal,          // Value to break
//           long *plHour,        // Hours
//           short *psMin,        // Minutes
//           short *psSec,        // Seconds
//           double *pdFrac)      // Fraction
// {
//     double dI,dF;
//     short sNeg = 0;
//
//     // --- Take out the negative ---
//
//     if (dVal < 0.0) { sNeg = 1; dVal = -dVal; }
//
//     // --- Break into Fractional Components ---
//
//     dF = modf(dVal,&dI);
//
//     // --- Determine the Hour ---
//
//     *plHour = (long) dI;
//
//     // --- Determine the Minutes And Seconds/Frac ---
//
//     *pdFrac = modf(dF * 3600.0,&dI);
//     *psSec = (short) RoundLong(dI);
// }
```

```

//      *psMin = (short) (*psSec / 60);
//      *psSec = (short) (*psSec % 60);
//
//      // --- Negative ? ---
//
//      return(sNeg);
//  }
//
//  -----
//
//  static const short  DateNGS[12] =
//  {31,28,31,30,31,30,31,31,30,31,30,31};
//  static const short  DateLGS[12] =
//  {31,29,31,30,31,30,31,31,30,31,30,31};
//
//  #define NORMAL_YEAR    365
//  #define LEAP_YEAR      366
//
//  void
//  sBreakDate(double dVal,          // Value to break
//             short *psYear,       // Year
//             short *psMonth,      // Month
//             short *psDay)        // Day
//  {
//      double dF,dI;
//      short  sDays;
//      const short *psMonths;
//
//      short sDay;
//      short sMonth;
//      short sYear;
//
//      // --- Break in the Integer and Fractional Components ---
//
//      if (dVal < 0.0) dVal = 0.0;
//      dF = modf(dVal,&dI);
//
//
//      // --- Compute the Year ---
//
//      sYear = (short) dI;
//      if ( (sYear % 4) == 0)
//      {
//          psMonths = DateLGS;
//          sDays     = LEAP_YEAR;
//      } else {
//          psMonths = DateNGS;
//          sDays     = NORMAL_YEAR;
//      }
//
//      // --- Compute the Day ---
//
//      sDay = (short) RoundLong(dF * (double) sDays);
//
//
//      // --- Compute the Month ---
//
//      sMonth = 0;
//      while (sDay >= psMonths[sMonth]) { sDay-= psMonths[sMonth];
//      sMonth++; }
//
//
//      // --- Ok ---
//
//      *psYear = sYear;

```

86 Appendix 2: Displaying Data Formats

```
//      *psMonth = sMonth+1;
//      *psDay   = sDay+1;
//    }
//
// -----
//
// double
// dMakeTime(long   lHour,          // Hour Value
//           long   lMin,          // Minute
//           double dSec)          // Second
// {
//     double dVal;
//
//     // --- Limit the Information ---
//
//     if (dSec > 30000000.0) dSec = 0.0;
//     else {
//         while (dSec >= 60.0) {lMin++; dSec -= 60.0;}
//         if (dSec < 0.0) dSec = 0.0;
//     }
//     if (lMin > 500000L) lMin = 0L;
//     else {
//         while (lMin >= 60L) {
//             if (lHour >= 0L) lHour++;
//             else lHour--;
//             lMin -= 60;
//         }
//         if (lMin < 0L) lMin = 0L;
//     }
//
//     // --- Compute fractional hour ---
//
//     dVal = (dSec + (double) (lMin * 60L)) / 3600.0;
//     if (lHour < 0) dVal = -dVal;
//
//     // --- Compute final value ---
//
//     return(dVal + (double) lHour);
// }
//
// -----
//
// double
// dMakeDate(short  sYear,          // Year
//           short  sMonth,        // Month
//           short  sDay)          // Day of the Month
// {
//     short  sDays;
//     const short *psMonths;
//     short  i;
//
//     // --- Validate the Date ---
//
//     if (sYear < 0) sYear = 0;
//     if ((sYear%4) == 0)
//     {
//         psMonths = DateLGS;
//         sDays    = LEAP_YEAR;
//     } else {
//         psMonths = DateNGS;
//         sDays    = NORMAL_YEAR;
//     }
// }
//
//
```

```
//      // --- Get the Month ---
//
//      sMonth--;
//      if (sMonth < 0) sMonth = 0;
//      if (sMonth > 11) sMonth = 11;
//
//
//      // --- Get the Day ---
//
//      sDay--;
//      if (sDay < 0) sDay = 0;
//      if (sDay >= psMonths[sMonth]) sDay = (short)
(psMonths[sMonth]-1);
//
//
//      // --- Add days in the previous months ---
//
//      i=0;
//      while (i < sMonth) sDay += psMonths[i++];
//
//
//      // --- Compute the Value ---
//
//      return((double) sYear + ((double) sDay / (double) sDays));
// }
#endif
```